Natural CO_2 Fluids in Italy: Implications for the leakage of geologically stored CO_2

Jennifer J. Roberts

Thesis submitted for the degree of Doctor of Philosophy

The University of Edinburgh

2012

Acknowledgements

Firstly, my thanks go to my primary supervisors Rachel Wood and Stuart Haszeldine. It has been a privilege to have their support and encouragement to freely explore and develop research ideas, and their clarity of thought when I have lost mine. It has been a delight to work with such brilliant characters, and I am particularly grateful for the time, energy and tea Rachel has provided to me.

Thanks to Mark Naylor and Andrew Bell for sharing their code, and for their constructive insight. I have greatly valued the discussion and guidance Mark Naylor and Mark Wilkinson have given me over the years. I will thank Mark Naylor again, alongside Emmanuel Cedillo, for being excellent field assistants, offering amusing company, constructive input and impressive negotiation of Italian roads. My thanks to Stuart Gilfillan for sharing the Foreign and Commonwealth Office grant which paid for this fieldwork, and for his constructive support.

Invaluable information and data has provided by Gerald Roberts (Birkbeck, UCL), Roberto Bencini (Independent Resources, Italy), Giovanni Chiodini (INGV) and Carlo Cardellini (Perugia) and to these people I am very grateful. Additionally, I value the hospitality, time and investment from Fedora Quattrocci (INGV) and Alfredo Pugliese, Michele Impala, Francesco Bertello and Jonathon Craig (ENI).

I would not have had the opportunity to conduct this research if the Scottish Centre for Carbon Storage and Knowledge Transfer Partnership had not provided the financial means.

Finally, BIG thanks to my ever supportive family and friends, without whom I would not be who I am, nor where I am today.

Declaration

I declare that the research presented in this thesis was entirely the work of the author, except where stated otherwise. No part of this thesis has previously been submitted for a degree or any other degree or professional qualification at this or any other university.

Jennifer J Roberts

October 2012

Abstract

A principle concern for engineered CO_2 storage is long-term security. Surface leakage ('seepage') of injected CO_2 to the surface is economically and environmentally undesirable. Italy is a region of intense natural CO_2 degassing; 308 CO_2 seeps are catalogued which exhibit different surface characteristics, and a number CO_2 rich reservoirs were discovered when drilling for hydrocarbons. These seeps and reservoirs provide excellent natural analogues for seeps that might arise from breached carbon stores. This thesis explores the geological controls on the crustal plumbing of CO_2 fluids to model the processes governing CO_2 seep locations and distribution, and characteristics; and their consequences on human health risk. Risk of human death from accidental CO_2 poisoning at all seep types is low (10^{-8} yr^{-1}) and several factors influence risk of human mortality. Seeps distribute on two spatial scales; on a local scale (<5 km) seeps are clustered and aligned with subsidiary geologic structures, while on large scales seep clusters are discrete, and align with regional structures. Within clusters, seep locations are influenced by fault maturity, the presence of lithological boundaries and seep manifestation, which is determined by the flow properties of the outcropping lithology and local topography. Sealing and seeping CO_2 reservoirs are identified, and their geological characteristics compared. Italian reservoirs successfully retain large CO_2 columns at a range of reservoir conditions. Reservoirs which have hydrostatic pressure conditions in the overburden, determined from well logs, are located close to surface CO_2 seeps and recent extensional faults. Where there is significant overpressure above hydrostatic in the overburden, there are no seeps present above the reservoir structure. Overpressure of reservoir fluids may enhance fluid flow rates but is not a necessary condition for CO_2 leakage. Geothermal conditions influences the style of leakage at depths and towards the surface. Total CO_2 degassing from dry Italian CO_2 seeps is 3.5 ± 0.5 $Mt_{(CO2)}yr^{-1}$. It would take thousands of years for the effectiveness of a commercial scale store to be significantly reduced if it leaks to form a single seep with the mean flux rates modeled in Italy. If a seep

cluster develops, the storage effectiveness will reduce more rapidly, and could negate engineered CO_2 storage as a climate mitigation strategy.

The research presented in this thesis contributes to a body of knowledge which directly informs site selection procedure for carbon storage and maximise the long term storage potential for CCS. Thorough scientific understanding of the geological processes governing fluid escape is crucial to assure the scientific, political and public communities that safe, long-term carbon storage can be realised as an effective climate mitigation technology.

Contents

List of Figures

List of Tables

List of Abbreviations

a.s.l	Above Sea Level
CCS	Carbon Capture and Storage
CDS	Campanian Degassing Structure
CGIAR-CSI	Consultative Group on International Agricultural Research - Consortium for Spatial Information
DEM	Digital Elevation Model
ENI	Ente Nazionale Idrocarburi
GIS	Geographical Information System
GW	Gigawatt
IFT	Interfacial Tension
INGV	Istituto Nazionale di Geofisica e Vulcanologia
IQR	inter quartile range
ISPRA	Istituto Superiore per la Protezione e la Ricerca Ambientale (Italian Institute for Environmental Protection and Research)
ISPRA	Istituto Superiore per la Protezione e la Ricerca Ambientale (Italian Institute for Environmental Protection and Research)
ISTAT	Italian National Institute of Satistics
ITHACA	ITaly HAzard from CApable faults
MMbl	Million barrels
MORB	Mid Ocean Ridge Basalt
Mt	Megatonne
NRI	No Recorded Incident
PDB	Pee Dee Belemnite
ppm	parts per million
t d^{-1}	tonnes per day
Tcf	Trillion Cubic Feet
TRDS	Tuscan Roman Degassing Structure
TVD	True Vertical Depth
ViDEPI	VIsibilità dei Dati afferenti all'attività di Esplorazione Petrolifera in Italia

List of Symbols

C%v.v	Percentage by volume
°C	Temperature, degree Celcius
A	Area
B	Buoyancy
k	permeability
ka	a thousand years
KE	effective permeability
m	meters
M	Earthquake Magnitude Scale
m^3	cubic meters
Ma	million years
mm	Millimetre
P	Pressure
Pa	Pascals
Pf	pore fluid
Q	Flux
R/Ra	Helium (He) isotope ratio, where R = 3He/4He in the sample; Ra = 3He/4He in air
s	Seconds
Ss	Specific Storage
T	Temperature
$\bar{x}$	mean
z	Depth
Δelev	change in elevation
μ	Viscosity
σ	standard deviation

Chapter 1

Introduction

Anthropogenically-produced CO_2 is affecting the stability of the Earth's climate (Solomon, 2007), and the consequences of recent and projected climate change are severe (IPCC, 2007c). If dangerous climate change is to be averted, atmospheric CO_2 concentrations must not exceed 450 ppm, which corresponds to 2°C temperature rise above pre-industrial levels (IPCC, 2007b). The rate of atmospheric CO_2 increase over the period 2002 - 2011 (2.07 ppm yr^{-1}) predicts that we will surpass this threshold in the next 15 years if CO_2 emissions are unabated. A global effort is therefore required to drastically reduce society's dependency on CO_2 emitting resources (IPCC, 2007a). Many nations acknowledge this necessity and are imposing legislation to reduce greenhouse gas emissions, for example, the Climate Change Act (2008) of the UK government has committed to reducing its greenhouse gas emissions by at least 80% by 2050, relative to 1990 levels.

Modern industrialised society is dependent upon fossil fuels to meet energy demands and will remain so for the foreseeable future (Scott et al., 2012). Fossil fuel combustion for energy is responsible for 80% of global CO_2 emissions (IPCC, 2007a). Decarbonising the energy sector is therefore one of the most important technological challenges of the modern era.

One of the most promising technological solutions to reduce emissions from large point sources is carbon capture and storage (CCS), whereby CO_2 is captured at source and injected in geological formations where it is stored (Bickle, 2009). CCS has potential to reduce global CO_2 emissions by 20% on decadal timescales, but requires a rapid technology roll-out (Haszeldine, 2009; IEA, 2009).

Pilot scale CCS projects are currently injecting CO_2 onshore and offshore, and there are many larger scale demonstrations planned (Scott et al., 2012). Several financial and political factors hinder upscaling of the technology, and one of the greatest challenges is long term security of the performance of the CO_2 store.

To benefit medium term climate mitigation efforts, stored CO_2 must remain isolated from atmosphere for at least 10,000 years (Lindeberg, 2002). Model estimates suggest that storage sites must therefore operate with less than 0.01 % y^{-1} (Hepple and Benson, 2005), or 1% CO_2 loss to the surface in 1,000 years (IPCC, 2005). Current EU legislation requires engineered stores to retain CO_2 'permanently' (Council, 2009).

Aside from negative climatic consequences, leakage of injected CO_2 from the storing reservoir, and subsequent seepage to the surface, is both economically and environmentally unfavourable, and is associated with direct negative health effects from CO_2 poisoning. Public acceptance can strongly influence the fate of new technologies. Public concern, motivated by fear of seepage, is hindering CCS deployment onshore (Johnsson et al., 2009; Shackley et al., 2009). To gain public and political acceptance it is therefore crucial that storage sites operate without containment failure.

There is no experience of commercial scale CCS with which to verify predicted risks of engineered storage failure. Naturally occurring CO_2 reservoirs have successfully retained CO_2 underground for geological time periods; reservoirs in Colorado contain up to 5.8 Gt CO_2 (Allis et al., 2001) and have successfully done so for 70 Ma (McElmo Dome (Gilfillan et al., 2008). CO_2 can be successfully trapped in complex and multi-layered, or simple reservoir-caprock systems, at a range of depths and pressure conditions (Lewicki et al., 2007; Pearce, 2005/6).

These natural reservoirs provide a unique opportunity for developing insight into the physical and chemical processes that retain CO_2 and the long term effects of CO_2 on the reservoir rocks (Baines and Worden, 2004; Gilfillan et al., 2009; Kampman et al., 2010; Lu et al., 2009; Oldenburg and Lewicki, 2006). These physical and chemical processes are difficult to represent in laboratory or modelling experiments given the long time scales required to simulate comparable scenarios and heterogeneity intrinsic to geological formations.

Similarly, instances of CO_2 leakage from naturally occurring reservoirs serve as direct analogues for the potential migration of CO_2 from geologic storage sites. These sites provide opportunity to assess:

- The controls on containment and migration of CO_2 fluids (Dockrill and Shipton, 2010; Nelson et al., 2009)
- The fate of CO_2 migrating from the reservoir (Baines and Worden, 2001; Kampman et al., 2010)
- Natural rates of gas loss towards the surface (Annunziatellis et al., 2008; Chiodini et al., 2004; Chiodini et al., 2010)
- The environmental hazards of surface seepage (Beaubien et al., 2008; Etiope et al., 2005; Raschi et al., 1997)
- New methods of site assessment and monitoring (Bateson et al., 2008; Wilkinson et al., 2009)

In Italy natural CO_2 is being generated and trapped at the present day. Some traps have failed, or have been bypassed by CO_2, such that unusually abundant seepage is widespread. This thesis seeks to elucidate the crustal processes governing CO_2 flow paths and seep characteristics (expression, flux, etc) in Italy. Estimates of total and mean CO_2 flux rates are presented, and, together with quantified human health risk at these CO_2 seeps, the implications of seepage on this scale from engineered stores are explored.

The remainder of this chapter presents an overview of the sources and trapping mechanisms of crustal CO_2, and crustal fluid pathways are discussed alongside CO_2

fluid behaviour considerations. Italy as a region of degassing is then introduced which leads to the research aims and objectives of the research presented in this thesis.

1.1 Naturally Occurring CO_2

Flux of CO_2 to the Earth surface occurs in many regions of the world. Notable study CO_2 provinces are the Colorado Plateau (USA), Eifel region (Germany), periAlpine region (France), Reykjanes (Iceland), the Pannonian basin (Hungary) and Italy (Baines and Worden, 2004; Kirk, 2011; Pearce, 2005/6; Stevens et al., 2001). These provinces demonstrate that CO_2 can seep to the Earth surface by a range of mechanisms, and can exhibit a range of surface manifestations; including dry gas seeps, geysering, travertine deposition, sparkling water springs, mud volcanoes, and gas venting (Lewicki et al., 2007; Pearce, 2005/6). Furthermore, the origins of CO_2 in these provinces are different.

1.1.2 Origins of CO_2

A number of geological processes generate CO_2 which can accumulate to high concentrations in geological reservoirs or be released to the Earth surface, these include:

- *Magmatic*; CO_2 is released as magmas depressurise during ascent.
- *Metamorphism*: CO_2 is liberated by mineral reactions in response to elevated pressure (e.g. burial or regional metamorphism) or temperature (e.g. burial or contact metamorphism). Carbonate rocks, or rocks derived from organic materials (e.g coal) can release large quantities of CO_2 through this process.
- *Biogenic*: CO_2 is liberated by the biodegradation or maturation of hydrocarbons, which includes processes of methanogenesis, oilfield biodegradation, kerogen decarboxylation, and hydrocarbon oxidation.

Carbon stable isotope ratios ($^{12}C/^{13}C$, expressed as $\delta^{13}C$ relative to the PDB standard) are commonly used to distinguish between different CO_2 sources, since each process has typical fractionation factors, as expressed in Figure 1.1. However the $\delta^{13}C_{(CO2)}$ PDB of natural gas fields where CO_2 is the major component frequently lies within a range of overlap between magmatic degassing and carbonate breakdown (Gilfillan et al., 2008).

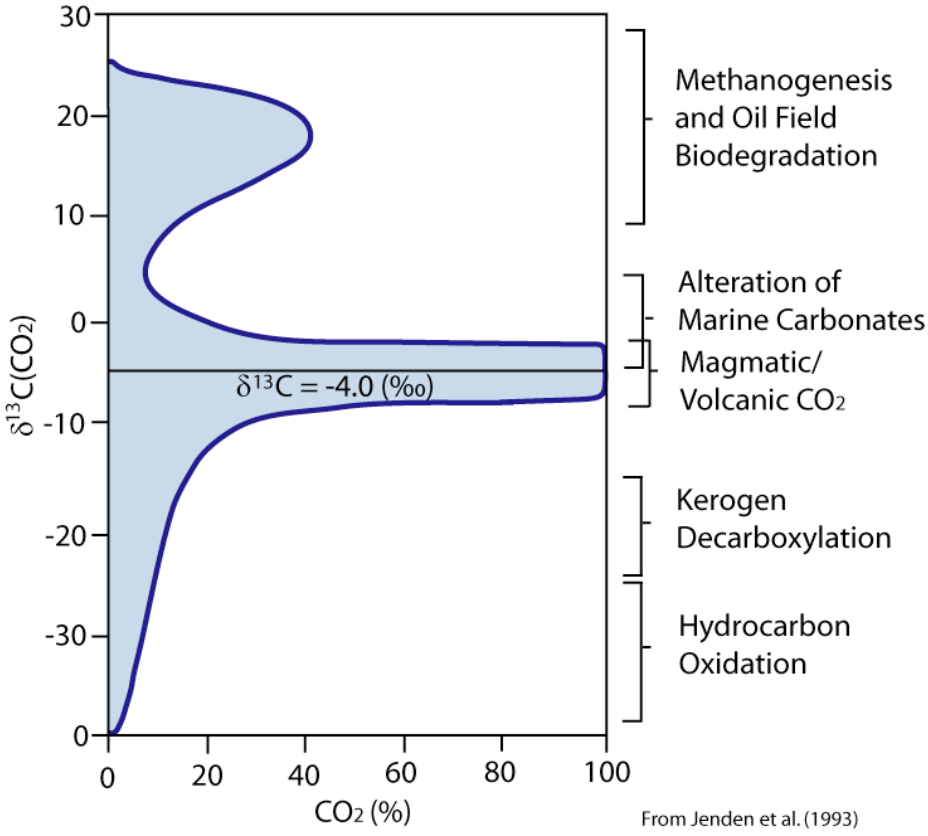

Figure 1.1: The range of $\delta^{13}C_{(CO2)}$ PDB signatures for different geological CO_2 generating processes. Note the overlap between the $\delta^{13}C_{(CO_2)}$ values for CO_2 derived from magmatic degassing or carbonate breakdown. Figure from (Gilfillan, 2006), redrawn from (Jenden et al., 1993).

Noble gases from the terrestrial atmosphere are isotopically and compositionally distinct from those of primordial and crustal sources. Noble gas isotopic and abundance measurements are therefore useful geochemical tracers for deep processes, including CO_2 origins and interaction with groundwater systems

(Gilfillan et al., 2008). Helium (He) isotope ratios are expressed as R/Ra values (R = $^3He/^4He$ in the sample; Ra = $^3He/^4He$ in air). Normal crustal R/Ra signatures are ≈ 0.02 (O'Nions and Oxburgh, 1988) whereas mantle signatures lie above this value, with MORB values at approximately 2.0 (Ballentine et al., 2002). The magnitude of fractionation of noble gases in subsurface reservoirs, can be used to quantify regional ground water movement through time, gas residence time, and groundwater volumes that have interacted with the trapped reservoir phase.

1.1.2 CO_2 trapping mechanisms

CO_2 can be retained in geological formations by a combination of physical and chemical trapping mechanisms. In order of increasing storage security, that is, decreased CO_2 mobility, these are:

Physical Trapping Mechanisms

- *Buoyancy Trapping*: Low-permeability sealing horizons (stratigraphic or structural) prevent upward migration of CO_2 fluids, which are less dense than formation waters. The majority of injected CO_2 is expected to be initially trapped in this way (Zweigel et al., 2004).
- *Residual Trapping*: Following CO_2 charge, 10 - 35% CO_2 will remain residually trapped as immobile droplets in the pore throat (Bennion and Bachu, 2008; Bickle, 2009). Residually trapped CO_2 will eventually dissolve into unsaturated wetting fluids where groundwaters experience hydrodynamic flow (Bickle, 2009).
- *Adsorption Trapping*: CO_2 molecules are adsorbed onto micropore surfaces. This is most significant in coal seams (IPCC, 2005).

Chemical Trapping Mechanisms

- *Solubility Trapping*: Free phase CO_2 will dissolve if it is in contact with unsaturated formation waters. The resultant CO_2-H_2O solution will be 1% denser than the initial formation waters and will sink, developing

convective mixing and ultimately enhancing solubility trapping (IPCC, 2005). Natural CO_2-rich reservoirs can show over 90% of initial CO_2 partitions to the aqueous phase (Gilfillan et al., 2009). CO_2 solubility in water is negatively affected by water salinity and temperature, but increases with pressure.

- *Mineral Trapping*: Dissolved CO_2 will dissociate to form carbonic acid. Mineral buffering in response may lead to the formation of new carbonate minerals. This immobilises the CO_2 and is therefore considered the most permanent form of trapping. However, the capacity for mineral trapping is limited and reaction rates may be slow. For example, a study of natural CO_2 reservoirs find maximum of 18% mineral trapping of CO_2 (Gilfillan et al., 2009) in siliciclastic rocks, which have greater potential for solubility trapping than carbonate reservoirs (Baines and Worden, 2004).

1.1.3 Migration of CO_2 Fluids from the Reservoir

In the CO_2 reservoir, free phase CO_2 will buoyantly migrate via matrix or fracture flow until it meets a sealing horizon. CO_2 may also migrate laterally due to advection. Flow rate can be retarded by factors such as decreased permeability due to formation heterogeneities, or changes in fluid buoyancy or relative permeability. These baffles to flow can lead to lateral spreading of the CO_2 phase during its ascent toward the reservoir top, increasing residual and solubility trapping by increasing the quantity of CO_2 in contact with unsaturated formation waters.

CO_2 can migrate from a reservoir structure by several mechanisms.

- *Regional groundwater flow:* Dissolved CO_2 will migrate with regional water flow if the reservoir is laterally unconfined. This may transport CO_2 from the reservoir unit.
- *Diffusion through the overburden:* Dissolved and free phase CO_2 can seep from the reservoir by diffusion. This is an extremely slow process (Bachu and

Bennion, 2008a), a study of North Sea oilfields found CO_2 diffused 12 metres into a mud rock seal in about 80 million years (Lu et al., 2009).

- *Capillary transport via pores or fractures in the overburden:* Capillary flow through rock pores or fractures (also referred to as matrix, or 'Darcy' flow) is governed by the Darcy equation:

$$\frac{Q}{A} = \frac{K_E \cdot \delta P}{\mu \cdot \delta z} \qquad [1.1]$$

where Q (flux) is CO_2 flux rate ($m^3 s^{-1}$) over the seepage area, A (m^2), K_E is the effective permeability of the fluid (m^2), $\delta P / \delta z$ is the pressure gradient,(Pa m^{-1}) where P is pressure and z is depth, and μ is CO_2 viscosity (Pa s^{-1}).

Equation [1.1] details how flow rates, Q, are enhanced by high fluid pressure gradients, high relative permeabilities and low viscosities. Pressure gradients can be elevated by buoyancy effects or fluid overpressure. Relative permeability is dependent on the fluid saturation of the mobile phase. Most reservoirs are water-wet, therefore for H_2O-CO_2 solutions K_E is equal to the rock bulk permeability, K_{seal}. However, for two phase flow, such as CO_2 flowing through a water-wet rock, the relative permeability, $Kr_{CO2,}$ describes the fraction of the total permeability accessible to each phase, therefore effective permeability for CO_2 is determined by:

$$K_E = K_{seal} \cdot Kr_{CO2} \qquad [1.2]$$

CO_2 saturation in porous rocks is typically between 30 - 60% (IPCC, 2005) and will vary with CO_2 viscosity (μ). Temperature and pressure conditions influence CO_2 viscosity, which is much decreased in the gas phase.

In order for the non-wetting fluid to invade the seal and initiate flow by capillary transport, CO_2 must overcome any capillary entry pressure of the pore or fracture. The capillary entry pressure is controlled by fluid interfacial

tension (IFT) which is influenced by the rock pore geometry and mineral chemistry, or fracture length, aperture and roughness. In a water-wet system, fluid IFT (and therefore capillary entry pressure) is considerably lower for dense phase CO_2 than for gaseous CO_2 (Hebach et al., 2002). IFT increases with pressure and decreases with temperature and salinity (Bachu and Bennion, 2008b; Chalbaud et al., 2009). Capillary entry pressures are lower where pore throat radii or fracture aperture is greater, thus fluids will flow more readily through these highly permeable pathways.

- *Unsealed faults or fractures in the overburden*: Fracture networks can exhibit high permeability and connectivity which, as previously discussed, will have lower capillary entry pressures than rock pores. Fractures may be present in a rock body from burial or tectonic deformation before CO_2 charge. Fractures often become mechanically sealed with confining pressure (depth) (Nara et al., 2011). Fractures can remain open at considerable depth where disparities on the fracture surface prevent total closure. Elevated formation pressures resulting from CO_2 charge can open fractures, or even induce fractures, thereby enhancing or creating fracture permeability. This will encourage fluid flow until the pressure is decreased and the fracture closes.

1.1.4 CO_2 migration in the shallow subsurface

Where no trap exists, or a trap structure has been filled to spilling point and subsequent CO_2 charge bypasses the trap, or CO_2 has migrated from a trap structure, free phase CO_2 fluids will continue their ascent from depth. Residual trapping and dissolution will attenuate these fluids during ascent, and they may accumulate in secondary reservoirs (Pruess, 2008).

Dissolved CO_2 will migrate with regional water flow. If these CO_2-rich waters rise towards the surface the accompanying pressure reduction will cause CO_2 to come out of solution. This can also be caused by heating these waters, or mixing with saline or thermal waters. The decreased density of the resulting mixture of gas and

water can enhance flow rate to the surface. This process is called 'gas lift' (Kirk, 2011) and can lead to geysering or vigorous degassing.

At depths shallower than ~700 m, ascending fluids will pass through two hydrologic zones; the phreatic, saturated zone and the vadose, unsaturated zone. CO_2 will be in gas phase at these depths, and will therefore be more buoyant than waters in the phreatic zone. Cool CO_2, however, will be denser than soil gas in the vadose zone which can encourage CO_2 lateral diffusion in the vadose zone (Kirk, 2011; Pearce, 2005/6). Flux measurements at natural CO_2 vents find elevated CO_2 concentrations extend beyond the actual edifice due to dispersion in the near surface (Annunziatellis et al., 2008).

1.1.5 Faults and crustal fluid flow

Crustal fluid flow is commonly controlled by faulting induced deformation (Faulkner et al., 2010). Fault zones are complex structures which evolve with slip activity (Wibberley and Shipton, 2010). They are composed of multiple deformation features (e.g. rocks with variable degrees of deformation states along one or several slip zones, with splays, Riedel shears and relay ramps) and their internal structure is a key control on their fluid flow properties (e.g., the thickness, nature and continuity of the fault rocks, the orientation, distribution and connectivity of slip surface and subsidiary faults and fractures (Faulkner et al., 2010; Kurz et al., 2008; Wibberley and Shipton, 2010).

As such their hydraulic properties vary with fault maturity and in all dimensions around the fault. Typically the 'damage zone', a fracture-dominated region of lower strain, acts as a conduit to fluids. This zone can be 10's to 100's of meters in width (Agosta and Kirschner, 2003; Faulkner et al., 2003) and surrounds a narrower, highly strained, 'fault core' (Figure 1.2 on following page). Here, the production of a low permeability fault gouge by persistent cataclasis, or entrainment of clay or shale into the fault, acts as a barrier to fluids. In addition, fluid flow along originally permeable fault features (cataclasites or fractures) may lead to preferential

cementation which can partially or completely remove porosity (Yielding et al., 1997).

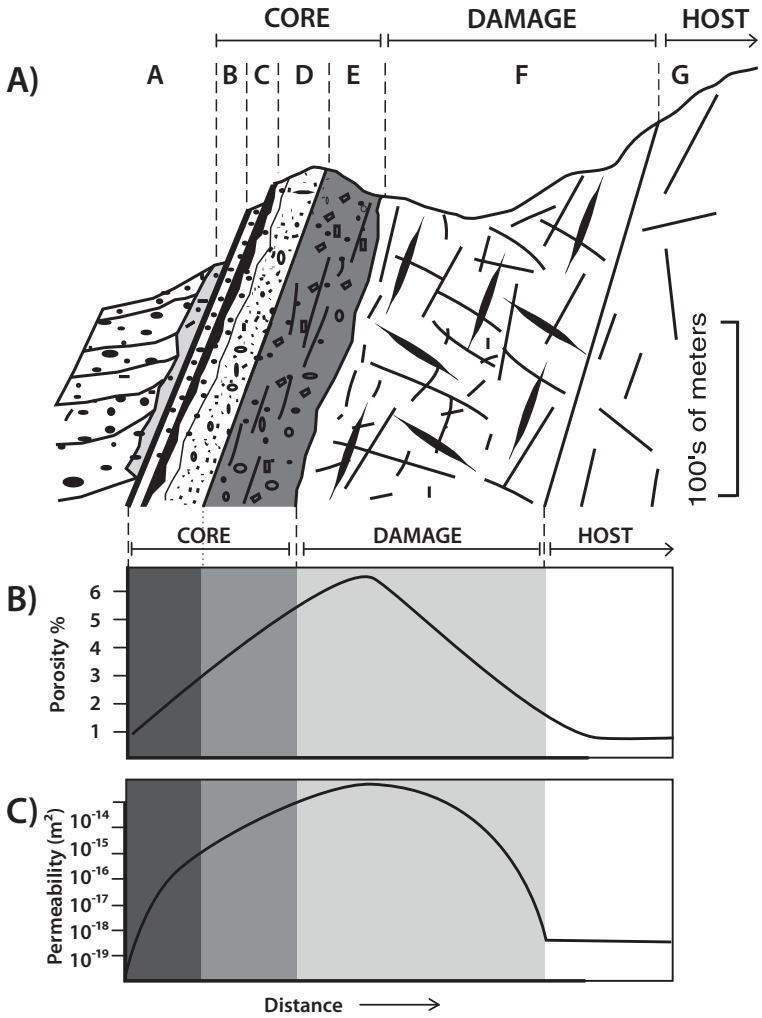

Figure 1.2 A: Schematic geologic section showing the architecture of a fault in carbonate host rock, where A: sediments in basin, B: hanging wall breccia, C: cemented zones, D: cataclasites, E: fault gouges, F: damaged host rock, H: host rock. **B:** The corresponding changes in measured porosity and permeability **(C)** from the fault core towards the damage zone (as indicated by shading). Adapted from (Agosta and Kirschner, 2003; Agosta et al., 2007).

Studies of active faults in the USA find the spatial variation in fault permeability influences groundwater flow and therefore spring location (Figure 1.3 below). The majority of ambient and hydrothermal springs are located in the fault tip or ramp where fractures propagate (Figure 1.3 C - D). Fewer springs are located at the fault trace, and spring temperatures cool away from the fault, though spring temperatures are less variable in evolved fault systems where linkage is well established (Anderson and Fairley, 2008; Curewitz and Karson, 1997). Spring locations correspond to regions of elevated stress which have enhanced crustal permeability, either by dynamic breakdown away from the existing fault or by kinematic opening of pre-existing fractures (Anderson and Fairley, 2008; Curewitz and Karson, 1997).

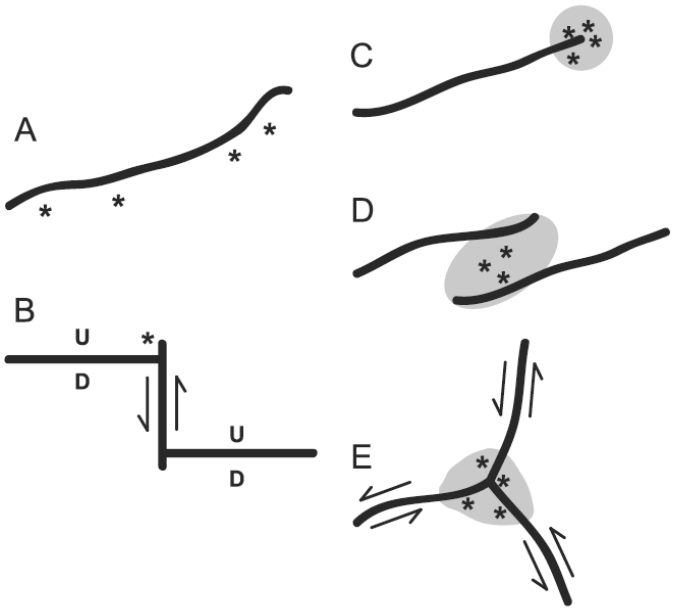

Figure 1.3: Structural settings of springs associated with faulting in the USA. Stars indicate the location of springs in each setting; breakdown regions are indicated by shading. (a) Fault trace; (b) Slipping fault intersection; (c) Fault tip; (d) Fault tip interaction area; (e) Locked fault intersection. Settings A-B kinematically maintained, C-E dynamically maintained. From (Anderson and Fairley, 2008) after (Curewitz and Karson, 1997).

1.2 Geological Setting of Italy

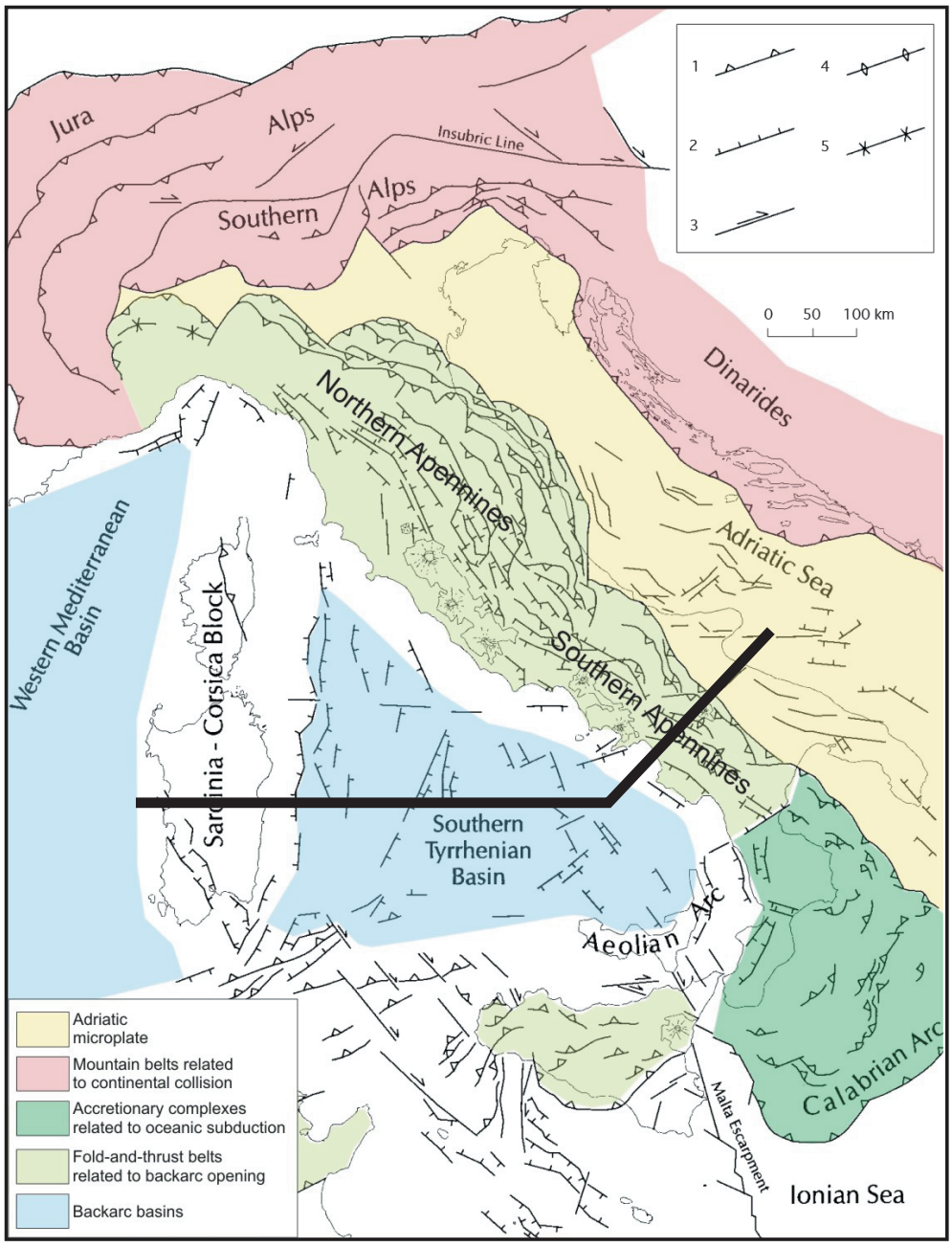

Figure 1.4: Simplified structural map of the Central Mediterranean region which shows the extent of the main tectonic domains, redrawn from (Serpelloni et al., 2006). Italy exhibits a diverse range of geodynamic processes which includes subduction, rifting, thrusting and strike-slip faulting. Black line of section for the following figure (Fig. 1.5). *Key: 1 – thrusts; 2 – normal faults; 3 – strike slip faults; 4 – Pliocene-Quaternary anticlines; 5 – Pliocene-Quaternary synclines.*

The tectonic setting of the Mediterranean region results from the complex evolution of oblique convergence between the African-Arabian and Eurasian plates which lead to the closure of the Tethyan Ocean. Current geodetic models estimate convergence is presently continuing at ≈ 5 mm y^{-1} (Serpelloni et al., 2006). Whilst the African and Eurasian plates remain relatively undeformed, the Adriatic Block records a variety of deformation processes. Geodynamic processes in Italy include subduction, back-arc spreading, rifting, thrusting, normal and strike-slip faulting (Figure 1.4).

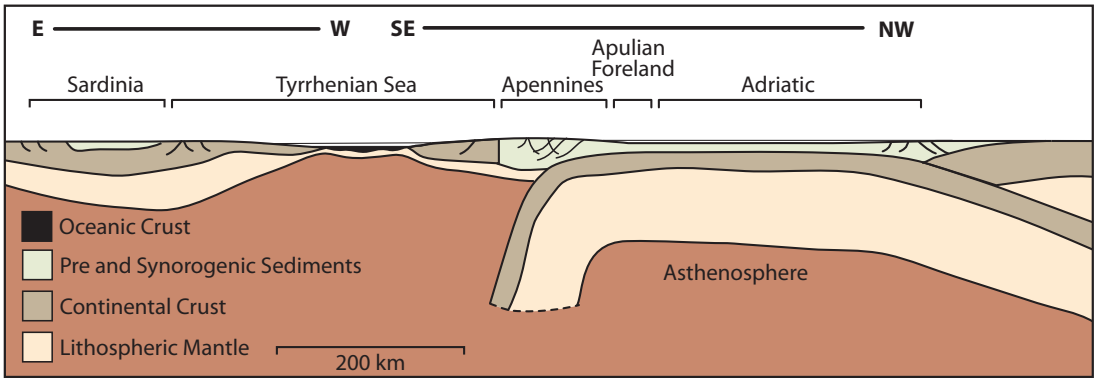

Figure 1.5: Lithospheric scale cross-section from Sardinia-Tyrrhenian-Central Italy (line of cross section shown in figure 1.4). The Adriatic microplate is subducted beneath the Corsica-Sardinia microplate of the European margin. Note the depth to Moho is much shallower East of Italy mainland. Adapted from (Carminati et al., 2010)

Westward subduction of the Adria plate beneath the European margin has developed a strong regional NW-SE structural grain in Italy (Fig. 1.4). In the Miocene, Jurassic-Eocene flysch units and synorogenic foredeep sediments were tectonically stacked above the thick, thrusted, semi-autochthonous Mesozoic-Tertiary carbonate platform sequence. Eastward younging foredeep and piggyback basins document the migration of the compression belt toward the foredeep at ≈ 4 cm y^{-1} related to slab retreat (Ghisetti and Vezzani, 2002; Patacca and Scandone, 2007; Scrocca, 2005). Coeval extension opened marine and continental basins, where

Messinian evaporites (mostly gypsum and anhydrite) formed, and the Tyrrhenian Sea.

During the Pliocene several granite bodies were emplaced and lamproitic and rhyolitic volcanism affected the Roman-Tuscan region. Since the Quaternary, volcanism has changed to K-rich undersaturated volcanism in central Italy (first in the Tuscan-Roman Magmatic Province and later in the Campanian Magmatic Province) and carbonatite magmas were extruded in intramontane areas of central Italy. The geochemistry of Quaternary magmas in the Roman and Campanian provinces show contamination of mantle melts by carbonate rich crustal material (Marziano et al., 2007).

Today, it is generally agreed that the Italian Adria - European collisional margin coincident beneath the Apennine Mountain belt (Figure 1.5) is no longer active and subduction is constrained to the Calabrian arc (Ghisetti and Vezzani, 2002). The Tyrrhenian sector preserves the older extensional system and exhibits a thinned crust (Figure 1.5) and associated high heat flow. Andesitic-rhyolitic and potassic volcanism in the peri-Tyrrhenian is still active.

Italy is a seismically active region, as testified by the distribution of earthquakes which focus in the Apennines (Figure 1.6). This mountain chain arcs from northwest Italy, down throughout the Italian peninsula, continuing southwest into Sicily. The Central and Southern Apennines are mostly characterised by thin-skinned tectonics (Calabro et al., 2003; Scrocca, 2005; Shiner et al., 2004) and are structurally composed of a carbonate duplex system overlain by a thick pile of platform and basin derived flysch nappes (the 'Allochthonous Complex'), Figure 1.7 (Patacca and Scandone, 2007).

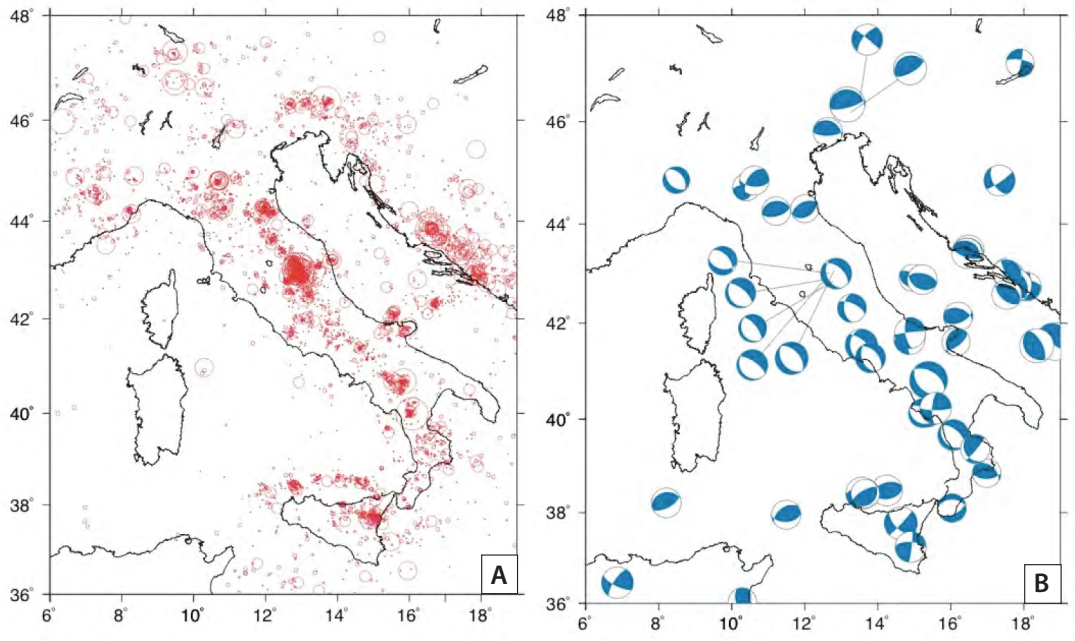

Figure 1.6 A : Earthquake hypocentres in the period 1989-1998 (M > 2.4). Note how seismic events mostly occur in the Apennine arc. **B**: Centroid moment tensor solutions for earthquakes shallower than 40 km in Italy. Images from (Carminati et al., 2010)

GPS velocity measurements find the Central and Southern Apennines are extending around 1.8 - 2.5 mm y^{-1} (Serpelloni et al., 2005), in response to gravitational collapse. Extension is accomplished by seismogenic normal faulting, and exposed fault scarps date from 12-18 Ka (Roberts, 2008). Most normal faults have comparable offsets (~2 km) and slip rates (~1-3 mm y^{-1}) but young from west to east (Ghisetti and Vezzani, 2002). The extensional domains of the Central and Southern Apennines are separated by the NE - SW Ancona-Anzio transpressive fault. Right lateral strike slip motion along this lithospheric fault at ≈ 2.8 mm y^{-1} has developed high crustal strain in this region. The Mesozoic carbonate sequence of the Central Apennines is represented mainly by pelagic limestones with the Burano formation at the base; a thick, laminate anhydrite sequence formed during the opening of the Tethys. Carbonate sequences to the South are composed of stacked overthrusts of platform, bypass margin, slop and pelagic facies.

The Apennines are bordered to the East by the Adriatic foredeep where compressional tectonics are ongoing. The foredeep is filled by deep Pliocene-Pleistocene deposits (Scrocca, 2005).

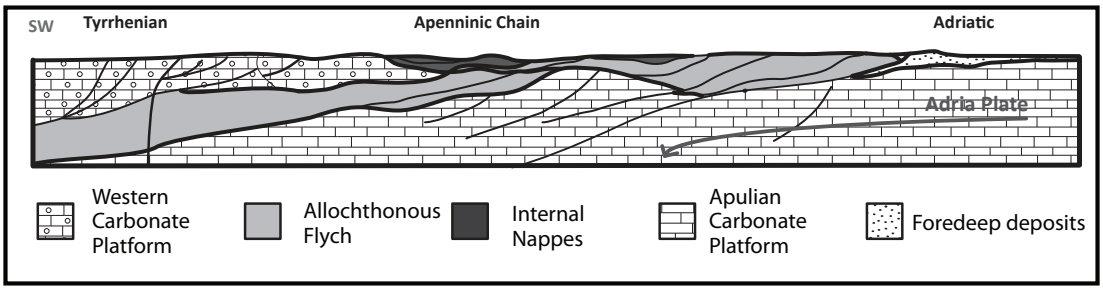

Figure 1.7: Schematic cross section of Italy showing major structural units, modified from (Improta et al., 2000). The Western Carbonate Platform, Apulian Carbonate Platform, Internal Nappes and the Allochthnous Units were once located on the same crystalline basement. The Adria Plate is subducted beneath the Corsica-Sardinia block of the European plate, the collisional margin is located under the Apenninic Mountain Chain.

1.3. Natural geofluids in Italy

Italy is a region of natural geofluid phenomena. Subsurface structures trap hydrocarbon oil and/or gas and/or CO_2 and seepage of these fluids is widespread; numerous CO_2, CH_4, and oil seeps are documented as well as many mud volcanoes (Chiodini et al., 2008; Etiope et al., 2007b; Gambardella et al., 2004; Katz et al., 2000; Martinelli and Judd, 2004; Minissale, 2004; Sani et al., 2004; Tassi et al., 2012). Figure 1.8 shows the distribution of gas and oil fields, mud volcanoes and CO_2 seeps.

In ancient Osco tradition, Mefite was the goddess 'in-between life and death' who oversaw the process steps important in life and was hence goddess of fertility. She acts between heaven and earth, between the underground and surface. Gas seeps were believed to source from her breathing within Earth. With such rich religious connections seeps are sites of archeological interest where many religious artefacts have been discovered, dating to 2000 years old (Chiodini et al., 2010).

Over 1000 natural gas (methane) seeps were documented in 1950, although few (< 30) presently exhibit continuous gas emissions following hydrocarbon exploitation over the last century (Etiope et al., 2007a). Hundreds of oil seeps are also documented, and these seeps guided early petroleum exploration. Today, Italy is the fourth most hydrocarbon endowed country of western Europe, following Norway, the UK and the Netherlands. According to 2009 figures, 1040 MMbbl of oil and 24.7 Tcf (700 billion m^3) of gas have been produced so far in Italy (Bertello et al., 2010).

In regions of hydrocarbon prospecting (wells, seismic lines) there is a wealth of subsurface information. Several subsurface structures are known to contain CO_2, either as a component of hydrocarbon reservoirs (Casero, 2005) or as nearly pure CO_2 (Collettini and Barchi, 2002; Heinicke et al., 2006). Reservoir structures include shallow (~1 km) or deep (~ 5 km) thrust related anticlines (Chiodini et al., 2010; Collettini and Barchi, 2002), extension related horst structures (Carapezza and Tarchini, 2007; Chiodini et al., 1995) or shallow gas pockets in Pleistocene sands (Barberi et al., 2007). Additionally, CO_2 reservoirs can show fluid pressures close to lithostatic (Collettini and Barchi, 2002).

Following several CO_2-related fatalities in the past 20 years, and recent scientific advances regarding the role of deep fluids and seismogenesis, there has been considerable investment into the documentation of all CO_2 seeps in Italy. Research concerning CO_2 fluids in the 1990's focussed on travertine formations and thermal springs (Duchi et al., 1995; Pentecost, 1995). A spate of research in the late 1990's addressed CO_2 origins and flux, and regional aquifer circulation (Chiodini et al., 2000; Italiano et al., 2000; Minissale et al., 2000). More recently, studies have focussed on the role of CO_2 on deformation and seep response to seismic events (Agosta and Kirschner, 2003; Agosta et al., 2008; Bonini, 2008, 2009; Collettini et al., 2008; Miller et al., 2004; Smith et al., 2008). Research attention at onshore Italian seeps, as analogues for breached CO_2 stores, are site specific, assessing the environmental effects, gas hazard, and monitoring methods (Annunziatellis et al., 2008; Bateson et al., 2008; Beaubien et al., 2008; Chiodini et al., 2007; Chiodini et al., 2010; Etiope et al., 2005) and structural control on CO_2 vent alignments at Panarea, offshore Sicily, have been investigated (Esposito et al., 2006). Studies of subsurface CO_2 accumulations in Italy

are few (Barberi et al., 2007; Bonini, 2009; Carapezza et al., 2003; Heinicke et al., 2010).

To date, over 308 CO_2 seeps at 270 locations have been catalogued in Italy (Chiodini, 2008). These are mostly low temperature gas emissions with various manifestations including vents, diffuse soil degassing, CO_2-driven mud volcanoes[1], and CO_2-rich groundwaters (springs and pools of bubbling water, see section 5.1 for seep type definitions). Several deep boreholes are also known to leak CO_2 (Chiodini et al., 2008; Heinicke et al., 2010; Mariucci et al., 2008). CO_2 degassing occurs in a range of geological environments; seeps are prevalent in areas affected by high heat flow and volcanism, and also in areas where there is no volcanic activity, such as Central and Southern Apennines (Frezzotti, 2009).

1.3.1 CO_2 Composition and Origins

At Italian seeps, CO_2 is released together with lesser amounts of N_2, H_2S, CH_4, H_2, Ar, He and CO (Minissale, 2004). The methane component in warmer seeps reflects abiotic sources whereas cooler seeps contain thermogenic methane (Tassi et al., 2012).

[1] There is some debate in the scientific community regarding the classification of these CO_2 driven 'mud-volcanoes'. While some authors refer to mud volcanoes (e.g. Bonini, 2009) others refer to the same edifices as CO_2 vents (Chiodini et al (2008); Etiope and Martinelli, 2009). (Etiope, G., and Martinelli, G., 2009, "Pieve Santo Stefano" is not a mud volcano: Comment on Structural controls on a carbon dioxide-driven mud volcano field in the Northern Apennines (by Bonini, 2009): Journal of Structural Geology, v. 31, p. 1270-1271.

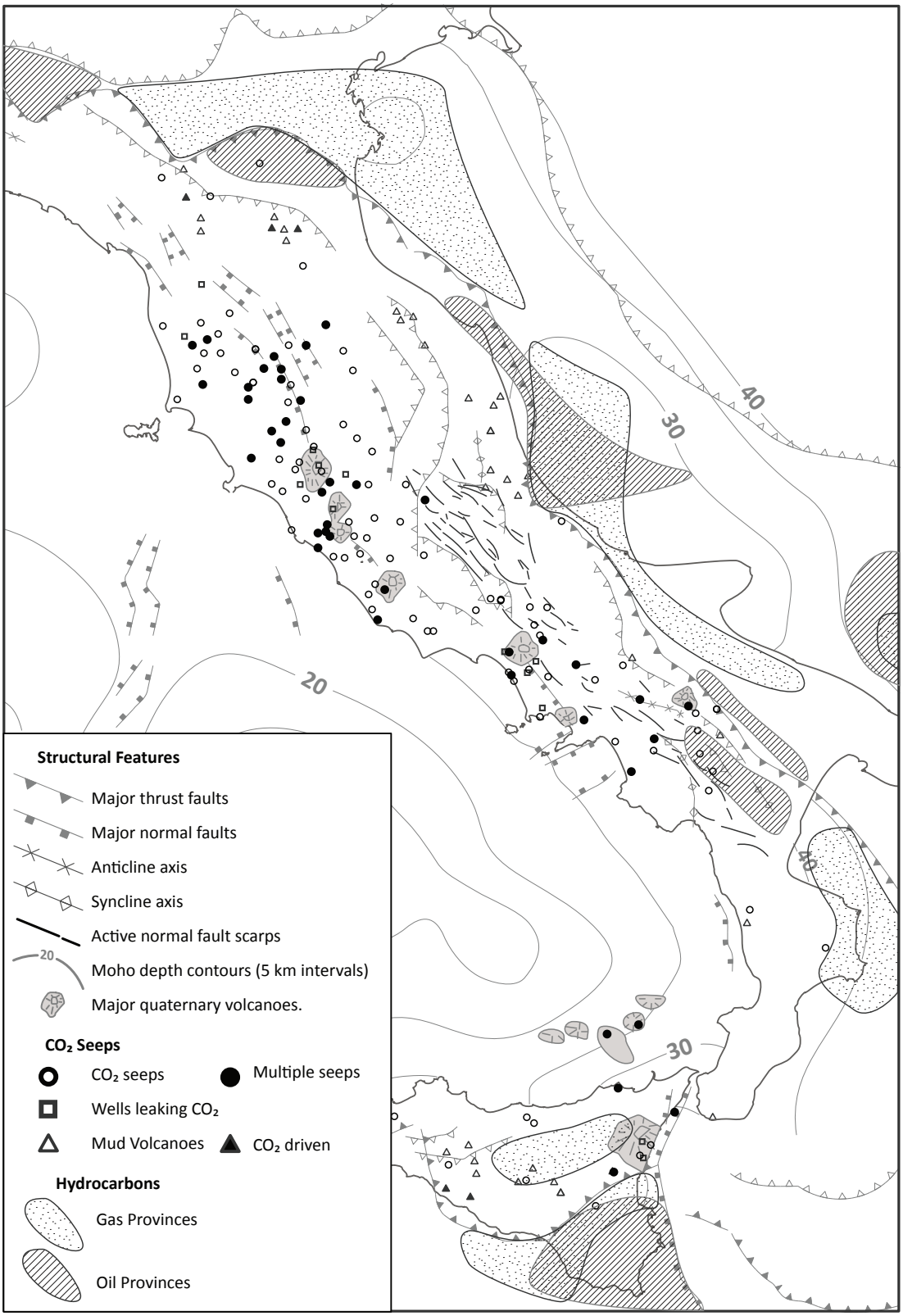

Figure 1.8: Schematic sketch of Italy showing major structural features (Ghisetti and Vezzani, 2002), major oil and gas petroleum provinces (Casero, 2004) and the location of CO_2 seeps (Chiodini and Valenza, 2009) and mud volcanoes (Martinelli and Judd, 2004).

Numerous geochemical studies have attempted to elucidate the diverse sources of CO_2 in Italy (Chiodini et al., 2004; Marziano et al., 2007; Minissale, 2004; Minissale et al., 1997) and several hypotheses have been proposed including CO_2 proportions from shallow biogenic processes, carbonate hydrolysis, mechanical breakdown or thermo-metamorphism of carbonates, and mantle degassing (Frezzotti, 2009; Italiano et al., 2008).

In volcanic or geothermal districts, CO_2 clearly sources from thermo-metamorphic reactions between magmas and carbonate country rocks (e.g., Alban Hills, Vesuvius, Colli Albani (Cinti et al., 2011; Frondini et al., 2004; Gambardella et al., 2004; Mariucci et al., 2008). However, these effects are local, and the majority of degassing occurs regionally, away from volcanically active areas (Frezzotti, 2009; Morner and Etiope, 2002). The geochemistry of magmas in the Roman and Campanian magmatic provinces show contamination of mantle melts by carbonate rich crustal material (Marziano et al., 2007). Since regional CO_2 flux increased in these provinces, it is argued that the most probable source of elevated regional CO_2 flux is the mantle wedge, enriched with subducted carbonates from the Adria plate (Chiodini et al., 2004; Collettini and Barchi, 2002; Frezzotti, 2009). This is supported by geochemical evidence that 43.3% of CO_2 dissolved in Apennine aquifers derives from deep sources (Chiodini et al., 2004).

Where degassing sites exhibit radiogenic helium compositions of crustal origins, $\delta^{12}C/^{13}C$ compositions have been interpreted to represent metamorphic CO_2 mixing with a proportion of biogenic CO_2 (Italiano et al., 2010; Vaselli, 1997) or the mechanical breakdown of CO_2 during seismogenesis (Italiano et al., 2008). In contrast, mantle R/Ra values at Mefite D'Ansanto similar to those at Vesuvius, located 60 miles away have been attributed to melt intrusions beneath the Southern Apennines (Italiano et al., 2000). Figure 1.9 shows the range of noble gas isotopic composition of CO_2 edifices in Central Italy. Even seeps with mantle R/Ra signatures show a strong crustal CO_2 contribution.

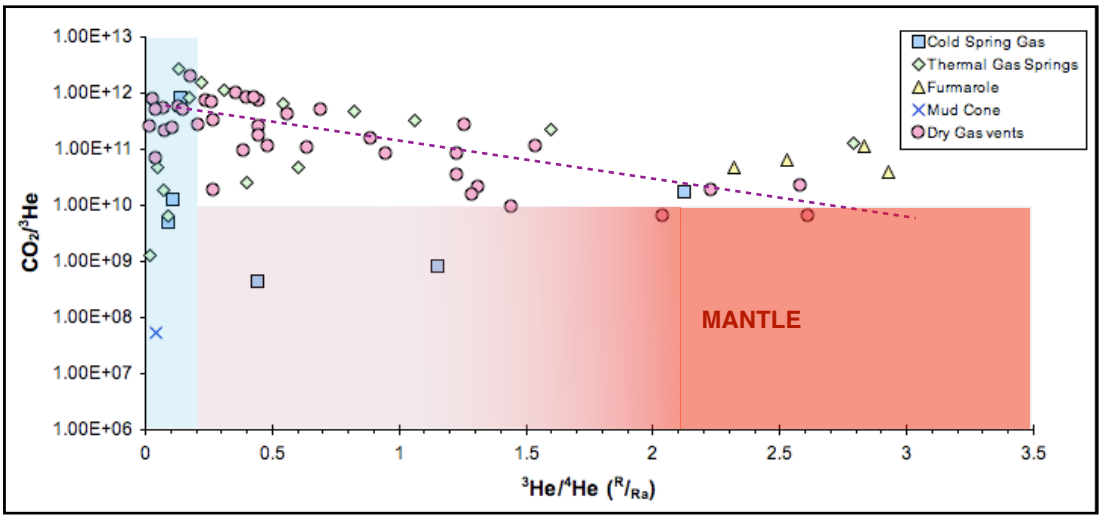

Figure 1.9: Crustal $CO_2/^3He$ values are greater than 1^{10}, so lower ratios indicate excess ^3He, which must be derived from the mantle. Normal crustal R/Ra values lies close to 0.2 (shown by blue background) whereas mantle R/Ra signatures exceed 2.0. Most of the gas seeps have crustal $CO_2/^3He$ values (> 1^{10}) despite showing mantle contribution R/Ra contributions. Several origins of CO_2 in Italy are proposed, with no consensus. Replotted from published data (Minissale, 2004).

1.3.2 Seep Flux

Seep density and flux is greatest towards the peri-Tyrrhenian. Here, two degassing structures relating to the Roman-Tuscan and Campanian magmatic provinces are identified (Chiodini et al., 2004), Figure 1.10. Archeological artefacts and historical records indicate that seepage has been established for at least 2000 years (Chiodini et al., 2011; Etiope et al., 2007b) and it is thought that regional CO_2 flux has remained elevated since volcanism began ~0.9 Ma (Minissale, 2004; Smith et al., 2008).

Seep flux varies between locations, from as little as < 1 ton per day (t d^{-1}) to in excess of 2000 t d^{-1} at Mefite D'Ansanto, which exhibits the greatest CO_2 flux from a single seep in the world (Chiodini et al., 2010). It is estimated that 9.2 $Mt_{(CO2)}$ y^{-1} from a mantle source is transported and released by Apennine aquifers (Chiodini et al., 2004). This is likely an underestimation since it does not include the contribution of CO_2 from the widespread gas seeps (Chiodini et al., 2010). Indeed, (Morner and

Etiope, 2002) estimate a total diffuse non-volcanic CO_2 output of 3–30 Mt y^{-1}. Such CO_2 flux is globally significant. Estimates of present-day global CO_2 discharge from sub-aerial volcanoes vary from 88 - 110 $Mt_{(CO_2)}y^{-1}$ (Kerrick, 2001) to 300 $Mt_{(CO_2)}y^{-1}$ (Morner and Etiope, 2002). Depending on which of these estimates are considered, the proportion of CO_2 discharging from aquifers in Italy accounts for between 3.1 - 9.4% of the global budget.

1.3.3 CO_2 fluids and Seismicity

It is well known in the Earth sciences that CO_2 gas emissions and tectonic activity are related (e.g (Irwin and Barnes, 1980). In Italy, CO_2 flux is much reduced in the Apennine Mountains where unusual seismic sequences indicate that trapped deep CO_2 fluids influence seismogenesis (Collettini and Barchi, 2002; Di Luccio et al.; Miller et al., 2004). CO_2 seep characteristics can vary in response to seismic events. In the Northern Apennines, seep fluxes are enhanced by seismic sequences (Bonini, 2009; Heinicke et al., 2006). In Southern Italy, degassing anomalies include temperature, conductivity, ^{222}Rn, CO_2 and NH_3 (Quattrocchi and Calcara, 1998). However in other regions, CO_2 seeps have appeared unaffected by high magnitude seismic events (Chiodini, 2010; Italiano et al., 2008).

1.3.4 CO_2 Fluids and Travertine Precipitation

Travertines and tufas are natural chemical precipitates from $Ca(HCO_3)_2$ saturated waters (terminology discussion can be found in a review by (Ford and Pedley, 1996)) and may therefore be considered as a form of mineral trapping of CO_2 at the surface. The processes of travertine formation is enhanced where groundwaters contain high dissolved CO_2 content pass through limestone aquifers. Dissolved CO_2 forms a weak acid, which encourage the dissolution of the limestone host. This process can saturate the waters in $CaCO_{3(aq)}$ which, when disturbed from equilibrium and the saturation potential of the waters is decreased (e.g. by reduction in pressure and temperature or release of the dissolved CO_2 phase), $CaCO_3$ is precipitated.

Active and inactive travertine deposits are widespread in Italy, where the oldest dated travertine is 0.5 Ma (Minissale, 2004). Some inactive deposits relate to paleoclimate cycles (Faccenna et al., 2008; Minissale et al., 2002). Travertine distributions are spatially related to regions of elevated CO_2 flux, indicating that their formation is encouraged by the elevated dissolved CO_2 contents in Italian groundwaters, relating to anomalous regional CO_2 degassing.

1.3.5 Crustal Controls on CO_2 seep formation

While the origins of CO_2 has been widely studied and debated, few studies have examined the crustal controls on seep locations or the processes that determine whether dry gas seeps or CO_2 springs develop. It has been observed that seep density and flux is greatest towards the Tyrrhenian (Chiodini et al., 2004; Chiodini et al., 2008; Minissale, 2004) where horst structures in buried Mesozoic carbonates are observed to correlate with areas of enhanced CO_2 degassing (Chiodini et al., 1995). Site specific studies note that seeps in the Northern Apennines align with subsidiary structures related to recent extensional faulting (Bonini, 2009), and in some locations gas fluxes are observed to be elevated towards faults (Annunziatellis et al., 2008; Etiope et al., 2005). Thermal springs, which indicate rapid fluid ascent, are observed to discharge in topographic lows close to faults at the contact between the Mesozoic limestones and overlying formations (Collettini et al., 2008; Minissale, 2004). Indeed, the presence of faults are evoked to account for the extraordinary gas flux at Mefite d'Ansanto (Chiodini et al., 2010) though these structures are not obvious from the surface geology.

A long term study at a number of closely spaced seeps in the Northern Apennines noted that seep water content exhibited some seasonal variation (Heinicke et al., 2006) and some edifices migrated several meters during the study period. It has been proposed that hydrological properties relating to lithology affects seep density and flux (Collettini et al., 2008). Models suggest that carbonate aquifers can dissolve 10 times more CO_2 than flysch, and 2.5 times more than volcanic rocks before gas

must leak at the surface (Collettini et al., 2008). To date, this concept has not been tested by field evidence at these CO_2 seeps.

1.4 Research aims and objectives

The overarching aim of the research presented here is to directly inform storage site assessment and monitoring strategy at engineered CO_2 stores by analysing controls on the distribution of natural CO_2 seeps and reservoirs in Italy. The research presented in this thesis draws on the wealth of regional surface and subsurface data available in Italy with the following objectives:

- CCS faces opposition regarding potential negative human health affects of CO_2 leakage from onshore storage sites, and there is no commercial scale CCS with which to verify predicted risks. Natural CO_2 seeps can therefore guide assessment of potential health risks from leaking stores. Here, historical records over the last 20 years of human death at CO_2 seeps in Italy are examined to quantify the health risk they present to the resident population, and to understand the factors that influence this risk. This allows evaluation as to whether current concerns regarding the negative health affects of leaking CO_2 stores are founded, as well as to guide risk assessment.
- Site specific research has identified that CO_2 seep locations associate with faults or deep structures, but these relationships have not, to date, been rigorously examined. I have used an extensive database to understand controls on the spatial location and distribution of CO_2 seeps in Italy and how this is related to geological structures in order to establish the first order controls on CO_2 fluid pathways in a range of structural settings.
- CO_2 seeps in Italy show a range of surface characteristics (seep type, flux, temperature). However, the controls on these seep characteristics are poorly understood. Models find that seep hosting lithology may influence seep type development and seep flux / density (Collettini et

al., 2008), and field observations note that seeps often emerge in valleys. The role of lithology or topography and seep characteristics and seep density are therefore here explored to elucidate the processes governing CO_2 seep characteristics.

- Resource exploration discovered a number of CO_2 bearing reservoirs in Italy, some of which are located close to CO_2 seeps. Studies of these reservoirs are few; only one reservoir has been studied to assess how CO_2 breaches the formation (Bonini, 2009). As a result, an appraisal of sealing and leaking CO_2 reservoirs in Italy is conducted to determine the geological factors that inhibit, or encourage, fluid escape.
- Total non-volcanic CO_2 flux from the Italian sector is not well quantified. This is because previous calculations of total non-volcanic CO_2 flux from the Italian sector consider only the CO_2 released from CO_2 rich springs (Chiodini et al., 2004), and in addition may be poorly constrained (Gambardella et al., 2004). Here, I have undertaken improved estimates of regional degassing by quantifying the contribution from catalogued dry CO_2 seeps.
- Modelled mean flux rates from breached geologic stores are smaller than the fluxes observed at Italian gas seeps (Pruess, 2004, 2008). Therefore I have sought to apply mean seep flux rates to geological storage scenarios to establish how seepage on the scale observed in Italy will affect CO_2 storage operations.

1.5 Data Sources and Methods

1.5.1 The Italian Seep Database

A national project involving over 50 Italian researchers was co-ordinated by the INGV-DPC V5 (Istituto Nazionale di Geofisica e Vulcanologia Dipartimento della Protezione Civile) during 2005–2007. The project's objective was to share knowledge and reduce health hazard from emission sites. To achieve this a web-based catalogue of degassing sites in Italy was created, which is referred to as the INGV Googas database (Chiodini and Valenza, 2009).

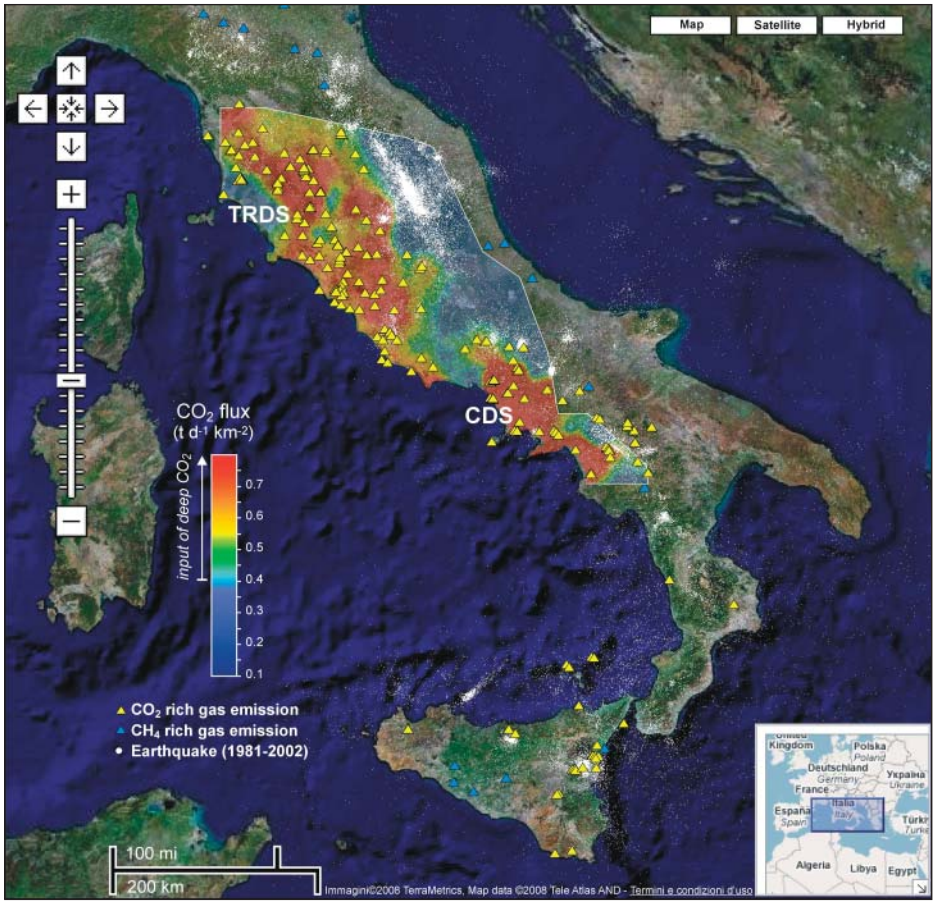

Figure 1.10: The Googas database showing CO_2 flux in Central Italy (Chiodini and Valenza, 2009). Two degassing structures are identified; the Tuscan Roman Degassing Structure (TDRS), and the Campanian Degassing Structure (CDS)

All known gas emission sites in Italy were surveyed and the results compiled into a GRS and published as an informative layer over maps which are publicly available through Google Maps as shown in Figure 1.10, below. The Web interface, called GOOGAS, is available at: http://googas.ov.ingv.it (Chiodini and Valenza, 2008)

The data available for each catalogued seep site include: name, coordinates, image, brief description of the site, type of gas emission, gas composition, temperature, gas flux magnitude, gas flux measurement method, gas hazard description, bibliographic references, downloadable files (such as images, maps, tables, articles, etc.), and the contact information of researchers who performed specific investigations.

Seep classifications, as described by INGV researchers (Cardellini, 2010; Chiodini, 2010) include:

- *Vent emissions*: expulsion of pressurised dry gas
- *Diffuse emission:* expulsion of dry gas at ambient pressures.
- *Springs*: Water spring with high dissolved CO_2 content derived from deep origin.
- *Bubbling Water*: pools of water degassing CO_2
- *Wells*: Man made deep well with high dissolved content of CO_2, or degassing CO_2.
- *Fumaroles*: High temperature emissions associated with volcanic edifices.

Gas concentration from focussed dry seeps were measured using an infrared analyser e.g. (Frondini et al., 2009) and flux measured by calculating air velocity with a hot-wire digital anemometer (Heinicke et al., 2006) and, in some cases, measurement of a gas river e.g. (Chiodini et al., 2010). Soil diffuse degassing was derived by geostatistical and statistical methods based on accumulation chamber measurements, or dynamic concentration measurements or Eddy Covariance. Fluxes of dissolved gas species were derived from the flow rate of the water and the dissolved gas content. The gas seeps are not exclusively CO_2 dominated; 287 seep sites were documented, of which 270 are CO_2 seeps, 16 are methane (CH_4) gas

emission sites and 1 is nitrogen N_2 dominated. In the remainder of this thesis 'seep' will refer to CO_2 seeps unless otherwise specified.

1.5.2 Italian well logs

Documents concerning Italian oil exploration have been made easily accessible by the ViDEPI[2] project (www.videpi.com, (ViDEPI, 2009)). Oil companies in Italy must, by law, provide UNMIG[3] with progressive technical reports on exploration activities relating to their permits and concessions. These reports information such as geologic and structural maps, final well logs and seismic lines.

The ViDEPI database makes all expired mining permits and concessions that were filed with UNMIG of the Ministry for Economic Development since 1957 publicly available to download as PDF files. The database of wells includes well logs of non-commercial Italian wells drilled between the period 1895 till 2010. Seismic lines, wells and expired permits, and links to the relevant documents can be geographically searched using a WebGIS, and can be downloaded as a Google Earth file[4]. The database is updated regularly. The Ministry of Economic Development made the data available to the Italian Geologic Society[5] and the project is funded by the Italian Petroleum and Mining Industry Association[6].

CO_2 bearing reservoirs can be identified from well test information from the well logs. Formation fluid analyses which are not noted on the well log are not currently available online for a number of wells, but they (or any other publicly available documents that are not hosted online) can be consulted by visiting the Library of

[2] '**VI**sibilità dei **D**ati afferenti all'attività di **E**splorazione **P**etrolifera in **I**talia' ('Visibility of Petroleum Exploration Data in Italy').

[3] '**U**fficio **N**azionale **M**inerario per gli **I**drocarburi e **G**eotermia' ('National Mining Office for Hydrocarbon and Geothermal Energy').

[4] Google Inc. (2009). Google Earth (Version 5.1.3533.1731) [Software]. Available from: www.google.com/earth

[5] Società Geologica Italiana

[6] Assomineraria

Rome University Tre (BAST)[7]. Some confidential data including formation fluid analyses and a report on CO_2 bearing wells is supplied by ENI[8].

1.5.3 Active Faults in Italy

The ITHACA (ITaly HAzard from CApable faults) database is the outcome of a project to document all tectonic structures capable of surface deformation, and evaluate the natural hazard these faults present. Each fault is attributed information regarding the fault type, fault kinematic and evidence of environmental hazard it poses. The project is regularly updated or modified, and the resulting GIS files are available from: http://sgi.isprambiente.it/geoportal/catalog/content/project/ithaca.page (ISPRA, 2007)

It is important to note that aseismic slip on evolved faults can lead to surface deformation, as observed in the mature extensional system in peri-Tyrrhenian (Collettini and Holdsworth, 2004). Faults in the ITHACA database may not necessary be seismically capable. Active normal fault scarps which offset 12-18 ka landforms in the Apennines have been accurately mapped and published (Roberts, 2008).

1.5.4 ISPRA[9] GeoMapViewer

The Geological Survey of Italy have made geological information available by a WebGIS accessed online at http://sgi1.isprambiente.it/GeoMapViewer/index.html (ISPRA, 2010). Relevant geological information includes: geological maps (at 1:25,000; 1:100,000; 1:500,000; 1:1,000,000 scales, where available); geophysical data (gravimetric measurement stations, gravity data and Bouguer anomalies); historical seismicity; geomorphological information; hydrologic information (rivers, basins

[7] Biblioteca di area scientifico tecnologica dell'Università Roma Tre ('Science and Technology Library')

[8] Ente Nazionale Idrocarburi

[9] **I**stituto **S**uperiore per la **P**rotezione e la **R**icerca **A**mbientale (translates to 'Institute for Environmental Protection and Research').

and lakes and springs); Italian landslides and sinkhole inventory, ViDEPI data. This information can be downloaded in Google Earth (KML) or GIS (Shapefile) format.

ISPRA state (translated from Italian):

> "*While recognizing that the GeoMapViewer is a powerful visualization tool, consultation and data query, please note that it is not a tool for detailed analysis. The Geological Survey of Italy noted that it is not responsible for any inaccuracies of the data and the degree of-date. It also specifies that for a proper use of the data item will be displayed taking into account the original scale. Remains valid intellectual property ISPRA, therefore any unauthorized use of data will be liable to prosecution*".
>
> (ISPRA, 2010)

The information elicited from the ISPRA GeoMapViewer is therefore treated as a guide to the geological structure, and, where possible other, more accurate information sources are used.

1.6 Methods

Data from the sources outlined above were compiled into a GIS dataset. This rich dataset, alongside field observations, formed the cornerstone of the research presented in this thesis. Detailed methodologies relevant to a specific body of work are presented in the corresponding chapters.

1.6.1 Geographical Information System

The Geographical Information System ArcGIS is populated with the data outlined in section 5 above, in addition to:

- The location of documented active and fossil travertines (Minissale, 2004).
- Published present day stress field information (Barba et al., 2009) constructed from geological, seismological, and contemporary stress data.
- SRTM[10] DEM[11] 90 m elevation data (Jarvis, 2008) from the CGIAR-CSI[12] GeoPortal (http://srtm.csi.cgiar.org)
- Isotherms at 1 and 2 km depth from the Geothermal Resources National Inventory (Geothopica, 2010).
- Published deep carbonate structure map (Nicolai et al., 2007) and tectonic terrains (Ghisetti and Vezzani, 2002).
- Location and magnitude of all detectable seismic events since 1983, publicly available from an online server provided by the INGV: ftp://ftp-server.rm.ingv.it/pro/bollet/

[10] Shuttle Radar Topography Mission

[11] Digital Elevation Model

[12] Consultative Group on International Agricultural Research - Consortium for Spatial Information

- Resident population information from the 2001 census, made available by the Italian National Institute of Statistics (ISTAT, 2001) accessed by the DaWinci online database: http://dawinci.istat.it/pl/index_eng.html
- Administrative information and urban information from the ArcGIS online resource centre: http://www.arcgis.com/home/webmap/viewer.html?useExisting=1

This rich dataset is used as a basis for investigating regional CO_2 seep trends in the proceeding research. Statistical techniques were applied to the seep dataset to characterise their spatial distributions and provide insight into the processes governing their locations and expressions. These methods, and specific ArcMap tools and plugins are detailed in the relevant chapter.

1.6.2 Fieldwork

Two field trips to Central Italy supplemented the seep database. The first field trip, in May 2009, was a short, four day scoping study visiting seep sites of different seep classifications in Campania. The second trip included sample collection from cores in Milan, courtesy of ENI followed by 5 days geological mapping and travertine sample collection in Campania. Field observations seeded the research questions outlined in Section 1.5.

1.7 Thesis Overview

Chapters 2 - 6 contain research papers which address the research questions formulated during fieldwork in Central Italy during 2009. Each paper is preceded by a foreword which frames the research context and followed by material supplementary to the paper.

Chapter 2: CO_2 is poisonous to humans at elevated concentrations. However, much of the Italian population are exposed to CO_2 seeps, which are located in both rural and urban areas in Italy. Field observations note that the surface expression of vents, fumaroles and high flux diffuse seeps are more obvious to the human eye than bubbling water and spring type seeps. The Googas seep database documents whether animal or human fatalities have occurred at seep sites. This information is coupled with resident population data and site specific information obtained from Googas collaborators to investigate the factors influencing health risk, and to quantify risk of human death at seep sites.

Paper 1: '*Assessing the health risks of CO_2 seeps in Italy*'.
[Published, PNAS, 2011[13]]

Chapter 3: CO_2 seeps are located in a variety of structural settings in Italy. Seep density is greatest towards the Tyrrhenian, but shows regional variation in seep density, seep types, and seep flux. Site specific studies identify that seep locations are guided by faults. In this chapter, spatial statistical methods investigate seep distribution on various scales and the GIS dataset is rigorously examined to elucidate how regional geological structures influence seep locations and distributions.

Paper 2: '*Structural controls on the spatial distribution of CO_2 seeps in Italy*'. [Submitted for publication]

[13] Published: Roberts, J.J., Wood, R.A., and Haszeldine, R.S., 2011, Assessing the health risks of natural CO2 seeps in Italy: Proceedings of the National Academy of Sciences of the United States of America, v. 108, p. 16545-16548

Chapter 4: The factors determining seep type development are unclear. Field observations noted that seeps often to emerge in local topographic depressions, or close to streams and rivers, and dry seeps sometimes occurred up slope from seeps associated with water. The GIS dataset is used to determine how the location of different seep types are influenced by topography, distance from rivers, and surface geology.

> Paper 3: '*Controls on the surface characteristics of CO_2 seeps: implications for leakage from engineered stores*'.
>
> [Submitted for publication]

Chapter 5: To date, studies of subsurface CO_2 accumulations in Italy are few. In this chapter, the subsurface conditions of CO_2 reservoir case studies are examined to assess which are seeping reservoir fluids to the surface. Common and disparate characteristics of seeping and sealing reservoirs are determined by comparing the geological characteristics and down well conditions of these case studies. Seepage rates from the reservoir are calculated to inform the fluid processes governing fluid escape from the reservoir at the fluxes observed at the surface.

> Paper 4: '*To Seep or not to seep? Case studies of CO_2 Reservoirs in Italy*'
>
> [Submitted as 2 publications]

Chapter 6: No estimate of total CO_2 flux from dry (vent and diffuse) gas seeps has yet been made. Using flux data available from the Googas dataset, total CO_2 flux at dry gas seeps in Italy was calculated. These calculations consider scenarios where seeps might be missing from the catalogue or seep flux measurements are biased. Average flux rates at Italian gas seeps are applied to engineered storage sites to investigate what rates of leakage these seeps would represent.

> Paper 5: '*Quantifying long term non volcanic CO_2 release in Italy and implications for engineered CO_2 storage efficiency*'.

Chapter 7: Each research paper in these chapters illuminates some the controls on the location, surface characteristics and consequences of seeping CO_2 fluids. Chapter 7 synthesises these research findings, together with research drawbacks.

Potential seeping mechanisms are explored, and a conceptual model of seep development is presented. The application of the research presented in this thesis to engineered CO_2 storage is evaluated.

Chapter 8: The chapter concludes the thesis, summarising principle research results and the ramifications of this body of research. Important research questions for future research are proposed.

Chapter 2

How Safe are Seeps?

While vents and high flux CO_2 seeps often have obvious physical expressions, many CO_2 seeps are subtle manifestations. There are several features which aid identification of nondistinctive seeps in Italy:

- Elevated CO_2 and associated H_2S in the air and soil gas encourage acidophilic ecosystems to establish (Raschi et al., 1997).
- If concentrations get so great that vegetation cannot survive (40-50% vol, (Smets et al., 2010)) and patches of bare earth can be seen. High gas concentrations can create a local light refraction effect (shimmer).
- The presence of dead animals provides a strong indication of CO2 seeps (Chiodini et al., 2008; Smets et al., 2010).
- H_2S, often released as a subsidiary gas, has a distinctive smell.

Seep hazard can therefore be difficult to perceive. Many Italian CO_2 seeps are unsigned and public access is unrestricted despite several accidental human deaths from CO_2 poisoning in recent years. These observations provided the stimulus to assess the risk the numerous seeps in Italy present.

2.1 Assessing the health risks of natural CO_2 seeps in Italy

Industrialised societies which continue to use fossil fuel energy sources are considering adoption of Carbon Capture and Storage (CCS) technology to meet carbon emission reduction targets. Deep geological storage of CO_2 onshore faces opposition regarding potential health effects of CO_2 leakage from storage sites. There is no experience of commercial scale CCS with which to verify predicted risks of engineered storage failure. Studying risk from natural CO2 seeps can guide assessment of potential health risks from leaking onshore CO2 stores. Italy and Sicily are regions of intense natural CO_2 degassing from surface seeps. These seeps exhibit a variety of expressions, characteristics (e.g., temperature/ flux), and location environments. Here we quantify historical fatalities from CO_2 poisoning using a database of 286 natural CO_2 seeps in Italy and Sicily. We find that risk of human death is strongly influenced by seep surface expression, local conditions (e.g., topography and wind speed), CO_2 flux, and human behaviour. Risk of accidental human death from these CO_2 seeps is calculated to be 10^{-8} $year^{-1}$ to the exposed population. This value is significantly lower than that of many socially accepted risks. Seepage from future storage sites is modelled to be less that Italian natural flux rates. With appropriate hazard management, health risks from unplanned seepage at onshore storage sites can be adequately minimised.

2.1.1 Introduction

Several factors currently hinder upscaling of Carbon Capture and Storage (CCS) (Bickle, 2009; Haszeldine, 2009) but one of the greatest challenges is the intrinsic uncertainty of integrity of geological storage. Uncertainty does not mean inevitable leakage from subsurface geological containment. The likelihood of surface leakage will be highly site-specific and, overall, will remain poorly calibrated until geological carbon storage has been practiced widely over decades.

Fear of surface leakage, together with a perceived lack of local benefit, is one of the prime foundations for negative public opinion towards CCS (Bradbury et al., 2009; Desbarats et al., 2010; Johnsson et al., 2009; Shackley et al., 2009) and is driving storage operations offshore or delaying project development (e.g., Mattoon, USA; Barendrecht, Netherlands). Public acceptance can strongly influence the fate of new technologies and onshore storage will usually be the least-cost domestic option for many countries. It is therefore crucial to assess the environmental hazards from leakage of CO2 to the surface using analogues, models, and pilot studies (Chiodini et al., 2010; Holloway et al., 2007; Lewicki et al., 2007; Pruess, 2004, 2008; Voltattorni et al., 2009). Developing and implementing suitable risk-assessment procedures will enable the accuracy of current concerns to be evaluated.

Italy is a region of widespread natural CO_2 degassing from well documented surface seeps. These CO_2 seeps provide excellent analogues for assessing the health risks of CO_2 leakage from onshore storage reservoirs. Italian gas seeps have already proven a valuable tool for developing storage site assessment, monitoring techniques, and understanding and predicting CO_2 leakage pathways and fluxes (Beaubien et al., 2008; Costa et al., 2008; Pearce, 2005/6; Voltattorni et al., 2006; Voltattorni et al., 2009). This study presents a quantitative analysis of human and animal injury from Italian CO_2 seeps during recent history. The aims are to calculate the risk that natural surface seeps present and understand the factors influencing human and animal health risk from surface CO_2 seeps. Data were elicited from Googas (Chiodini and Valenza, 2008), a web-based catalogue of degassing sites in Italy constructed as a national project by the Istituto Nazionale di Geofisica e Vulcanologia (INGV), communication with Googas collaborators, fieldwork, and published scientific literature.

2.1.2 Results

Italian Gas Seeps

Natural CO_2 degassing is most abundant in western Italy (Chiodini et al., 2004; Chiodini et al., 2008; Minissale, 2004) (Figure 2.1). Here there are over 270 documented CO_2 seeps exhibiting a range of surface expressions (Figure 2.2), flux, and temperatures (Chiodini et al., 2008; Minissale, 2004), see supplementary information. Seeps can be found in both rural and urban regions and public access is usually unrestricted, with little or no warning signposts. Degassing sites are typically geographically related to volcanic edifices, known natural CO_2 reservoirs, and CO_2-rich aquifers.

2.1.3 Health Hazards of Italian CO_2 Seeps

Here, *hazard* refers to a fatal outcome and *risk* as the likelihood of fatality according to historical records. Documentations of nonfatal events are not robust and are therefore disregarded. At the Earth's surface, CO_2 is a colourless and odourless gas, which is chemically unreactive and hence undetectable by the human senses. Elevated CO_2 concentrations (1- 3% air by volume, $C_{\%}v.v$) cause no physical damage but lead to rapid breathing, headaches, and tiredness. Above 3% ($C_{\%}v.v$) incomplete gas exchange in the lungs causes CO2 concentration in the blood to increase hence altering the pH (D'Alessandro, 2006). This condition is called hypercapnia and leads to brain malfunction, loss of consciousness, and death at concentrations above 5–10% $C_{\%}v.v$. At Italian gas seeps co-released gases such as hydrogen sulphide (H_2S) also present a significant hazard. H_2S is beneficial to human health in extremely low concentrations but quickly becomes toxic above $3 \times 10^{-3}\%$ ($C_{\%}v.v$), causing irreversible tissue damage. The strong "rotten-egg" odour of H_2S is identifiable at trace (parts per million, ppm) concentrations although human sensing of the gas rapidly decreases after exposure. Current European Union (EU) legislation would allow subsidiary gases such as sulphur species to constitute a minor component of injected flue gas (Council, 2009) and pipeline corrosion is not a concern if H_2S

concentrations remain below 200 ppm. The H_2S component of analysed Italian seeps averages 0.32 × 10^{-6}% ($C_{\%}v.v$) (Minissale, 2004) which is well within the legal contaminant levels for geological CO_2 storage.

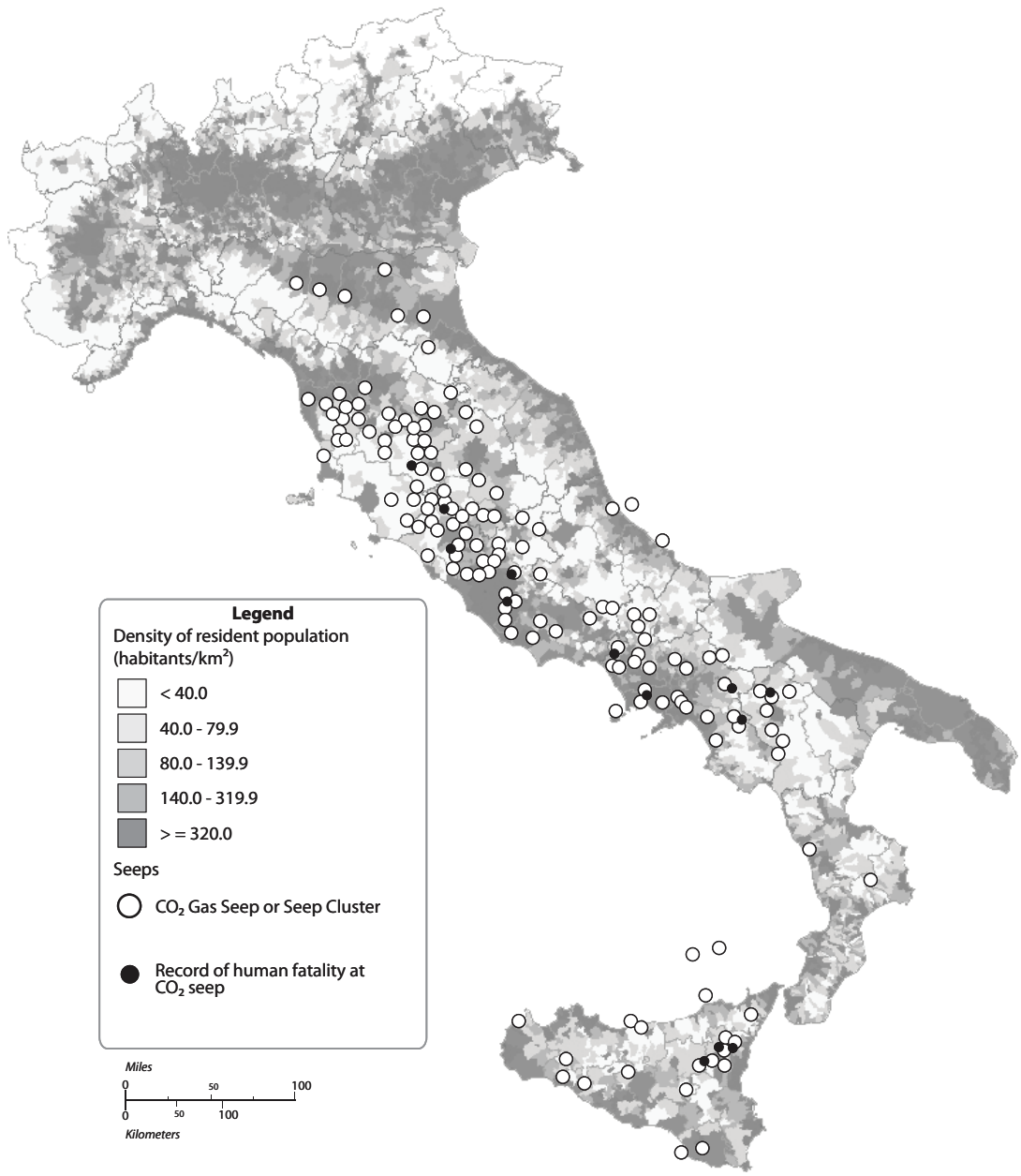

Figure 2.1: Map of resident population and seep locations in Italy (2001 census, map modified from Italian Institute of Statistics). Seeps where human death has occurred over the past fifty years are in black (http://dawinci.istat.it/pl/index_eng.html) (ISTAT, 2001). Seeps concentrate in the Western sector of Italy and Sicily.

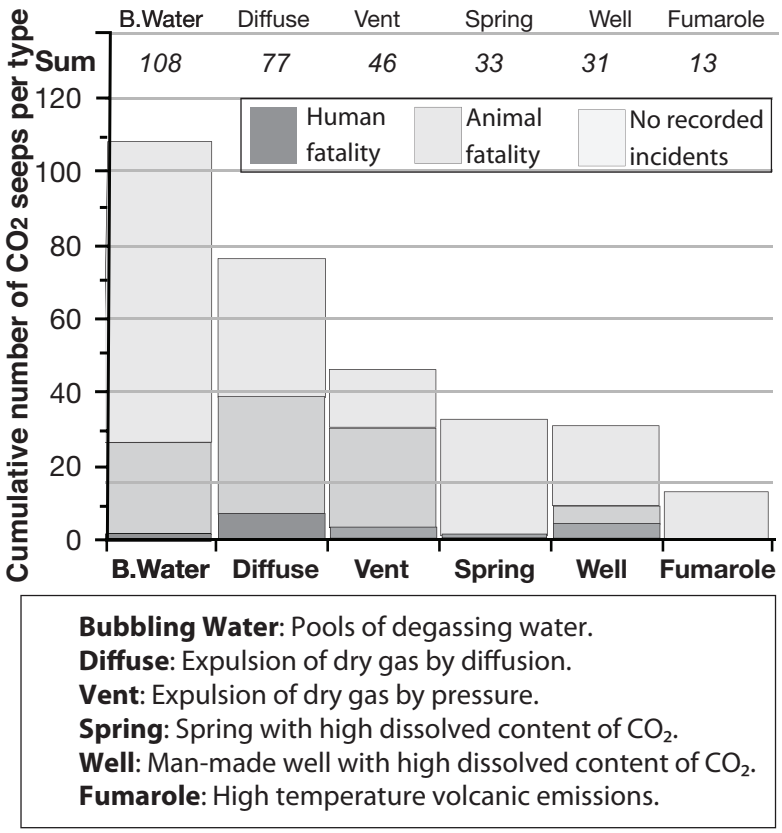

Figure 2.2: Record of health incidents according to seep type from the past fifty years. There are six different seep types classified according to surface expression. Dual-system seeps are treated as two separate occurrences here. The number of fatalities relate to seep type rather than relative abundance; the most dangerous seeps being diffuse and vent (dry seeps). Only fumaroles record no fatal injury to humans.

2.1.4 Factors Influencing Risk at Italian Gas Seeps

Seep classification

Historically all seep classifications except springs and fumaroles present serious health hazard to animals (Figure 2.2). A third of all known seeps are responsible for animal fatalities. Only thirteen seeps are responsible for loss of human life, the majority of which are dry seep types (diffuse and vent). Dual-system seeps, where two seep types occur in one location, are particularly high risk; ⅔ have claimed

animal lives (Figure 2.2). Dual seeps are commonly diffuse classification coexisting with vent or bubbling-water types. There are no recorded human fatalities at fumaroles, which may be for two reasons:

- Fumaroles have distinct surface expressions and high temperatures (>90 °C) which signal to humans and animals to be cautious.
- Fumaroles are found close to volcanic edifices or geothermal fields which are sparsely populated, sparsely vegetated, and hence less visited by humans, and more exposed to wind, which disperses CO_2 gases.

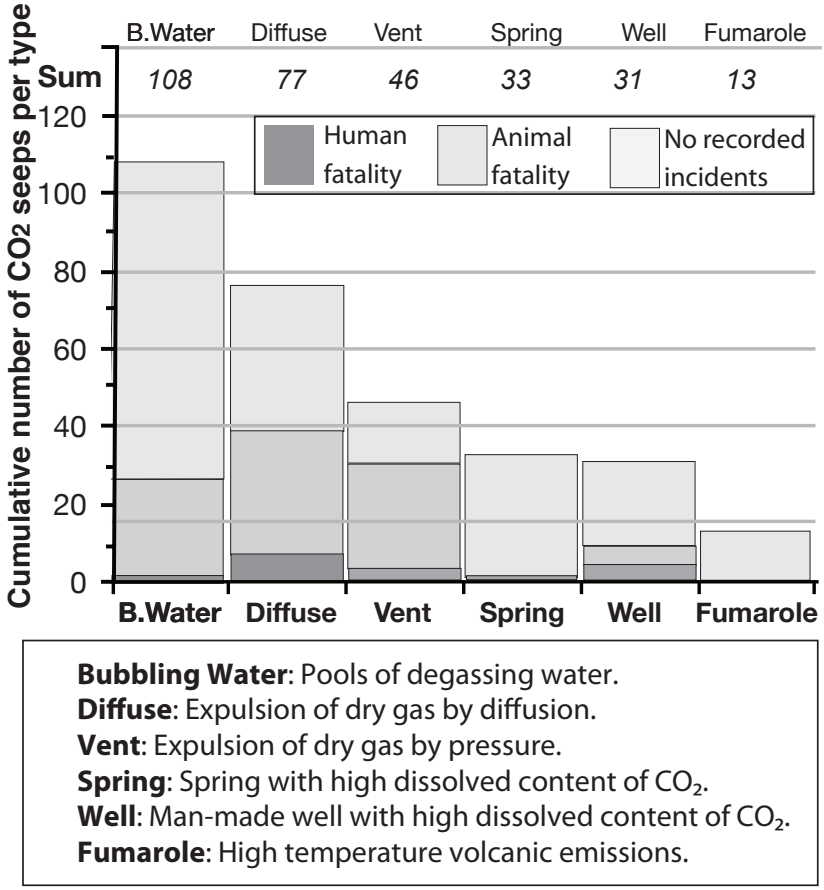

Figure 2.3: Flux data for 169 of the 286 CO_2 seeps in Italy. Flux is measured by the CO_2 t d^{-1} and class as "low" (<1 t d^{-1}); "medium" (1–10 t d^{-1}); and "very high" (>100 t d^{-1}). These data are represented above according to seep type (lines) on the left axis and total number of seeps in each flux class on the right axis (block grey). High flux seeps are most common, however it is expected that these seeps have been preferentially studied.

Seep flux

Italian seeps most commonly degass between 10– 100 tonnes of CO_2 per day (Figure 2.3). Monitoring studies over several years have not detected temporal variances that challenge the flux classifications assigned to measured seeps (Italiano et al., 2000). Italian gas seeps do not show intermittent geyser-style emissions, although characteristics such as water content are known to show minor variation at some gas seeps (Heinicke et al., 2006). The influence of gas-flux and other seep characteristics are therefore considered to be constant factors affecting seep hazard.

Seep type affects the relationship between risk of death and CO_2 gas-flux. Risk positively correlates with gas-flux at dry seeps ($r^2 = 0.9$ and 0.6 for vent and diffuse seeps respectively). In contrast, at wet seeps the correlation if any, is much weaker; similar numbers of deaths have occurred at both low flux and high flux seeps.

Seep temperature

All measured seep temperatures are cool enough such that both CO_2 and H_2S are denser than air at atmospheric pressures, which can lead to gas pooling in sheltered locations. Seeps with emergent temperatures warmer than 34°C record no injury to humans or animals, implying that low-temperature seeps present the greatest risk of fatalities (Figure 2.5 in Supplementary Information). The increased health risk at low-temperature seeps is important because low-temperature dry seeps are analogous to CO_2 leakage from engineered storage sites. The observed relationship between cool temperature and greater risk could be attributed to the relative abundance of cooler seeps and their coincident high flux, or simply that elevated temperatures invoke precautionary behaviour taken by animals and humans in the same way as hypothesised for fumaroles.

Local topography

Gas pooling from topographic effects can account for high risk but low flux wet seeps. For example, *Santa Maria De Luco* (Potenza) is a low flux seep in a sparsely populated rural region. Although located in pasture fields, discrete metre-scale

topographical depressions allow CO_2 to accumulate to dangerous concentrations (Chiodini and Valenza, 2008). Gas pooling in this manner will be more rapidly accomplished by higher flux emissions but is certainly achievable by any seep located in the correct environmental conditions. Density-driven accumulations can flow like a river. The paths of these gas-rivers are visible as grey scars on the landscape (Chiodini et al., 2010; Sorey et al., 1998) where the CO_2 and H_2S gas mixtures modify or kill the local vegetation (Beaubien et al., 2008; McGee and Gerlach, 1998; Raschi et al., 1997). Abnormal vegetation is common at gas seeps and might assist gas hazard recognition if the animal or human is aware of such phenomena.

Human population and behaviour

Incidents of human fatality are greatest in the most populated areas where exposure to the gas hazard can be assumed to be greatest but some deaths have occurred in sparsely populated regions (Figure 2.1). Where fatality occurred in a rural area the victim was commonly engaged in an activity placing them close to the ground; either the victim was breathing close to the surface (swimmers; low-lying hunters) or lower than the surrounding surface (in a ditch or basement). The increased risk when breathing close to the ground is illustrated by the greater than 6:1 proportion of animal to human fatalities (Figure 2.2). Hence the height or behaviour of animals and humans influences their risk of death where even slight density pooling occurs.

2.1.5 Quantifying Risk from Italian Gas Seeps

Between 1990 and 2010, a time period considered to represent the fullest record, there were a total of 11 accidental fatalities at Italian CO_2 seeps. To quantify risk we consider regional resident populations in the western sector of central and southern Italy and Sicily, see SI Text. These 20 million (M) people were exposed to unfenced, unsigned, open-access seeps during this 20-year period. These deaths equate to 2.8×10^{-8} risk of fatality from CO_2 seeps per annum. Table 1 places this value alongside socially accepted hazards and events for context. CO_2 poisoning at Italian gas seeps

is markedly lower risk in comparison to most low-probability events, with 1 in 36 million chance of death per annum for exposed populations.

In risk analysis the expression *Risk = Probability × Consequence* is commonly applied. Death by CO_2 poisoning is a "critical" consequence. However, the probability of death occurring is so small in this case that risk would usually classify as '*low*'.

Event	Risk/yr
Killed in car accident (It, 2006)	1.8×10^{-4}
Struck by lightning (USA)	2.3×10^{-5}
Accidental domestic death from CO poisoning (UK)	9.2×10^{-7}
Winning the lottery jackpot (UK)	7.1×10^{-8}
CO_2 poisoning at seeps (western sector of central and southern Italy and Sicily)	2.8×10^{-8}

Table 2.1: Comparison of risk of fatality from CO_2 seeps in Italy alongside other hazards and events that many societies are exposed to. Many members of society choose to accept these risks so as to, for example, enjoy the benefits of travelling by car. United Kingdom national lottery statistics represents a positive risk that people are familiar with, and many United Kingdom citizens choose to take despite low-returns.

2.1.6 Discussion

Natural analogues can provide an understanding of important processes which are otherwise unfeasible or unethical to test, but their comparability to engineered scenarios does have limitations. Large quantities of natural CO_2 in Italy originate from volcanic, mantle, and biogenic sources (Chiodini et al., 2004), rather than a single injector source. Italian gas seeps include trace components (H_2S, H_2, light hydrocarbons) that industrial flue gas may not constitute. Only a proportion of the seeps considered in this study arise from reservoirs analogous to CO_2 stores. These seeps reflect established fluid migration pathways from carbonate reservoirs in a

tectonically complex region rather than new emerging pathways from reservoirs more geologically suitable for CO_2 storage.

The purpose of CCS is to undertake storage in deeply buried geological reservoirs for 'long' periods of time. In the context of reversing anthropogenic forcings, long refers to many (perhaps hundreds of) thousands of years (Shaffer, 2010; Tyrrell et al., 2007). Such time scales are difficult to reconcile with legislative and commercial operations, and thus long typically means 1,000 y in the context of human planning. The EU CCS Directive (Council, 2009) expects a CO_2 storage site to operate under zero, or very small and predictable, leakage. There is, as yet, no standardised value for tolerable seepage, and this will be specific to any storage site. As a minimum standard of performance, the (IPCC, 2005) suggested retention of at least 99% stored CO_2 during a 1,000 year period. In this manner, leakage of 10- 100 tonnes per day (t d^{-1}), a common flux at Italian seeps, would be deemed a reasonable leakage (0.1–1%) from a storage facility injecting 3.6 Mt per year. Modelled leakage rates from storage to surface, based on well established knowledge of complex fluid flows, are typically several orders of magnitude lower than that from Italian gas seeps (Pruess, 2004, 2008).

In the unfortunate case of surface leakage of CO_2 from an engineered site risk management procedures will be implemented. It is expected that public access to any surface leak site would be restricted unlike described Italian natural analogues. Furthermore, local communities would be informed of the dangers of CO_2 gas seeps, hazardous behaviours around seeps, and how to recognise a seep. Under EU legislation (Council, 2009) if any 'significant irregularities' in the storage operation are experienced, injection would have to immediately cease, strict remediation procedures would have to be followed, and the operator would be penalised. Consequent pressure decrease is predicted to reduce or cease leakage flux. In addition the seep quantity, spread and affected population is likely to be much reduced in the case of leaking onshore CO_2 stores. As such, risk calculations here can only overestimate the risk of death by CO_2 poisoning from leaking onshore scenarios.

CCS offers rapid remediation of CO_2 emissions. While CCS development and deployment is delayed, many megatonnes of CO_2 are being released into the atmosphere without abatement. Anthropogenic CO_2 release is contributing to a process which will have catastrophic effects on human lives across the globe (Peng et al., 2010; WHO, 2009). Without decarbonisation by CCS and other methods, risk of death from climate change will be much greater than that from breached engineered CO_2 stores.

2.1.7 Summary

While CO_2 degassing sites are indeed capable of causing death, the frequency of these incidents is extremely rare. According to 20 years of recent historical records from 286 seep locations in Italy, the risk that gas seeps present to the population is orders of magnitude lower than many other natural or socially accepted hazards. The risk of death from CO_2 poisoning to the population is extremely low at $2.8 \times 10^{-8}\ y^{-1}$.

Seep characteristics (type, temperature, and flux), as well as the surrounding environment and human behaviour all have strong effects on the risk that each seep presents (Figure 2.6 in Supplementary Information). Cool and dry seeps pose greater risk than hot or wet seeps. Risk from wet seeps poorly correlates with seep flux, unlike dry seeps which show a strong positive relationship. Simple human behaviour which maintains breathing height above ground and avoids regions of low topography greatly reduces the risk of death. The factors we identify to influence health risk at Italian gas seeps are readily assessable and can be managed to achieve a reduced-risk environment at these sites or seeps which might arise in the event of leakage from CO_2 storage operations. Therefore, in the event of onshore CO_2 leakage from engineered storage operations the ensuing health risk to the local population would be significantly lower than that from Italian gas seeps.

CCS cannot operate with zero risk. We have shown here that even if all containment fails and stored CO_2 leaks to the surface, the risk of death is extremely low. Hence

the current public concern regarding death by CO_2 leakage from onshore storage sites appears overamplified.

2.2 Supplementary Information

2.2.1 Supplementary Methodology

Information from all known seeps were compiled into a database, simplified, and analysed (see Appendix 1). Many documented seeps lack precise information other than location, type, and safety. For example, 41% of all seeps have poorly quantified flux and over half have no temperature record or gas hazard assessment. Where more than one seep classification is expressed at a single location it is treated as several individual seeps and any repetition that results are accounted for when investigating death risk. There are 270 seep locations, 308 individual seeps overall that are dominantly CO_2 composition, and 15 further seeps which dominantly degass CH_4 or N_2.

Seep safety was assessed and classified by the INGV according to historical incidence of injury to humans and/or animals. For animals "injury" equates to mortality and for simplicity only cases of human fatality are considered in this study, discarding cases of human injury (or near-misses). This simplification is considered to be justifiable; very few cases of human injury are recorded, seeps responsible for human injury are ubiquitously responsible for human fatality, and the effects of CO_2 poisoning are difficult to recognise and therefore will be underrepresented in the data.

Robust documentation of historical incidents is lacking beyond several decades, see Figure 2.5, indeed the earliest modern recording of human injury dates to the 1960's although historical chronicles describe CO_2-related deaths in the 17th Century

(Chiodini et al., 2008) and Roman times (Chiodini and Frondini, 2001). For this reason we consider only the past 20 y in calculations of risk of human fatality. Additional detail about incidents of death were provided by the acknowledged Googas collaborators upon request. In the past 20 y, human deaths have occurred at the following CO_2 seeps (see Table 2.2 for detail): *Le colline* (1 death), *Veiano* (2 deaths), *Cava dei Selci cava* (1 death), *Mefite D'Ansanto* (3 deaths), *Casa* (2 deaths), *Galleria drenante Ponteferro* (1 death), and *Contrada Pescheria* (1 death). There are four seeps which have no date of death information either in the Googas database, Googas collaborators, or in published literature. For these seeps (*S. Maria De Luco, Cava dei Selci vignette, Fossa del Bue, Pozzo One*) it is assumed that the fatality cannot have occurred in the past 20 y otherwise more precise information would be available.

Regional population cartography from the 2001 census (ISTAT, 2001), car accident deaths in Italy in 2006, and Italian resident population in the same year source from the Italian National Institute of Statistics (ISTAT, 2006a, b). Risk calculations included regional populations from the 2009 databases (ISTAT, 2009). CO_2 seeps locate in only the western sector of central and southern mainland Italy. Human population is evenly weighted between the West and the East in both the Central region and the Southern region, therefore 50% of the population for each (11.8M × 0.5 and 14.2M × 0.5 respectively) were summed with the population of insular Italy (32.5 M) to represent the population exposed to CO_2 hazard (20 M). We favour this simple approach because we do not have information to which communities encounter CO_2 seeps. Risk calculations which considered only the population within 5 km radius of a CO_2 seep (from the population density per commune, 2001 census) find a similar risk factor when the risk factor was averaged for all seeps. Additionally, the risk factors presented in Table 1 were all calculated by a similar, simple approach.

The annual death rate from CO poisoning sourced from the Department of Health campaign from 2008 (DoH, 2008) and verified by the Carbon Monoxide Gas Safety Society database (COGS), and the number of residential dwellings in 2009 source

from the Department of National Statistics (DCLG, 2009). The risk of being struck by lightning in the USA was taken from published sources (Adekoya and Nolte, 2005).

National Lottery statistics can be derived from probability calculations: In the United Kingdom National Lottery, players pick six numbers from the range of integers between 1 and 49. When the lottery draw takes place, six numbers are drawn and to win the Jackpot all six numbers must be accurately predicted by the player. There are 49!/(6!*(49-6)!) combinations of six numbers from 1–49. The calculation equates to 1 in 13,983,816 (approximately 1 in 14 million) chance of winning the right combination.

2.2.2 Supplementary Results

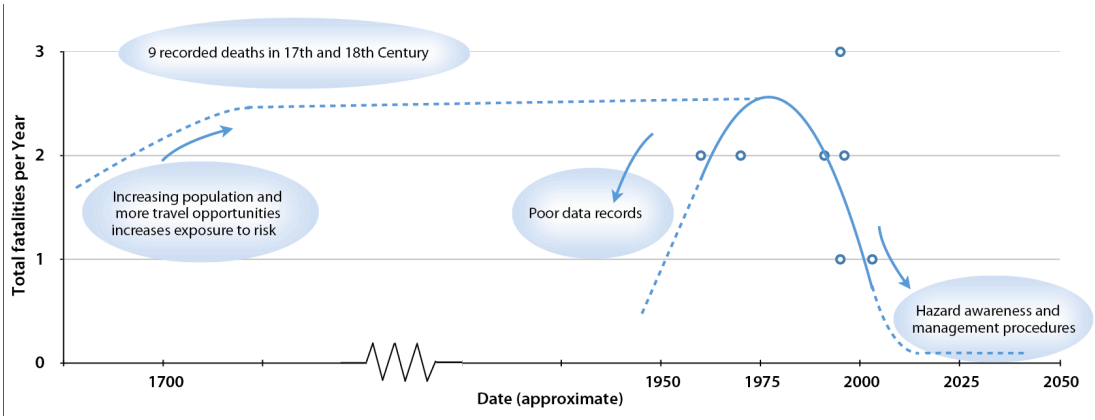

Figure 2.4: The historical and projected trend in human fatalities at CO_2 seeps. Detail of these deaths are documented in Table 2.2

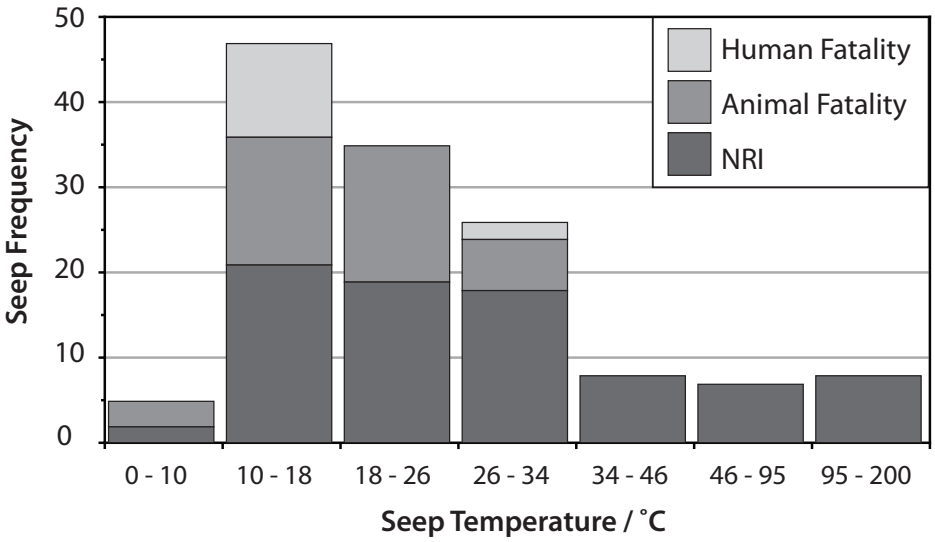

Figure 2.5: Animal and human fatalities according to seep emergent temperatures. The majority of high-risk seeps are characterised by temperatures between 10- 18 °C. Seeps warmer than 34°C record no injury to animals or humans. NRI = No Recorded Incidents.

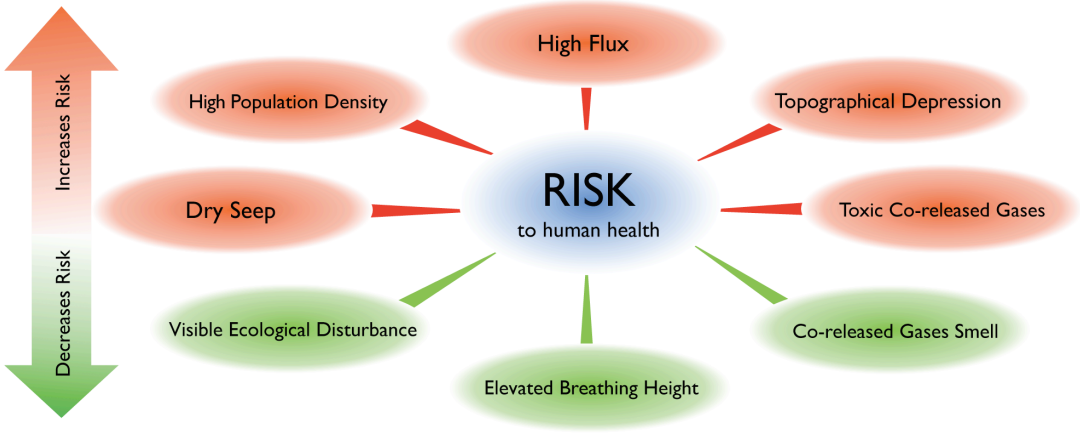

Figure 2.6: A summary diagram of the factors influencing human death risk at Italian CO_2 seeps.

Seep	Type	Incident	Note	Source
Cava dei Selci cava	Diffuse	Death	In a small river. Slight depression in the soil.	(Chiodini et al., 2008)
Contrada Pescheria	Diffuse	Injuries	Man digging a trench felt sleepy and fainted, but was rescued “several years ago”	(Giammanco, 2010)
Le colline	Diffuse & Vent	Death	Hunter died in 2003	(Chiodini et al., 2008)
Galleria drenante Ponteferro	Well	Death	Local inhabitants drank from this open access spring, which was on private property. In 1995 an elderly man collecting water on a still day fainted and drowned in the spring channel. After this accident, the owners restricted access to the spring and covered it with metal plates.	(Giammanco, 2010)
S. Maria De Luco	Bubbling Water	Injuries	No information known	(Chiodini and Valenza, 2008)
Cava dei Selci vigneto	Diffuse	Injuries	No information known	(Chiodini and Valenza, 2008)
Fossa del Bue	Diffuse	Injuries	In a small river. Slight depression in the soil.	(Chiodini and Valenza, 2008)
Casa	Well	Death	2 locals died in basement lift (1996) and similar near-miss with workers (1992). Cause of death could have been H_2S or CO_2	(Chiodini, 2010)

Pozzo 1	Well	Injuries		(Chiodini and Valenza, 2008)
Mefite	Diffuse & Vent	Death	3 deaths in the 1990's were researchers visiting the site. 9 deaths prior to this. Lethal concentration of CO_2 can be present up to 2-3 m of height inside the river valley	(Chiodini, 2010; Chiodini et al., 2008) (Chiodini, 2010)
Veiano	Diffuse & Vent in Pool	Death	2 hunters died in 1991	(Chiodini and Valenza, 2008)
Lago della Regina-Acque Albule	Spring	Death	2 boys swimming here in the 70's died	(Chiodini et al., 2008)
Galleria drenante Acquasecca	Well	Death	2 men killed digging in the well in the 60's	(Giammanco, 2010)

Table 2.2: Summary of the available information regarding CO_2 poisoning at CO_2 seeps. Where the Googas database notes that human injuries have occurred, but no further information is known, we assume 1 person died at this seep prior to 1990 since otherwise there would be more detailed information available.

Chapter 3

CO_2 seeps and geologic structures

This chapter presents the results of a large body of work whereby the spatial data described in Section 1.5 is rigorously examined using spatial statistical methods. First the two-point correlation function, which describes the distributions of data points, is performed for seep location data to establish whether seeps exhibit correlation patterns between seep points or if they are effectively random. Then, once we establish that seeps show organised distributions, the relationships that seep location and characteristics exhibit with different geological structures are investigated to elucidate the first order controls on seep locations. These inform the first order controls on near surface CO_2 pathways in a range of geological settings.

The code for the two-point correlation function (in Appendix 2) was adapted from script written by Andrew Bell.

3.1 Structural Controls on the Spatial Distribution of Natural CO_2 Seeps in Italy

Site selection for the geological storage of carbon requires an understanding of the controls on containment, migration and surface seepage of CO2 fluids. The study of natural analogues can provide insight into these geological controls. Natural CO_2 degassing to the surface at 270 known sites in Italy occurs as a variety of seep types. Here, we statistically interrogate the relationship between seep spatial distribution, structural features, and CO_2 seep characteristics (type, flux, temperature). We find that seeps distribute differently on two spatial scales corresponding to geological structure. On large scales (>5 km radius) seeps isotropically distribute and align with regional structures. On local scales (<5 km radius) seeps are clustered and aligned with subsidiary geologic structures, and seep locations are influenced by fault maturity, the presence of lithological boundaries and seep type. These findings will assist seepage risk assessment and surface monitoring strategy at engineered carbon stores.

3.1.1 Introduction

Industrialised societies which continue to use fossil fuel energy sources are considering adoption of Carbon Capture and Storage (CCS) technology to meet carbon emission reduction targets. Natural CO_2 seeps provide a unique opportunity for developing insight into the containment of CO_2 trapped deep below ground for geological time periods. This can inform on the long-term security of performance of engineered CO_2 storage.

In Italy natural CO_2 is being generated and trapped at the present day. Some traps have failed, or have been bypassed by CO_2, such that unusually abundant seepage is widespread (Chiodini et al., 2004; Minissale, 2004). In central and southern Italy and Sicily over 308 CO_2 seeps at 270 locations have been documented and these exhibit a variety of surface expressions (seep 'types'), temperatures and fluxes. CO_2 can be released as a free-phase by focused gas emission sites or as a dissolved

constituent of springs. CO_2 release from regional aquifers in western central Italy is estimated to account for over 10% of the present-day global CO_2 discharge from sub-aerial volcanoes (Chiodini et al., 2004). This 10% approximates to the quantity of CO_2 emitted annually by a 2.5 GW coal-fuelled power plant.

Analyses of Italian gas seeps have already proven valuable for developing techniques of storage site assessment, monitoring, and evaluating potential health risk from CO_2 escape (Annunziatellis et al., 2008; Roberts et al., 2011; Voltattorni et al., 2006). Seeps can also provide insight into the long term plumbing of CO_2 fluids. Here we present the first quantitative analysis of the controls on the spatial distribution and characteristics of CO_2 degassing sites. Understanding of such controls is imperative to effective storage site selection, appraisal and consequent surface monitoring strategies of engineered storage projects.

3.1.2 Geological Setting

Westward subduction of the Adria plate beneath the European margin and subsequent tectonic stacking of the Mesozoic-Tertiary carbonate platform and synorogenic foredeep sediments has developed a strong regional NW-SE structural grain in Italy (Ghisetti and Vezzani, 2002). Extension followed the NE-migrating compression belt since 7 Ma, opening marine and continental basins and the Tyrrhenian Sea. Most faults trend NW-SE and ENE-WSW although variance in crustal shortening developed E-W trending strike-slip tectonics, and small-scale faults and fractures exhibit more complex orientations locally (Agosta et al., 2009; De Paola et al., 2007). Average fault spacing of normal faults (~5 km) are half the spacing of thrust faults in Italy (~11.4 km) (Morellato et al., 2003).

Today, subduction is considered to have ceased, and seismogenic normal faulting concentrates in the Apennine Mountain belt in response to gravitational collapse. The Tyrrhenian sector preserves the older extensional system and exhibits a thinned crust, associated high heat flow and volcanism from Pleistocene to present day. Here, CO_2 degassing at surface seeps is most widespread (Chiodini et al., 2004; Minissale, 2004). CO_2 seep density and flux is much reduced in the Apennines

where CO_2 flux varies in response to seismological events (Chiodini et al., 2004; Heinicke et al., 2006; Heinicke et al., 2010; Heinicke et al., 2000). Here, fault scarps date from 12-18 Ka (Roberts, 2008) and trapped CO_2 fluids at depths > 5 km play a critical role in the nucleation and evolution of seismogenesis and therefore deformation style and geodynamics of the region (Di Luccio et al.; Miller et al., 2004).

3.1.3 CO_2 seeps and their origins

The distribution of subaerial CO_2 seeps is shown in Fig 3.1 A. Five types of natural seep are identified: vents, diffuse seeps, springs, bubbling pools of standing water and volcanic fumaroles (see Fig 3.1C for explanation of seep types). Several deep boreholes are also known to leak CO_2 ; these seeps are classified as 'wells'. CO_2 is degassed together with lesser amounts of N_2, H_2S, CH_4, H_2, Ar, He and CO. Gas flux can vary between locations from < 1 to > 2000 tonnes/day (t d^{-1}) (Chiodini et al., 2010; Chiodini and Valenza, 2008), most commonly between 10-100 t/d (Roberts et al., 2011), see Section 2.1.4.

Numerous geochemical studies have attempted to elucidate the diverse sources of CO_2 in Italy (Chiodini et al., 2004; Marziano et al., 2007; Minissale, 2004; Minissale et al., 1997). Carbon and noble gas isotope studies identify several contributions to regional CO_2 degassing in varying proportions, including shallow biogenic processes, carbonate hydrolysis, mechanical breakdown or thermo-metamorphism of carbonates, and mantle degassing (Chiodini et al., 2004; Italiano et al., 2000; Italiano et al., 2008).

Active and fossil travertine systems are widespread in western Italy and the oldest travertine dates to 0.5 Ma (Minissale, 2004). Italian travertine carbon isotopes may show evidence of CO_2 contributions from deep sources (Minissale, 2004). Volcanism in western Italy has been active since 0.9 Ma and so it is probable that the regional flux of CO_2 has remained elevated within the past ~1 Ma (Minissale et al., 2002; Smith et al., 2008).

Energy resource exploration has discovered several subsurface CO_2 reservoirs (Bonini, 2009b; Casero, 2004; Chiodini et al., 2010). Both CO_2 and hydrocarbon reservoirs typically form in the crests of fault propagation anticlines capped by allochthonous, tectonised overburden. Other CO2 trapping structures include buried limestone horsts (Carapezza and Tarchini, 2007; Chiodini et al., 1995).

3.1.4 CO_2 Pathways

High-permeability pathways are required to bring fluids from depth to the surface and crustal fluid flow is commonly controlled by deformation-induced permeability of fault and fracture networks. In carbonate rocks the damage zone is rarely greater than 100 m from the fault (Agosta and Kirschner, 2003; Cello et al., 2000). Studies of active faults in the USA find the majority of hydrothermal springs are located in the fault tip or ramp where fractures propagate. Fewer springs are located at the fault trace, and spring temperatures cool away from the fault (Anderson and Fairley, 2008). Case studies of Italian CO_2 seeps have found that faults, often through impermeable rock formations, focus and localise CO_2 ascent pathways, and the flux of ascending gases increases towards the fault plane (Beaubien et al., 2003; Ciotoli et al., 2005) and seabed vents at Panarea (offshore Sicily) align with local faults (Esposito et al., 2006).

Here we use spatial statistical methods to analyse the spatial distribution of subaerial seeps analogous to seepage from engineered carbon stores (vents, diffuse, bubbling water and spring type seeps). We use the results to elucidate the competing crustal controls on natural CO_2 fluid pathways in Italy.

Figure 3.1A: Structural sketch of Italy and Sicily (Brozzetti, 2011; Improta et al., 2000; Patacca et al., 2008) showing the location of CO_2 seeps, seismogenic normal faults (Roberts, 2008) and moho depth contours (Di Stefano, 2011). Filled symbols show multiple seeps. **B:** Polar plot of normalised azimuths from the analysed fault datasets (modern Apennine faults (Roberts, 2008) in dark grey). **C**: Proportion of CO2 seep types (a according to surface expression, n = 308 (Chiodini and Valenza, 2008)). Seep classes can be grouped into aqueous ('wet') and non-aqueous ('dry') categories. Wells are artificial leaking pathways.

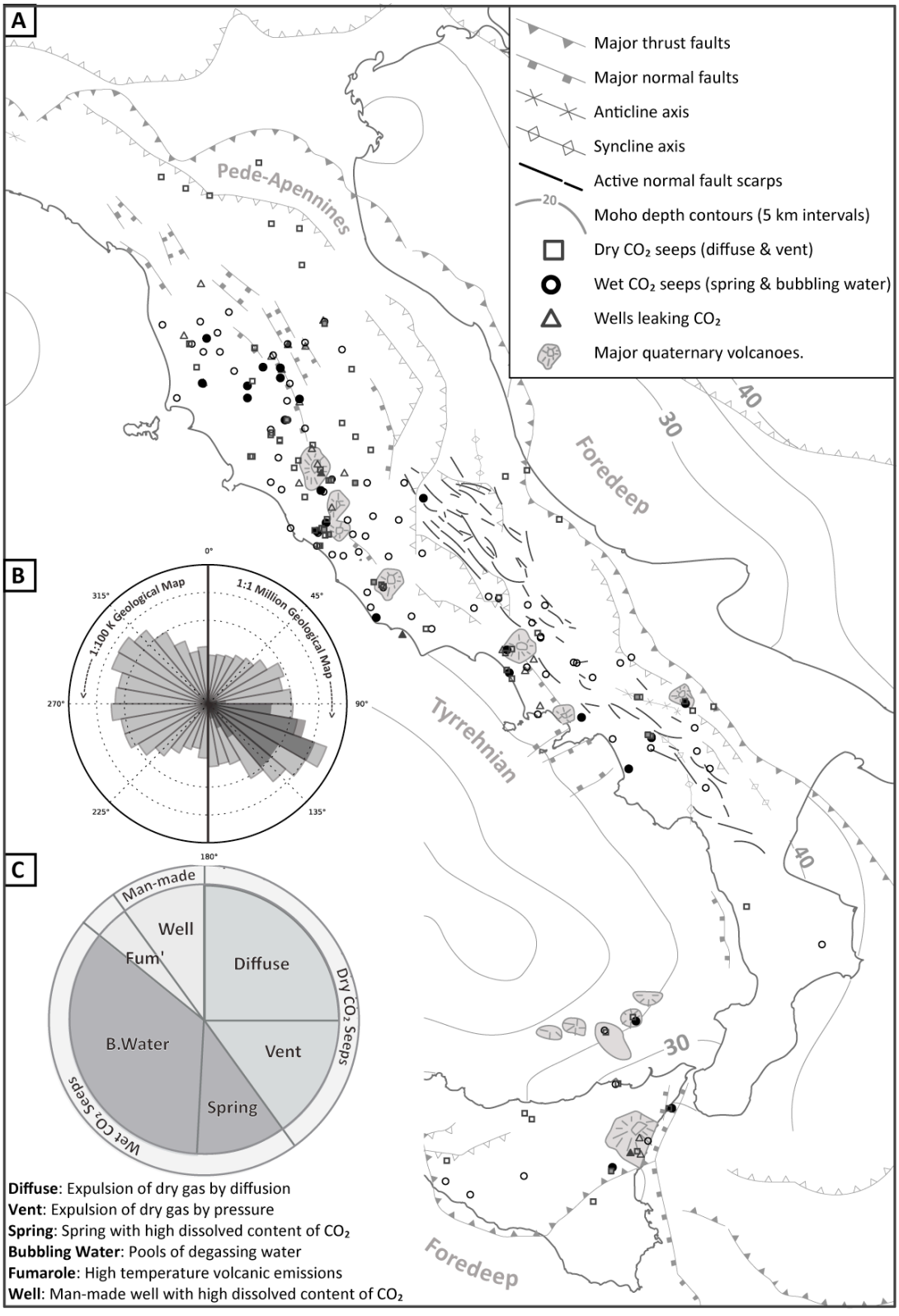
A
Major thrust faults
Major normal faults
Anticline axis
Syncline axis
Active normal fault scarps
20
Moho depth contours (5 km intervals)
Dry CO_2 seeps (diffuse & vent)
Wet CO_2 seeps (spring & bubbling water)
Wells leaking CO_2
Major quaternary volcanoes.
Pede-Apennines
Foredeep
Tyrrehnian
Foredeep
40
30
40
30
B
1:100 K Geological Map
1:1 Million Geological Map
0°
45°
90°
135°
180°
225°
270°
315°
C
Man-made
Well
Fum
Diffuse
Vent
B.Water
Spring
Dry CO_2 Seeps
Wet CO_2 Seeps
Diffuse: Expulsion of dry gas by diffusion
Vent: Expulsion of dry gas by pressure
Spring: Spring with high dissolved content of CO_2
Bubbling Water: Pools of degassing water
Fumarole: High temperature volcanic emissions
Well: Man-made well with high dissolved content of CO_2

3.1.5 Methods

Seep location, type, flux, gas composition and temperature were elicited from Googas (Chiodini and Valenza, 2008) a web-based catalogue of degassing sites in Italy and Sicily. Flux classifications (low = <1 t d^{-1} ; medium = 1-10 t d^{-1} ; high = 10-100 t d^{-1} and very high = >100 t d^{-1}) are only possible for 60% of seeps. The five natural CO_2 seep classifications are grouped into wet (bubbling-water, spring) and dry (vent, well) systems.

We populated a geospatial information system (GIS) with lithology, facies and ascribed permeability class, significant fault traces at 'regional' 1:1 million scale and 'local' 1:100,000 scale); gravity data; seismically capable faults and scarps; stress field data, elevation data, seismic events 1981-2002, subsurface carbonate structure, relevant well logs, travertine distribution (active and inactive) and Googas seep data. We generated a synthetic dataset of randomly (Poisson) distributed points within the areal extent of Italy as a 'control' for comparison with seep distributions.

The properties of spatial distribution can be analysed using the two-point spatial correlation function, a technique developed for cosmology (Peebles, 1980) and previously used in earth science to quantify the spatial distribution of earthquake aftershocks (Huc and Main, 2003; Richards-Dinger et al., 2010). The method permits the quantification of the departure from homogeneity of a distribution of points, expressed as the probability of finding a pair of points within incremental radius and azimuth. The correlation function plots as a power law, $P \propto r^{\varkappa}$, where P is probability, r is radius, and the constant $\varkappa$ describes the spatial distribution. For randomly distributed points we expect $\varkappa = 2$. If points are clustered, that is, they are spatially closer together than expected from a random distribution, k<2. For points that are randomly distributed on a line, the $\varkappa = 1$. The distribution of azimuths between all point pairs can also be measured by this technique as a measure of anisotropy in the distribution.

Clustering (the tendency for points to occur near other points) was measured by the nearest neighbour technique (Clark, 1954) and Ripley's K-function (RKF) which

investigates spatial clustering as a function of distance. Near-analyses determined the distance and azimuth of seeps to the nearest fault or lithological boundary. These techniques permit us to analyse the scale dependence of point spatial relationships and test the association of seeps with geological structures and geological boundaries.

3.1.6 Spatial Distribution of CO_2 Seeps

Figure 3.1 shows the distribution of seeps and a structural sketch of Italy. A regional NW-SE trend is noticeable by eye, and on closer observation seeps can be aligned with normal faults (e.g. Tiber Valley region), thrust faults (e.g. Pede-Apennines) else seem to exhibit little alignment.

Nearest neighbour analyses find CO_2 seeps are significantly clustered compared to a spatial random (Poisson) process (99.9% confidence). When separated for seep type, all seeps show clustering of equal significance except springs, which alongside travertine exhibit a near random distribution (see supplementary information Table 3.1). RKF computations find wet (predominantly bubbling water) seeps have ~ 5 km clusters, whereas dry seeps show ~2 km clusters spread approximately ~15-20 km apart. Seeps are no longer clustered at separation distances greater 40 km (see supplementary information Fig 3.1).

Figure 3.2A shows the two-point correlation function for seep data, and for comparison a synthetic dataset of points randomly distributed within the areal extent of Italy. The results show:

- At separation distances between 5 and 100 km the correlation function is the same for seep and synthetic data and $\alpha = 2$, indicating these points are randomly distributed in space. The roll-off at distances greater than 100 km is a finite size effect from the spatial extent of Italy. Roll-off is less notable in the synthetic data because points are distributed across the width of Italy whereas seeps are located west of the Apennines.

- At separation distances of <5 km, ϰ decreases to ~0.5-1, indicating spatial clustering above random (ϰ = 1 indicates seeps are aligned). The synthetic dataset is not clustered so has few point pairs below 10 km.

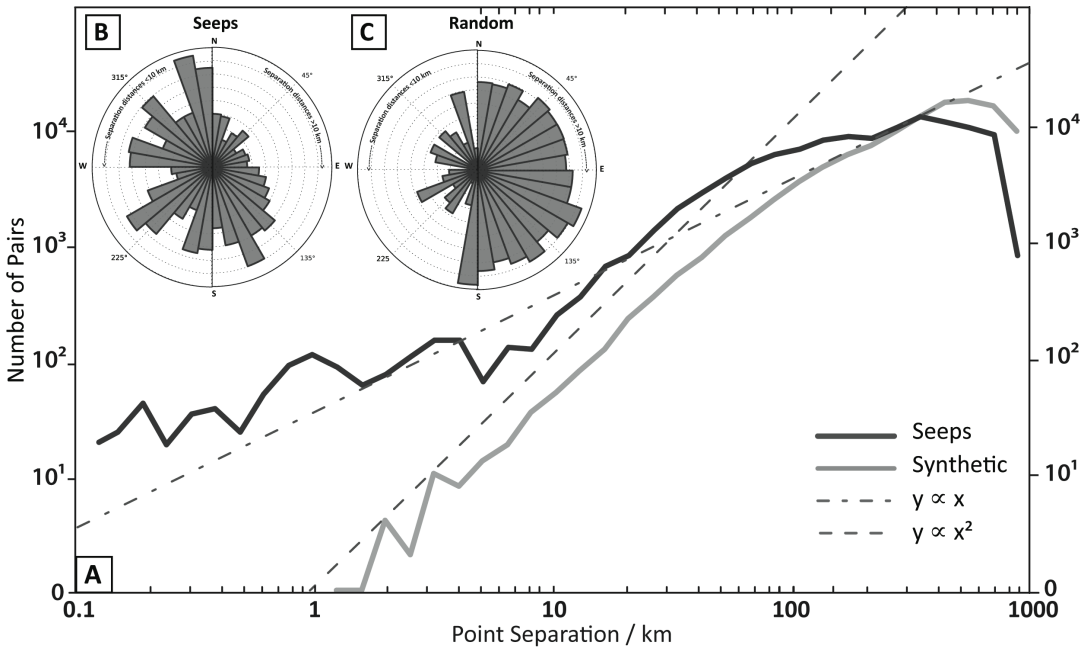

Figure 3.2A: Point-distance correlation functions for seep and synthetic data. Note the break in slope for seep data around ~5 km and roll-off towards ~100 km in both datasets. Inset: Distribution of azimuths for points below 10 km (anticlockwise) and above 10 km (clockwise) for seeps (**B)** and synthetic (**C)**. Seeps show several favoured orientations below 10 km, and NW-SE trend above 10 km separation.

Figures 3.2B & C show the distribution of azimuths between all pairs of seeps and synthetic points separated above and below 10 km.

At separation distances below 10 km seeps show several orientations approximately 30-40° apart. Synthetic data show marked peaks relating to few point pairs rather than a preferred orientation. Above 10 km, seep pairs show a preferred NW-SE (140-160°) orientation which synthetic data does not exhibit.

Seeps and seismic events are regionally distinct. In the Central Southern Apennines (Campania-Apulia region), where M > 5.0 seismicity is active, CO_2 degassing and seismogenic faulting occur together unlike the Central Apennines where seismogenic faulting is regionally distinct from CO_2 seeps.

3.1.7 Roles of Geological Structures

Mature Fault Traces

We find that seeps locations relate with non-seismogenic faults, see Figure 3.3. Dry seeps are exponentially more common closer to fault traces whereas springs seeps show a weaker, linear, increase (see Figure 3.3c). 90% of vent seeps are located within 0.5 km of a fault, increasing to 1 km for diffuse and bubbling water seeps, and 2 km for springs. Fumarole locations show no trend with fault distance. These relationships are consistent for smaller faults. Seep-fault azimuths are principally SW (-NE).

Most seep temperatures are in the range 15-30°C (mean and mode 22°C, greater than ambient temperatures). Large fault traces weakly influence the emergent temperature of seeps within 2 km and only influence spring and well temperatures at greater distances. Vent temperatures are inversely affected; they warm away from regional and local fault traces. Medium flux seeps show strongest fault distance dependence and very high flux seeps the weakest, but overall we find gas flux is not controlled by proximity to fault traces, although this might result from the incomplete flux dataset.

Active Fault Traces

Seep locations are not strongly associated with active fault traces, found in the Apennines. The few (37) CO_2 seeps which are located within 10 km of a young normal fault scarp are spring-type seeps (70%) with high fluxes (15 of the 16 seeps with quantified flux degas >10 t d^{-1}). Unlike seeps in the peri-Tyrrhenian, we find seeps in the Apennines are located SSE of active faults. We observe these are located

toward the fault tip region, or at fault ramp structures between two neighbouring fault tips (Figure 3.4).

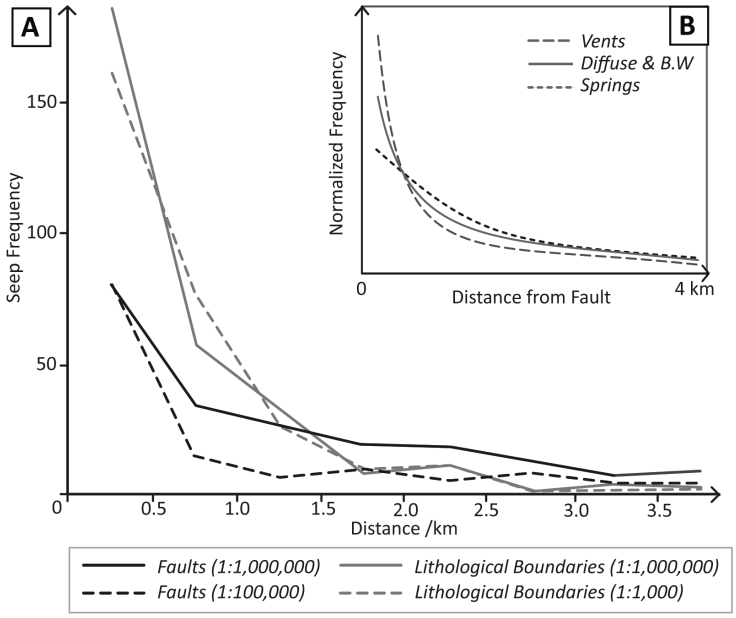

Figure 3.3A: Line histogram of seep distances from geological features. Lithological boundaries control seep locations more than faults at both scales. **3B** (inset): Normalised line histogram of seep types and distances from faults (B.W refers to bubbling water seeps).

Lithological Boundaries

Seeps are preferentially located towards lithological boundaries; 76% of all seeps are located within 1 km of lithological boundaries from the 1:500k geological map (see Figure 3.3A). Seeps show no favoured orientation from lithological contacts, only a weak NE-SW trend. At both scales, all springs are located within 1 km of a lithological boundary (Fig 3b). Diffuse, vent and bubbling water seeps show a weaker, near-linear relationship. As with faults, gas flux does not appear to be controlled by seep distance to lithological boundaries.

Subsurface Structure

Where subsurface structure is known we find that seeps and CO_2 reservoirs correlate with the structural highs of Mesozoic carbonate. Seeps are located above anticline crests known to host CO_2 reservoirs (Figure 3.4). They are also located

above local highs of the steep dipping flanks of these structures. Few seeps are located above nappe décollements where carbonate depth is greatest.

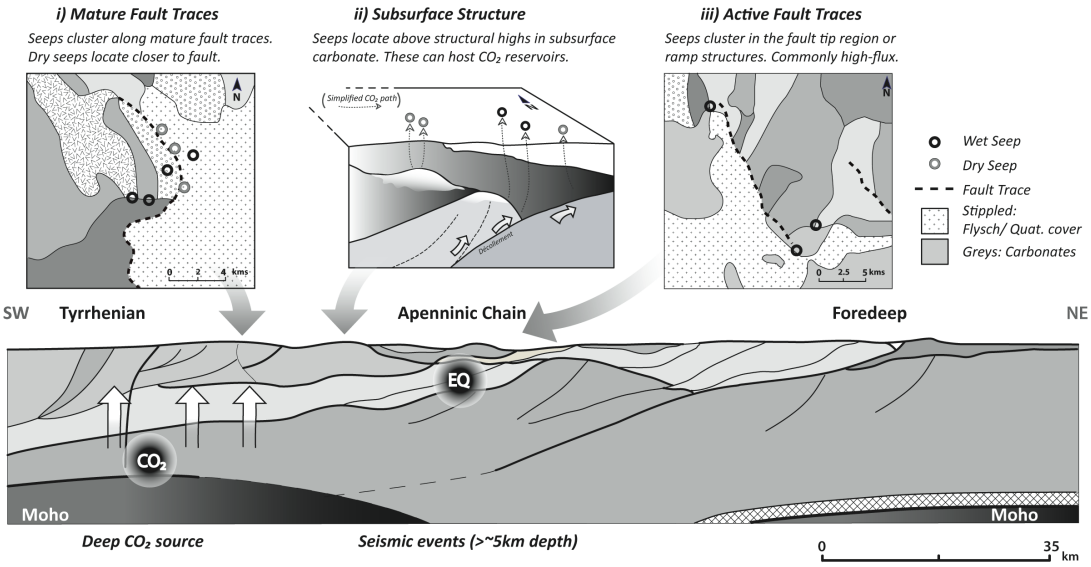

Figure 3.4: Crustal cross-section of the Central-Southern Apennines (Calabro et al., 2003; Ghisetti and Vezzani, 2002; Improta et al., 2003). Above cartoons adapted from real examples depict the major structural controls on CO_2 seeps: *i) mature fault traces ii) subsurface structure iii) active fault traces*. Lithological structure influences seep type and location In all these settings. Seep type is lithology dependent and lithological contacts govern seep locations.

3.1.8 Subsurface plumbing of CO_2 fluids

We can consider how the observed relationships between CO_2 seeps and geological structures can account for the scale dependent distribution style of CO_2 seeps. The distance-dependent distribution observed for CO_2 seeps corresponds to a change from a clustered to isotropic spatial distribution around ~5 km. RKF analyses support these results, finding dry seeps clusters are ~2 km radius and wet seep clusters ~ 5 km radius. Clusters may represent several seeps fed by one source/ reservoir or several utilising the same leakage pathways

Seeps locations are determined by the presence of large-scale faults. Field studies find the permeable fault damage zones are rarely wider than 100 m from the fault

core in carbonate rocks. We find the spatial relationship between faults and seeps extends beyond the damage zone (up to ~2 km). The distribution of seeps from faults is seep type dependent, thus we propose that seep type is an indicator of CO_2 spread the near surface from a deeper feed structure (fault).

As they evolve, faults develop low permeability fault cores mantled by a more permeable fault damage zone (Agosta and Kirschner, 2003). The fault trace can thus provide both a lateral barrier and a vertical conduit to fluids. The relationship between seeps and faults indicate these properties guide CO_2 fluids at depth in Italy. In young faults the impermeable core may be less developed. We observe seeps emerge at fault tips and fault ramps of modern Apennine faults, so opening-mode fractures rather than barrier/conduit properties must govern fluid pathways here. Springs show the weakest relationship with faults and the strongest relationship with lithological boundaries. This implies that gaseous pathways are controlled by structural features whereas aqueous fluids are also guided by hydrologic regime.

While seep locations show strong dependency on geological structures which show a NW/WNW trend, within clusters seeps show several preferred point pair azimuths. The orientation of seep azimuth peaks indicate that synthetic and antithetic minor faults (from NW-SE faults) are guiding seep distribution. It seems that towards the surface the larger NW-SE faults must no longer provide the most significant fluid pathways and deformation related geological features below the resolution of the studied faults are influencing the location of seeps within clusters. The CO_2 distributes away from the main fault and towards different fates (seep types).

The distance-dependent distribution observed for CO_2 seeps find that seep clusters tend to lie NW-SE of each other in accordance with the structural trend of both compressional and extensional structures in Italy. We find CO2 seeps are located above structural highs in the high-permeability tectonised Mesozoic carbonate platform. These structures are fault-bend folds confined by the flysch overburden. CO_2 is known to accumulate in these structures (perhaps supplied by the thrust décollement) and must migrating through the overburden to supply surface seeps.

Fluid pathways may be faults and fractures relating to thrust propagation or extensional faulting, or perhaps flysch heterogeneities. Similar processes are observed in carbonate horsts seeping CO_2 (Carapezza and Tarchini, 2007) and tar migration through the Majella anticline to the North (Agosta et al., 2009).

We deduce that regional controls such as large faults, décollements and geologic structures such as nappes/horsts are governing CO_2 delivery between seep clusters, which we find are typically 15 km or so apart.

3.1.9 Application to Carbon Capture and Storage

Understanding CO_2 seep pathways assists seepage risk assessment and surface monitoring strategy at engineered carbon stores. Historical documentation of health incidents at Italian gas seeps find dry type seeps to be most hazardous (Roberts et al., 2011, see Section 2.1.4). Our results suggests that seepage will be expressed at a number of sites in a small area within which seeps are broadly aligned according to local geologic structures. Active faults will channel fluids towards fault tips and fault ramps whereas mature faults will guide fluids along the fault trace. The seep type will vary with distance from these features; vents locating within 0.5 km of the fault, bubbling water and diffuse seeps within 1 km, and springs will emerge at lithological boundaries within 2 km of the fault trace. Potential seep locations and type can therefore be identified given thorough geological knowledge of the units overlying a CO_2 store.

3.2 Supplementary Information

3.2.1 Supplementary Methods

Seep data were elicited from Googas (Chiodini, 2008), a web-based catalogue of degassing sites in Italy constructed as a national project by the Istituto Nazionale di Geofisica e Vulcanologia (INGV), communication with Googas collaborators, fieldwork and published scientific literature (Chiodini et al., 2011; Duchi et al., 1995; Minissale, 2004). To verify seep classifications we compare Googas data (Chiodini, 2008) with previously published catalogues (Minissale, 2004).

'Wells' are man-made and therefore are not considered to represent natural CO_2 leakage pathways but rather indicate the presence of subsurface CO_2 reservoirs. It is noted that some dry gas emissions are man-made, for example at Cava dei Selci and Solftara at Colli Albani where removal of impermeable deposits due to quarrying and mining respectively have enabled gas to escape (Carapezza and Tarchini, 2007) but the location of the majority of seeps has not been determined by human activity.

In the Googas database, each record was assigned information (including seep type, flux, historical safety, gas composition, site description, published research) although many documented seeps lack precise information other than location, type and safety (Roberts et al., 2011).

Flux and seep type are considered permanent since seeps do not exhibit geyser style eruptions although there is some evidence of seep water content variation with seasonality (Heinicke et al., 2006) and flux variations with seismicity (Bonini, 2009a; Heinicke et al., 2006; Heinicke et al., 2010). Seep locations are also considered permanent since archeological discoveries at Mefite D'Ansanto indicate this seep has been active since Roman times (Chiodini et al., 2010). Edifices in the Tiber Valley have been observed to migrate several meters seasonally (Heinicke et al., 2006) however this is below the accuracy of the GIS dataset.

When conducting the cluster analysis we tested both 'separated' and dual-system (where more than one seep type is expressed at one location) point locations. In total we have analysed 286 seep locations (323 seeps total; of which 308 seeps at 270 locations are dominantly composed of CO_2, 15 of CH_4 and 1 of N_2).

The geospatial information system, ArcGIS, with an azimuth plugin(Jenness, 2005) was populated with geological information (geology, gravity data) made available by ISPRA, mapped fault scarps(Roberts, 2008) and seismically capable faults(ISPRA, 2007), stress field data(Barba et al., 2009), SRTM 90 m elevation data (Jarvis, 2008), seismic data (CSI 1.1 Catalogo della Sismicità Italiana 1981-2002, filtered for events from Mt Etna to remove intense clustering bias), depth to moho data (Di Stefano, 2011), subsurface carbonate structure (Nicolai et al., 2007) relevant well logs (available by the ViDEPI project (ViDEPI, 2009)).

We extracted information about the distance of the seeps to significant lithological boundaries and the nature of the relationships between seeps and the surrounding geological environments. Mindful of the large scale, fault information were extracted as a *guide* to the structural grain in Italy.

A variety of spatial statistic methods are available to quantify geographic patterns. These were adapted to investigate the spatial distribution of CO_2 seep locations to identify interactions between migrating CO_2 and crustal structure. In particular we used:

- The nearest neighbour technique (Clark, 1954) tests the degree of clustering in spatial distributions by comparing the observed mean distance of points with the expected mean distance given a random distribution and was performed using the Euclidean distance method which measures distances as a straight line between the two points.
- Two-point azimuth analysis (Bleacher et al., 2009) measures the significance of alignments between point data (CO_2 vents, seismic events, spring points).

- Two-point correlation function measures the significance of distance between points on their distribution (Peebles, 1980; Richards-Dinger et al., 2010). The excess probability (p) of there being a neighbouring point (above what is expected for an unclustered random Poisson distribution) is calculated at incremental radial distances (r) from each point by:

$$p = n^2 \cdot [1+\xi(r)] \cdot A$$

Where ξ is the correlation function; n is the point density in an area A.

This provides information on the characteristics of the relationship between neighbours. For example, the correlation function can inform on the dispersion or clustering of points, the degree and size of these clusters, and can indicate if the points are aligned or more broadly distributed.

Correlation analyses was performed for CO_2 seeps, non-volcanic seismic events and spring points and compared to a synthetic random dataset (where $n_{rand} = n_{seeps}$ for consistency), seep Appendix 2 for script used to calculate the two-point correlation function.

We investigated the effect of point extent and rock type on the spatial distributions of points. The synthetic data were clipped to the seep extent (with point densities similar to the seeps) and analyses performed on points that lay within the three major seep hosting lithologies.

3.2.2 Supplementary Results

Cluster analysis of seeps

The average nearest neighbour technique compares the average distance between point features with the average distance expected if these points were randomly distributed. We find that seeps are significantly clustered to 99.9% confidence. Isolated seep types are also significantly clustered, except springs which together with travertine show a near random distribution (see Table 3.1).

	Z	CI	Signif.	Distribution
Seeps (sep)	-23.58	0.31	99.9%	Clustered
Seeps (dual)	-23.23	0.34	99.9%	Clustered
Dry (diff + vent)	-13.19	0.4	99.9%	Clustered
Wet (spring + bw)	-12.95	0.44	99.9%	Clustered
Spring	1.15	1.65	75%	Dispersed
Bubbling Water	-11.63	0.42	99.9%	Clustered
Diffuse	-6.98	0.53	99.9%	Clustered
Vent	-7.3	0.5	99.9%	Clustered
Fumarole	-3.5	0.49	99.9%	Clustered
Seismic events	-22.32	0.38	99.9%	Clustered
Travertines	-0.9	0.95	<65%	Random

Table 3.1: Results of Point Cluster Analysis. Z-scores and Cluster Index of point data in Italy. The cluster index (CI) value signifies if the points are clustered (CI<1) or dispersed (CI>1). The Z-score is a measure of standard deviation (σ) from the mean. Critical Z-score values for 95% and 99% confidence intervals are ±1.96 and ±2.58 respectively. The area considered for these calculations influences the results. We set the area of computation to the area which obtains a random distribution for a random scenario (320 points randomly distributed throughout Italy). Sep = Seep separated (dual seep types treated as two seeps), dual = dual seep types treated as one seep, diff = diffuse, bw = bubbling water seep.

Ripley K-Function

$$KF \bullet r = \sqrt{\left[\frac{A}{\pi \bullet n \bullet (n - 1)} \right]}$$

Where KF is the K-function, r is separation distance between features, n is the number of features and A is the area.

Radial distances considered for the Ripley K-Function (RKF) computations were considered at 0.5 km intervals from 0.5 - 50 km radius. The synthetic data informed the 'expected' random gradient given the area of Italy. K-values inform whether the distribution is more clustered ($K_{(obs)} > K_{(exp)}$) or more dispersed ($K_{(obs)} < K_{(exp)}$) than a

random distribution at that scale. Results show that wet seeps have ~ 4 km clusters within 10 km, whereas dry seeps show ~2 km clusters approximately ~15-20 km apart. Seeps are no longer clustered at separation distances greater 40 km (Figure 3.5).

Are seep alignments an artefact of the lithological outcrop?

To test if the two scale distribution and alignment observed for CO_2 seeps was an artefact of outcropping lithology or increased seep density in the Tyrrhenian, we analysed the spatial distribution and azimuth for synthetic points located in:

- The same areal extent of the CO_2 seeps
- Andesitic rocks
- Platform carbonate rocks.
- Turbiditic Rocks

The point azimuths and the two point correlation results are presented in Figures 3.6 and 3.7. We find the synthetic data exhibited random point distributions, no clustering and no distance dependent point distributions, even when clipped to the most prominent seep hosting lithologies (turbidites, andesites and basalts, platform carbonates). Thus the two-scale point correlation we observe for CO_2 seeps is not an artifact of the shape or extent of outcropping lithology.

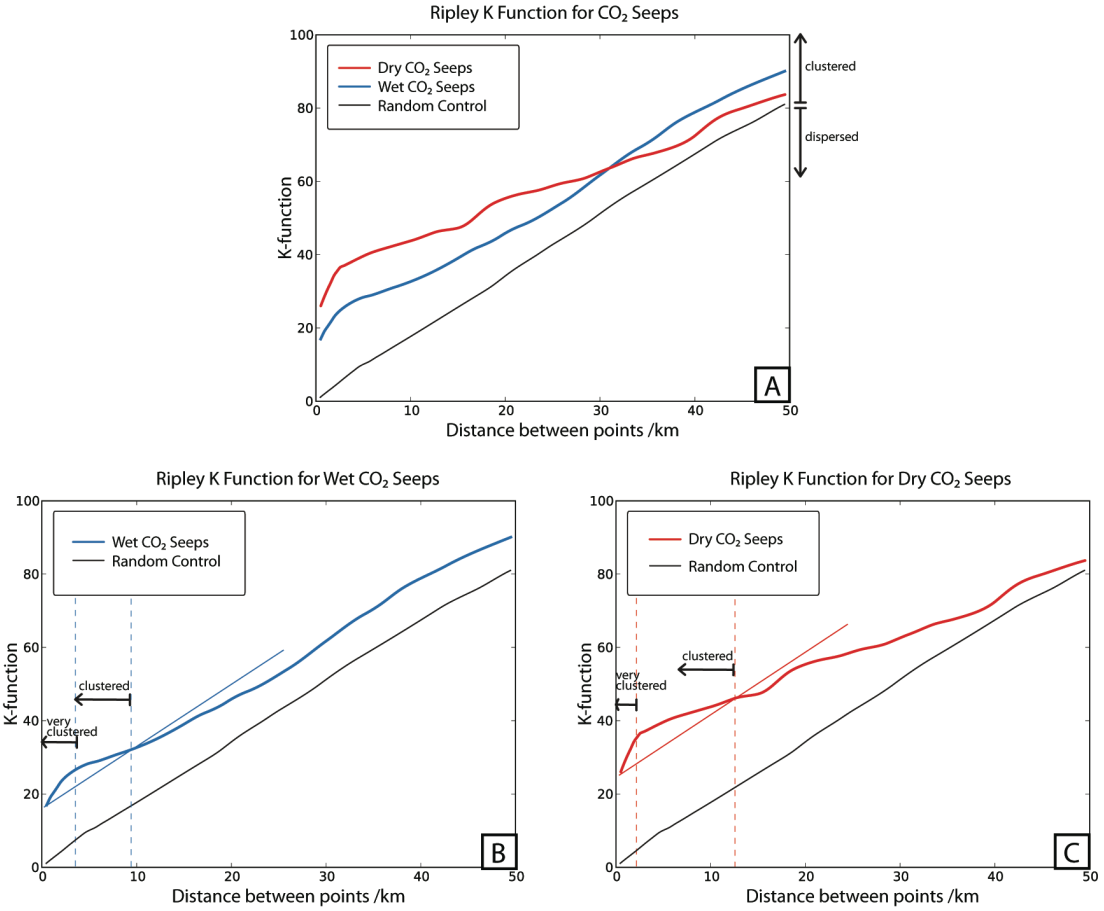

Figure 3.5 A: Ripley K Function for wet and dry seeps and the synthetic random dataset. The seeps are clustered when the K function slope is steeper than that of the synthetic data, and no longer clustered when the K function slope is shallower than that of synthetic data. Seeps are clustered at all scales compared to the synthetic random control. Beneath are interpreted graphs for wet (**B**) and dry (**C**) seeps. Most clustering occurs within ~10 km point separation, and most significantly ('very clustered') below ~4 km point separation for wet seeps and ~ 2 km point separation for dry seeps.

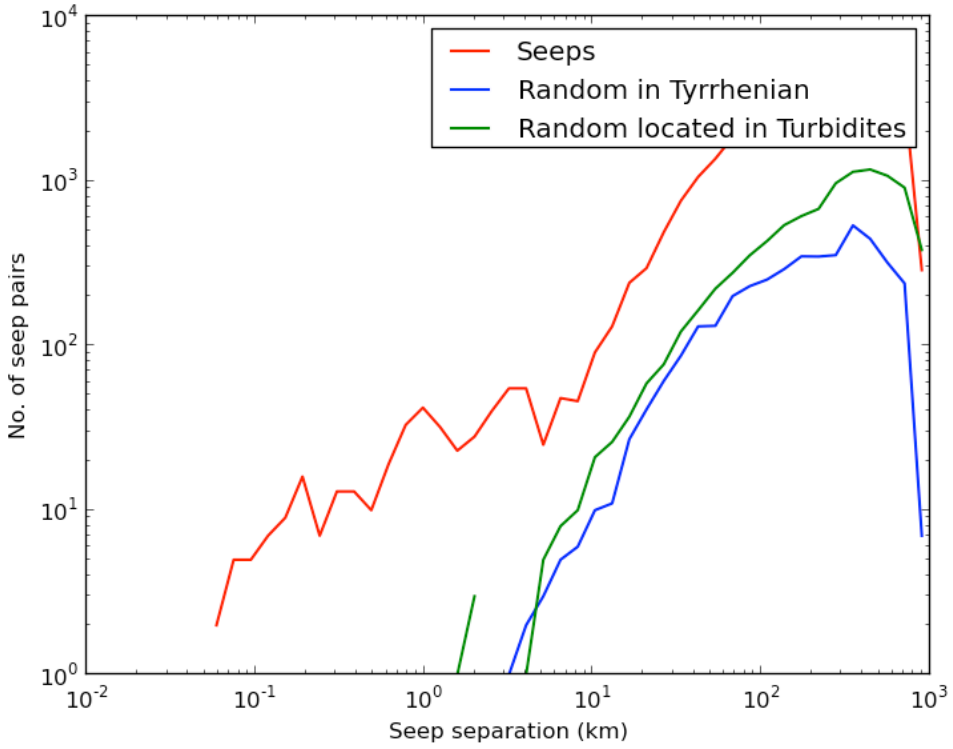

Figure 3.6: Two-point correlation results for seep data compared with results of synthetic points located in the Tyrrhenian sector (the extent of the CO_2 seeps), hosted by turbiditic rocks. Seeps show two-scale distribution. Synthetic points do not.

Figure 3.7: Point azimuth analysis results for synthetic data distributed in the Tyrrhenian or hosted by platform carbonates (P.Carbonates), andesites or turbidites, which are the most common rock types in the Tyrrhenian sector of Central Italy where most seeps distribute. At distances above 10 km, seep azimuths (Figure 3.2B) show similarities to the azimuths displayed by these random data. At distances below 10 km, the seep azimuths are markedly different to the synthetic data azimuths, which are also much fewer. This supports the conclusion that seeps are distributed on two spatial scales, and within seep clusters (5 km radius) seep distributions are non-random.

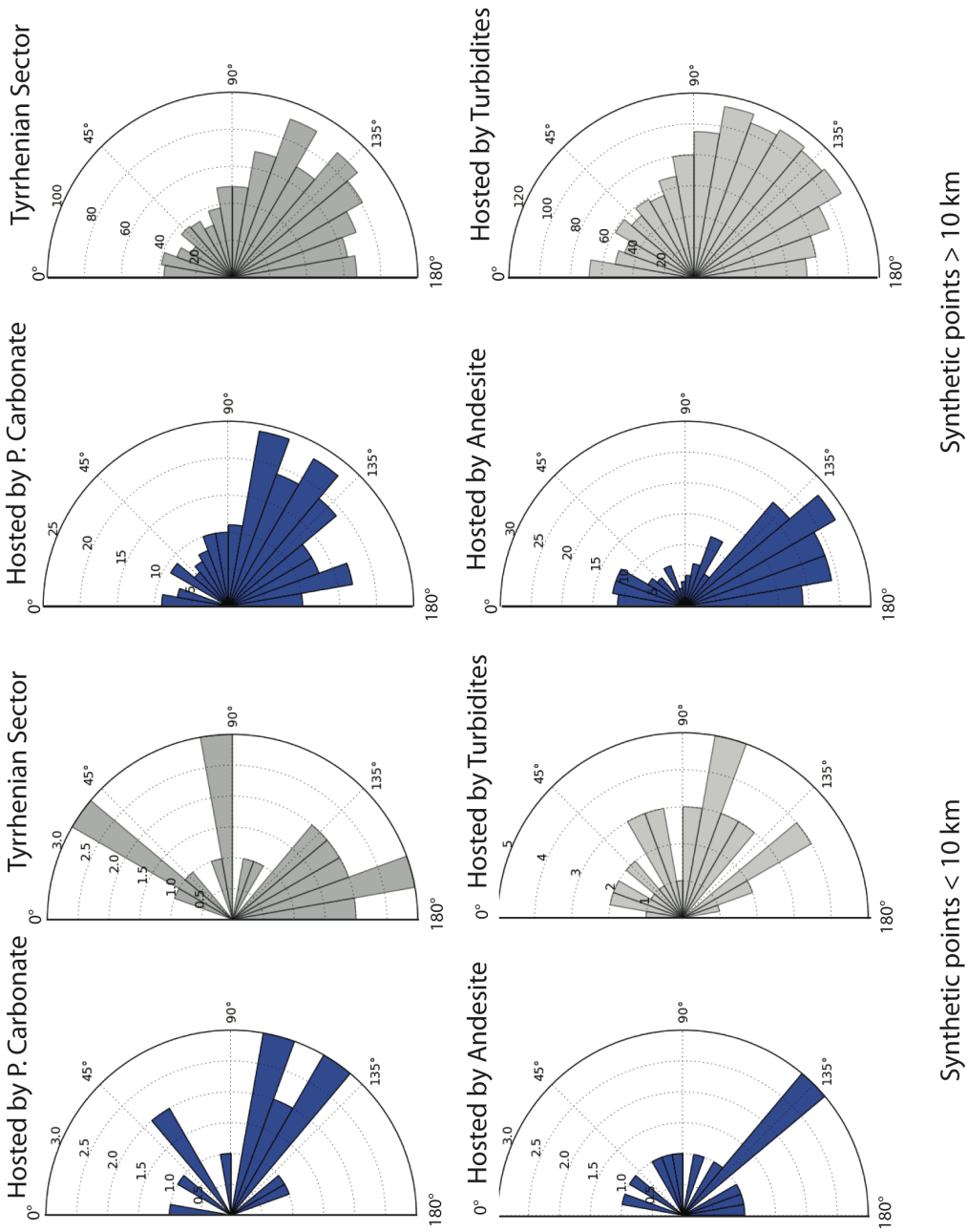
Tyrrhenian Sector
Hosted by Turbidites
Hosted by P. Carbonate
Hosted by Andesite
Tyrrhenian Sector
Hosted by Turbidites
Hosted by P. Carbonate
Hosted by Andesite
Synthetic points > 10 km
Synthetic points < 10 km

Chapter 4

What determines CO_2 seep characteristics?

The spatial investigations presented in the previous Chapter find that seeps distribute differently from geological structures according to seep type. Field observations note that seeps often emerged in local topographic depressions or close to streams and rivers, and the topographic distribution of seep types seemed systematic. To test this, the spatial dataset is further examined to assess the geological and topographic controls on seep characteristics. Since the investigation of historical human death at CO_2 seeps in Chapter 2 find seep type influences the risk of CO_2 poisoning at seeps, the ability to assess which seeps may establish from breached onshore storage operations is important for risk assessment and management procedure.

4.1 Surface controls on the characteristics of natural CO_2 seeps: implications for engineered CO_2 stores

Long-term security of performance of engineered CO_2 storage is a principle concern, as seepage of injected CO_2 to the surface is economically and environmentally undesirable. In Italy, natural CO_2 degassing to the surface via seeps is widespread, providing an insight into the various styles of subsurface plumbing as well as surface expression of CO_2 fluids. While deep geological structures control the spatial distribution, alignment and clustering of Italian CO_2 seeps, here we investigate the surficial controls on the distribution of seep characteristics (type, flux and temperature) using a large geographical and historical dataset. When observed seep locations are compared to a statistically random dataset, we find that the nature of the CO_2 seeps and their distance from geologic structures are determined by the flow properties of outcropping lithology, together with local topography. Where low permeability rocks outcrop (e.g. turbiditic mudstone, shales and quaternary cover) there are numerous dry seeps exhibiting a range of fluxes. CO_2 'vents' occur along faults. Where CO_2, laterally supplied by these faults, emerges from the vadose (water unsaturated) zone, 'diffuse' dry seeps develop, whereas wet 'bubbling water' seeps arise where CO2 supply enters the phreatic zone or an aquifer (e.g. fractured carbonates). 'Spring' seeps emerge where valleys erode into CO_2 aquifers and these are wet, high flux seeps that are positioned close to lithological boundaries. 'Fumaroles' are associated with active volcanism. Seep type is known to influence human mortality, therefore identifying such controls on potential seep locations and type, above engineered CO_2 storage operations is crucial to targeted site monitoring strategy and risk assessment. We find that seep monitoring efforts should target elevated low-permeability rocks near faults.

4.1.1 Introduction

Industrialized societies which continue to use fossil fuel energy sources are considering adoption of Carbon Capture and Storage (CCS) technology to meet carbon emission reduction targets. Naturally occurring CO_2 seeps provide a unique opportunity to understand the crustal fluid pathways of CO_2 migrating from depth. This not only informs the long-term performance security of engineered CO_2 storage but also enables the development of more accurate seepage risk assessment and surface monitoring strategies.

In central and southern Italy and Sicily over 308 CO_2 seeps at 270 locations have been spatially and historically documented (Chiodini and Valenza, 2009). The CO_2 release is globally significant - discharge from regional aquifers in western central Italy is estimated to account for over 10% of the present-day global CO_2 budget from sub-aerial volcanoes (Chiodini et al., 2004).

Groundwater pollution, ecosystem damage and CO_2 poisoning of animals and humans are associated with CO_2 leakage. Italian seeps exhibit a variety of surface expressions (seep 'types'), temperatures and fluxes. Our previous work examined the health risk from natural seeps. The environmental hazard of seeps is dependent on how CO_2 is dispersed rather than the flux alone (Hepple, 2005), and indeed, as presented in Chapter 2 of this thesis, historical records of very rare human deaths at Italian gas seeps have found that dry seeps pose the greatest death risk. Investigation of the spatial distribution of CO_2 seeps in Chapter 3 established that large faults and folds control CO_2 seep location at a regional scale. These structures supply CO_2 to seep clusters, where CO_2 can be released as a free-phase 'dry' gas, or as a dissolved constituent of wet springs.

The local factors governing seep characteristics and distance from deep geological structures are not currently known, so here we examine the influence of near-surface geological structures, in particular host lithology and topography, on the distribution of CO_2 seep types, temperature and flux.

4.1.2 Italian CO_2 seeps and their origin

The distribution of subaerial CO_2 seeps in Italy is shown in Figure 4.1A. Five types of natural seep are identified: vents, diffuse seeps, springs, bubbling pools of standing water and volcanic fumaroles (Chiodini and Valenza, 2008); where bubbling water, and diffuse seeps are the most common (Figure 4.1B). Several deep boreholes are also known to leak CO_2; these seeps are classified as 'wells'. CO_2 is degassed together with lesser amounts of N2, H2S, CH4, H2, Ar, He and CO (e.g. (Minissale, 2004). Gas flux can vary between locations, from < 1 to > 2000 tonnes/ day (t d^{-1}), but most commonly between 10-100 t d^{-1} (as presented in Section 2.1.4).

CO_2 degassing is greatest towards the Tyrrhenian sector, where the crust is thinned and there is high heat flow. Crustal extension is currently active in the Apennine Mountains where CO_2 flux is much reduced and trapped CO_2 fluids at depths > 5 km are known to affect the seismicity and deformation style of the region e.g. (Di Luccio et al.; Miller et al., 2004).

There are nineteen sites where more than one seep type is expressed at a single location ('dual-system seeps'). In Section 2.1.4 it is observed that diffuse seeps are often one of these seeps, paired with either vents or bubbling-water seeps. While flux, seep types and seep locations are considered constant here, there is evidence of seasonal seep water content variation and concomitant migration of edifices by several meters (Heinicke et al., 2006). Additionally, flux variation at several seeps can be affected by deep seismic events (Bonini, 2009a, b; Heinicke et al., 2010).

Numerous geochemical studies have attempted to elucidate the sources of CO_2 in Italy (Chiodini et al., 2004; Marziano et al., 2007; Minissale et al., 1997). Carbon and noble gas isotopes identify several regional contributions to CO_2 degassing including shallow biogenic processes, carbonate hydrolysis, deep burial mechanical breakdown or thermo-metamorphism of carbonates, and mantle degassing during volcanism (Chiodini et al., 2004).

Discharges of both thermal and cold CO_2 fluids are fed by a regional aquifer within Mesozoic carbonates (Goldscheider et al.; Minissale, 2004). Travertines are a direct

consequence of dissolved CO_2, and active and inactive (fossil) travertine systems are widespread. Travertine carbon isotopes show evidence of CO_2 contributions from metamorphic and mantle sources (Minissale, 2004). Travertines, thermal springs, and seeps may be associated with karst collapse sinkhole environments which often follow active faults (Santo et al., 2011), showing long-term groundwater flux.

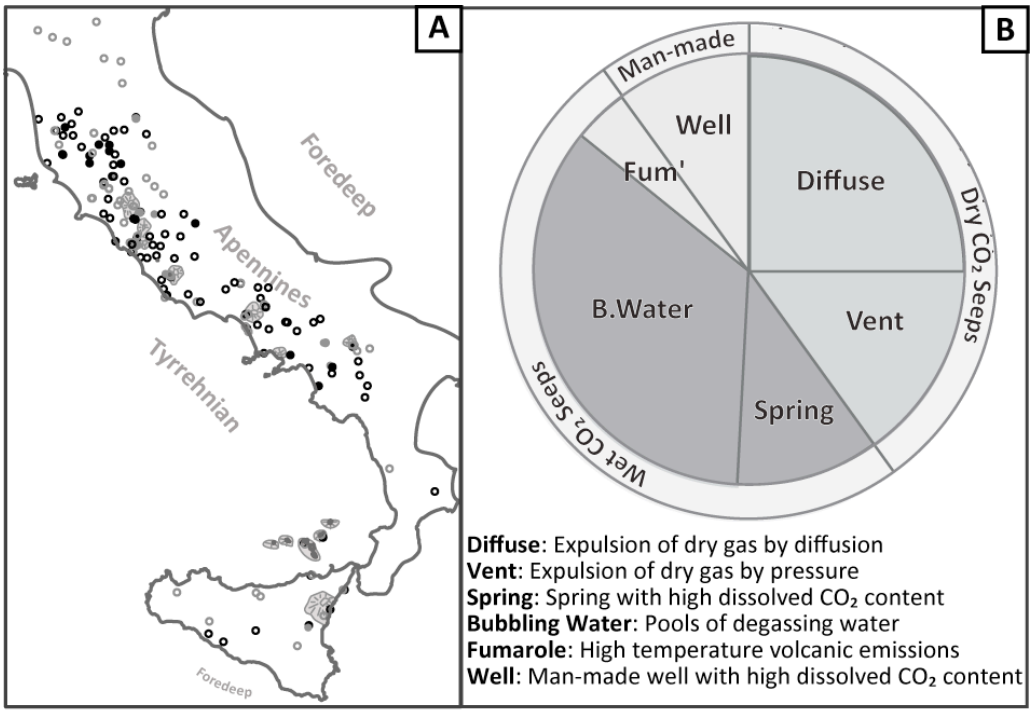

Figure 4.1 A: Sketch of Italy and Sicily showing the location of CO_2 seeps (circles). Filled symbols show multiple seeps. **B**: Proportion of CO_2 seep types (classified according to surface expression, n = 308). Seep classes can be grouped into aqueous ('wet') and non-aqueous ('dry') categories. Wells are artificial leaking pathways.

4.1.3 Theoretical CO_2 pathways

High-permeability pathways are required to bring fluids from depth to the surface and crustal fluid flow is commonly controlled by deformation-induced permeability of fault and fracture networks (e.g. (Agosta et al., 2010; Agosta et al., 2007; Faulkner et al., 2010; Kurz et al., 2008). The regional study of onshore CO_2 seeps in Central and Southern Italy and Sicily presented in Chapter 4 found that faults and regional subsurface structures govern large scale (> 10 km) seep distribution. Seeps emerge at fault tip and ramp structures near active faults in the Apennine Mountains, whereas they tend to position along the fault trace of more evolved fault systems (see Section 3.1.7). Faults feed seep clusters of 2-5 km radius, which represent the dispersal of CO_2 in the near surface by subsidiary structural features, along which the seeps are broadly aligned. It was observed that several seep types occur within these clusters and are related to the seep distance from the (non-seismogenic) fault, with vents closest and springs furthest away.

As CO_2 fluids ascend from depth to the surface there are several changes to the subsurface environment that will affect fluid flow:

Fracture aperture

The damage zone and impermeable core properties of evolved faults behave as a fluid barrier-conduit system. In the shallow crust uncemented macro-fractures dominate fluid flow. These macro-fractures might be subsidiary faults and fractures associated with large faults or bedding planes and joints (Agosta et al., 2010; Agosta and Kirschner, 2003; Billi, 2005). The permeability of these fractures rapidly decreases with depth, as they become mechanically sealed. Micro-fractures seal less rapidly so increasingly dominate rock permeability at depths > ~1.5 km (Nara et al., 2011). At depths below this, fluid flow is governed by matrix and micro-fracture permeability. Here faults will remain important, since micro-fracture density is greatest in fault damage zones and scales with fault displacement (Mitchell and Faulkner, 2012).

Hydrologic Zones

Fluids migrating from depth will pass through two shallow depth hydrogeological zones on ascent from ~700 m to the surface: the phreatic (water saturated) zone followed by the vadose (unsaturated) zone. A proportion of gaseous CO_2 will dissolve into phreatic (saturated) pore fluids during this ascent. In the phreatic zone, gaseous CO_2 is less dense than the pore fluids, so CO_2, driven by buoyancy, will migrate via matrix or fracture flow. In the vadose zone, gaseous CO_2 is denser than soil-gas and therefore may collect and laterally disperse above the water table. Dispersion in the vadose zone will lead to CO_2 seepage over a larger area than that of the point of emission from the saturated zone.

Pressure (P) and temperature (T)

P-T conditions will decrease during the shallow ascent of aqueous fluids with conflicting effect on CO_2 solubility. As deep circulating CO_2 saturated waters rise towards the surface, CO_2 solubility will first increase (temperature effects), pass a peak and then decrease (pressure effects), whereafter dissolved CO_2 will begin to be released from solution and two-phase flow conditions become established. The transition from dense-phase to gaseous-phase CO_2 is associated with increased buoyancy and increased interfacial tension (IFT) with water. Gaseous CO_2 is therefore likely to have different near-surface leakage pathways than aqueous fluids.

It has been proposed that lithology affects seep density and flux (Collettini et al., 2008). The carbonate aquifers of the Apennine Mountains can accommodate great volumes of fluids and allow long residence periods with effective mixing. Models suggest that these aquifers can hold 10 times more CO_2 than flysch, and 2.5 times more than volcanic rocks before gas leaks at the surface (Collettini et al., 2008). It can therefore be predicted that seeps from volcanic rocks will be more numerous and dry, whereas wet seeps or rarely high flux dry seeps will emerge from aquifers such as carbonates. This supports observations that thermal springs, which indicate rapid fluid ascent, tend to discharge in topographic lows along faults at the contact

between the Mesozoic limestones and overlying volcano-sedimentary formations (Collettini et al., 2008; Minissale, 2004). Cluster analyses presented in Section 3.2 (Table 3.1) confirm that CO_2 springs are not clustered when individual seep type distributions are considered separately, unlike all other seep types.

Hydrogeological features can theoretically influence the dispersion of CO_2 fluids in the vadose zone. Here, we investigate the relationship between seep characteristics (type, flux, temperature) and distribution with respect to their host lithology, the landform (as a proxy for ground water level) and travertine deposits.

4.1.4 Methods

Seep data were elicited from Googas (Chiodini and Valenza, 2008), a web-based catalogue of degassing sites (where CO_2 flux > background) in Italy constructed as a national project by the Istituto Nazionale di Geofisica e Vulcanologia (INGV). Additional communications have been made with Googas collaborators, alongside personal fieldwork and a review of current published scientific literature. There are 286 seep locations, 323 seeps overall, of which 308 are of dominantly CO_2 composition rather than CH_4.

Six CO_2 seep types (bubbling-water, diffuse, fumarole, spring, vent and well) are classified by the Googas seep catalogue (Chiodini and Valenza, 2008). Wells are man-made and therefore are not considered to represent natural CO_2 leakage pathways but rather indicate the presence of subsurface CO_2 reservoirs. In the Googas database, seep location, type and safety is recorded alongside additional information such as flux, temperature and composition. Flux is measured in tonnes per day (t d^{-1}) and categories are low (<1 t d^{-1}), medium (1-10 t d^{-1}), high (10-100 t d^{-1}) and very high (>100 t d^{-1}). We here refer to low-end (low and medium) and high-end (medium and high) flux seeps.

A geospatial information system, ArcGIS was populated with seep data, SRTM 90 m Digital Elevation Model (DEM) (Jarvis, 2008) together with fault information, surface lithology, and travertine distribution. Where more than one CO_2 seep

classification is expressed at a single location it is treated as several individual seeps and proceeding calculations are corrected to account for this.

Lithological information was extracted from a 1:500 000 scale geological map of Italy. The 128 different lithologies were classified into 18 broad rock types then further sub-divided into 6 general rock categories (Igneous; Metamorphic; Basin slope; Terrestrial; Platform margin and Platform interior; see 3). The number of seeps emerging from each rock type was normalised to the total outcrop area. Travertine is a surface deposit formed from waters with high dissolved CO_2 content. We therefore do not consider it as a seep hosting lithology.

The elevation above sea level (a.s.l) of each CO_2 seep was extracted from the DEM. To investigate how rock type and topography relate in Italy, the elevations a.s.l for rock types in the peri-Tyrrhenian were determined by analysing the host rock type and elevation of points located within 30 km of a seep from a synthetic Poisson dataset of 10,000 points distributed within Italy.

Channel network analysis in ArGIS identifies where water should flow given topography, and depicts stream networks for basins of given sizes. To define stream networks, the DEM was prepared using standard fill and flow routing algorithms (Tarboton et al., 1991). Critical drainage areas were defined at 8 km² to extract streams of different channel volumes. Strahler stream order (Strahler, 1952) was calculated from the resulting valley bottom network. The channel sizes considered are herein referred to as ‘stream’ (order 100) and ‘river’ (order 1000). Here, we are interested in identifying topographic lows in the land surface so do not verify whether predicted channel networks correspond with real rivers, streams or stream type. Elevation of seeps from the nearest (geodesic) channel (referred herein as $\Delta elev_{stream}$ and $\Delta elev_{river}$) was calculated by performing a near-analysis from seeps to stream lines to create points. The elevation of these points was interpolated from the DEM.

To test the deterministic control of shallow geology on CO_2 seep type and distribution, analyses were repeated for a synthetic Poisson (random) dataset (with the same number of points as the seep database) distributed within Italy. This

comparison enables us to test if the observed data is significantly different from random.

4.1.5 Results

Topography

Figure 4.2A shows that bubbling-water and spring type seeps are more common in topographic lows than vents and synthetic, randomly distributed, points (66% are located within 500 m of a river). By contrast, CO_2 vent and fumarole positions are not controlled by topographic depressions. Diffuse seeps are more common towards topographic lows than synthetic data, but not as frequent as wet seeps.

The $\Delta elev_{river}$ of seeps within 500 m of the nearest river are shown in Figure 4.2B. Wet seeps tend to emerge in topographic lows, while diffuse seeps show similar elevation distribution as synthetic data. Vents, while similar to diffuse and synthetic distributions show a peak in their abundance between 200 - 300 meters elevation from rivers.

Spring, bubbling-water and diffuse seeps locate at a similar elevation to the river channel (Figure 4.2C). Vents show the greatest $\Delta elev_{river}$ compared to other natural seeps. Despite similar distribution from rivers, diffuse seeps show much smaller interquartile range (IQR) and mean $\Delta elev_{river}$ than synthetic data. For streams, not shown here, only bubbling-water seeps show any significant difference from the synthetic control, exhibiting little elevational difference from the nearest stream. For all seep types we find mean elevation and elevation from channels has no correlation to CO_2 flux.

Springs are the warmest seeps ($\bar{x}_{temp}$ ~35°C), bubbling water seeps are cooler ($\bar{x}_{temp}$ ~26°C) and dry gas seep temperatures are coolest ($\bar{x}_{temp}$ ~18 - 20°C). There is no significant change in seep temperatures with distance from the channel base.

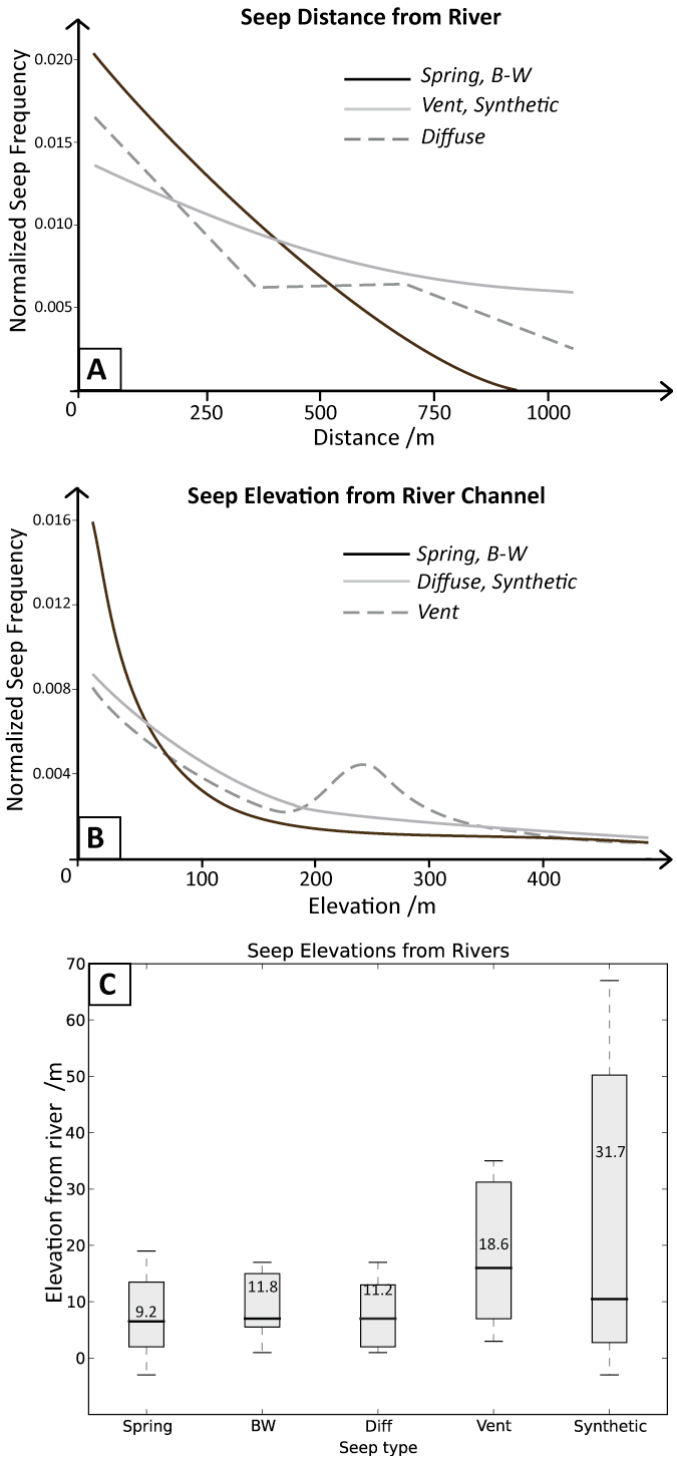

Figure 4.2: Normalised and smoothed line histogram summarising seep distance **(A)** and elevation **(B)** from 'river' channels according to seep type. Fumaroles are too rare to be presented as statistically significant data **(C)** Seep and active travertine elevations within 500 m of the nearest river ($\bar{x}_{elev}$ values additionally shown in the box plot). (BW = bubbling water, Diff= Diffuse.)

Travertines

18 CO_2 seeps are associated with travertine deposition. Most of these seeps are wet seeps, with only 5 dry (all diffuse) seeps associated with travertine. There are only 13 currently active travertines in Italy, and 10 of these have co-occurring CO_2 seeps, which are all located upslope from the travertine. Inactive travertines are found at a similar elevation to the associated present day CO_2 seep.

Host Lithology

Rock type is strongly related with elevation a.s.l (see Figure 4.3A). Limestone lithologies form the Apennine Mountains; therefore carbonate platform rock categories (margin, interior and basin and slope) show much greater elevations a.s.l. than terrestrial and igneous rock categories. Elevation analysis finds that seep types show different elevation distributions and all non-volcanic seeps have lower mean elevations ($\overline{x}_{elev}$) than synthetic data (see Figure 4.5 in Supplementary Information). Spring and bubbling-water seeps show the lowest $\overline{x}_{elev}$, which is ~100 m less than dry seep types and 160 m below synthetic $\overline{x}_{elev}$. Vents show no significant difference in elevation than synthetic data. Fumaroles, which are volcanic edifices, show the highest $\overline{x}_{elev}$ and lowest range, despite igneous rocks generally outcropping at considerably lower elevation than the platform rock categories.

Figure 4.3B shows how different seep types are associated with different rock categories. Seeps emerge from two dominant rock categories which represent four principal rock types. In order of prevalence (when seep frequencies are normalised to outcropping area) these are: igneous (rhyolites/ dacites, and andesites/ basalts), and basin slope sediments (muds/marls, and turbidites). Limestones (rock type numbers 7 - 11) commonly host seeps.

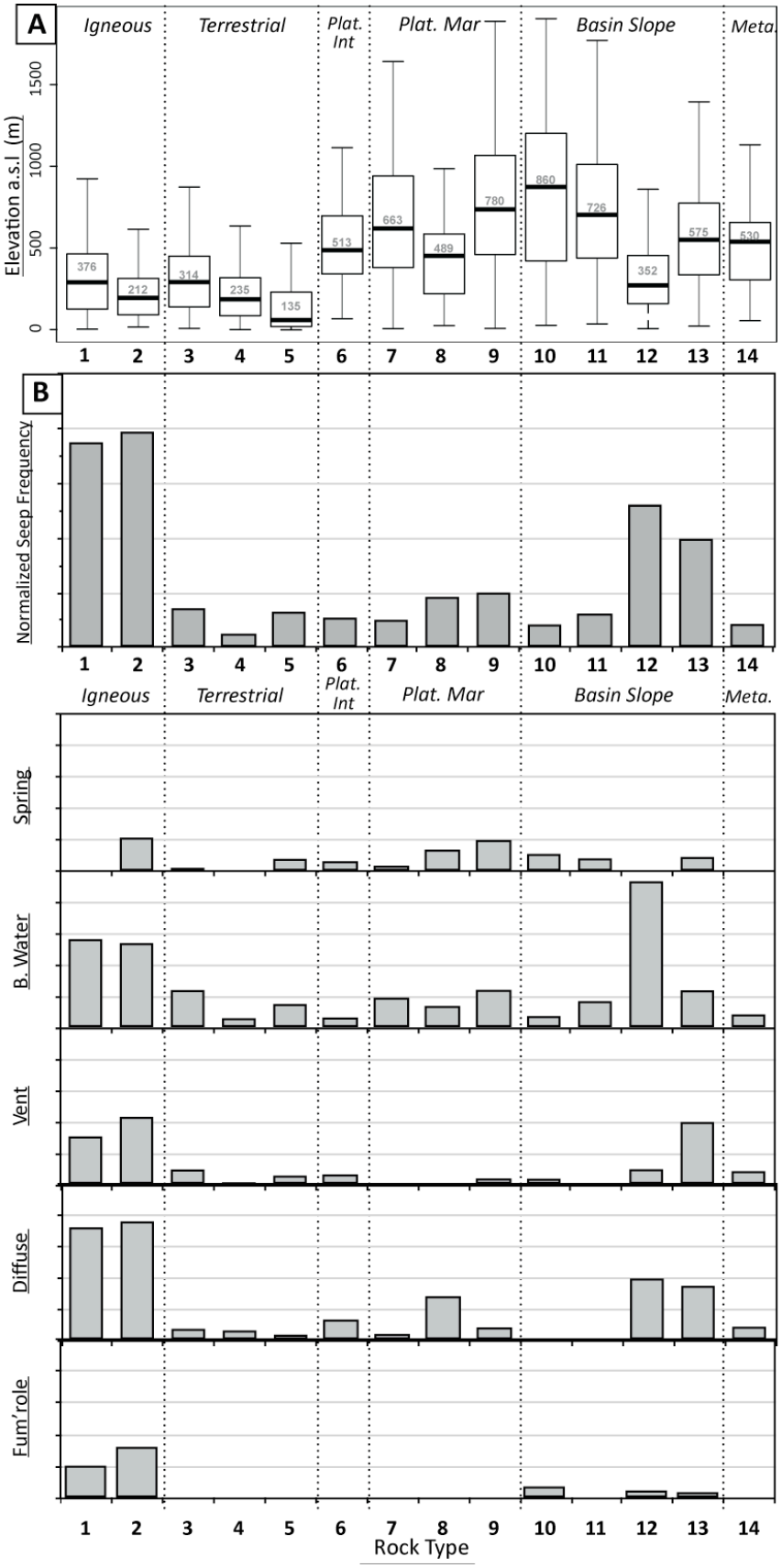
A
Igneous
Terrestrial
Plat. Int
Plat. Mar
Basin Slope
Meta.
Elevation a.s.l (m)
0
500
1000
1500
376
212
314
235
135
513
663
489
780
860
726
352
575
530
1 2 3 4 5 6 7 8 9 10 11 12 13 14
B
Normalized Seep Frequency
Spring
B. Water
Vent
Diffuse
Fum'role
Rock Type

Figure 4.3A: Rock type elevations above sea level, divided into rock category (Plat. Int = Platform Interior, Plat.Mar = Platform Margin, Meta = Metamorphic). Only seep hosting rock types are shown. **B**: Seep hosting rock types, and host lithologies for natural seep types. Seep frequency is normalised to the rock outcrop area.

Rock Types: 1 Andesites & Basalts, 2 Dacites & Rhyolites, 3 Conglomeritic Sands, 4 Glacial Cover, 5 Quaternary Cover, 6 Evaporites, 7 Dolomitic Limestone, 8 Limestone and Sandstone, 9 Platform Carbonate, 10 Detrital Limestone, 11 Pelagic Limestone, 12 Mudstones and Marls, 13 Turbidite, 14 Metasediments (Travertine, a surface deposit directly related to CO_2 rich ground waters, is not considered as a host lithology).

Unsurprisingly, fumaroles are hosted almost exclusively by igneous rocks which also host numerous high flux dry seeps. Platform carbonates and turbidites host all seep types, however, dry seeps are virtually absent in carbonates and far more common than wet seeps in turbidites (Figure 4.3B). Carbonate units host the majority of wet seeps (often high flux - although these also have the greatest quantity of seeps with unknown flux), and no CO_2 vents. Springs are absent from andesites/basalts, metasediments, muds/marls, and conglomeritic sands which host numerous other seeps. Seeps emerging from low permeability rocks (e.g turbidites, Quaternary cover) are more likely to have low fluxes (see Figure 4.6 in Supplementary Information).

4.1.6 Discussion

In Italy CO_2 seep clusters are delivered by deep geological structures (Section 3.1.7). The influence of meso/macro fractures is greatest at depths above 1.5 km, although fluid pressure can sustain fracture apertures at greater depths. Seep clustering indicates that towards the Earth surface, competing processes govern fluid flow, dispersing CO_2 fluids. Analyses presented in Section 3.1.7 show how seep type varies with distance from regional faults; with CO_2 vents locating closest to fault traces, bubbling-water and diffuse seeps exhibiting a weaker relationship with fault distance, and spring locations being controlled mainly by lithological boundaries.

However, the local factors governing seep characteristics (such as type, flux, temperature) and distance from the geological structures were previously unknown.

We here demonstrate that the shallow hydrogeologic environment influences the dispersion and expression of CO_2 fluids. The fate of rising CO_2 fluids depends on rock type, water table depth and topography. CO_2 seeps that are preferentially located toward the local topographic base level must either be interacting with the water table, delivered via degassing CO_2 saturated waters, or river channels are preferentially eroding geological features such as faults which are conduits for deep-derived CO_2 . Since we find that wet seeps emerge in channel bottoms, even though these seeps are found furthest from fault traces, the observed importance of channels on wet seep location must be controlled by the position of the local water table rather than faults.

In contrast to wet seeps, CO_2 vents show no difference to synthetic data in their distribution from river channels (Figure 4.2A) yet differ from synthetic data in their elevation distribution (Figure 4.2B). The location of vents must be independent of the water table, and is simply determined by fault location. It is unclear why these seeps tend to emerge 200 – 300 m up-slope from topographic lows (Figure 4.2B), but it may be that these vents are preferentially located above subsurface structural highs; which we observe in the previous Chapter (Section 3.1.7), and is the case at Mefite D'Ansanto, Italy's highest flux CO_2 seep (Chiodini et al., 2010).

The relationship between diffuse seeps and topographic lows is more complex. Their distance distribution from river channels is similar to wet seeps until 300 m (Figure 4.2A), after which the frequency plateaus until 700 m. This is unlikely to be an artifact of a small dataset since diffuse seeps are the most common (see Figure 4.1B). Further than 700 m from a river, diffuse seep frequency distribution lies between wet seeps and vent/synthetic. In contrast, the elevation distribution of diffuse seeps from channels is no different from synthetic data. In Chapter 2 (Section 2.1.4) we find diffuse seeps commonly constitute one of the 'dual system seeps'; paired with bubbling water or vent seeps, and analyses in Chapter 4 show bubbling water and diffuse seeps exhibit similar frequency distributions from fault traces. We

suggest that diffuse and bubbling-water seeps represent similar fluid leaking paths. Where the water table is at the surface, bubbling water seeps occur, whereas diffuse seeps rise through the unsaturated vadose zone, emerging close to river channels. Diffuse seeps represent near surface CO_2 dispersion from CO_2 vents. This is supported by two further observations: firstly, the only dry seeps to co-locate with active travertines are the diffuse type, where it is likely that CO_2 degassed from the travertine-precipitating waters emerges from the vadose region above the spring, and secondly, while both bubbling water and diffuse seeps emerge from low permeability rocks, bubbling water seeps are more prevalent in rocks which outcrop at low elevations a.s.l (such as mudstones and marls, or quaternary cover) and are therefore more likely to have a shallower water table.

We observe that springs only emerge from permeable lithologies, and these are often high flux. This agrees with models of rocks with high infiltration rates (Collettini et al., 2008). However, these models also suggest that dry seep density will be greatest in more impermeable rocks. We find, however, that igneous extrusive rocks rather than (less permeable) turbidites are the most common seep hosting lithology and, moreover, seeps hosted by igneous rocks are often high-end flux. This may be explained by the elevated geothermal gradients associated with igneous provinces. Here, not only will igneous processes be supplying greater quantities of CO_2, but these rocks will also have Na-Cl type pore waters. Increased temperature and salinity both reduce CO_2 solubility in water and will therefore reduce the attenuation of dry CO_2 fluids by dissolution.

A large proportion of high flux seeps (> 10 t d^{-1}) are dry types emerging from turbidite mudrocks. Since these are generally low permeability rocks, the flux is not controlled by inherently high rock infiltration rates. We suggest that these rocks with low vertical permeabilities are acting as a seal to inhibit the seepage of CO_2 fluids from an underlying lithology. Opportunities for these buoyant fluids to escape through the impermeable cover may be few. Therefore, where a pathway exists, such as at a faults or lithological contacts, the resulting seeps are the only regional pathways to release these fluids, resulting in increased gas flux and perhaps increased gas pressure, drawn from a wider lateral region.

Seep elevations a.s.l vary between seep types (Figure 4.3A) and reflect the influence of outcropping rock type on seep development and topographic preferences. For example, the mean elevation of springs is lower than diffuse and vent seeps even though springs most commonly emerge from limestone rocks which show greatest elevations a.s.l. This reflects the tendency for springs to emerge in valley bottoms unlike dry seeps. These dry seeps are more likely to emerge away from topographic lows in the lower lying igneous rocks and low permeability marine sedimentary facies such as mudstones and marls and turbidite rocks. Synthetic data show greatest spread in elevation a.s.l because these points do not concentrate in the peri-Tyrrhenian and are independent of topography.

The research presented in Section 2.1.4 finds local topography surrounding a seep, together with seep type influences the health risk posed to humans. Sheltered areas enhance density-driven pooling of CO_2 which can rapidly increase CO_2 concentrations to dangerous levels. Although more deaths have occurred at dry seeps than wet seeps (Chapter 2), we find dry seeps do not preferentially emerge in valley bottoms, and in fact CO_2 vents emerge upslope of a river so decreasing their health risk. It is therefore most important that seep risk assessment identifies where diffuse seeps may emerge at low elevation or where density driven CO_2 streams may develop. Seep monitoring efforts should therefore target elevated low-permeability rocks near faults. Low lying permeable rocks at the surface above a CO_2 store (where there is a high water table) will decrease human health risk from CO_2 seeps, since the interaction of CO_2 with ground waters attenuates dry seepage.

Figure 4.4 proposes a model of seep type development that summarises the major controls on seep type, location and flux. Seeps emerging from more permeable rock categories (e.g. fractured carbonates) are typically wet, high flux, and emerge in valley bottoms. Previous research identified that wet seeps tend to be located close to lithological boundaries (Section 3.1.7) whereas dry seeps are positioned closer to faults. Seeps emerging from low permeability rocks are more numerous and can exhibit a range of fluxes. Seep types in these rocks are determined by elevation, which we suggest increases the depth to the phreatic zone. If these low permeability rocks are at low elevations a.s.l (e.g. mudstones and marls, quaternary cover) then

diffuse and bubbling water seeps are most likely to develop, whereas if these rocks have greater elevations a.s.l (e.g. evaporitic rocks, turbidites) then diffuse and vent seeps are more likely to develop. This model suggests that where ascending CO_2 fluids meet a permeable horizon in the unsaturated zone, CO_2 will spread laterally, dissolving into pore waters if present, and subsequently emerge at springs. Free phase CO_2 gas that spreads through this permeable horizon may then emerge as either diffuse seeps or as bubbling water seeps, depending on the position of the water table.

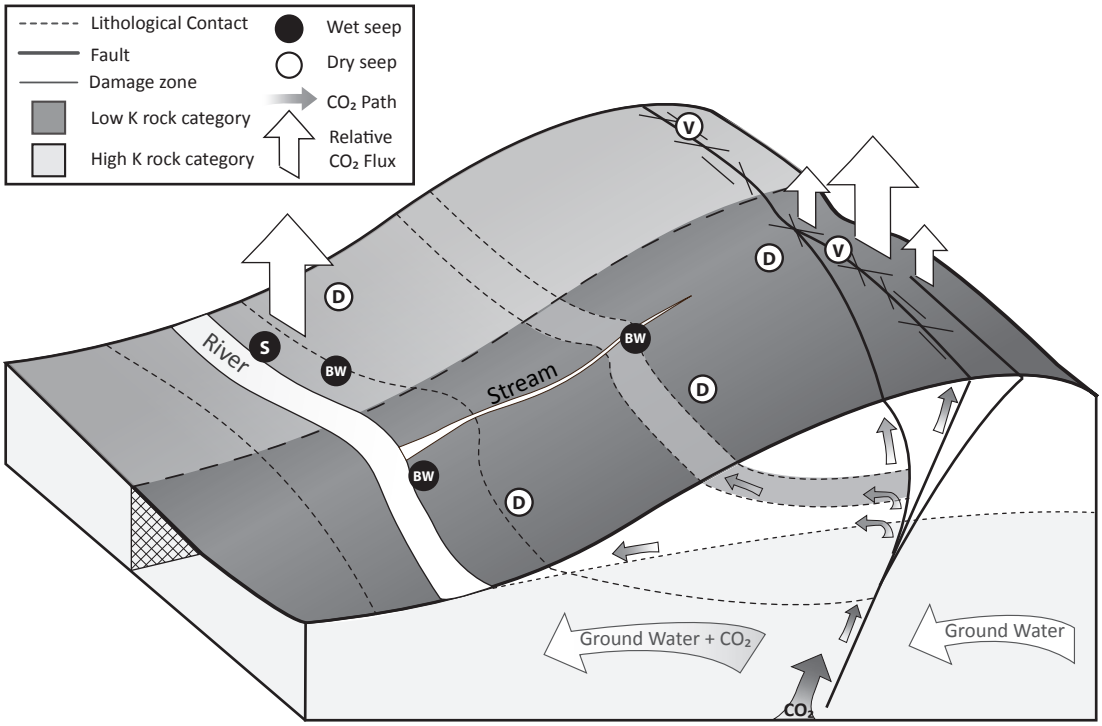

Figure 4.4: Schematic of the role of geological structure, topography, host lithology and local water table on seep type development. Where host rocks are high permeability (k) rock categories (e.g. fractured carbonates) seeps are more likely to be wet, high flux and emerge in valley bottoms. Research presented in the previous chapter find wet seeps tend to position close to lithological boundaries. Where low permeability (k) rocks outcrop (e.g. turbidites, muds and marls and quaternary cover) more numerous dry seeps form which can exhibit a range of possible fluxes. Diffuse seeps are more common in topographic lows whereas vents show no relationship. These also locate closer to the fault trace than wet seeps. Seep types: D = diffuse, V = vent, S = spring, BW = bubbling water.

4.2 Supplementary Information

4.2.1 Supplementary Results

Elevation analysis find CO_2 seeps locate at a range of altitudes but all non-volcanic seeps have lower mean elevations ($\bar{x}_{elev}$) than synthetic data (Figure 4.5). Spring and bubbling-water seeps show the lowest $\bar{x}_{elev}$, which is ~100 m less than dry seep types and ~200 m below synthetic $\bar{x}_{elev}$. Vents show no significant interquartile range (IQR) difference than synthetic data. Fumaroles, which are typically located on volcanic edifices, show the highest $\bar{x}_{elev}$ and lowest Inter Quartile Range (IQR). The elevation IQR for synthetic data points is much greater than seeps, this may reflect the reduced CO_2 seep density towards the Apennines and other mountainous regions, so all seeps are preferentially located towards valleys rather than emerging on mountain tops.

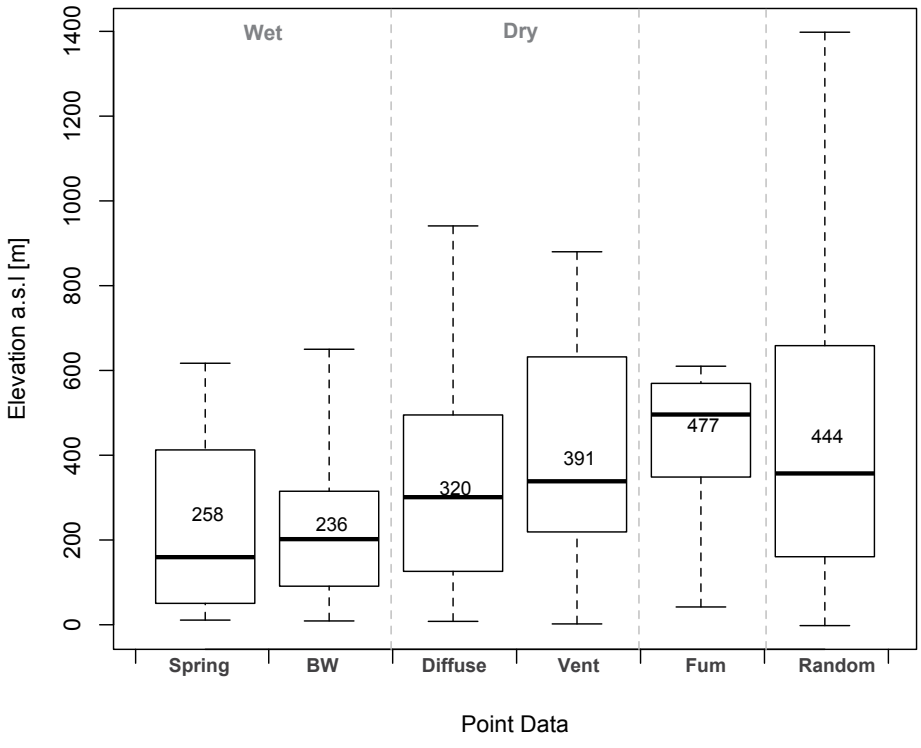

Figure 4.5: Box plot of natural seep type elevations a.s.l in Italy and random data selected within 30 km of a seep. Wet seeps are typically found at lower elevations than dry seeps.

There is evidence that seep hosting lithology influences seep flux, as proposed by (Collettini et al., 2008). The majority of low flux seeps emerge from igneous rock types, although Andesites also host a number of high flux seeps. Carbonate units 9 - 11 (platform, detrital, and pelagic carbonates), host only low and medium flux seeps, whereas unit 8 (limestone and sandstone) host seeps with high fluxes, where flux is quantified. Mudstones and marls (unit 12) and turbidite (unit 13) host the majority of high-end flux seeps. Quaternary cover (unit 4) hosts few seeps, but these are high flux.

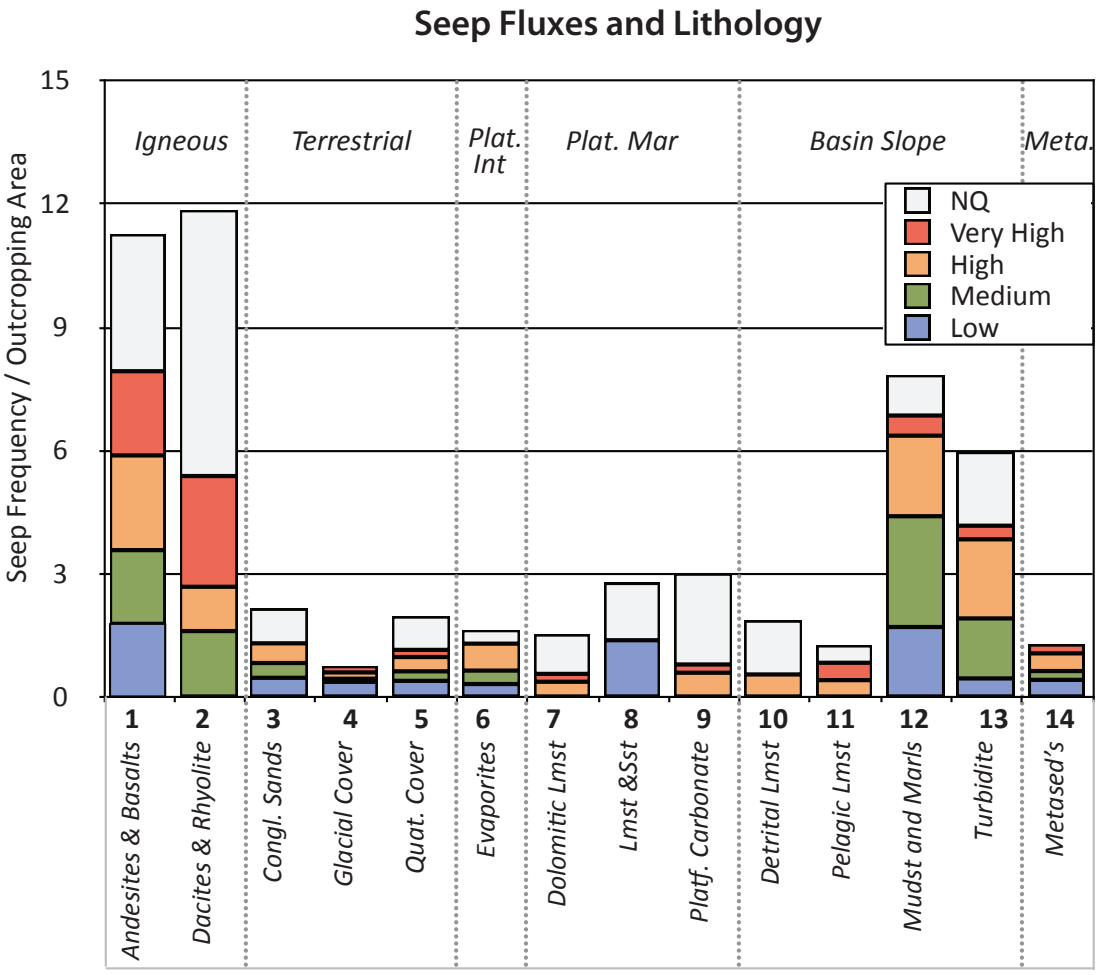

Figure 4.6 A: Seep frequencies per rock type normalised to rock outcropping area, showing flux categories.

Rock Types: 1 Andesites & Basalts, 2 Dacites & Rhyolites, 3 Conglomeritic Sands, 4 Glacial Cover, 5 Quaternary Cover, 6 Evaporites, 7 Dolomitic Limestone, 8 Limestone and Sandstone, 9 Platform Carbonate, 10 Detrital Limestone, 11 Pelagic Limestone, 12 Mudstones and Marls, 13 Turbidite, 14 Metasediments (Travertine, a surface deposit directly related to CO_2 rich ground waters, is not considered as a host lithology).

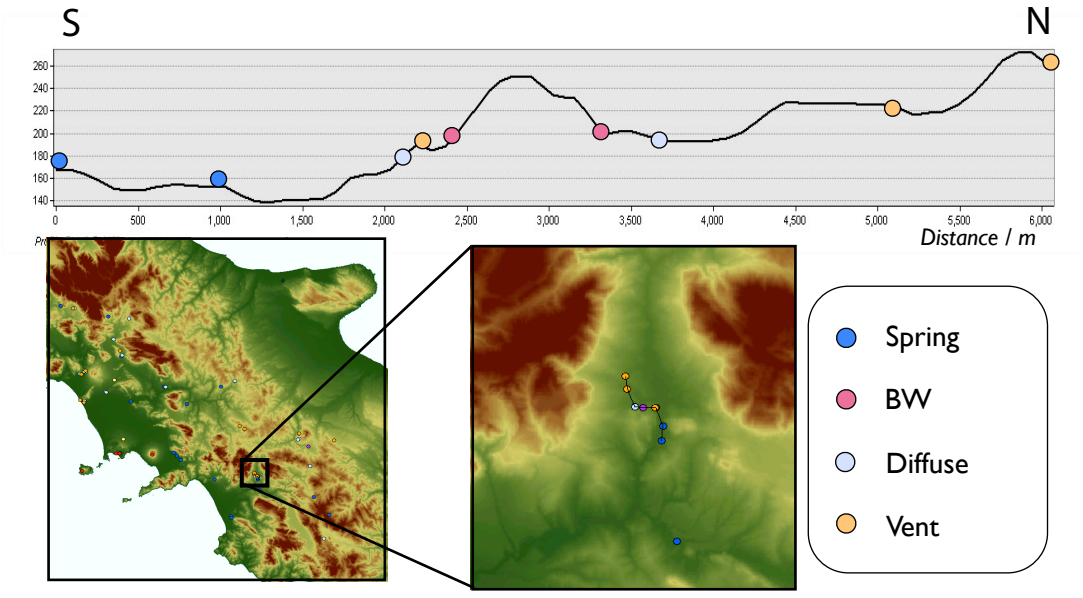

Figure 4.7: Topographic profile of a seep cluster (Contursi cluster, explored further in Chapter 5) showing the elevation distribution of seep types. Location and line of profile shown beneath. CO_2 springs are located towards valley bottoms. Diffuse and bubbling water (BW) seeps are located upslope from these, while vents locate at the highest elevation. In this cluster, seeps outcrop along the lithological contacts between a tectonic window ('klippen') of carbonate and terriginous sediments in the Sele graben, in a relay zone of the Irpinia normal fault. Seeps within this cluster will show N-S and E-W alignments (Section 3.1.6).

Chapter 5

To Seep or not to Seep?

Hydrocarbon exploration drilling in Italy discovered large CO_2 accumulations in Italy. Where CO_2 reservoirs are located close to surface seeps, these reservoirs can be considered to be leaking. This Chapter presents a substantial body of work, comparing the characteristics of seeping and sealing CO_2 reservoirs in Italy. The majority of the boreholes were drilled from the 1960's to the 1980's before modern logging tools were developed. Using the data available, the down well conditions evidenced from the well logs are used to model CO_2 behaviour and depth at these reservoirs. CO_2 properties are modelled using a sophisticated equation of state (Huang et al., 1985; Span and Wagner, 1996). I adapted an R code written by Mark Naylor to calculate CO_2 properties from drill mud weights and uncertain geothermal and depth conditions.

The following paper is presented in two parts. Part I describes and compares the geological characteristics of the reservoir, and Part II assesses the rate of CO_2 leakage and potential mechanisms enabling such fluid escape.

5.1 To Seep or not to Seep: A Comparison of Seeping and Sealing CO_2 Reservoirs in Italy

A principle concern for engineered CO_2 storage is long term security, as seepage of injected CO_2 to the surface is economically and environmentally undesirable. In Italy, natural CO_2 degassing to the surface occurs at over 308 seeps which show a variety of surface manifestations. In addition, several hydrocarbon exploration wells discovered CO_2 rich reservoirs (CO_2 > 90 %). CO_2 seeps close to CO_2-bearing wells could indicate reservoir breaching. Here, we compare sealing and seeping CO_2 rich reservoirs in Italy to elucidate the mechanisms enabling or preventing fluid escape. These reservoirs are hosted in carbonate rocks capped by flysch overburden, and CO_2 is retained in gas or supercritical phase at various depths and pressure conditions. Sealing reservoirs show overpressured overburden, whereas seeping reservoirs are located close to modern extensional faulting and show overburden at hydrostatic conditions. Fluid seep rates from top reservoir conditions are applied to investigate the geological conditions required for fluid escape. Formations waters have the potential to dissolve large quantities of CO_2 and could therefore transport CO_2 to the surface at considerable rates. However geologically unrealistic permeabilities would be required for these waters to ascend at the rates necessary to supply high flux CO_2 seeps. Rapid CO_2 flux will always be more achievable by seeping free phase CO_2. Significant (>100 tonnes per day) leakage of dense phase CO_2 from the reservoir can be achieved by Darcy flow without the need for faults or enhanced permeability pathways. In contrast, to enable the same CO_2 flux for gas phase CO_2, fault permeabilities and areas are necessary since seepage through the overburden would require geometrically unlikely areal extent of seepage. Changes in CO_2 properties during ascent from the leaking reservoir therefore lead to fluid channeling along high permeability pathways such as faults. These findings will directly inform site selection procedure at engineered storage sites.

5.1.1 Introduction

Industrialised societies which continue to use fossil fuel energy sources are considering adoption of Carbon Capture and Storage (CCS) technology to meet carbon emission reduction targets. For effective climate mitigation, the injected CO_2 must remain secure in the subsurface for tens of thousands of years (Shaffer, 2010).

Instances of CO_2 migration to the surface from naturally occurring reservoirs serve as direct analogues for the potential migration of CO_2 from geologic storage sites. These provide a unique opportunity to assess the conditions required for CO_2 to leak from the reservoirs and to understand the crustal fluid pathways of CO_2 migrating from depth. Similarly, instances where CO_2 has been successfully retained for geologically long time periods offer opportunity to assess the conditions required for effective storage. This not only informs the long-term performance security of engineered CO_2 storage, but also guides effective site assessment and injection strategy. In this paper we refer to the release of CO_2 at the Earth surface as CO_2 *seepage*, and CO_2 migration from its containing reservoir as CO_2 *leakage*.

Italy is a region of natural geofluid phenomena, and numerous CO_2 and CH_4 gas seeps, oil seeps and mud volcanoes are documented (Chiodini, 2008; Etiope et al., 2007; Katz et al., 2000; Sani et al., 2004). Italy is also the fourth most hydrocarbon-endowed country in Europe to date, and over 7000 wells have been drilled for hydrocarbon exploration and production (Bertello et al., 2010). These have revealed the presence of CO_2 accumulations (Casero, 2004; Chiodini et al., 2010; Heinicke et al., 2006).

In total, over 308 CO_2 seeps at 270 locations have been catalogued in Italy (Chiodini et al., 2008). These are mostly low temperature emissions and can manifest in a variety of ways, including CO_2 vents (pressurised CO_2 release), diffuse soil degassing, CO_2-driven mud volcanoes, and CO_2-rich springs and pools of bubbling water (Chiodini, 2008; Minissale, 2004; Roberts et al., 2011). Several shallow and deep boreholes are also known to seep CO_2; these are not natural seeps but do indicate the presence of subsurface CO_2 accumulations.

Here, we draw on this wealth of surface and subsurface information to identify CO_2 reservoirs and establish which are located close to CO_2 seeps and therefore may be leaking. We compare reservoir and overburden characteristics of these case studies to elucidate the geological and structural conditions which determine if a CO_2 reservoir is sealing or not. CO_2 fluid properties (density, buoyancy, solubility) at top reservoir conditions are calculated to establish the minimum CO_2 flux from seeping reservoirs and investigate the permeabilities necessary to enable such fluid escape.

5.1.2 CO_2 Properties in Geological Formations

Flow of CO_2 fluids in the reservoir

Free phase CO_2 fluids are retained in geological formations in either a free dense or light phase or dissolved form (where we define 'dense' as CO_2 with densities greater than the critical density (ϱ_c = 464 Kg m^{-3}) and 'light' as CO_2 fluids with densities below the critical density). Free phase CO_2 will dissolve if it is in contact with unsaturated formation waters (Gilfillan et al., 2009), increasing the water density (Spycher et al., 2003). In contrast, free phase CO_2 will be less dense than surrounding pore waters and will buoyantly rise and may become structurally trapped beneath a sealing horizon, if such a structure is present.

Fluid flow through pore space in rocks is commonly approximated by capillary (or 'Darcy' flow), which is governed by the equation:

$$\frac{Q}{A} = \frac{K_E}{\mu} \cdot \frac{\delta P}{\delta z} \qquad [5.1]$$

where Q (flux) is CO_2 flux rate (m^3s^{-1}) over the seepage area, A (m^2), K_E is the effective permeability of the fluid (m^2), $\delta P/\delta z$ is the pressure gradient,(Pa m^{-1}) where P is pressure and z is depth, and μ is CO_2 viscosity (Pa s^{-1}). $CO_{2(d)}$ is more viscous and less-buoyant than $CO_{2(g)}$ and will therefore flow less readily according to equation [5.1].

Single phase flow accesses all rock permeability. Therefore, if CO_2 saturated and CO_2 unsaturated waters are assumed to behave as one phase, as is the case for many reservoir simulators, for CO_2 saturated water flowing through a water-wet rock, K_E is equal to the rock bulk permeability, K_{rock}.

However, for two phase flow, such as CO_2 flowing through a water-wet rock, the relative permeability, $Kr_{CO2,}$ describes the fraction of the total permeability accessible to each phase, therefore effective permeability for CO_2 is determined by:

$$K_E = K_{rock} \cdot Kr_{CO2} \quad [5.2]$$

A rock volume will commonly exhibit a distribution of fluid pathway geometries due heterogeneity intrinsic to geological units and the presence (and orientation) of rock fractures. Here, K_{rock} represents the bulk permeability of a rock volume, where permeability is provided by matrix or fracture flow (Bogdanov et al., 2007; Paluszny and Matthai, 2010).

Relative permeability is influenced by the formation water saturation in the pores or fractures through which the CO_2 is flowing. Experiments to determine Kr_{CO2} in carbonates are few, but (Bachu and Bennion, 2008) find Kr_{CO2} varied from 0.06 to 0.53 at irreducible water saturations (i.e. minimum water saturation excluding drying out effects) and that $CO_{2(d)}$ typically has lower Kr_{CO2} than $CO_{2(g)}$. Once flow is established at the maximum CO_2 saturation in relative permeability experiments, Kr_{CO2} may increase further by 'drying' effects, whereby formation fluids dissolve into the flowing CO_2 phase.

The role of fractures

Crustal fluid flow is commonly controlled by deformation induced permeability of fault and fracture networks (Faulkner et al., 2010). The damage zone and impermeable core properties of evolved faults behave as a fluid barrier-conduit system. The permeability of uncemented fractures in the damage zone is a function of effective normal stress, and is influenced by many factors including fracture size,

aperture, and orientation to the stress field (and therefore the stress state of the fracture). Connected, uncemented macro/mesoscale fractures dominate fluid flow in the shallow crust but become mechanically sealed with confining pressure (depth). Microfractures dominate rock permeability at depths below ~1.5 km (Nara et al., 2011).

Rocks are weak in tension, so to open fractures the fluid pressure only needs to exceed the rock tensile strength or minimum stress. Elevated fluid pressures can lead to hydraulic opening of fractures and enhanced permeability (Gudmundsson et al., 2001; Yang and Manga, 2009). CO_2 buoyancy or fluid pressure could therefore increase the rock fracture permeability and, in extreme cases can encourage rock failure (Collettini et al., 2008).

Fluid Mass Transport

Mass transport considerations must be addressed when investigating the movement of fluids in the subsurface. Conservative mass transport refers to flow of fluids which experience no chemical alteration and no interactions with the rock matrix (and so the rate of fluid accumulation is the difference between fluid mass inflow and the fluid mass outflow). The distribution of flow pathways (matrix, fracture - i.e. relative permeability) will result in both longitudinal and lateral dispersion. In reality, reactive transport processes (sorption, dissolution or decay) can occur as a result of fluid interaction with the rock matrix. Therefore the fluid mass that flows into a rock volume can be quite different to the fluid mass that flows out of the rock volume.

The mass balance equation describing hydraulic flow for a unit volume can be expressed as:

$$Q = Ss \frac{\partial P}{\partial t} - \nabla \left(\frac{k}{\mu} (\nabla P + \varrho g \nabla z) \right) \qquad [5.3]$$

where Ss is the specific storage (Pa^{-1}), P the pressure, k the permeability, μ the fluid dynamic viscosity, ϱ the fluid density, g the acceleration of gravity, z the depth, and Q is the flow rate (s^{-1}).

The specific storage term refers to the volume of fluids released from a saturated aquifer per unit decrease in hydraulic head. Hydraulic head can decrease in response to fluid pressure decrease or effective stress increase. The specific storage therefore represents mechanical compaction in response to stress, or by change in fluid volume in response to thermal or pressure effects (McDermott et al., 2006) which relates to the fluid compressibility. CO_2 compressibility is determined by the CO_2 state; light phase CO_2 is more compressible than dense phase. Examining equation [5.3] shows how responsive the CO_2 flux (Q) is to the pressure conditions, which include confining pressure related to depth, or CO_2 fluid pressure from overpressure or buoyancy effects.

Migration of CO_2 from the reservoir

Dissolved and free phase CO_2 can seep from the reservoir by diffusion, but this is an extremely slow process (Bachu and Bennion, 2008; Lu et al., 2009; Zweigel et al., 2004). More rapid migration of CO_2-bearing waters may be achieved by pressure (hydraulic head, reservoir over pressure) or thermal effects. However, high seep rates through the overburden of natural reservoirs will most likely arise from a buoyant CO_2 phase which may seep by (i) capillary transport through pores or microfractures in the reservoir overburden, or by (ii) unsealed faults (Zweigel et al., 2004). Otherwise, the overburden units may be bypassed if CO_2 'spills' from a trapping structure. In this case, the reservoir overburden has not been compromised, but the space for CO_2 in the reservoir has simply been exceeded.

The capillary entry pressure of CO_2 determines the CO_2-column height in the reservoir before CO_2 to invades the seal by capillary transport. The capillary entry pressure is a product of the fluid interfacial tension (IFT) and the contact angle in the wetting phase (i.e.water), and influenced by the rock pore and pore throat geometry, or fracture length, aperture and roughness (Bachu and Bennion, 2008; Naylor et al., 2011).

Subsidiary reservoir fluids can affect CO_2 capillary entry pressures, wettability and fluid mobility. For example, small proportions of CH_4 mixed with CO_2 will increase the IFT and decrease the density (Naylor et al., 2011) of the fluid mixture, whereas H_2S decreases IFT (Bennion and Bachu, 2008; Savary et al., 2012).

Following capillary breakthrough, CO_2 flow through the seal and overlying overburden occurs at capillary pressures below the entry pressures due to hysteretic effects.

CO_2 migration through the overburden to surface seepage

The area of degassing at Italian CO_2 seep sites is relatively discrete, often degassing over an areal extent less than ~100 m². However, seepage from the reservoir may have occurred over a greater area and fluids have become more channelized during shallow ascent. A proportion of the CO_2 charge will become residually trapped in the pore throats. If the rock pore fluids are hydrodynamically replenished by unsaturated fluids, the residually trapped CO_2 will progressively dissolve into the surrounding pore waters, reducing the free fraction. Where pore waters are not flowing, residually trapped CO_2 will equilibrate.

Significant CO_2 dissolution requires adequate mixing with formation waters. Such mixing will only occur at the CO_2 flood front, where CO_2 is mobile and in contact with pore fluids. Residually trapped CO_2 is isolated and so dissolution can only occur slowly across boundaries involving surface tension effects. Low permeability rocks and channelised flow along permeable pathways does not encourage significant CO_2 mixing with pore fluids. Some CO_2 will dissolve into the formation waters during ascent, especially if the seeping fluids accumulate in overlying secondary reservoirs (Pruess, 2008). When leak paths establish, the amount of free CO_2 can also attenuate by several mechanisms, and CO_2 leakage from a subsurface reservoir may not initially result in CO_2 seepage to the surface.

CO_2 solubility in water varies with CO_2 density, and therefore rapidly declines across the phase transition from dense to gas phase (Spycher and Pruess, 2005; Spycher et al., 2003). If CO_2 bearing waters mix with saline or thermal waters the

CO_2 will be rapidly released from solution. At depths shallower than ~700 m, CO_2 will pass through two hydrologic zones; the phreatic, saturated zone and the vadose, unsaturated zone. CO_2 will be in gas phase at these depths, and will therefore be more buoyant than waters in the phreatic zone. Cool CO_2, however, will be denser than soil gas in the vadose zone which can encourage lateral CO_2 dispersion above the water table (Annunziatellis et al., 2008; Kirk, 2011).

5.1.3 Regional Geological Setting

Westward subduction of the Adria plate beneath the European margin has developed a strong regional NW-SE structural grain in Italy. In the Miocene, Jurassic-Eocene flysch units and synorogenic foredeep sediments were tectonically stacked above the thick, thrusted, semi-autochthonous Mesozoic-Tertiary carbonate Platform sequence (see Figure 5.1A). Eastward younging foredeep and piggyback basins document the migration of the compression belt toward the foredeep, related to slab retreat (Ghisetti and Vezzani, 2002; Patacca and Scandone, 2007; Scrocca, 2005). Coeval extension opened marine and continental basins and the Tyrrhenian Sea.

Today, it is generally agreed that the Italian Adria - European collisional margin coincident beneath the Apennine Mountain belt is not longer active and subduction is constrained to the Calabrian Arc (Ghisetti and Vezzani, 2002). The Tyrrhenian sector preserves the older extensional system and exhibits a thinned crust and associated high heat flow, and here CO_2 degassing at surface seeps is most widespread (Chiodini et al., 2004), see Figure 5.1B. Andesitic-rhyolitic and potassic volcanism in the peri-Tyrrhenian has been active since ~0.9 Ma, which likely coincided with elevated regional CO_2 flux.

Seismogenic normal faulting is currently active in the Apennine Mountains in response to gravitational collapse. Exposed fault scarps date from 12-18 Ka (Roberts, 2008), and most normal faults have comparable offsets (~2 km) and slip rates (~1 mm y^{-1}) but young from west to east (Ghisetti and Vezzani, 2002). Here, trapped CO_2 fluids at depths > 5 km play a critical role in the nucleation and evolution of

seismogenesis, and therefore deformation style and geodynamics of the region (Miller et al., 2004). The Apennines are bordered to the East by the Adriatic foredeep, which is filled by deep Pliocene-Pleistocene deposits (Scrocca, 2005). Crustal heat flow and CO_2 flux in the Adriatic domain is much reduced, instead the foredeep is characterised by CH_4 seeps and mud volcanoes (Etiope et al., 2007; Martinelli and Judd, 2004).

Our study focusses on Central Italy where CO_2 flux is greatest. In this region there are several stacked domains which derive from the paleogeographic structure of the carbonate platform (see Figure 5.1A). These domains, presented from East to West in table 5.1, were originally located on the same Apulian Paleozoic crystalline basement (Scrocca, 2005) and often several first order thrusts separate tectonic units of the same stratigraphic succession. CO_2 seep and subsurface reservoir locations correlate with deep Mesozoic carbonate structures (Roberts et al., 2012).

Table 5.1: Geological Domains in Italy detailing the 6 geological units shown in Figure 5.1A. Most CO_2 reservoir case studies are hosted by the Apulian Carbonate Platform (ACP) in the Inner Thrust Belt, and the Allochthonous Complex form the overburden. These domains correlate with particular deformation styles, crustal permeability (Ghisetti and Vezzani, 2002) and geofluid phenomena. Lacustrine or continental Plio-Pleistocene deposits are common basin deposits throughout Italy.

Domain	Unit	Era	Geological Description		Extra Information
A: Internal nappes	*Liguride-Sicilide basin*	Cretaceous - early Miocene	Sediments from the Neotethyan oceanic domain.		
B: peri-Tyrrhenian domain	*Western Carbonate Platform (WCP)*	Late Triassic - early Miocene	A thick succession (up to 5 km) of shallow-water carbonates overlain by hemipelagic and siliciclastic deposits. Typically detached along an intra-Triassic surface. Dissected by systems of NW–SE oriented, west-dipping normal faults that merge with low-angle normal faults (Ghisetti and Vezzani, 2002).		High crustal heat flow from the thinned crust and magmatism has developed hydrothermal fluid systems. CO_2 degassing is most widespread in this domain; there are several CO_2 bearing structures but, despite some wildcat discoveries, no commercial hydrocarbon reservoirs (Casero, 2005)
C: Allochthonous Complex (Flysch)	*Lagonegro*	Middle Triassic-Early Cretaceous	Basinal carbonates composed of two superimposed nappes of distal (upper) and proximal (lower) basinal facies.		Tectonised by imbricate and out of sequence thrusting over the carbonate Platform units and conformably overlain by later thrust-top deposits. Cross cut by subsequent normal faults.
	Sannio	Late Cretaceous-early Miocene	Pelagic deposits ~ 1500 m thick, including the Argille Varicolori (Varicoloured Clays) and sandstones. Separated from the underlying Lagonegro by a detachment.		
	Molise	Messinian	Foredeep deposits; completely detached from their original substratum.		
D: Inner Thrust Belt	*Apulian Carbonate Platform (ACP)*	Mesozoic - Miocene	5 - 7 km thick unit of shallow water carbonate platform. Shows low permeabilities (<0.01 mD) if unfractured, whereas fractured ACP show over 100 mD permeabilities. Overlies the Burano formation, a ~ 2 km sequence of upper Triassic evaporitic rocks.	Stratigraphically overlain by upper Messinian and Pliocene terrigenous deposits. Characterised by Plio-Quaternary basins bounded by steep dipping (50–70°) NNW–SSE oriented normal faults and filled by continental lacustrine sequences.	Commercial and non-commercial hydrocarbon discoveries are hosted by the fractured ACP in eastern margin of the overthrust belt (Casero, 2005). Italy's largest CO_2 seep, Mefite D'Ansanto is located above a CO_2 reservoir in this domain (Chiodini et al., 2010)
E: Outer Thrust Belt				Structurally beneath the Inner, overthrusted, counterpart. Pliocene–Pleistocene normal faults dip >60° and separate preserved thrust units.	CO_2 seeps are rare, and few hydrocarbon accumulations have been discovered in the outer thrust.
F: Adriatic foredeep	*Bradanic Trough*		The Adriatic foredeep and Apulia foreland, where folding, thrusting and strike-slip tectonics are still active. The foredeep is filled with Pleistocene deposits.		Here gas and condensate deposits are found and mud volcanoes and methane seeps are common, but there are no CO_2 seeps.
G: Thrust sheet top units		*Miocene - Pliocene*	Sedimentary units (turbidites, muds, sandstones and conglomerates) which unconformably overlie the thrust sheets of the Allochthonous Complex.		There are many thrust sheet top units, including the siliciclastic *Castelvetere Formation* and *Torrente Calaggio Complex*. All thrust top units are sometimes grouped together and referred to as the 'Irpinia Formation'.
		Pleistocene	Pleistocene terrigenous deposits unconformably overlie the outer margin of the Apennine Mountain chain.		They represent sudden rapid deposition filling structural depressions related to the development of extensional tectonics at the Pleistocene/middle Pleistocene boundary

5.1.4 Part I: Case Study Reservoirs

5.1.4.1 Methodology

Non-commercial well logs in Italy have been made publicly available (www.videpi.com) along with associated drilling notes. We identified case studies where reservoir fluids in well tests are dominantly composed of CO_2. CO_2 seep location, type, flux, gas composition and temperature were elicited from Googas (Chiodini, 2008) a web-based catalogue of degassing sites in Italy and Sicily. Collaboration with ENI, Independent Resources and Googas researchers, and personal fieldwork broadened our dataset. Spring type seeps in this catalogue are selected for those showing significant deep CO_2 contributions. Seep flux is measured in tonnes per day ($t_{(CO2)}d^{-1}$) and classified into low (<1), medium (1-10), high (10-100) and very high (<100) categories.

We examined a geospatial dataset of drilled wells, CO_2 seeps and geological information (see supplementary information for detail). Where CO_2 reservoirs are not associated with surface seeps these reservoirs are considered to be sealing.Wells located close to CO_2 seeps which do not show CO_2 are also selected since i) these wells may contain CO_2 in its dissolved form, or ii) may have been drilled off the CO_2 bearing structure, if present, and can therefore provide information on the subsurface structure and conditions.

Many of the selected wells were drilled in the 1960s and 1970s and therefore lack downhole information available from modern technologies. Pressure information was derived from the mud density of drilling fluids and by formation tests. Pressures obtained from mud density will systematically over estimate the formation pressure by approximately 10%, which we correct for.

A number of the wells lack information required to calculate corrected geothermal gradient from down hole temperature measurements. Where down well temperatures are unavailable or they are unusually cool, the geothermal gradient

for that well was interpolated from a 1 km isotherm from the Ministry of Economic Development National Inventory of Geothermal Resources (Geothopica, 2010).

5.1.4.2 Case Studies

The location of the studied wells (both CO_2 bearing and neighbouring dry wells) and seeps closest to these wells are shown in Figure 5.1B, and further well information is detailed in SI Table 5.3. Figure 5.1 also shows the locations of nearby wells which are known to contain CO_2 but are not publicly available so not studied here (Castelpagano 001, Vallauria). 7 CO_2 bearing wells are spatially located close to CO_2 seeps (wells MF1, Tr1, SAT1, MT1, Ac1, and PSS1).

The studied CO_2 bearing wells are from five CO_2 fields in Central Italy; Frigento, Benevento, Acerno, and Muscillo, and the Pieve Santo Stefano CO_2 reservoir in the Northern Apennines. Figures 5.2 shows the location and 5.3 A-D show the structure of these fields. In the following section, we first detail the geological structure of the CO_2 reservoir case studies, then compare the geological characteristics of leaking and sealing reservoirs.

Figure 5.1A: Cross section of Italy modified from (Improta et al., 2000) detailing the 6 domains described in Table 5.1. Most CO_2 reservoirs are hosted by the Apulian Carbonate Platform (ACP) in the Inner Thrust Belt, and the Allochthonous Complex form the overburden. **1B: Structural sketch of Italy** modified from (Patacca et al., 2008) detailing topography and the location of CO_2 seeps (dry and wet) and studied wells, terrain boundaries (Ghisetti and Vezzani, 2002), and moho depth contours (Di Stefano, 2011). The Pieve Santo Stefano 1 (PSS1) well and nearby Caprese Michelangelo seep cluster are shown to the North of the Apennines. **1C: Map of the Southern Apennine region**, showing the location of CO_2-bearing wells, depth to top APC carbonate structure (Nicolai et al., 2007) where known, stress field data (Barba et al., 2009) and mapped seismogenic normal faults (Roberts, 2008). **Table inset:** Detail of seeps shows in (C), including name, seep type and flux information. **Abbreviations**: Ben1 = Benevento 001, Ben2 = Benevento 002, BS1 = Benevento Sud 001, Tr1 = Tranfaglia 1; SAT1 = S. Arcangelo di Trimonte 1, MF1 = Monte Forcuso 001, MF2 = Monte Forcuso 002, Cic1 = Ciccone 1; Ac1 = Acerno 1, Co1 = Contursi 1; Mu1 = Muscillo 1.

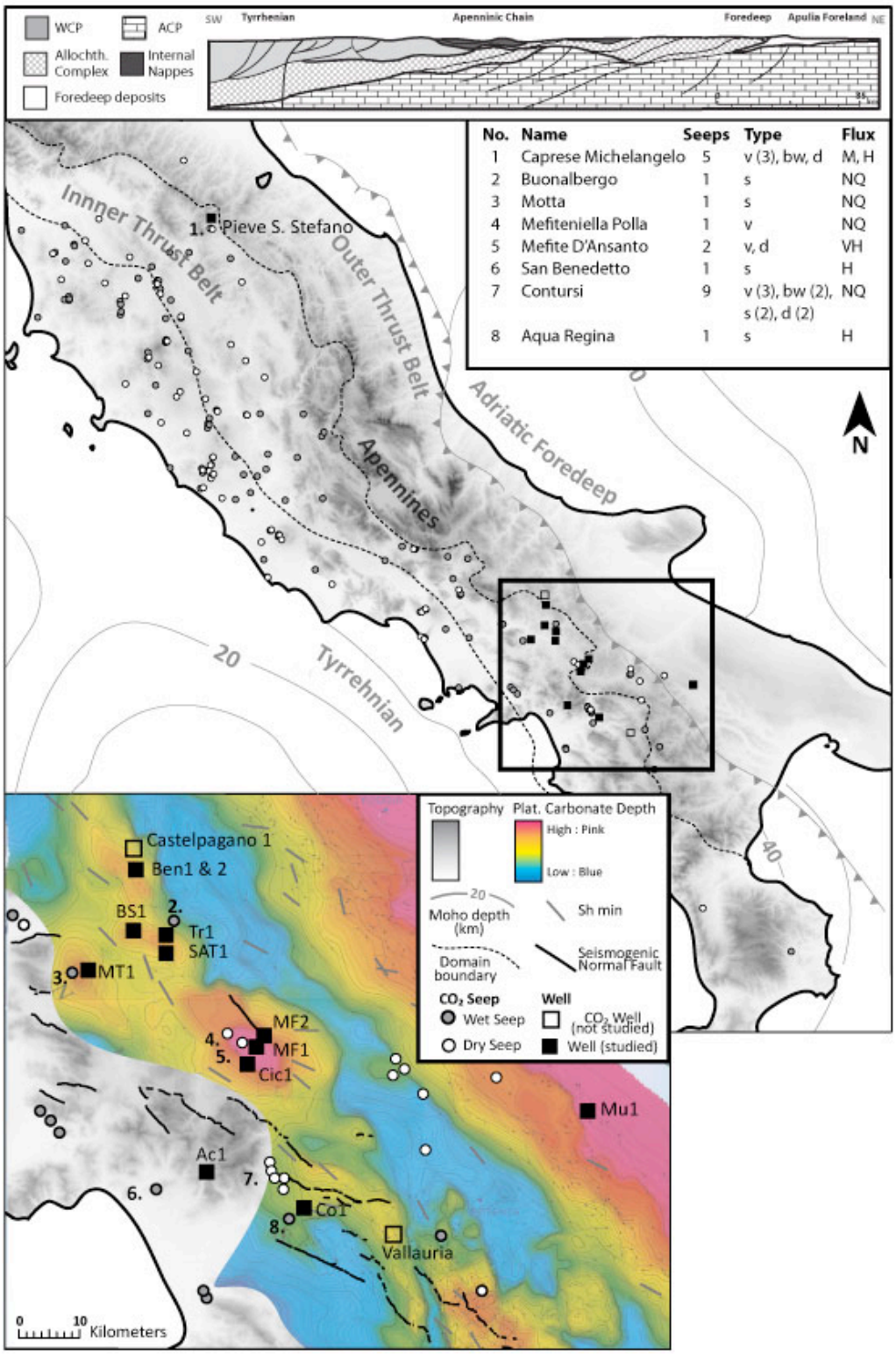
WCP
ACP
Allochth. Complex
Internal Nappes
Foredeep deposits
SW
Tyrrhenian
Apenninic Chain
Foredeep
Apulia Foreland
NE
No. Name Seeps Type Flux
1 Caprese Michelangelo 5 v (3), bw, d M, H
2 Buonalbergo 1 s NQ
3 Motta 1 s NQ
4 Mefiteniella Polla 1 v NQ
5 Mefite D'Ansanto 2 v, d VH
6 San Benedetto 1 s H
7 Contursi 9 v (3), bw (2), s (2), d (2) NQ
8 Aqua Regina 1 s H
Inner Thrust Belt
Outer Thrust Belt
Apennines
Adriatic Foredeep
Tyrrehnian
Pieve S. Stefano
20
40
N
Topography
Plat. Carbonate Depth
High : Pink
Low : Blue
Moho depth (km)
Sh min
Domain boundary
Seismogenic Normal Fault
CO2 Seep
Wet Seep
Dry Seep
Well
CO2 Well (not studied)
Well (studied)
Castelpagano 1
Ben1 & 2
BS1
Tr1
SAT1
MT1
MF2
MF1
Cic1
Mu1
Ac1
Co1
Vallauria
0 10 Kilometers

5.1.4.3 Case Study Characteristics

Benevento CO_2 Field

The large Benevento CO_2 field is documented by three wells (BS1, SAT1, Tr1, see Figure 5.2) where, regionally, the ACP deepens northeastward (1.5 km in SAT1 to 2.7 km in BS1, see Figure 5.1C). There are continuous CO_2 shows from ~2707 m to 4139 m in the BS1 well (1432 m gross CO_2 column). Methane (CH_4) is the primary gas in the Tr1 well from 400 m depth until CO_2 reservoir, and BS1 shows up to 5.1% CH_4 fluid composition by volume (*C%v.v*). The CO_2 reservoirs are at hydrostatic pressure for BS1 and Tr1, which both have a thin Miocene evaporite cap, but show overpressure in the shallower SAT1 well. CO_2 in this field exists in dense (BS1) and gaseous (Tr1) phase, and the SAT1 contains CO_2 at conditions close to the phase transition. The Allochthonous Complex overburden record overpressure above 10 MPa in all three wells. The Buonalbergo CO_2 spring is located 3.5 km from TR1 well but no further information is known about this seep (flux, temperature etc).

To the North, the Benevento 001 (Ben1), and Benevento 002 (Ben2) wells also find CO_2 at ~ 3 km depth. These wells drill a broad structural high (see Figure 5.1C), and are also found to contain some light hydrocarbons (max 6.2% CH_4 *C%v.v*) at ~3.3 km (Ben2). These wells show significant overpressure above hydrostatic in the overburden, but the reservoirs are hydrostatically pressured. There are no CO_2 seeps in the vicinity of these wells and are therefore considered to be sealed.

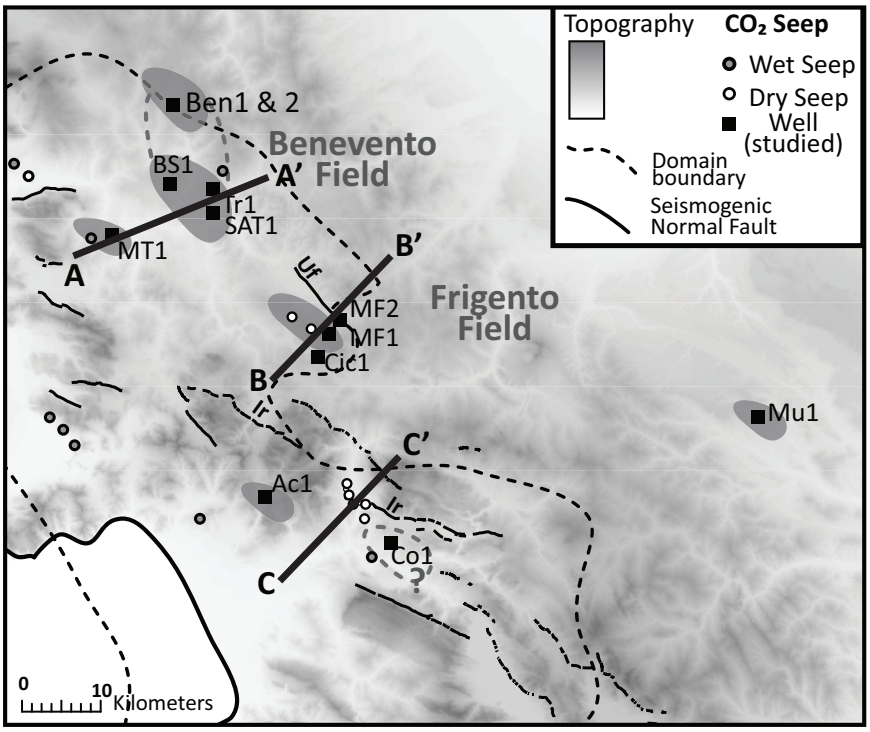

Figure 5.2. Location map of case study CO_2 fields and cross sections presented in figures 5.3A-C.

Monte Taburno CO_2 Reservoir

To the East of the Benevento CO_2 field, the Monte Taburno (MT1) well drills a separate structure containing CO_2 at 2.6 km depth (Figure 5.3). The reservoir is directly capped by mio-pliocene thrust top deposits. Overburden pressures are hydrostatic, but the CO_2 reservoir shows ~9 MPa overpressure to SAT1 and contains CO_2 in its supercritical state. The MT1 well is located 7 km from the Montesarchio and Ioannis seismogenic normal faults (Roberts, 2008), and 1.6 km from Motta, a thermal spring with small CO_2 emission (Chiodini, 2008) for which no further information (flux, temperature etc) is known.

Muscillo CO_2-CH_4 Reservoir

The Muscillo (Mu) well, located in the Outer Thrust domain, documents a shallow CO_2-CH_4 reservoir (See Figure 5.3). The CH_4 leg shows low gas saturation and overlies a CO_2 gas and water '*mixture*' which starts at 694 m below the surface. Down well pressures are hydrostatic in the overburden and the reservoir and there are no CO_2 seeps in the vicinity of this well.

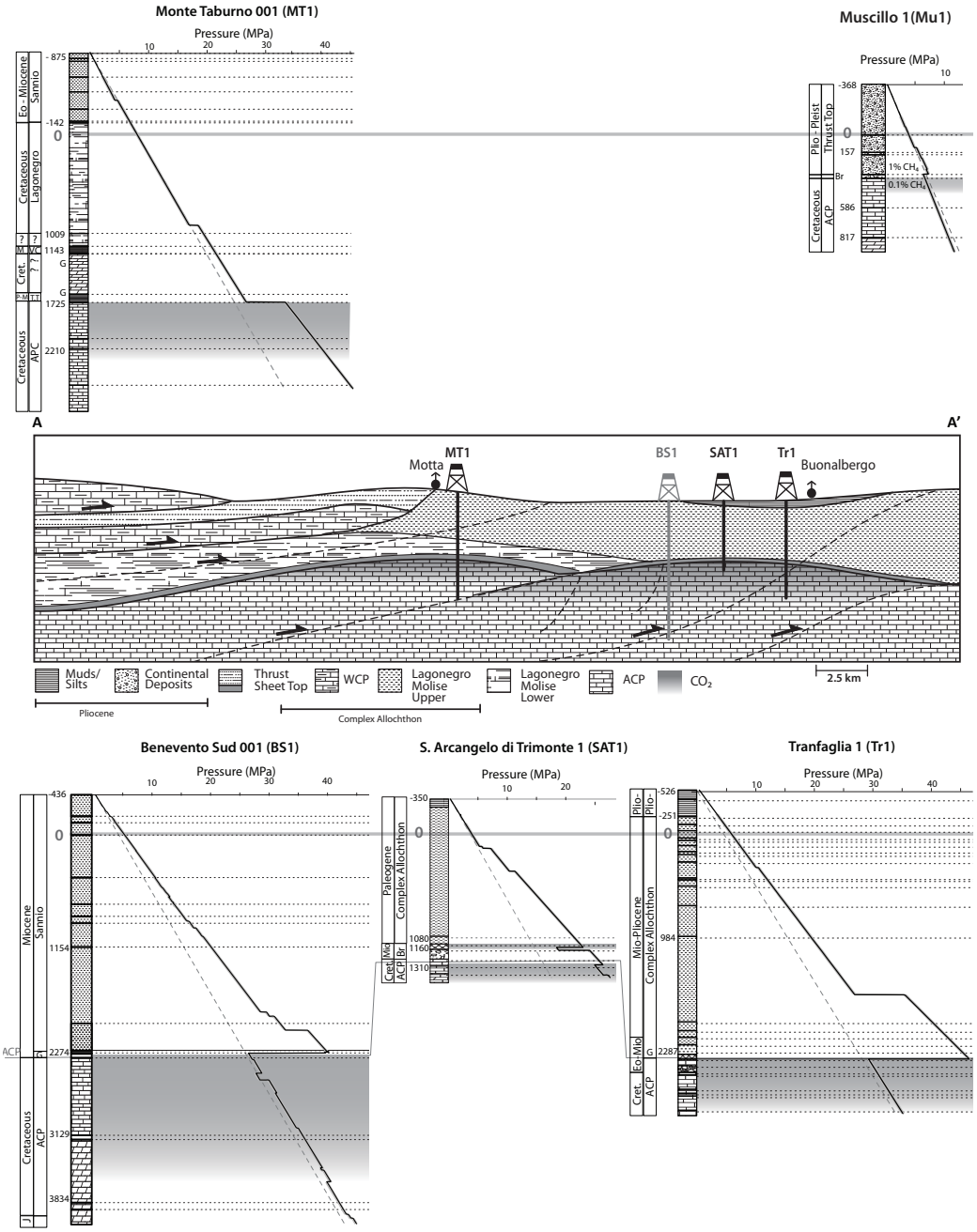
Monte Taburno 001 (MT1)
Pressure (MPa)
10
20
30
40
Eo - Miocene
Sannio
Cretaceous
Lagonegro
Cret.
APC
-875
-142
0
1009
1143
1725
2210
Muscillo 1(Mu1)
Pressure (MPa)
10
Plio - Pleist
Thrust Top
Cretaceous
ACP
-368
0
157
Br
586
817
1% CH4
0.1% CH4
A
A'
MT1
Motta
BS1
SAT1
Tr1
Buonalbergo
Muds/
Silts
Continental
Deposits
Thrust
Sheet Top
WCP
Lagonegro
Molise
Upper
Lagonegro
Molise
Lower
ACP
CO2
2.5 km
Pliocene
Complex Allochthon
Benevento Sud 001 (BS1)
Pressure (MPa)
10
20
30
40
Miocene
Sannio
Cretaceous
ACP
436
0
1154
2274
3129
3834
S. Arcangelo di Trimonte 1 (SAT1)
Pressure (MPa)
10
20
Paleogene
Complex Allochthon
Cret.
ACP
-350
0
1080
1160
1310
Tranfaglia 1 (Tr1)
Pressure (MPa)
10
20
30
40
Plio
Mio-Pliocene
Complex Allochthon
Eo-Mio
Cret.
ACP
-526
-251
0
984
2287

Figure 5.3 A: Benevento and Monte Taburno structures and pressure-depth profiles for the Tranfaglia (Tr1), S. Arcangelo di Trimonte (SAT1), Benevento Sud (BS1), Monte Taburno (MT1) and Muscillo wells. It is unclear if the Motta and Buonalbergo CO_2 springs are related to the subsurface CO_2 fields, though they do exhibit significant deep CO_2 contributions. Note that BS1 and Tr1 show ACP at hydrostatic conditions. All three wells show significant overpressure in the overburden. SAT1 pressures indicate this reservoir is not connected to neighboring reservoirs, although this may be an artefact of poor mud weight information (as outlined in Table 5.2 accompanying text). In contrast, MT1 shows hydrostatic overburden and overpressured ACP reservoir. *Geological Units in 5.3A-D*: Lagonegro, L; Breccia, Br; Gypsum and Anhydrite, G; Undefined, ?; Thrust Top Deposits, T. T; Western Carbonate Platform, WCP; Apulian Carbonate Platform, ACP; Dolomite, D; Varicoloured Clay, VC. *Geological Eras*: Pleistocene, Pleist; Pliocene, Plio / Pl; Miocene, Mio / M; Eocene, Eo; Cretaceous, Cret/C; Triassic, Tri/T.

Frigento CO_2 Field

The Monte Forcuso 001 and 002 (MF1, MF2) and Ciccone (Cic1) wells drill the Frigento Antiform, see Figure 5.3B. This local structure in the ACP (Improta et al., 2003a) correlates with a gravity and thermal anomaly; the 1 km geotherm here reaches over 90°C/km at the crest of the structure. The MF1 well documents a ~472 m gross CO_2 column in the ACP at just over 1 km depth, above a fresh water leg. The MF2 and Cic1 wells located on the flanks of the anticline contain no CO_2, only fresh water (with traces of CO_2) and saline water respectively. The differences in formation salinity and pressure in Cic1 suggests structural partitioning from the MF1 and MF2 reservoir.

The regional stress field (Barba et al., 2009) shows NW-SE extensional faulting which is currently active. The 1980 Irpinia earthquake (M 6.9) nucleated on the Irpinia fault to the South of the reservoir and Ufito normal fault scarp is located less than a kilometer to the NE of the MF2 well (see Figure 5.2)(Improta et al., 2003b; Roberts, 2008). This fault lies above a the terrain boundary; a thrust detachment dividing the Inner and Outer Thrust belt (Ghisetti and Vezzani, 2002), so the ACP deepens drastically to the NE.

Loss of drilling fluid circulation or significant mud absorption can be useful indicators of geological horizons with enhanced permeability, or where the rock fracture gradient has been exceeded. There are no significant mud losses while drilling the MF1 well, but the operators experienced circulation loss at the reservoir top and again at 1787-1800 m. This caused a CO_2 blowout at 731 m depth following which the well was plugged. Regardless of whether the uncorrected borehole temperatures or isotherm temperatures are applied, the reservoir conditions in the Frigento structure show that CO_2 will be in gas phase, and CO_2 density increases with depth away from the anticline crest.

Mefite D'Ansanto and *Mefitiniella polla* CO_2 vents (seep no. 4 & 5 in Figure 5.1) are located close above the structural high point of the Frigento Antiform. These seeps are characterized by moderate temperature dry CO_2 venting (~15 - 30°C (Chiodini, 2008; Minissale, 2004)). Mefite D'Ansanto is Italy's highest flux CO_2 seeps which degasses over 2000 $t_{(CO2)}d^{-1}$ and exhibits a high mantle component ($R/Ra = 2.58$, $\delta^{13}C_{CO2} = 0.73$ (Minissale, 2004)). On the flanks of the Frigento antiform, less than 3 km from the gas seeps, are the San Teodoro thermal springs (~15-27°C, flow rates ~7 Ls^{-1} (Minissale, 2004)). These are Ca-CO_3-SO_4 type waters and their geothermometry suggests a reservoir temperature of ~ 125°C (Duchi et al., 1995). These chemical features indicate deep water circulation in carbonate rocks, and the springs are thought to arise from rapid fluid ascent related to faulting (Duchi et al., 1995). A travertine precipitating fluid seepage system might have once existed in this area since travertine deposits have been mapped within 5 km of the seeps but there have been no geochemical investigations to distinguish their age or CO_2 source.

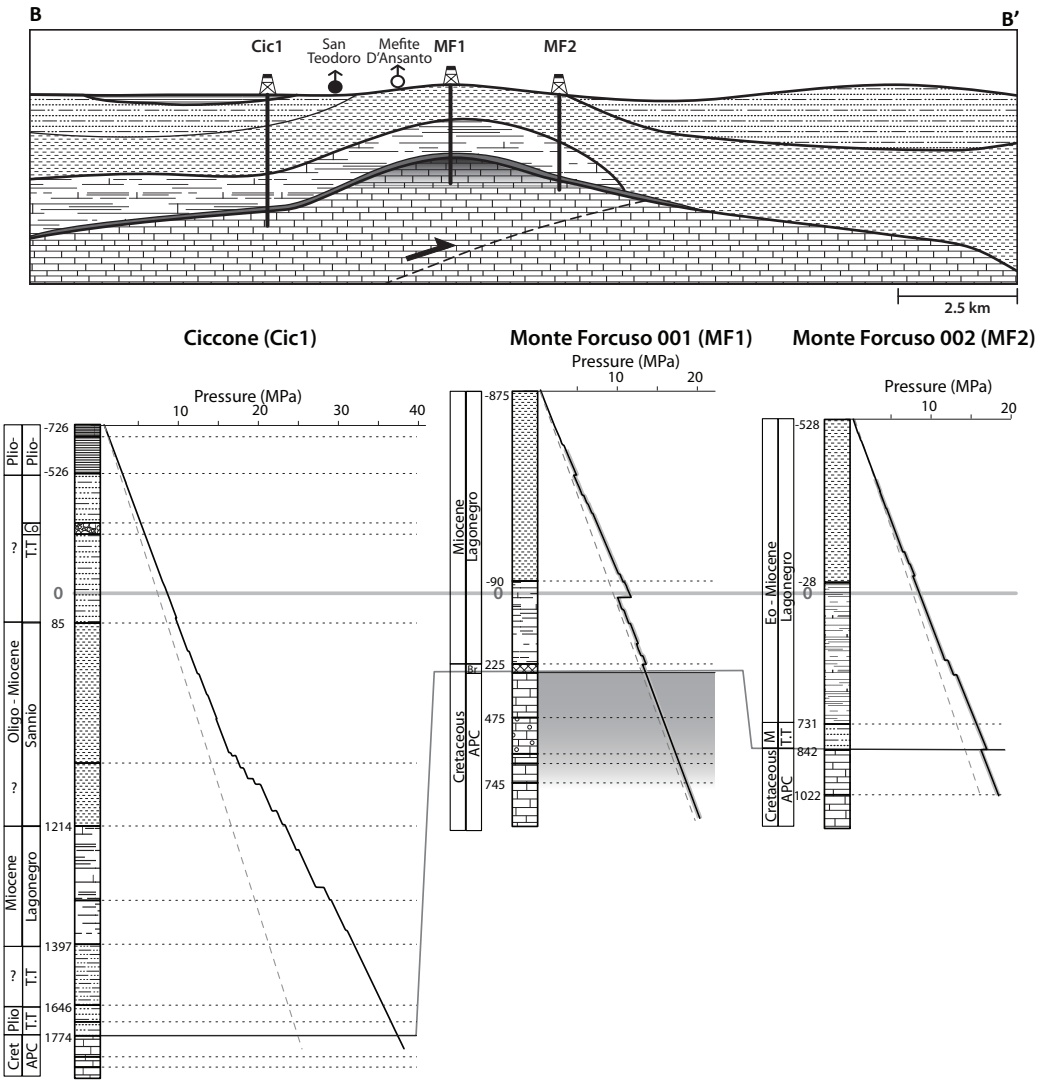

Figure 5.3B: Subsurface structure and the location the wells (Ciccone, Cic1; Monte Forcuso 1, MF1; Monte Forcuso 2, MF1) that drill the Frigento Formation. MF1 drills a CO_2 accumulation in the ACP at hydrostatic pressure, but MF2 and Cic1 drill into the water leg. Mefite D'Ansanto (and Mefitiniella polla not shown here) are high flux CO_2 vents. San Teodoro, located on the SW flank of the antiform, is a sulphurous thermal spring that does not degass CO_2.

Acerno CO_2 Reservoir

The Acerno well (Ac) penetrates the deepest CO_2 reservoir, located in a horst structure 4263 m beneath Mount Picentini (Figure 5.3C). Overpressure in the overburden continues into the ACP reservoir (λv=0.6). There was only one drill stem test, over a 192 m interval, yielding over 90% CO_2 in the dense phase. There are no CO_2 seeps located above the Acerno CO_2 bearing structure, but it is located 11 km ENE of the high flux San Benedetto CO_2 spring, and 15 km NW of the Contursi seep cluster (Figure 5.1B).

Contursi CO_2 Structure

The Contursi (Co) well is located within 5-10 km of a large seep cluster (seep no. 7 and 8) which includes CO_2 vents and diffuse degassing, CO_2 springs and bubbling waters, and one travertine depositing spring (see Figure 5.1C). These are located in a tectonic 'window' where the WCP is outcropping. The gases sampled from one of these edifices indicate a mantle contribution to the CO_2, little biogenic component ($R/Ra = 1.37$, $\delta^{13}C_{CO2} = 0.34$ (Minissale, 2004)) and high fluxes. Similar to the San Teodoro spring, the geochemistry of Contursi spring waters (seep cluster 8, Figure 5.1) is characteristic of deep carbonate circulation and is thought to represent rapid ascent related to faulting in the region (Duchi et al., 1995) although the spring flow rate is relatively low (1 Ls^{-1}). The dry gas seeps are cool (4.5°C) whereas springs exhibit a range of temperatures 15 - 44°C (Chiodini, 2008; Santo et al., 2011). The seep cluster is located in the relay zone between two normal fault scarps (see Figure 5.1) of the Marzano and Picentini Mountains, where karst collapse sinkholes are known (Santo et al., 2011).

Significantly, the Contursi well (see Figure 5.3B) does not reach the ACP and finds no CO_2 manifestation at depth, only 30 m column of fresh water at the top of the Western Carbonate Platform reservoir at ~1 km depth. The down well pressure profile shows only minor overpressure, and CO_2 conditions at depth are close to the CO_2 phase transition (see Appendix 4).

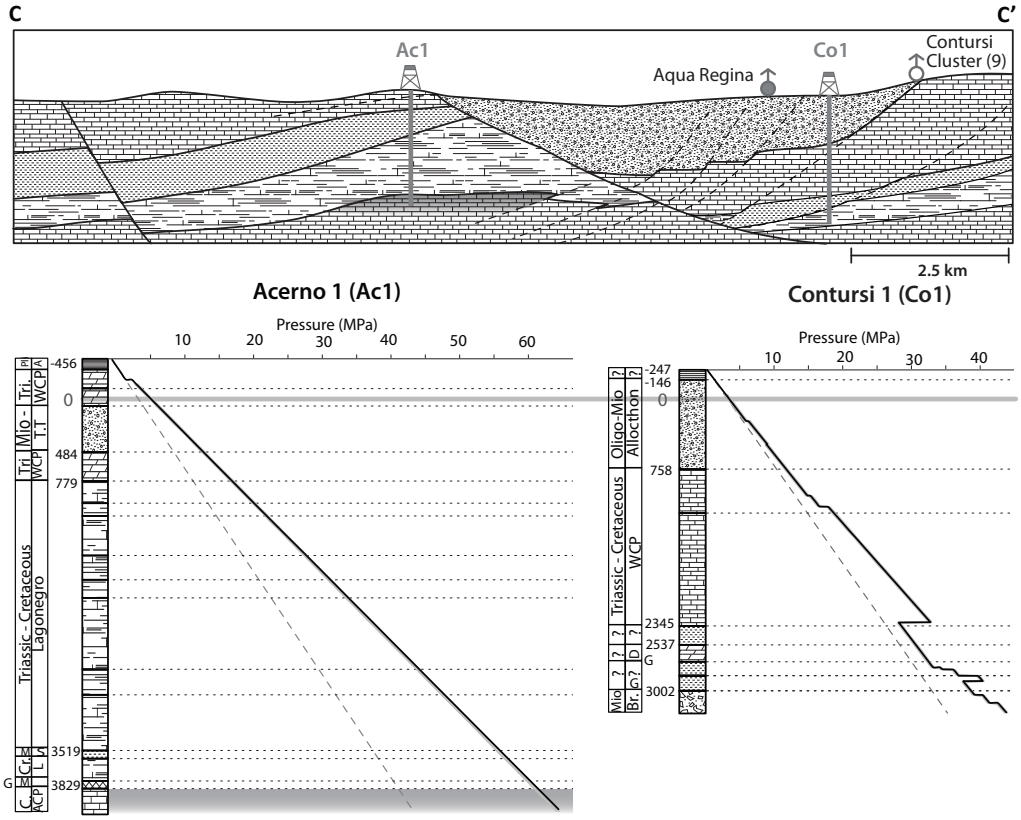

Figure 5.3C: Cross section of the Acerno and Contursi structures showing the location of the Acerno (Ac1) and Contursi (Co1) wells. The Contursi seep cluster is composed of 9 different CO_2 seeps located in a tectonic window of the WCP in the relay zone of theIrpinia seismogenic normal fault. The Contursi well did not discover any CO_2 accumulation at depth, but did not penetrate the ACP. No seeps are located above the Acerno horst structure.

Pieve Santo Stefano (P.S.Stefano) CO_2 Reservoir

To the North, the Pieve Santo Stefano (PSS1) well commercially exploits a multilayered CO_2 reservoir at ~3.6 km depth (Figure 5.3D). The well documents near hydrostatic overburden conditions and notes significant mud losses while drilling. The main CO_2 reservoir lies 300 m beneath a thin CO_2 accumulation and hosted by dolomites and evaporites of the Triassic Burano group (Bonini, 2009). These units are significantly overpressured and show saline formation waters. The regional subsurface structure here is poorly known.

The PSS1 well is located only 2.5 km from the Caprese Michelangelo (CM) seep cluster, which consists of 3 vents, 1 bubbling water and 1 diffuse type seep (seep no. 1 in Figure 5.1). The two seeps with quantified flux classify as medium and high flux seeps. The vents align E-W, along NE-SW trending faults in the NW-SE trending Tiber Valley graben (Bonini, 2009). The reservoir is located in the footwall Alto-Tiberina fault (Collettini and Barchi, 2002), which is an active structure and regional seismic events are common (Heinicke et al., 2006; ISPRA, 2007). Flux and degassing characteristics are observed to vary with local seismic events at these seeps (Bonini, 2009; Heinicke et al., 2006).

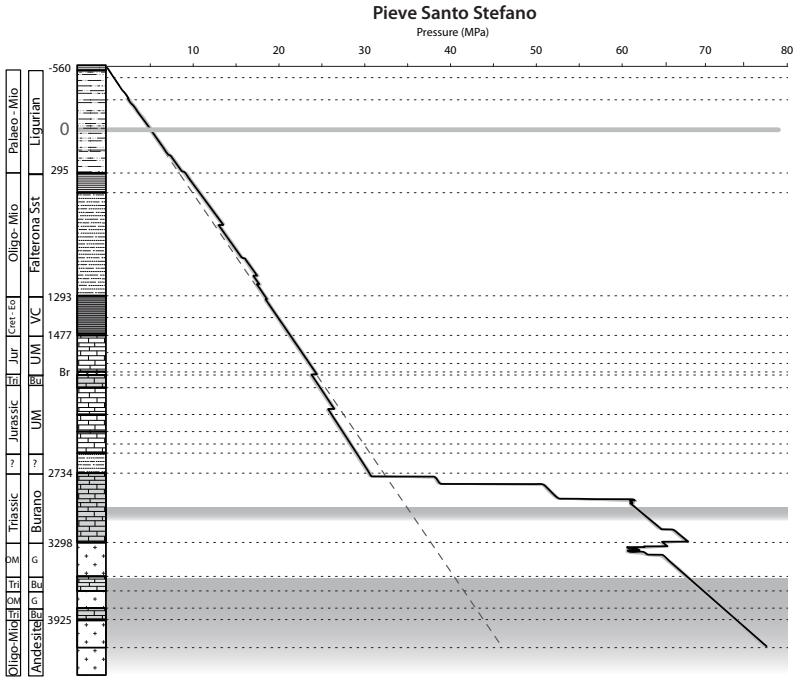

Figure 5.3D: Pieve Santo Stefano depth profile. CO_2 in this reservoir is hosted by the Burano Formation and is significantly above hydrostatic pressure conditions. The Caprese Michelangeo and Fungaia CO_2 vents are located near to the Pieve Santo Stefano well and are considered to represent surface seepage of the reservoir.

5.1.4.4 Analysis

The geological structure of the case studies are broadly similar; CO_2 reservoirs are hosted by anticline or horst structures in the Mesozoic carbonate units and are is typically capped by Thrust Top deposits and Allochthonous Complex overburden (see Table 5.1, C and G respectively for description). The thrusted contact between reservoir and overburden is marked by a tectonic breccia or by a Messinian evaporite unit in several wells.

Thermal springs in Italy tend to indicate rapid ascent from the buried ACP carbonate reservoir, facilitated by faults (Duchi et al., 1995). The Motta thermal CO_2 waters are likely sourced from the WCP or ACP but it is unclear if this represents leakage of the CO_2 reservoir discovered in MT1. With no further information regarding the Buonalbergo CO_2 spring, its relationship with the underlying Tr1 CO_2 structure is inconclusive. In all cases, the relationship between seeps and subsurface CO_2 reservoirs are hypothetical since both reservoir and seeping fluids lack sufficient geochemical information that would enable direct linkage.

Overpressure and Seepage

Some deviation from hydrostatic pressure is expected while drilling low permeability units since there is poor connectivity between the drill mud and the surrounding rocks, and so it is best practice to overestimate the pore pressure. Additionally, since the Allochthonous Complex and thrust top deposits have

experienced compressional tectonics and it is unsurprising if they preserve elevated pore fluid pressure (Osborne and Swarbrick, 1997).

Wells with overpressure in the overburden exhibit a significant pressure decrease when the ACP is initially penetrated. For all wells, penetrating the ACP is often associated with significant mud losses or circulation loss, indicative of overestimate pressure (and increased rock permeability). The reservoir carbon units have deformed differently to the overburden flysch and are often connected to the surface. Reservoir overpressure is observed in two CO_2 fields; P.S.Stefano and Monte Taburno. SAT1 well shows overpressure but, as noted in the text accompanying Table 5.2, mud weights here may overestimate the pressure conditions. The overpressure observed in the PSS reservoir (28 MPa above freshwater hydrostatic) is much greater than the error incurred by applying a freshwater hydrostatic profile to the saline formation waters of the Burano evaporites. In both PSS1 and MT1 the pressure gradient is close to hydrostatic.

Where the overburden has higher fluid pressures than the reservoir, the net pressure gradient over the reservoir-overburden interval is opposite to the lithostatic gradient. Fluids would therefore preferentially flow into the reservoir rather than up from the reservoir into the overburden. Since high pore fluid pressures are symptomatic of limited fluid flow, this net transport cannot occur. For these reasons, pressurisation of overburden units to decrease or reverse the fluid pressure gradient is proposed as a remediation option should leakage from a reservoir occur (Reveillere and Rohmer, 2011).

Reservoir and overburden pressure characteristics of CO_2 bearing wells are summarised in Table 5.2 and displayed in Figure 5.4. Where there is a significant CO_2 reservoir and the overburden is not overpressured, seeps are present at the surface (MT1, MF1, PSS1; Mu1 records low gas saturation and is therefore not a significant CO_2 reservoir). Where the overburden is significantly overpressured beyond hydrostatic pressure there are no (obviously connected) seeps present above the reservoir structure (BS1, SAT1, Ac1; Tr1), see Figure 5.4. The Co1 well, which did not penetrate the ACP, has near hydrostatic conditions in the overburden and is

located close to surface seeps. Aside from SAT1, these wells have evaporitic Miocene thrust top units directly overlying the ACP, which may be providing an effective seal.

We interpret that the Frigento, P.S.Stefano and Monte Taburno reservoirs are leaking, and postulate that, if present, a CO_2 reservoir in the ACP beneath the Contursi structure would also be leaking. Significantly, these wells are also located near seismogenic normal faults (Figure 5.1B).

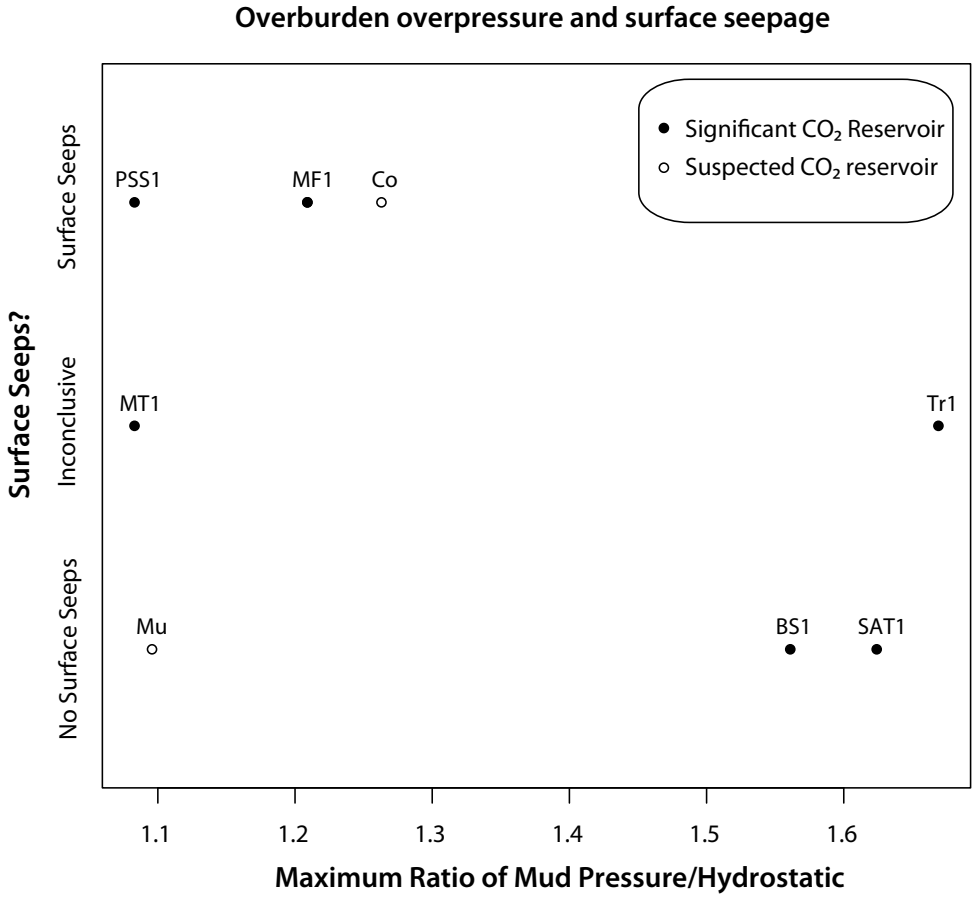

Figure 5.4: Overburden overpressure for studied CO_2 bearing wells, and the presence/absence of surface seeps. Significant CO_2 reservoirs with little overpressure in the overburden have surface CO_2 seeps spatially located at the surface. In contrast, significant CO_2 reservoirs with high overpressure beyond hydrostatic in the overburden do not have obvious surface seeps associated.

CO_2 Properties at Reservoir Conditions

CO_2 properties are modeled at top reservoir conditions (Huang et al., 1985; Span and Wagner, 1996) and we test their sensitivity to pressure and temperature uncertainty at 10 m intervals, for which we assume a standard error of ± 0.1 MPa and ± 5 °C, to 2 standard deviations. Many CO_2 reservoirs lack enough information to determine CO_2 column heights from which CO_2 buoyancy can be calculated. Formation pressure measurements are not sufficiently regular, nor are mud weights sensitive enough, to distinguish the reservoir CO_2/water legs from the pressure profiles. Formation tests for BS1 and MF1 document the transition from CO_2 to the water leg, and minimum column heights can be inferred from the well tests in some CO_2 reservoirs.

The buoyancy pressure (B) is calculated at the crest of the reservoir where column heights are known:

$$B = (\varrho_{H2O}-\varrho_{CO2}) \cdot g \cdot h_{CO2} \quad [5.4]$$

where ϱ_{H2O} is the density of water (Kg m^{-3}), ϱ_{CO2} is the density of the CO_2 (Kg m^{-3}), h_{CO2} is the CO_2 column height (m), and g is the gravitational acceleration (ms^{-2}).

Pressure and ϱ_{CO2} and, where possible, CO_2 buoyancy drive at top reservoir conditions in CO_2 bearing wells are shown in Figure 5.4. We find all the case study reservoirs contain CO_2 in gas or dense phase, and in some cases this CO_2 can be close to the critical point (see Table 5.2). No reservoirs contain liquid phase CO_2 (see figure 5.5). Pressure and temperature uncertainty lead to moderate calculated ϱ_{CO2} variation (± 10 Kg m^{-3}), although these effects are increased towards the phase transition.

CO_2 buoyancy alone does not determine whether a CO_2 reservoir is sealing or leaking. The sealing BS1 reservoir shows greater CO_2 buoyancy than the leaking MF1 reservoir. If BS1, SAT1 and Tr1 drill the same structure, buoyancy effects will be

greater in the Tr1 and SAT1 wells where the APC is considerably shallower. Applying BS1 CO_2 column heights to these wells find CO_2 buoyancy is 7.3 and 6.4 MPa m^{-2} respectively. Despite such potential buoyancy, these reservoirs are not obviously leaking. Relative permeability effects will restrict the mobility of CO_2 in Muscillo reservoir because gas saturation is so low. This therefore negates the buoyancy of these gaseous fluids.

When calculating CO_2 properties the effect of CH_4 and H_2S subsidiary gases were ignored. These gases are present in trace (<0.1% *C%v.v*) quantities in many of the case studies. Sealing reservoirs Ben2, BS1 and Mu1 show CH_4 compositions >5% *(C %v.v)*. CH_4 is less dense than CO_2 at the same conditions, therefore the buoyancy of the CO_2-CH_4 gas mixture in these wells will be underestimated. However, the increased IFT of the CO_2-CH_4 mixture will lead to an overall increase in capillary entry pressures. Minor quantities of CH_4 may therefore be enhancing reservoir sealing at these sites.

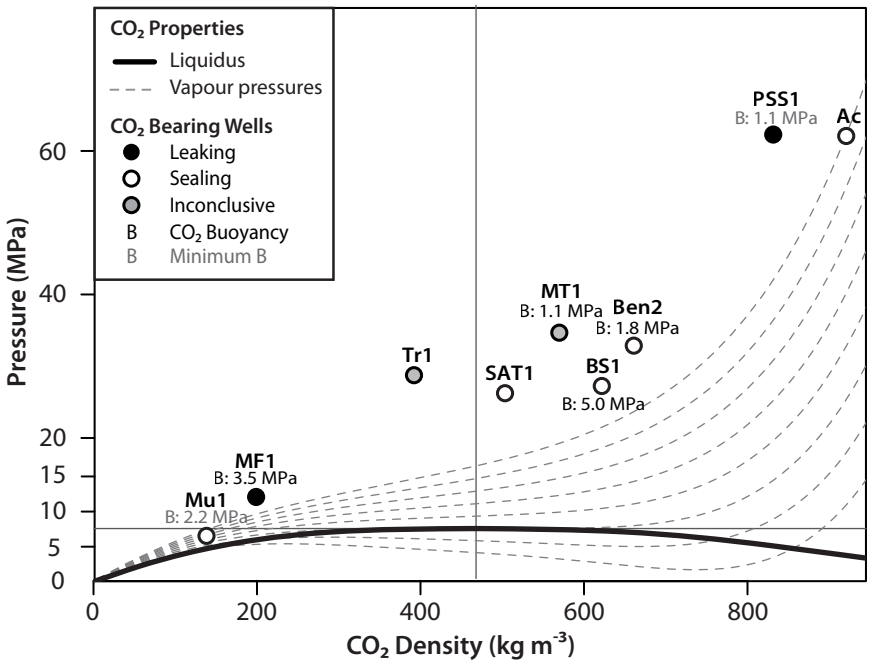

Figure 5.5: CO_2 pressure-density phase diagram detailing CO_2 density at reservoir/seal boundary of CO_2 bearing reservoirs. Calculated CO_2 buoyancy is shown next to the data points where information is available. In these case studies CO_2 exists as gas or dense phase. Neither CO_2 density nor buoyancy determines if a reservoir is sealing in these case studies.

Depth Profiles for CO_2 Properties

Wells with geothermal gradients cooler than 40 °C/km which show overpressure in the overburden (Ac1 and Ben1/2) exhibit depth-ϱ_{CO2} profiles that pass through the liquidus. Here, ϱ_{CO2} of CO_2 ascending form the reservoir changes very little until the phase transition from liquid to gas which is associated with ϱ_{CO2} decrease of ~600 Kg m^{-3}. These reservoirs are sealing.

Figure 5.6 shows ϱ_{CO2} variation with depth below surface using pressures derived from mud weights for end-member leaking CO_2 reservoirs PSS1 (28.4°C/km) and MF1 (93.3°C/km). To investigate the effects of reservoir overpressure, modeled ϱ_{CO2} at hydrostatic pressure conditions are plotted for the overpressured PSS1 reservoir, and ϱ_{CO2} for 10 MPa reservoir overpressure is plotted for the hydrostatically pressured MF1 reservoir.

Figure 5.6: Down well pressure-ρ_{CO2} profiles for MF1 and PSS1 plotted on a vapour pressure curve (A) and down well depth and density difference ($\rho_{H_2O\text{-}CO_2}$) profiles (B). Hydrostatic reservoir conditions are modeled to show the effect of the observed ~27 MPa overpressure in PSS1 CO_2 reservoir. MF1 reservoir exhibits hydrostatic conditions, which are modeled beyond the MF1 bottom hole depth to compare with the PSS1 profile. The effect of 10 MPa overpressure in the MF1 reservoir is modeled. Increased reservoir pressure decreases the density difference between CO_2 and CO_2 saturated waters, thereby decreasing the buoyancy drive of the fluids. This effect is particularly enhanced in the gaseous MF1 reservoir, which, if over pressured by 10 MPa, would show decreased buoyancy drive towards the reservoir top. The **vapour pressure curve (A)** shows how the cooler PSS1 passes closer to the liquidus, which leads to more rapid changes in density **(B)** as the fluids ascend to approach 1 km depth, and a pronounced change in solubility in fresh water **(3C)**. Note the rapid change in CO_2 solubility in both cases towards the phase transition.

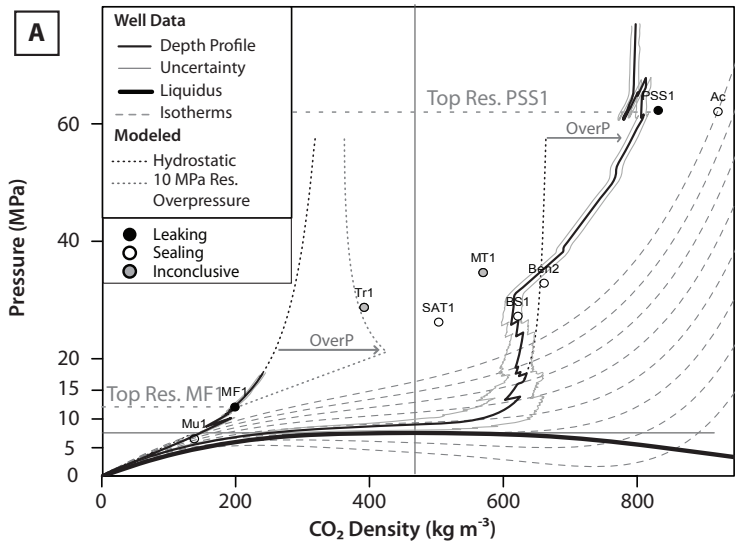
A
Well Data
Depth Profile
Uncertainty
Liquidus
Isotherms
Modeled
Hydrostatic
10 MPa Res.
Overpressure
Leaking
Sealing
Inconclusive
Top Res. PSS1
Top Res. MF1
OverP
PSS1
Ac
MT1
Bon2
BS1
SAT1
Tr1
MF1
Mu1
Pressure (MPa)
CO2 Density (kg m-3)

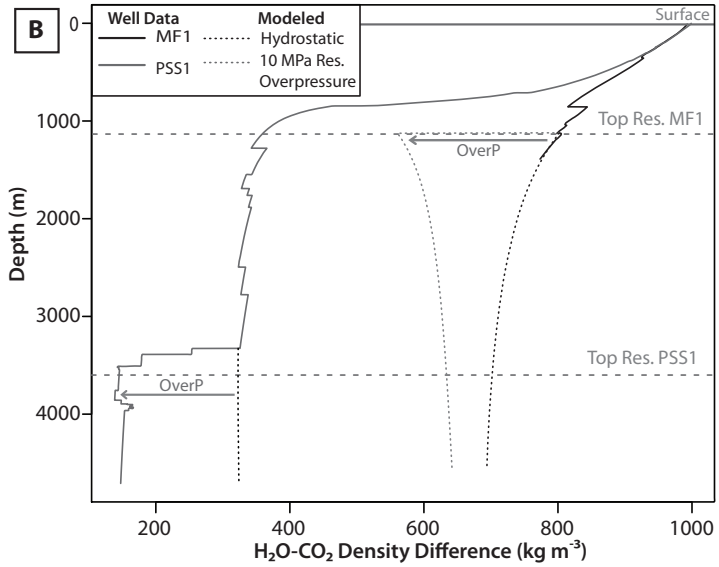
B
Well Data
MF1
PSS1
Modeled
Hydrostatic
10 MPa Res.
Overpressure
Surface
Top Res. MF1
OverP
Top Res. PSS1
OverP
Depth (m)
H2O-CO2 Density Difference (kg m-3)

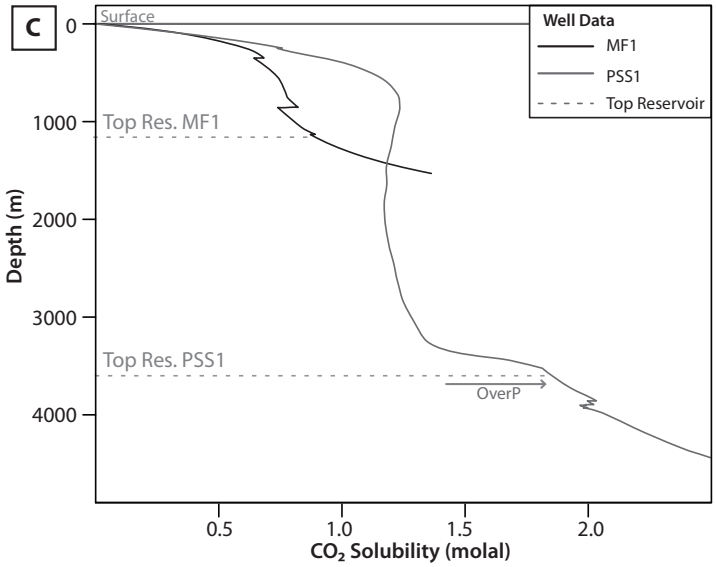
C
Surface
Well Data
MF1
PSS1
Top Reservoir
Top Res. MF1
Top Res. PSS1
OverP
Depth (m)
CO2 Solubility (molal)

CO_2 leaking from the P.S.Stefano reservoir passes close to the liquidus during its ascent at hydrostatic pressure conditions and so experiences a rapid increase in CO_2 buoyancy approaching 800 m depth (for example, the ascent from 1250 - 750 m in PSS1 is associated with 325 Kg m^{-3} ϱ_{CO2} decrease). In contrast, CO_2 ascending from the Frigento reservoir will progressively increase buoyancy (for example, the ascent from 1250 - 750 m in MF1 is associated with ~75 Kg m^{-3} ϱ_{CO2} decrease). Reservoir overpressure increases ϱ_{CO2} at reservoir conditions, decreasing CO_2 buoyancy in the reservoir.

CO_2 solubility in fresh water at reservoir conditions is typically between 1-1.5 molars (~40 - 60 $Kg_{(CO2)}$ $m^{-3}_{(H2O)}$), see Table 5.3 in supplementary information. Formation waters therefore have potential to dissolve significant quantities of CO_2 at reservoir conditions. Change in down well CO_2 solubility is non-linear due to conflicting effects of pressure and temperature (see Figure 5.6C). Solubility peaks just below the CO_2 phase transition depth, and rapidly decreases toward the surface. As fluids ascend, CO_2 solubility in water will first increase (by over 3 $Kg_{(CO2)}$ $m^{-3}_{(H2O)}$ in MF1) before rapidly decreasing. Attenuation of free phase CO_2 fluids during ascent by dissolution will therefore be most pronounced at the depths just below the CO_2 phase transition. These calculations do not account for the effects of subsidiary gases on CO_2 solubility. For example, H_2S decreases CO_2 solubility in water (Savary et al., 2012). H_2S is present in all CO_2 reservoirs but in trace quantities, therefore its effects on CO_2 solubility will be minor.

Table 5.2. Summary of down well pressure conditions for CO_2 bearing wells and any nearby seeps.

If conditions are 3 MPa above hydrostatic it is considered overpressured. Further detail about the seeps (type, flux, temperature) are tabulated in Figure 5.1B.

*SAT1 is the oldest well in this study and the mud densities are not clearly documented. Upon penetrating the ACP, multiple mud losses were experienced before the well was plugged after 300 m of drilling the reservoir which may suggest these mud densities were overestimating the pressure conditions.

Fig	Well	CO_2 (*C%v.v*)	ρ(CO_2)	Res. depth /m	OverP Overburden?	OverP Reservoir?	Surface Seeps (no.)	Distance (km)	Interpretation
2A	**BS1**	98.5	624 ± 15 (gas)	2710	Y	N	None	-	Sealing
	SAT1	Undefined	503 ± 11 (gas/SC)	1520	Y*	Y	None	-	Sealing
	Tr1	98	279 ± 6 (gas)	2773	Y	N	Buonalbergo (2)	3.3	Inconclusive
	MT1	>90	569 ± 10 (SC)	2600	N	N	Motta (1)	1.6	Inconclusive
	Mu1	97	139 ± 19 (gas)	694	N	N	None	-	Kr_{CO2}restricts flow
2B	**Ac1**	97	919 ± 8 (SC)	4262	Y	Y	San Benedetto (6) Contursi cluster (7)	11 15.5	Outside the Acerno horst structure
	Co1	-	-	-	N	Minor	Contursi cluster (7) Aqua Regina (8)	3.7 - 10.2 3.7	Leaking
2C	**MF1**	99.7	200 ± 5 (gas)	1128	Y	N	Mefiteniella polla (4) Mefite D'Ansanto (5)	5.4 1.8	Leaking
2D	**PSS1**	100	830 ± 8 (SC)	3600	N	Y	C. Michelangelo (9)	2.5 - 3.6	Leaking

5.1.4.5 Discussion of Case Study Characteristics

Confining pressure (reservoir depth) improves seal quality by increasing the minimum stress, and therefore rock strength, therefore greater fluid pressures are required for the seal to mechanically fail (Osborne and Swarbrick, 1997). Confining pressure also reduces rock pore-throat sizes and fracture apertures by compaction and cementation (Becker and Lynds, 2012). However, both shallow and deep CO_2 case studies show overpressure in the overburden, and both shallow and deep case studies leak CO_2.

Away from recent faults, overpressure from the previous compressional regime may be present in the heterogeneous and compartmentalised Allochthonous Complex. The exception to this trend is the Mu1 well which is located away from recent faults yet shows only minor deviation from hydrostatic. However this reservoir is very shallow and the Thrust Top overburden consists of sands, silts, clays and conglomerates which may be permeable to fluids. Sealing reservoirs have Messinian evaporite bearing unit directly overlying the CO_2 reservoir. Evaporite deposits are known to be particularly effective seals (Becker and Lynds, 2012). The units in the studied well logs vary from massive anhydrite deposits, which will have negligible permeability, to resedimented evaporites or evaporites interbedded with marls which could possess some (very low) permeability.

The overburden units of CO_2 reservoirs located close to seismogenic normal faults are hydrostatically pressured. The overburden here may posses greater pressure connectivity from the presence of a recent 'open' extensional fault, or because favourably oriented meso- and macro- scale fractures in the rock body are open (until confining pressures ~ above 1.5 km depth close these features and fluid flow becomes governed by microfracture or matrix permeability).

Leakage of buoyant CO_2 fluids and thermal waters from the Frigento field located next to the Ufito normal fault may therefore be facilitated by open fractures in the overburden or fault damage zones. The high confining pressures in the deep

P.S.Stefano will have closed mesoscale fractures, unless they are opened locally by overpressured fluids.

Rocks are weak in tension, so to open fractures the fluid pressure only needs to exceed the rock tensile strength or minimum stress. The effect of pore fluid pressure (Pf) on rock strength can be represented by the pore fluid factor, λv (Streit and Cox, 2001). This is the ratio of pore fluid pressure (i.e. reservoir pressure, $P_{(res)}$) to lithostatic stress:

$$\lambda v = \frac{P_{(res)}}{\varrho_{rock} \cdot g \cdot z} \qquad [5.5]$$

where ϱ_{rock} is 2500 Kg m^{-3}, g is acceleration due to gravity (ms^{-1}), and z = reservoir depth.

The λv ratio (Table 5.3 in the Supplementary Results) indicates how close a *coherent* rock body is to failure, and will therefore be underestimated when applied to a fractured rock unit. The high fluid pressure of the PSS1 reservoir (λv = 0.7) may therefore be sufficient to open fractures, locally enhancing rock fracture permeability and enabling fluid leakage. Additionally, elevated fluid pressures increase the pressure gradient and hence encourage fluid flux according to the Darcy flow equation [5.1]. Pressure pulses associated with seismicity will increase seepage of these fluids, which has been observed at the Caprese Michelangelo (CM) seeps (Bonini, 2009).

Due to the opening of fractures, abnormally high reservoir pressures will decrease the CO_2 column heights that can be achieved before capillary breakthrough occurs. This is, to some extent, counteracted by increased ϱ_{CO2} at reservoir conditions (see Figure 5.6A). Once the capillary threshold is exceeded, the elevated pressure gradient and increased fluid buoyancy upon leaving the reservoir will enhance the fluid seep rates. The associated volume increase may open fractures to locally enhance permeability and enable continued fluid flow through the overburden.

5.1.5 Part II: Reservoir Leakage to Surface Seepage

5.1.5.1 Methods

CO_2 properties at reservoir conditions are used to calculate the seepage rate of free phase or dissolved CO_2 from the reservoir top to supply seeps at a given flux, assuming no CO_2 attenuation during ascent.

For end member seeping reservoirs; the shallow, warm Frigento Field and the deep, cool P.S.Stefano Field, we model the CO_2 viscosity and density (ϱ_{CO2}) at top reservoir conditions (Huang et al., 1985; Span and Wagner, 1996) and apply reservoir pressures to calculate the minimum seepage rate (m^3s^{-1}) from the reservoir to enable free phase CO_2 delivery at 100, and 2000 $t_{(CO2)}d^{-1}$ (measured at the Caprese Michelangelo seep near PSS1, and the Mefite seep near MF1, respectively). A seep cluster may represent individual leak pathways from the reservoir, or near surface dispersion of a larger quantity of CO_2 leaking from the reservoir.

The change in CO_2 solubility from reservoir conditions to the surface can indicate the minimum volume of water required to ascend from the reservoir to supply CO_2 to the surface at the same flux rates. Down well CO_2 solubilities were calculated (Spycher et al., 2003) for fresh water since APC formation tests show low salinities in most wells.

We rearrange equation [5.1] to calculate the overburden effective permeability (K_E) and area required to allow such fluid seep rates from the reservoir. For CO_2 saturated fluids, Kr approximates to 1 therefore K_E is K_{seal}. For free phase CO_2, K_E represents $K_{seal} \cdot Kr_{CO2}$. Seep rates at 100 t d^{-1} from both the Frigento and P.S.Stefano reservoirs are calculated to compare the effect of CO_2 properties on seep rate.

The permeability ratio of CO_2 and CO_2 saturated water will indicate the Kr_{CO2} conditions where free phase CO_2 shows fluid seepage area equal to CO_2 saturated water.

5.1.5.2 Reservoir Leakage

Leakage Rates

Figure 5.5 shows the area and effective permeability (K_E) requirements at the reservoir top necessary for reservoir fluids (free phase or dissolved CO_2) to seep at 100 t d^{-1} from PSS1 reservoir conditions and 100 and 2000 t d^{-1} from MF1 conditions. The table inset shows the volume of fluids which must leak from the reservoir to achieve these flux rates. For the same CO_2 flux, the fluid volume seeping from the P.S.Stefano reservoir (ϱ_{CO2} = 830 Kg m^{-3}) is a quarter of the volume seeping from the Frigento reservoir (ϱ_{CO2} = 200 Kg m^3). The difference in water fluid volumes between the two case studies is less pronounced. CO_2 leaking from the reservoir in its dissolved phase requires six times greater fluid volume than $CO_{2(d)}$, or up to ten times for the less soluble $CO_{2(g)}$. These calculations do not consider Kr_{CO2} and will therefore underestimate the seepage areas and permeabilities required.

Estimates of minimum area of seepage at P.S.Stefano and Frigento case studies are shown in Figure 5.7. The main area of degassing at the Caprese Michelangelo seep cluster close to the PSS1 well takes place over 400 m^2 (Heinicke et al., 2006) whereas the area of degassing at Mefite close to the MF1 well occurs over 4000 m^2 (Chiodini et al., 2010). Table inset in Figure 5.7 shows that in order to to seep from the reservoir over such discrete areas,$K_E \sim 10^3$ mD is required.

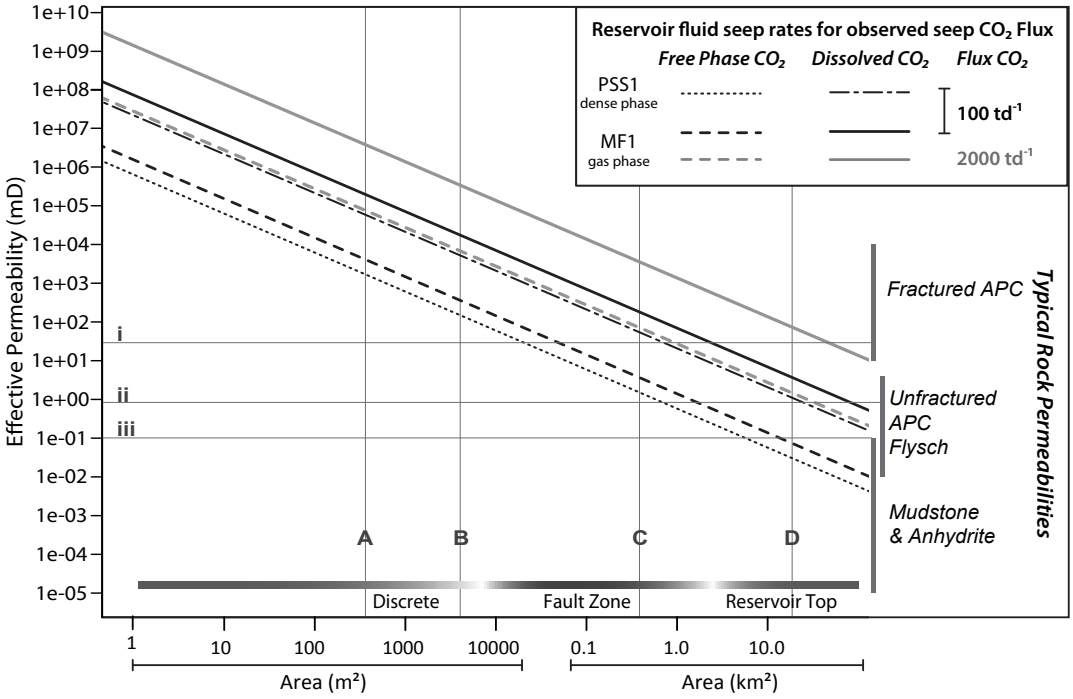

Case Study		MF1 2000 t d^{-1} CO_2		PSS1 100 t d^{-1} CO_2	
Top Reservoir Seep Rate (m^3s^{-1})		Free Phase 0.116	Dissolved 0.032	Free Phase 0.0014	Dissolved 0.027
Path	**Area**	**Permeability (mD)**		**Permeability (mD)**	
Discrete	A & B	6.9e+03	3.6e+05	1.6e+03	5.3e+04
Cluster Area	C	2.5e+01	1.3e+03	2	6.9e+01
Reservoir Top	D	2.2	1.1e+02	-	-
Path	**K (mD)**	**Area**		**Area**	
Fractures	10^4	2770 m^2	144000 m^2	63.4 m^2	2117 m^2
(i)	24	1.15 km^2	60 km^2	0.025 km^2	0.88 km^2
Sannio (ii)	0.8	276 km^2	14400 km^2	0.79 km^2	26.5 km^2

Figure 5.7: The area and effective permeability requirements at the reservoir top necessary for reservoir fluids (free phase or dissolved CO_2) to seep at 100 $t_{(CO_2)}d^{-1}$ from PSS1 reservoir conditions and 100 and 2000 $t_{(CO_2)}d^{-1}$ from MF1 conditions.Typical rock permeabilities and seepage area are annotated to the right of the plot. Permeabilities from well logs are annotated: i = Jurassic Umbria-Marche overburden in PSS1; ii = Allochthonous Complex overburden in MF1 well; iii = APC in MF2. Vertical lines A-D show estimates of minimum area of seepage at P.S.Stefano and Frigento case studies: (**A**) Main area of degassing at the Caprese Michelangelo (**B**) Area of degassing at Mefite (**C**) cluster area at the Caprese Michelangelo (0.2 km x 1.52 km) and the Mefite and Mefitiniellapolla vents (3.5 km x 0.1 km) and (**D**) minimum area of seepage from the Frigento CO_2 reservoir top (2 km radius circle). Table inset show calculated seep areas using relevant permeabilities, and permeability calculations using areas A-D. See text for discussion.

The area of seep clustering provides a minimum estimate for a distributed seepage area at depth and is similar for both Caprese Michelangelo and Mefite seeps (~0.35 km^2). Calculations here will underestimate the permeability since total seep flux from the cluster will be greater than the fluxes from one seep used in the calculations. Free phase CO_2 leaking through the PSS1 overburden (maximum 24 mD) requires a seepage area smaller than the cluster area of the Caprese Michelangelo seeps. However, seepage areas five times greater than the cluster area is necessary if these calculations are performed for the minimum measured permeability of the PSS1 (0.1 mD). Regardless, a fault or enhanced permeability pathway may not be necessary for free phase CO_2 fluids to leak from the PSS1 reservoir at 100 t d^{-1} since permeabilities feasible of flysch and unfractured carbonate are required for seepage over the cluster areal extent (see Figure 5.6).

In contrast, to deliver 2000 t d^{-1} to Mefite, Darcy flow of free phase CO_2 through mudstones (maximum permeability ~ 0.8 mD) would require seepage areas larger than the CO_2 reservoir top. Therefore seepage from MF1 conditions requires permeabilities provided by pervasive fracturing of the overlying low permeability units (10^2 mD) over areas reasonable for moderate faults, as can be observed in Figure 5.7.

We learn that CO_2-waters could be capable of delivering large fluxes of CO_2 to the surface providing very high permeability pathways exists. In both PSS1 and MF1, CO_2 bearing waters would require over an order of magnitude greater effective permeability. CO_2 seepage in its dissolved phase will always require larger K_{seal} or seeping areas to achieve the same flux as free phase CO_2, unless Kr_{CO2} is below 0.02 ± 0.01. Such low Kr_{CO2} is unlikely for long duration seep paths due to 'drying out' effects, and so significant (> 100 t d^{-1}) CO_2 seepage to the surface is more easily achieved by free phase CO_2.

5.1.5.3 Discussion

CO_2 transport by formation waters

Seep rate calculations consider waters that are CO_2 saturated, which requires effective water mixing and may be difficult to achieve. Therefore water seep rates are probably underestimated in these calculations, and it is more geologically reasonable that high flux seeps arise from leaking free phase CO_2 fluids. For example, for 2000 t d^{-1} to be transported and released from CO_2 saturated waters, 480 Ls^{-1} must ascend from the Frigento reservoir. Such flow rates are not impossible, since spring flow rates in Italy can exceed 800 Ls^{-1}. However, rock permeabilities over 10^7 mD are necessary for ascent over 10 m^2 area, which is difficult to achieve unless the rocks are karstic. Karst environments require carbonate units in the vadose zone, which is not the case for the Frigento reservoir.

Karstification is observed in the Contursi region, where karst-collapse sinkholes are attributed to meteoric water mixing with deep derived fault-channeled fluids (Santo et al., 2011). The Contursi well did not penetrate the ACP and discovered no CO_2 accumulation at depth, only a 30 m column of fresh water in WCP reservoir at 1 km depth. At reservoir conditions this fresh water could dissolve 44.3 $Kg_{(CO2)}$ per cubic meter of fresh water. These waters are close to the peak solubility depth, so by ascending and cooling to 15°C, they could release over 42 $Kg_{(CO2)}$ per cubic meter of water. There are 10 seeps located close to Contursi. If we estimate that CO_2 flux at this cluster is approximately 100 $t_{(CO2)}d^{-1}$ (10 seeps, each degassing 10 $t_{(CO2)}d^{-1}$) a

minimum flow rate of 27 Ls^{-1} of CO_2 saturated water is required to seep from the WCP, a moderate spring flow rate.

Travertine is precipitated at one of the springs in the Contursi seep cluster, and is a process which often accompanies CO_2 release from saturated waters. Flow rates at this spring are quite low; and spring gas flux is unquantified, but if the fluids were CO_2 saturated they should degas ~0.06 t d^{-1} which would classify as low flux (Chiodini and Valenza, 2008).

The San Teodoro springs, located on the flanks of the Frigento anticline do not release CO_2 when emerging nor precipitate travertine. If these waters source from the Frigento reservoir, the reservoir formation waters cannot be CO_2 saturated, otherwise the waters of the San Teodoro spring (7 $L_{(H2O)}s^{-1}$) would release ~0.4 t d^{-1} during ascent from the reservoir and classify as low flux according to the INGV classification system (Chiodini and Valenza, 2008). The San Teodoro springs may therefore represent thermally driven seepage from a CO_2 unsaturated water leg of the Frigento formation while the Mefite CO_2 vents represent seepage from the gas leg.

Rock permeability

Effective permeability, K_E, is the product of K_{seal} and Kr_{CO2}. Experimentally derived Kr_{CO2} from carbonate rocks with similar porosity values to the APC carbonates (~10%) range from 0.06 - 0.54 Kr_{CO2}. For free phase and dissolved CO_2 fluids to require equal seep area to achieve the same CO_2 flux, Kr_{CO2} would need to be even lower than these experimentally derived values ($Kr_{CO2} < 0.02 \pm 0.01$). It will therefore always be easier for free phase CO_2 to seep significant quantities of CO_2.

The Caprese Michelangelo and Mefite seeps are long established degassing sites (Chiodini et al., 2010; Chiodini et al., 2008; Heinicke et al., 2006), so the CO_2 saturation in the fluid pathway is likely to be towards the upper limits of the experimental range. This will reduce the permeability necessary for flow by <1 order of magnitude which does not change the geological feasibility of the previous area calculations.

These seeps are cool temperature CO_2 vents, characterized by dry CO_2 release at the surface at above ambient pressure (Roberts et al., 2011). At surface temperature and pressure conditions, CO_2 is denser than air, therefore subsurface pressure must be driving the escape of these fluids rather than buoyancy alone. Pressurized fluid escape implies that fluid flow is restricted at depth. CO_2 flow can be impeded by various fluid and rock properties during ascent.

Denser fluids require smaller permeability-area combinations for a given CO_2 flux rate. As dense CO_2 ascends from depth and ϱ_{CO2} decreases, seepage area or rock permeability must increase to enable steady state CO_2 flux. This might be dynamically achieved as the reduction in confining pressure at shallow depths progressively opens mesoscale fractures. Else fluid pressure (and therefore flow rate) may increase from buoyancy effect alone, or from fluid pressure head which gathers as flow is impeded. Otherwise, rock permeability may be actively (kinematically) increased by the opening of fractures by elevated fluid pressure. Therefore, while free phase CO_2 fluids may not need fault induced rock permeability to leak from the PSS1 reservoir, such pathways may be necessary for CO_2transport to the surface, where the Caprese Michelangelo seeps emerge along fault traces (Bonini, 2009).

Other baffles to flow may encourage the channeling of ascending fluids. Fracture connectivity and rock permeability will not be continuous during fluid ascent from the reservoir. Indeed, above the PSS1 reservoir there are several rock units which will show much reduced permeability than the carbonate units directly overlying the reservoir (e.g. Varicoloured Clay units, see Figure 5.3D). Fault induced rock permeability will be necessary for fluid transport through these units.

Relative permeability variation will also impede fluid flow and can arise from CO_2 exsolving from rising CO_2 waters. As previously discussed, these effects will be most pronounced towards the phase transition depth, where solubility rapidly decreases (see Figure 5.6C). When CO_2 waters degas, two phase flow conditions are established. The relative permeability of the parent waters will rapidly decrease, retarding flow rate, though the water buoyancy may be increased by the resulting

gas-water mixture. Fluid pressure will accumulate in response which, in extreme cases can lead to geyser-style seepage. The buoyant, high IFT, free phase CO_2 may follow a different flow path to its parent waters, subsequently forming several seep types in a seep cluster, as observed at the Contursi and CM seep cluster. If the hydraulic head of ascending waters is not great enough to enable the fluids to reach the surface, only dry CO_2 seeps will manifest.

In this way, CO_2 can be transported from the reservoir in its dissolved phase and seep as a free phase at the surface. Conversely, CO_2 can leak from the reservoir as a free phase and dissolve into overlying aquifer units during ascent, and seep as a dissolved constituent in springs. This process may be occurring above the Monte Taburno reservoir, the Motta seep may either be supplied by low seepage rates of free phase CO_2 which dissolves into the overlying WCP, or, the CO_2 capillary entry pressures have not been overcome and instead reservoir waters with moderate CO_2 content are seeping.

5.1.6 Conclusions

We have examined the subsurface conditions of CO_2 reservoir case studies in Italy to assess the geological conditions enabling CO_2 leakage from the reservoir and seepage to the surface. We find these reservoirs successfully retain CO_2 in gaseous phase or dense phase, and in some cases this CO_2 can be close to the critical point. Where the reservoir overburden is at hydrostatic pressure, CO_2 seeps are present at the surface. These case studies are located near seismogenic extensional faults, which may be responsible for subsurface pressure connectivity at these sites. Where the overburden is apparently overpressured there are no seeps present above the reservoir structure. In these case studies, overpressured fluids in the overburden is symptomatic of an effective reservoir seal, which in these cases may be enhanced by evaporite bearing caprocks.

Fluid seep rates from top reservoir conditions are applied to investigate the geological conditions required for fluid escape. Formations waters have the potential to dissolve large quantities of CO_2. Very high permeabilities are required for these waters to ascend at the rates necessary to supply high flux CO_2 seeps. Rapid CO_2 flux will always be more achievable by seeping free phase CO_2. Significant (> 100 t d^{-1}) leakage of dense phase CO_2 from the reservoir can be achieved by Darcy flow without the need for faults or enhanced permeability pathways. In contrast, to enable the same CO_2 flux for gas phase CO_2, fault permeabilities and areas are necessary since seepage through the overburden would require geological unlikely areas.

Changes in CO_2 properties during ascent from the leaking reservoir therefore lead to fluid channeling along high permeability pathways such as faults. These changes may also lead to CO_2 venting and seep clustering observed in Italy.

5.2 Supplementary Information

5.2.1 Supplementary Methods

GIS Dataset

To identify wells located close to seeps, the GIS was populated with the well (ViDEPI, 2009) and seep information (Chiodini and Valenza, 2008), mapped seismogenic fault scarps (Roberts, 2008), present day stress field data (Barba et al., 2009), seismically capable faults (ISPRA, 2007), SRTM 90 m elevation data (Jarvis, 2008), subsurface carbonate structure (Nicolai et al., 2007), and isotherms at 1 and 2 km depth (Geothopica, 2010) which are referred to as T1 and T2 respectively.

Deriving Geological Information from Well Logs

Geological information such as formation descriptions, names and ages, salinity information and drill stem tests (which provide fluid composition and pressure information) were elicited from the well notes, and subsurface structures of these reservoirs and the nature of nearby surface seeps from published literature.

We correct deviated drilling to the true vertical depth (TVD) and assume a standard depth error, intrinsic to depth while drilling measurements, of approximately ± 10 m and normally distributed to 1 standard deviation. See Appendix 4 for the code to calculate TVD from deviation information.

Pressure information was derived from the mud density of drilling fluids and by formation tests. To prevent a well blowout mud densities must maintain a pressure between hydrostatic and lithostatic. Pressures obtained from mud density will systematically over estimate the formation pressure by approximately 10%, we therefore assume formation pressures are 90% of the calculated pressures from mud density. See Appendix 4 for the code to calculate pressures from mud weights.

Mud weights greater than the formation pressure can, alongside thermal cooling from drilling muds, encourage the formation of drilling induced fractures. Loss of circulation or significant mud absorption can therefore be useful indicators of where the well encounters a significantly more permeable horizon, or, where the rock fracture gradient has been exceeded. Significant mud loses are therefore noted in this study.

The geothermal gradient is calculated from down hole temperature measurements. Drilling mud can cause erroneous formation temperature measurements, and so various borehole correction methods are usually applied.

Modelling CO_2 behaviour

The methods described above allow us to construct the down well pressure and temperature conditions, which allows us to model the down well CO_2 behaviour for each well (CO_2 bearing or not) using the (Span and Wagner, 1996) equation of state. Fresh water viscosities at reservoir conditions are calculated using the polynomial equation for variable temperature and pressure (Likhachev, 2003). The effect of dissolved CO_2 on water viscosity is neglected. The viscosity ratio of CO_2 and CO_2 saturated water indicate the magnitude difference in permeability and/or seepage area required to deliver CO_2 from the reservoir at a given flux rate, as either a free phase or dissolved form. The code for the function to calculate the effects of uncertainty, and graphical results of down well models for each well can be viewed in Appendix 4.

Calculations of CO_2 saturated water ascent from depth assuming an emergence temperature of 15°C, where the solubility of CO_2 in freshwater at 10 m depth is ~0.042 molal.

5.2.2 Supplementary Results

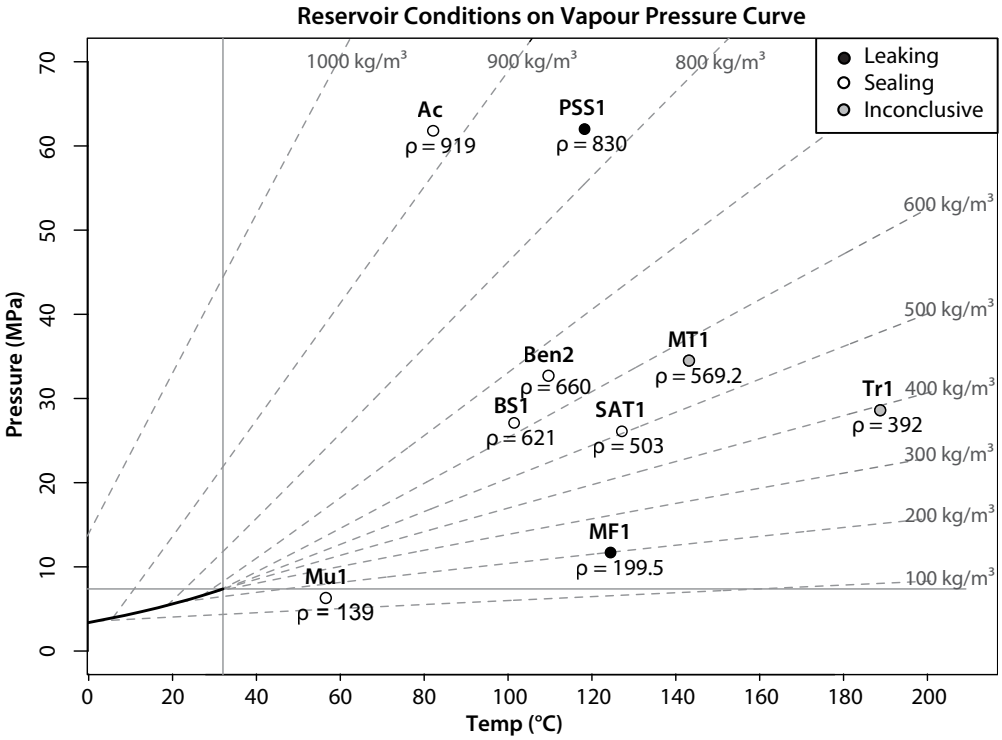

Figure 5.8: Vapour pressure curve detailing CO_2 density at reservoir-seal boundary, with fluid density shown next to the data points. CO_2 densities above the critical density (464 Kg m^{-3}) are 'dense' phase and below the critical density are 'gas' phase. Note that no reservoirs contain liquid phase CO_2, but both seeping reservoirs can contain CO_2 in dense or gas phase.

No	Well	a	b	c	d	e	Direct Overburden		Trap Style	f	g	h	i	λv	CO_2 Sol (molal)
							Rock Type	Age							
1	Monte Forcuso 1 (MF1)	1951	1,800	99.7	472	1,128	Flysch	Miocene	Antiform (1)	33.8*	495 ± 54	SC/Gas	0.3	0.4	1.14
										93.3	200 ± 5	Gas			0.88
2	Monte Forcuso 2 (MF2)	1963	1,690	-	-	1,366				60.8	358 ± 14	Gas	2.1	0.4	1.03
3	Ciccone (Cic)	1982	2,673	-	-	2,506	Anhydrite	Messinian		71.1	483	Gas	12.7	0.6	4.19
4	Tranfaglia 1 (Tr1)	1982	3,357	98	>803	2,773	Anhydrite + S&S sst	Mio-Pliocene	Antiform(2)	64.1	279 ± 6	Gas	1.3	0.4	3.19
5	S. Arcangelo Trimonte 1 (SAT1)	1961	1,917	yes	-	1,520	Breccia	Eo-Miocene		62.1	503 ± 11	SC/Gas	9.1	0.6	1.40
6	Benevento Sud 1(BS 1)	1976	4,502	98.85	1432	2,710	Anhydrite + Lagonegro	Miocene	Antiform (2)	31.5*	621 ± 15	SC	0.5	0.4	1.27
7	Benevento 001 (Ben1)	1973	3,112	-	-	2,959	Sicilide VS	Miocene	Antiform (2)	30.2*	759 ± 10	SC	13.5	0.4	1.51
8	Benevento 002 (Ben2)	1974	3,939	95.2	>610	3,052				30.4*	660 ± 12	SC	2.5	0.6	1.39
9	Monte Taburno 001 (MT1)	1996	3,733	>90	>282	2,600	ACP dolomite	?	Antiform (2)	49.1	569 ± 10	SC	9.0	0.5	1.82
10	Acerno (Ac)	1995	4,625	97	>182	4,262	Evaporite + Lagonegro	Messinian	Horst?	20.0*	919 ± 8	SC	20.0	0.6	1.60

No	Well	a	b	c	d	e	Direct Overburden		Trap Style	f	g	h	i	λv	CO_2 Sol (molal)
							Rock Type	Age							
11	Contursi (Co)	1963	2,142	-	-	1,004	S&S sst	Mio-Pliocene	Faulted Synform (3)	50.2	330 ± 25	Gas	1.3	0.5	1.03
12	Muscillo 001 (Mu)	1983	1,296	97	>100	694	Breccia	Eocene	?	58.6	139 ± 9	Gas	-0.5	0.4	0.84
13	Pieve San Stefano (PSS1)	1984	4,936	100	comple x >324	3,600	Dolomite (w. evaporite)	Cretaceous	? (4)	28.4*	830 ± 8	SC	26.8	0.7	1.85

Table 5.3: Summary information for the wells identified for study. Depth refers to uncorrected bottom hole depth. Geothermal gradients were determined by down well temperature gradients (indicated by *) and where no data was available an interpolated gradient was used. ACP = Apulian Carbonate Platform, WCP = Western Carbonate Platform, S&S = Sannio/Sicilide, VS = Varicolored Shale (of the Sicilide Complex), B = Burano formation. In the seeps column, '?' indicates where it is uncertain whether seeps represent leakage from that reservoir. Structure references: (1) (Chiodini et al., 2010; Improta et al., 2000; Nicolai et al., 2007) (2) (Di Bucci et al., 2006; Improta et al., 2003) (3) (Improta et al., 2003; Scrocca, 2005) (4) (Bonini, 2009; Heinicke et al., 2006). Where a) Year drilled b) Bottom hole depth c) CO_2 %, d) CO_2 column, e) Reservoir depth f) Geothermal gradient g) CO_2 density at reservoir conditions, h) CO_2 state at reservoir conditions, i) overpressure beyond hydrostatic (MPa).

Chapter 6

CO_2 flux from non-volcanic seeps in Italy

Previous calculations of total deep derived CO_2 flux in Italy do not consider the contribution from numerous dry seeps in Italy. Additionally, natural CO_2 seeps can inform potential flux rates from breached CO_2 stores. Seep flux information documented by the Googas database allow CO_2 flux from dry seeps to be quantified for the first time, and mean seep flux rates for different seep types to be examined. The consequences of these seep rates on storage effectiveness is assessed.

6.1 Natural flux rates of CO_2 seeps in Italy and implications for effective geological storage.

Italy is a region of natural geofluid phenomena. Over 308 CO_2 seeps are documented which exhibit variable seep type and CO_2 flux. Non-volcanic CO_2 seeps are potentially similar to seeps which could arise if engineered geological CO_2 storage selected poorly-sealed reservoirs. Analysis of Italian seep characteristics can therefore provide 'worst case' scenarios of CO_2 leakage by natural fluid pathways. Here, we quantify the total CO_2 flux from all types of natural non-volcanic CO_2 seeps in Italy in order to refine the annual budget of natural earth degassing from Italy. Total estimated CO_2 flux from all non-volcanic seeps in Italy contributes 13 ± 2 % to 3.2 ± 1.2 % of the global non-volcanic CO_2 budget. We investigate how the physical expression of seeps affects flux rates, and apply natural CO_2 gas flux rates to commercial scale carbon storage scenarios to quantify the effect of these seep rates on long-term storage effectiveness. We find that leakage of injected CO_2 at flux rates similar to the studied gas seeps would represent <1% annual injection at commercial scale carbon stores. If a single seep established with the mean seep flux rate for non-volcanic CO_2 seeps in Italy, such stores would remain 86-96 % effective over 1,000 years.

6.1.1 Introduction

Carbon Capture and Storage (CCS) is a direct and rapid method of reducing CO_2 emissions from large industrial sources. In this technology chain, CO_2 is captured from exhaust gasses from industrial processes, then transported, and injected into suitable rock formations. Pilot-scale CCS sites inject ~1 Mt y^{-1}, and moderate CO_2 storage operations (1 -1.5 GW coal fired power plant) proposed will inject 5 Mt y^{-1} where the injection phase is expected to continue for ~40 years. For effective climate mitigation, the injected CO_2 must remain secure in the subsurface for tens of thousands of years (Hepple and Benson, 2003; Shaffer, 2010). To benefit medium term mitigation efforts, a storage site should operate with less than 1% CO_2 loss to the surface in 1,000 years (Haugan and Joos, 2004; IPCC, 2005), though current EU legislation requires engineered stores to retain CO_2 'permanently'(Council, 2009).

Natural CO_2 reservoirs demonstrate that billions of tonnes of CO_2 can be successfully trapped in complex and multi-layered or simple reservoir-caprock systems, at a range of depths and pressure conditions (Fleet et al., 1998; Lewicki et al., 2007; Pearce, 2005/6). These reservoirs retain CO_2 securely for geologically long time periods (e.g. 42-70 Ma, Colorado) and several show no evidence of surface seepage (Allis et al., 2001; Gilfillan et al., 2008). Instances of CO_2 leakage, however, from naturally occurring reservoirs serve as direct analogues for the potential migration of CO_2 from geologic storage sites and can indicate the natural rates of CO_2 loss towards the surface and its subsequent fate.

Globally, the annual rate of natural CO_2 Earth degassing is orders of magnitudes smaller than the gigatonnes of CO_2 trapped in the subsurface. Estimates of global non-volcanic subaerial CO_2 flux range from 0.044 Gt y^{-1} (Kerrick, 2001) to 0.6 Gt y^{-1} (Morner and Etiope, 2002). CO_2 delivery and flux within and between non-volcanic degassing sites are highly variable. Comparison of measured flux rates at global seep sites show that flux varies by eight orders of magnitude (Kirk, 2011). This suggests there is no flux 'threshold' required for CO_2 to seep at the Earth surface, and all that is required is a permeable pathway to the surface.

6.1.2 Italian CO_2 seeps

Italy is a region of intense natural Earth degassing. CO_2 flux is greatest in western Central Italy where, besides fumaroles, CO_2 seeps locate away from the flanks and craters of volcanoes and therefore represent non-volcanic degassing (according to definition in (Kerrick, 2001)). Archaeological records indicate that seepage has been established for at least 2000 years (Chiodini et al., 2011; Etiope et al., 2007a) but it is likely that regional CO_2 flux has remained elevated since volcanism initiated ~0.9 Ma (Minissale, 2004; Smith et al., 2008). In total, over 308 CO_2 seeps at 270 locations have been catalogued (Chiodini and Valenza, 2008; Chiodini et al., 2008). These are mostly low temperature emissions (where mean and mode temperature is <22°C (see Section 3.1.7) and can manifest as vents, diffuse soil degassing, CO_2-driven mud volcanoes, and CO_2-rich springs and pools of bubbling water. Several deep boreholes are also known to leak CO_2; these wells are not natural seeps but do indicate the presence of subsurface CO_2 accumulations. In Chapter 4 we learn that the spatial distribution of Italian gas seeps shows that seeps usually form clusters over a small area, thought to indicate the near-surface dispersion of one seepage pathway at depth.

Gas flux varies between seeps, most commonly classifying between 10 - 100 tonnes per day (t d^{-1}), see Chapter 2. Mefite D'Ansanto (Southern Apennines, Italy) releases 0.73 Mt y^{-1} (Chiodini et al., 2010), and is the most effusive known non-volcanic CO_2 seep in the world. It is estimated that 9.2 Mt y^{-1} CO_2 derived from a mantle source is transported and released by Apennine aquifers (Chiodini et al., 2004) which then contributes between 3 - 9.4% of the present-day global CO_2 discharge from sub-aerial volcanoes (Kerrick, 2001; Morner and Etiope, 2002). However, this is likely to be an underestimation since it does not include the contribution of CO_2 from the widespread dry gas seeps located in Italy (Chiodini et al., 2004).

Here, we quantify the total CO_2 flux from all types of natural non-volcanic CO_2 seeps in Italy in order to refine its contribution to the annual budget of natural Earth degassing. We investigate how the physical expression of seeps affects flux rates, assess the conditions required at depth to deliver CO_2 at these rates and therefore

the geological processes which enable CO_2 escape from the reservoir. Finally, we apply natural CO_2 gas flux rates to carbon storage scenarios to quantify the effect of these seep rates on long-term storage effectiveness.

6.1.3 Methods

Seep data were elicited from Googas (Chiodini and Valenza, 2008) a web-based catalogue of degassing sites in Italy and Sicily. Each seep is assigned a seep classification, flux and gas composition. There are four natural non-volcanic (NNV) CO_2 seep classifications. We refer to these as either 'wet' (bubbling-water, spring) or 'dry' (vent, diffuse). Other seep types include fumaroles and wells. Mean seep flux calculations consider only natural non-volcanic CO_2 seeps which are most comparable to seeps arising from naturally breached stores (rather than, say, improperly abandoned boreholes).

CO_2 flux is measured in tonnes per day (t d^{-1}) and logarithmically categorised into 'low' (<1 t d^{-1}); 'medium' (1-10 t d^{-1}); 'high' (10-100 t d^{-1}) and 'very high' (>100 t d^{-1}). The most effusive seep, Mefite D'Ansanto, degasses over 2000 t d^{-1} (Chiodini et al., 2010). In general, background soil CO_2 flux is <0.00001 (t d^{-1}) (Kirk, 2011), therefore the upper and lower seep flux limits are conservatively set to 0.01 (min) - 2000 t d^{-1} (max). We use the logarithmic mean of flux category bounds in calculations where the uncertainty intrinsic in logarithmic categorisation is ±log(30%).

Flux Calculations

A third of all seeps lack flux data, and as seeps can be subtle manifestations it is likely that the catalogue is incomplete. To calculate the contribution of CO_2 from each seep type with unquantified fluxes we consider two potential models:

- *Flux Model One (FM1)*: Assumes there are no unidentified seeps (n=308) and no bias towards any flux category when measuring CO_2 seep flux. Therefore the number of seeps from each category are equally represented in the dataset.

- *Flux Model Two (FM2)*: Assumes that seep documentation and flux measurements are biased towards high flux seeps as these are most noticeable and have greatest perceived health risk, and therefore all high flux seeps are catalogued. Here, the number of low-end flux seeps not yet documented can be predicted by extrapolating a polynomial fit to the high-end flux categories (n=924).

Mean seep flux for each model is calculated using the modelled total seep frequency and the modelled total seep flux.

Storage Effectiveness

Seep flux rates from NNV seeps are applied to engineered storage scenarios to explore the consequences of such seepage on storage effectiveness if seepage occurs post-closure. Here, storage effectiveness, *E*, represents the fraction of CO_2 stored in the formation:

$$E = \left[1 - \frac{Q \cdot t}{I_T} \right] \times 100 \qquad [6.1]$$

where Q is annual flux of leaked CO_2, t is duration of leakage in years, and I_T is total injected CO_2, and E is expressed as a percentage.

Commercial scale CO_2 storage operations are expected to inject 5 Mt y^{-1} for an injection period of approximately 40 years. Following CO_2 charge a proportion of CO_2 will remain residually trapped in the pore throats due to capillary forces. Experiments determine between 20 - 40% CO_2 will remain residually trapped, so only a proportion of injected will be mobile (Bachu and Bennion, 2008). We can apply the calculate mean flux rates to assess how long it will take for all mobile CO_2 to leak from the store, assuming 20% residual trapping.

Research on the spatial distribution of CO_2 seeps presented in Chapter 4 has shown that seeps often emerge as clusters, within which seeps exhibit a variety of seep types and fluxes. The number of seeps in a cluster varies, but here, for simplicity, we assume a cluster size of 5 seeps which all exhibit mean flux rates.

6.1.4 Results

Flux Estimates

Total CO_2 flux estimates from CO_2 seeps in Italy are shown inset Figure 6.1A. Seeps with flux measurements release 5.3 Mt y^{-1}, of which 4.7 Mt y^{-1} is from NNV seeps. The total quantity of CO_2 from all seeps calculated by FM1 and FM2 is 5.5 – 8.3 Mt y^{-1}, respectively.

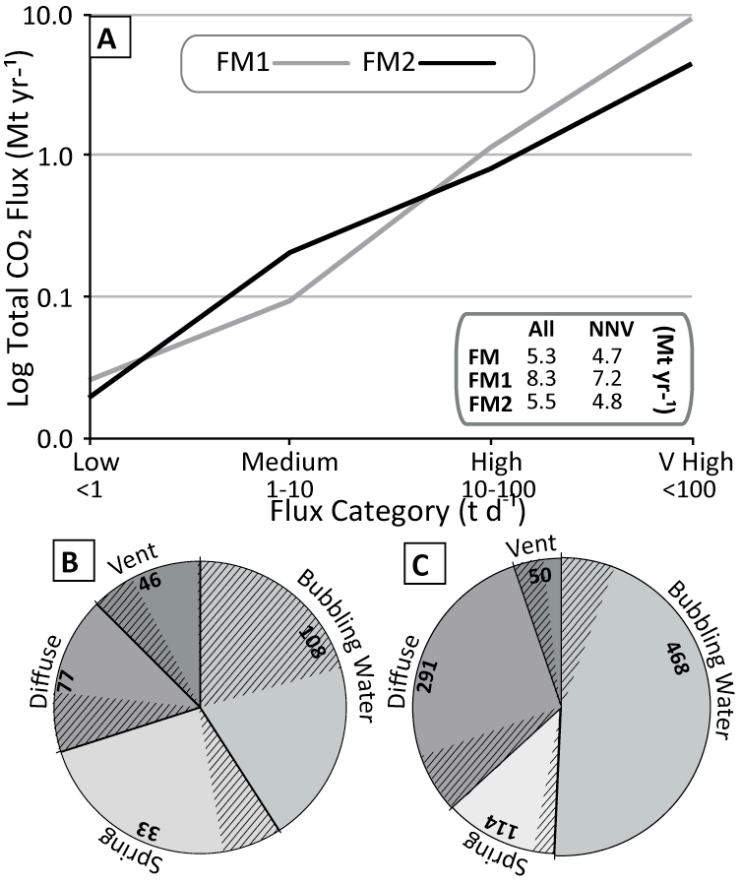

Figure 6.1 A: Log-Log plot showing total modelled CO_2 release per flux category. Note that a small number of very high flux contribute greatly towards total annual flux. **Inset:** Table of total flux from measured (M) and modelled seeps (NNV = natural non-volcanic). Flux contributions from each seep type are shown in **(B)** FM1 (n = 308) and **(C)** FM2 (n = 924). Shading shows proportion of seeps with quantified fluxes).

When total flux from NNV seeps are averaged (5.2 ± 0.3 Mt y^{-1}), these quantities contribute between 6.8 ± 1.9 (Kerrick, 2001) to 1.7 ± 0.8% (Morner and Etiope, 2002) of the global annual non-volcanic sub aerial CO_2 budgets. Previous estimates considered only CO_2 release from springs. Here we find all other natural non-volcanic seep types in Italy release half of the calculated total annual CO_2 flux.

FM2 predicts a further ~600 low-end flux seeps have yet to be documented in Italy (see Figure 6.1B, and Figure 6.2), the majority of which are bubbling water and diffuse types. Mean calculated seep flux from FM2 (20 t d^{-1}) and FM1 (78 t d^{-1}) classify in the 'high' flux category. Figure 6.3 shows how the total annual flux and mean seep rate varies between seep types. Fumaroles and springs show greatest mean seep rates (~150 t d^{-1}) though both flux models find the total contribution from dry seeps is ~1 Mt y^{-1} greater than wet seeps.

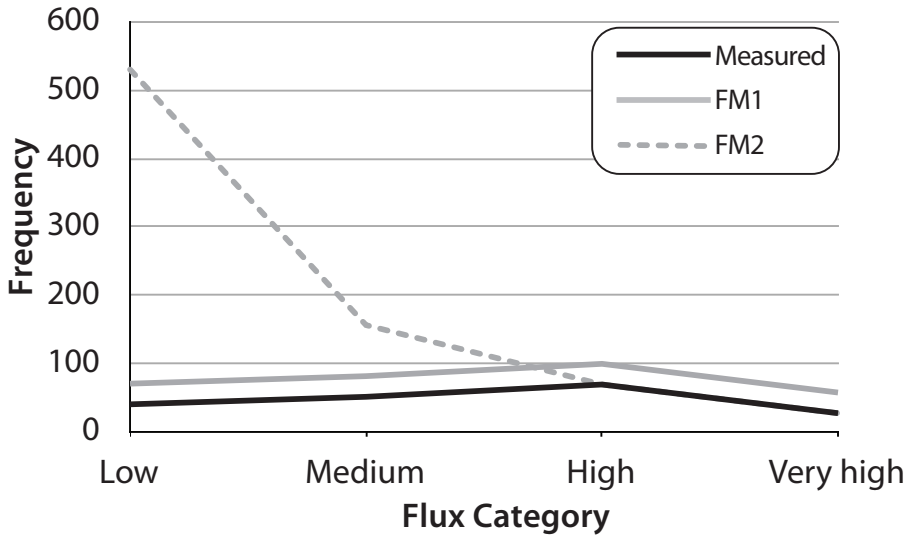

Figure 6.2: Total seep numbers for each category predicted for each flux model. Known seep numbers are labeled as 'measured'.

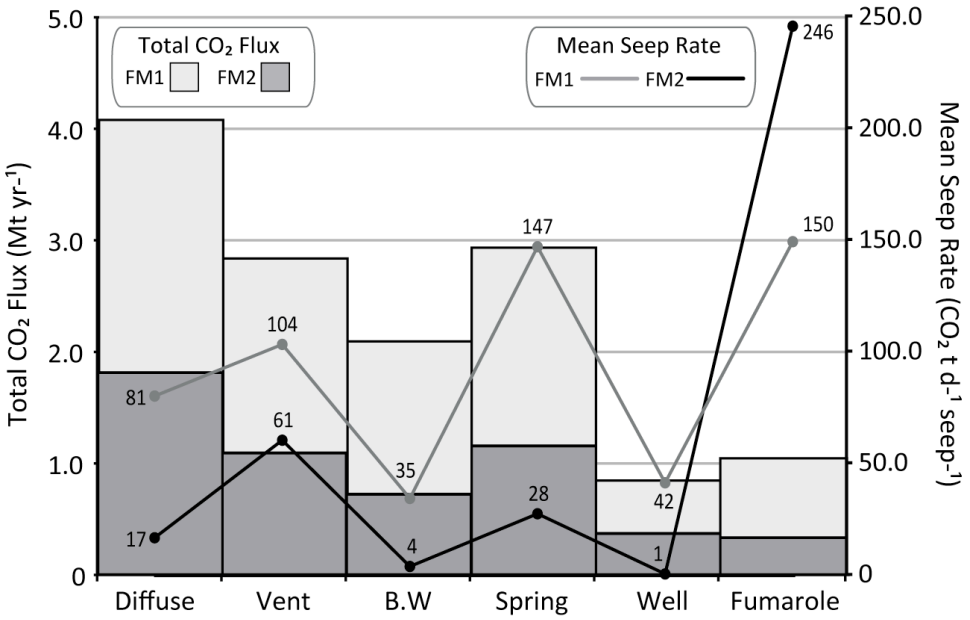

Figure 6.3: Estimated annual quantity of CO_2 released from each seep type (bars, left axis), together with mean flux rate (lines, right axis, figures shown) results from two flux models; FM1 and FM2 (see text for detail). B.W = bubbling water.

Italian Seeps and Engineered Storage

Table 6.1 summarises how seepage from engineered stores at flux rates exhibited by NNV seeps in Italy would affect storage effectiveness. Stores that breach post-closure will still take considerable time periods (> 1,000 ys) for mobile CO_2 to be released back to the atmosphere (see figure 6.4 in the supplementary information). The store would remain 86-96 % effective over 1,000 years. However, previous research on the spatial distribution of CO_2 seeps (Chapter 4) show that it is geologically more likely that a cluster of seeps establish. If we assume a seep cluster is composed of 5 seeps, 1% of the injected CO_2 could be released in decades (Table 6.1).

Seep		Flux t d^{-1}	5 Mt/y				
			% I y^{-1}	% T	$t_{1\%}$	$t_{80\%}$	E_{1000} %
Mefite		*2,000*	14.0	0.37	2.7	220	-
Mean	*FM1*	*78*	0.60	0.01	70.1	5,620	86
	FM2	*20*	0.14	0.04	274	21,920	96
Cluster (5)	*FM1*	*390*	2.84	0.07	14.1	1,130	29
	FM2	*100*	0.73	0.02	54.8	4,380	81

Table 6.1: Italian seep rates are applied to engineered storage scenarios at pilot and commercial scale. The seep rate is expressed as a percentage of annual CO_2 injection (I y^{-1}), and the time (t) in years required to leak 1% of the storage volume at these seep rates and 80% (assuming 20% residual trapping) are expressed. Resulting storage effectiveness (E) for seepage at these rates are presented for commercial scale stores.

6.1.5 Discussion

Annual CO_2 Flux

Here we determine that the total estimated annual CO_2 flux from dry (diffuse/vent) CO_2 seeps is 3.3 ± 0.8 Mt y^{-1}, which can account for 3.6 ± 1.0 % (Kerrick, 2001) to 0.9 ± 0.4% (Morner and Etiope, 2002) of the global Earth budget from non-volcanic sub areal CO_2 release. Total CO_2 release from all non-volcanic CO_2 seep types is 6.5 ± 1.1 Mt y^{-1} which constitutes 6.8 ± 1.9 % (Kerrick, 2001) to 1.7 ± 0.8 % (Morner and Etiope, 2002) of the global non-volcanic sub areal CO_2 budget.

Total deep derived CO_2 transported by Apennine aquifers and released at springs (and wells) totalled 9.3 Mt y^{-1}. These models were based on measurements at springs, and total measured deep derived CO_2 was 2.9 Mt y^{-1} (Chiodini et al., 2004). We can test the accuracy of our model by comparing the CO_2 flux contribution we calculate from springs to these previous calculations. Our model finds spring release a smaller quantity of CO_2 than previous measurements (2.1 ± 0.3 Mt y^{-1}, see Figure

6.2), but we note that springs selected for the Googas catalogue were selected for those which contained high proportions of deep derived CO_2 (Chiodini, 2010), suggesting that the Googas spring dataset is incomplete, but that all seeps in the Googas dataset represent the seepage of deep derived CO_2.

If we combine our modelled CO_2 release from vent, diffuse and bubbling water seeps (3.5 ± 0.6 Mt y^{-1}) with previous estimates of total deep derived CO_2 degassing from Apennine springs, we find that natural non-volcanic earth degassing in Italy contributes 13 ± 2 % (Kerrick, 2001) to 3.2 ± 1.2 % (Morner and Etiope, 2002) of the global budget. To place these quantities in context, such natural, non-volcanic CO_2 flux is only ~ 1.5% of the total anthropogenic CO_2 emissions from Italy in 2010 (EEA, 2012).

FM2 predicts that an additional ~ 600 low-medium flux NNV seeps remain uncatalogued in Italy. While >900 seeps may seem extensive, over a thousand methane/light hydrocarbon seeps were documented in Italy in the 1950s (Etiope et al., 2007b). Bubbling water and diffuse seeps are the most undocumented NNV seep, and indeed the surface expression of these seep types are the most subtle (Roberts et al., 2011).

FM1 assumes flux measurements are not biased towards any flux category and that the seep catalogue in Italy is complete. Total CO_2 release is significantly greater than FM2 because high-end flux seeps strongly influence total flux calculations (Figure 6.1). Mean seep rates for both flux models classify as high flux category (10-100 t d^{-1}), the mode category for seeps with quantified flux (Roberts et al., 2011).

Application to Engineered CO_2 Storage

Natural non-volcanic seeps are most comparable to seeps which establish from engineered carbon stores, where injected CO_2 seeps to the surface by natural CO_2 pathways. Storage sites will be selected for specific sealing characteristics whereas CO_2 reservoirs in Italy are effectively randomised. Surface seepage from these reservoirs occur because they are not ideal stores; the reservoirs are bisected or flanked by active faults and capped by highly heterogeneous and tectonised

sediments. Faulted reservoirs with heterogeneous or poorly permeable overburdens will not be selected as storage sites. In addition, these seeps are long duration fluid pathways which will have decreased the CO_2 column heights, and have minimised the wetting phase saturation by 'drying' effects (see Section 5.1.2) and have therefore increased the CO_2 relative permeability. Newly established fluid pathways may have quite different flow conditions and consequently different flow paths which will be slow when compared with evolved, long duration seeps such as those in Italy.

However, we can apply mean CO_2 seep flux rates at seeps in Italy to investigate the consequences of seepage rates on this scale from of non-ideal stores. We find that mean seep rates would release less than 1% of annual CO_2 injection at commercial scale carbon stores, and the site would be ~86-96 % effective over 1000 years. If a cluster of 5 seeps form, which is common in Italy, the store would be 30 - 80% effective over this period.

Poorly completed wells may also provide seepage paths if the selected store is a depleted hydrocarbon reservoir (IPCC, 2005). If seepage rate from a well bore post-closure of a commercial scale store was similar to the mean seep rate at Italian wells (~ 40 t d^{-1}) the effectiveness of the store over 1000 years would be 92.7%, which would fail the recommended standards (IPCC, 2005).

Even if carbon stores leak a small fraction of the injected CO_2, this is arguably more favourable than unabated CO_2 emissions from industrial sources without CCS (Scott et al., 2012). To effectively mitigate climate change, CO_2 stores of this scale must seep no more than 5.8 t d^{-1} CO_2. Such seepage would classify as medium flux according to the INGV classification (Chiodini and Valenza, 2008), and the majority of seeps in Italy are 10 - 100 t d^{-1} ('high') flux.

6.1.6 Conclusions

Natural non-volcanic seeps represent CO_2 seepage via natural fluid pathways from non-ideal stores. They provide an estimate of potential seep flux rates from engineered stores which were not selected for sealing characteristics, and therefore exhibit much greater fluxes than have been modelled from breached storage reservoirs e.g., (Pruess, 2008).

CO_2 degassing at surface seeps in Italy is globally significant. Previous flux calculations underestimated total regional CO_2 release in Central Italy, since only springs (and wells) were considered. Total CO_2 release from non-volcanic CO_2 seep types previously omitted from flux calculations is 3.5 ± 0.6 Mt y^{-1}. Total CO_2 release from all non volcanic CO_2 seeps can account for 13 ± 2 % (Kerrick, 2001) to 3.2 ± 1.2 % (Morner and Etiope, 2002) of global estimates of non volcanic sub areal CO_2 degassing.

6.2 Supplementary Information

6.2.1 Supplementary Results

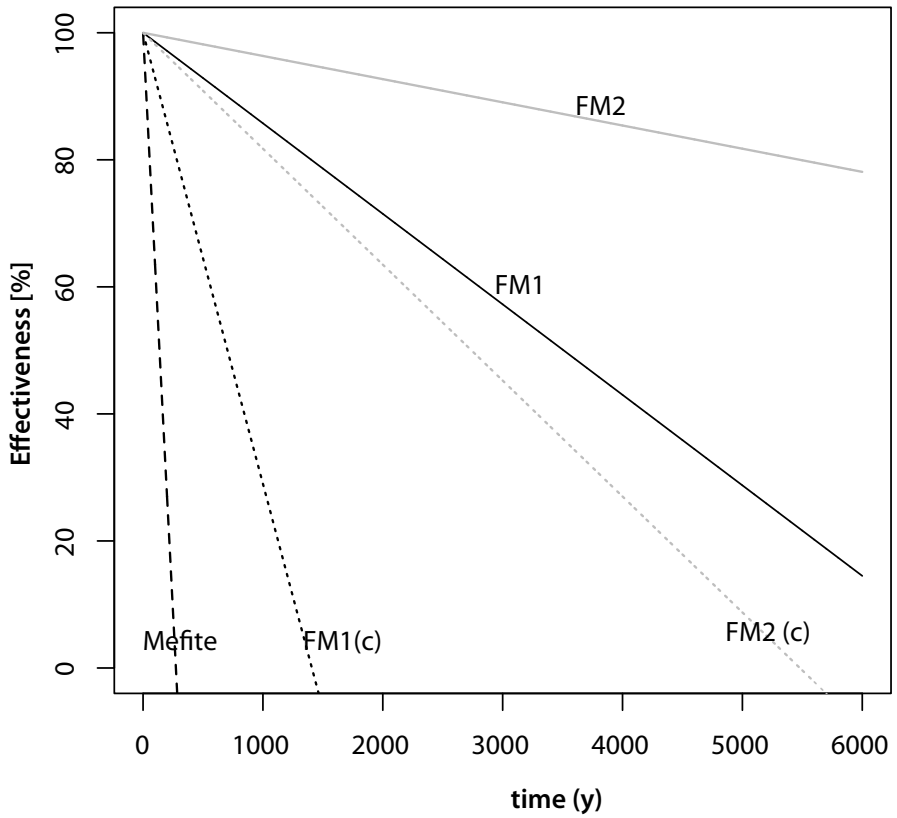

Figure 6.4: Effectiveness of a CO_2 store where 5 Mt y^{-1} was injected for 40 years, and t = 0 is the onset of CO_2 seepage from the store, post injection. Calculations performed for maximum and modeled mean (MF1 and MF2) seep rates of CO_2 seeps in Italy. Dotted lines show storage effectiveness if clusters of five mean-flux seeps develop, rather than individual seeps. For effective climate mitigation, CO_2 stores must remain 99% effective for over 1,000 years. Seepage at flux rates observed at NNV CO_2 seeps in Italy would render a store ineffective. Seep cluster development, or seeps with fluxes as great as Mefite D'Ansanto would be catastrophic for CCS.

6.2.2 Reservoir Capacity Estimates

Seeps may be fed by subsurface CO_2 reservoirs. A minimum capacity estimate of these reservoirs can be calculated by assuming CO_2 flux from the reservoir has delivered CO_2 to the surface seep at a steady state for a given time-period during which there was no significant replenishment. We consider that seepage has been steady state for 2000 years, as has been the case for Mefite D'Ansanto (Chiodini et al., 2010), and the results are in table 6.2. The reservoir volume fraction that seeps each year is 1/2000 (0.0005%), which is below the recommended seep rate for effective CCS (Hepple and Benson, 2005; IPCC, 2005).

This is a very conservative model since these seeps are still active and therefore considerable quantities of CO_2 are still present in the subsurface. In addition, capillary trapping will structurally retain a proportion of CO_2 and seeping fluids are likely to attenuate (e.g. dissolve in pore waters) during ascent and so a proportion of CO_2 will be unaccounted for.

Seep		Flux t d-1	Capacity CO_2 (Gt)
Mefite		2,000	1.46
Mean Flux Rate Model Result	*FM1*	78	0.06
	FM2	20	0.01
Seep Cluster (5)	*FM1*	390	0.28
	FM2	100	0.07

Table 6.2: Estimated CO_2 reservoir capacity from total CO_2 released at seep sites since historical records began (2 ka). Seep scenarios include maximum known seep rate (Mefite D'Ansanto, >2000 $t_{(CO2)}d^{-1}$) and mean seep flux rates from FM1 and FM2 have been applied to a single seep site or a cluster. These seeps will release approx. 0.0005 % of the total reservoir volume.

A second method of estimating CO_2 reservoir capacities in Italy is to calculate the CO_2 volume that can be contained in hydrocarbon reservoirs in Italy. These reservoirs have commercial interest and therefore their capacities have been well constrained. The Val D'Agri hydrocarbon reservoirs in the Southern Apennines have a comparable geological structure to CO_2 reservoirs in Italy (Bertello et al., 2010; Casero, 2004; Masini et al., 2011; Shiner et al., 2004). The Monte Enoc and Monte Alpi reservoirs of the Val D'Agri hydrocarbon province have estimated capacities of 100 - 400 million barrels (mb) respectively. A 100 mb reservoir can contain between 6 - 9 Mt CO_2 (depending on the geothermal gradient and reservoir depth, see table 6.3. The percentage of the reservoir volume which the seeps represent remains below 0.5% the total reservoir volume.

Geotherm	2 km depth	5 km depth
°C/km	$Mt_{(CO_2)}$	$Mt_{(CO_2)}$
40	8.2	8.9
60	5.8	6.9

Table 6.3: CO_2 reservoir capacity, assuming similar capacity to Italian hydrocarbon reservoirs. Reservoir capacity increases with depth (pressure) and cooler geothermal gradients.

Chapter 7

Discussion: uncertainties and ambiguities

Results presented in this thesis offer a valuable insight into multiscale processes governing the fate of CO_2 fluids at depth. There are several uncertainties, ambiguities and overarching considerations which are discussed in this Chapter.

7.1 Research limitations

7.1.1 Limitations of the dataset

A GIS dataset comprised of the Googas seep catalogue; geological, geophysical and resource information; and topographical and population data formed the cornerstone to much of the research presented in this thesis. While this dataset was rich and broad, there were several limitations that hindered the precision quality of the research. These shortcomings have been made clear in the relevant chapters, but relate to:

- Incomplete cataloguing of the CO_2 seeps. In Chapter 6, the number of undiscovered or uncatalogued CO_2 seeps is estimated by assuming complete cataloguing of high and very high flux seeps, and a power law relationship between seep frequency and seep flux. This model finds 600 low and medium flux natural non-volcanic CO_2 seeps are unaccounted for. These seeps can have little or minor physical expression and are therefore more like to be poorly catalogued. As noted in Chapter 6, over 1000 CH_4 and hydrocarbons were catalogued in Italy in the 1950's. CH_4 had greater IFT than CO_2 and therefore seeps less readily from reservoirs than CO_2.
- Incomplete cataloguing of CO_2 seep characteristics. Chapters 3-5 makes reference to the fact that many seeps lack information other than location, name and type. The absence of seep temperature and flux information is particularly pertinent in Chapter 5 and 6, since it meant it was difficult to quantify flux from known seeps and to ascertain if seeps were related to subsurface CO_2 reservoirs.
- No further information could be determined regarding human fatalities at three CO_2 seeps, which are recorded in the Googas database (Chiodini and Valenza, 2008). Since so few fatalities have occurred at CO_2 seeps, the number

of deaths and the nature of the victim behaviour would be valuable information.

- Structural and geological information was only available at broad scales. Research methods presented in Chapter 3 uses lithological and structural information from the 1:500,000 and 1: 1,000,000 scale geological map. Unfortunately 1:100,000 scale information was not available for the entire seeping region. While these datasets were fit for investigating regional scale controls on seep locations, it hampered investigation into the role of local scale structures on seep locations, which we instead investigate by assessing the role of lithology and topography in Chapter 4.
- The relationship between seeps and reservoirs in Chapter 5 is speculative, and without detailed geochemical information it is impossible to establish if CO_2 reservoirs nearby CO_2 seeps are causally related. The only exception is for the Pieve Santo Stefano reservoir and nearby Caprese Michelangelo seep cluster. This CO_2 reservoir is commercially exploited and so gas samples from the fertile CO_2 horizon have been studied by researchers at University of Florence[1] (Vaselli, 2012), and the CO_2 fluids are related. All other CO_2-bearing wells are closed.
- In Chapter 5, the geothermal gradient was interpolated from a raster constructed from the publicly available isotherm data (Geothopica, 2010). While appropriate for the broad scale of this research, the geothermal gradient has huge effect on the down well CO_2 properties, and so well constrained geothermal gradients can confidently inform the CO_2 properties at depth.
- Modern down well technology allow accurate logging and correction while drilling. In the absence of information these tools provide, information such as CO_2 column heights could not be determined from down well pressure changes. Few permeability measurements are available for overburden and reservoir rocks, which would allow more accurate seepage-area investigations in Chapter 5 to constrain the mechanisms of CO_2 leakage from the reservoir.

[1] Università degli Studi di Firenze

7.1.2 Relevance to Engineered CO_2 storage

By their nature, analogues studies cannot accurately represent unnatural processes and so the applicability of the natural CO_2 seeps and reservoirs studied in this thesis to engineered CO_2 storage will have limitations.

Not all seeps in Italy will necessarily be fed by large subsurface CO_2 reservoirs. Carbonate aquifers in Italy can retain and transport significant quantities of CO_2 (Chiodini et al., 2004). These waters have had long residence times (Minissale, 2004), and CO_2 fluids have distributed sources and mixed origins (Chiodini et al., 2004); they are not fed by a single deep reservoir. Therefore seeps that arise from degassing regional aquifers are not direct analogues to the seeps that might arise from breached 'young' engineered stores where the majority of CO_2 is structurally trapped. However, they are excellent analogues for leakage from 'mature' engineered stores in aquifers, where a significant proportion of the injected CO_2 has had time to dissolve into formation waters, which could be on the order of 1000 years (IPCC, 2005).

Large CO_2 reservoirs located near CO_2 seeps were studied in Chapter 5. These seeps are most analogous to those that may arise from breached 'young' CO_2 stores. Globally, there are few examples of reservoirs that directly feed surface CO_2 seeps, so the leaking CO_2 reservoirs in Italy are valuable analogues. When considering flux rates and seep paths at such reservoirs it must be remembered that they are flawed. Surface seepage from these reservoirs occur because they are not ideal stores; the reservoirs are bisected or flanked by active faults and capped by highly heterogeneous and tectonised sediments. Storage sites will be selected for specific sealing characteristics; faulted reservoirs with heterogeneous or poorly permeable overburdens will not be selected as storage sites. It is interesting, and reassuring, that the majority of such geologically imperfect CO_2 reservoirs appear to be effectively sealing, although there remains the possibility that these reservoirs are leaking and the CO_2 is trapped or dispersed in the subsurface rather than seeping to the surface.

Natural CO_2 seeps will be migrating by natural, steady state, fluid pathways. In contrast, in the context of CCS, the greatest risks of CO_2 leakage from engineered stores are improperly sealed boreholes (IPCC, 2005), complications relating to CO_2 injection (Haszeldine, 2009) and geomechanical effects from the pressure response to CO_2 injection. In Italy, deep wells leak CO_2. These can be exploration wells, geothermal wells, or wells for water supply, and can provide some indication of the seepage rates of CO_2 from improperly abandoned wells for CCS (Section 6.1.4). The Pieve Santo Stefano reservoir studied in Chapter 5 is likely to be leaking as a result of high fluid pressure in the reservoir. This process is analogous to leakage arise from geomechanical failure at CO_2 stores. As such, natural analogues in Italy can provide some information about seeps that may arise from 'CCS induced' fluid pathways. It is important to consider that CO_2 seeps in Italy are long duration fluid pathways which will have minimised the wetting phase saturation by 'drying' effects and therefore increasing the CO_2 relative permeability. Newly established fluid pathways may have quite different flow conditions and consequently different flow paths when compared with evolved, long duration seeps such as those in Italy.

7.1.3 Wet and Dry Seepage; Wet or Dry leakage?

In this thesis, CO_2 migration from the reservoir is referred to as 'leakage' while ascent to the surface is referred to as 'seepage'. There is a distinction between fluid processes at depth and fluid processes toward the surface.

What does wet or dry seepage actually represent?

'Dry' surface seepage may not represent CO_2 delivery from depth as a free phase. In Chapter 5, we learn that CO_2 solubility in water rapidly reduces toward the CO_2 phase transition. Therefore most CO_2 transported as a dissolved constituent of saturated waters will be released as these formation waters ascend, and the quantity of dissolved CO_2 will be much reduced when these deep waters reach phreatic depths (~ 700 m). CO_2 could also be

delivered from depth as a free phase, especially if fluids are channelised along permeable pathways.

Regardless of the origin or transport pathways of buoyant CO_2 in the phreatic zone, when CO_2 reaches the vadose zone, it will no longer be less dense then surrounding pore fluids (in this case, air). The CO_2 buoyancy is therefore reduced, encouraging lateral dispersion.

Depending on surface geology, 'wet' or 'dry' surface seeps may develop. For example, in Chapter 4 we suggest that both bubbling water and diffuse seeps represent CO_2 dispersion processes in the shallow subsurface; diffuse CO_2 emissions result from CO_2 dispersion in the vadose zone, while bubbling water emissions results from CO_2 dispersion in the phreatic zone or in perched aquifers where CO_2 reaches the surface together with this groundwater. Dry CO_2 migration even in the near surface can hence lead to 'wet' CO_2 delivery at the surface.

These considerations effect the total calculated flux from Apennine aquifers CO_2 in Italy. Modelling of CO_2 transport and release from Apennine carbonate aquifers are considered to underestimate total regional CO_2 flux since the contribution from dry gas manifestations are not included (Chiodini et al., 2004). We present new calculations of CO_2 flux from dry gas seeps in Chapter 6. If CO_2 released at diffuse and bubbling water seeps represent CO_2 degassing from aquifer waters, the CO_2 budget transported and released by aquifer groundwaters is greater than previously thought, and total CO_2 degassing not related to groundwater transport will be reduced. However, it may be impossible to determine the proportions of CO_2 which interact with groundwaters without rigorous noble gas geochemical studies. Regardless, total modelled CO_2 flux at dry CO_2 seeps is less than total modelled CO_2 flux from wet seeps and Apennine springs, therefore in the context of CCS, it could be inferred that more CO_2 will be dissolved in groundwaters than will be released at dry gas seeps. Historically, dry seeps present greater health risk to humans than wet seeps, and so wet seepage may be considered more favourable.

Seep type ambiguities: What are bubbling water seeps?

"Bubbling Water", as defined by Googas researchers (Chiodini and Valenza, 2008) is an ambiguous seep classification. There are two feasible mechanisms which cause CO_2 to bubble through water:

- Waters release CO_2 as they emerge at the surface. CO_2 bubbles form, in the same way as sparking water. These are 'wet' seeps.
- CO_2 seeps towards the surface as a free phase, but emerges where there is standing water pools. CO_2 bubbles through these pools. These are 'dry' seeps.

Bubbling water and springs show the same distributions and elevations from computed river paths (see 4.1.5). This suggests that bubbling water seeps are wet seeps. However other observations suggest that the two seep types are distinct:

- Bubbling water seeps are the only seep type to show distributions from computed stream paths (an order of magnitude smaller than rivers, see section 4.1.4) different to the synthetic control, including springs. This implies that bubbling water seeps preferentially develop towards minor, topographic depressions which do not determine the location of springs.
- The temperature distribution of CO_2 springs and dry (vent/diffuse) seeps are distinct (Figure 7.1). Springs are warm, while dry seeps are cool. Spring type CO_2 seeps are warm, while diffuse/vent seeps are cool. However, bubbling water seeps show temperature characteristics in the range between springs and dry seeps, and show greatest similarity with wells.
- Bubbling waters commonly colocate with diffuse seeps at dual system seeps (see section 2.1.4). Springs are never partnered with other seep types.

- Cluster analyses performed for individual seep types (section 3.1.6) find clustering is a feature for all natural seep types except for springs, which are discrete manifestations.

Wells are effectively groundwaters with high dissolved CO_2 contents and the similarity in temperatures between bubbling water and well seeps only informs us that the waters that are bubbling are likely to be groundwaters rather than poor ground drainage. These observations show that bubbling water seeps are distinct from springs, however, they do not differentiate whether these seeps represent dry or wet CO_2 delivery at the surface.

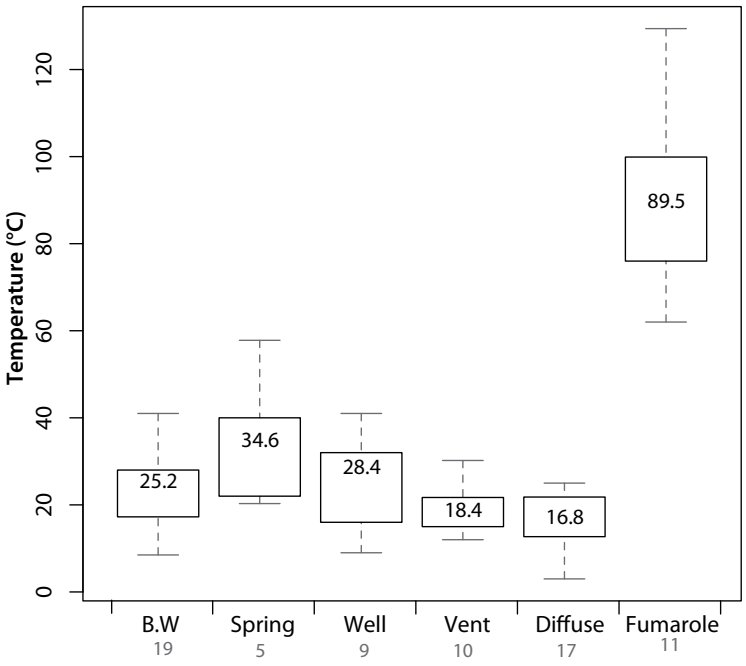

Figure 7.1: Box plot of seep temperature characteristics for each seep type. The mean temperature for each seep type is noted in the boxes, which show the interquartile range. The number of seeps with temperature measurements in each seep category is shown in grey beneath the seep type labels.

7.2 The Role of the Geothermal Gradient

From the Apennines to the Tyrrhenian the geothermal gradient increases from 30°C to 70°C, with gradients over 250 °C in the volcanic geothermal regions. The geothermal gradient determines the CO_2 properties with depth, and therefore consequences on CO_2 flow properties and solubility which will influence the fate of CO_2 fluids.

7.2.1 CO_2 Leakage and the Geotherm

The geothermal gradient determines the shape of the downhole CO_2 property profiles which in turn determine the flow characteristics (density, solubility, buoyancy, IFT) and therefore the flow path of CO_2 fluids. To enable rapid CO_2 flux from the reservoir in the gas phase, permeability-area conditions indicative of faults are necessary, but for equivalent CO_2 flux in the dense phase fluids can leak from the reservoir without the needs for deformation enhanced fluid pathways (Section 5.1.5). Fault related permeability becomes necessary for conserved CO_2 flux at depths towards the phase transition, which is dependent on the geothermal gradient.

The case studies in Chapter 5 exhibit geothermal gradients from 28°C/km to 93°C/km. Figure 7.2 shows the pressure density profiles for CO_2 fluids over this range of geothermal gradients (for at hydrostatic conditions, and surface temperatures of ~15 °C). The corresponding depth-density profiles are show in Figure 7.3. The only profile to 'touch' the vapour pressure curve at hydrostatic conditions is the 20°C/km geothermal gradient. This has marked consequences on the rate of change of CO_2 density during ascent from depth, and therefore buoyancy drive and permeability-area combinations necessary to maintain flow rates (see section 5.1.5). At geothermal gradients over 50°C/km, CO_2 density depth profiles are smooth (Figure 7.3) and CO_2 remains in gas phase at over 3 km depth.

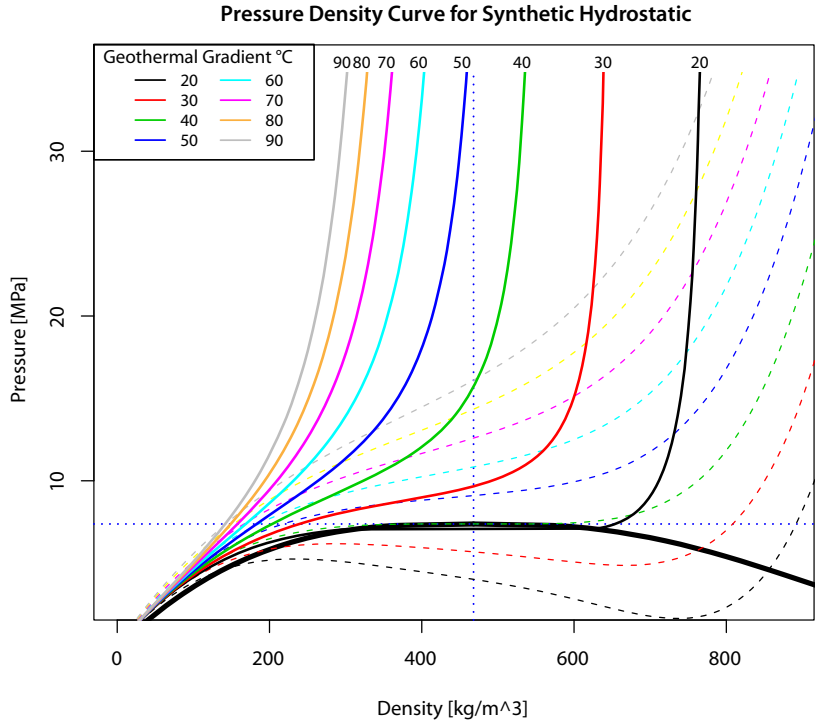

Figure 7.2: Pressure - CO_2 density plot for CO_2 fluids at hydrostatic pressure conditions at the range of geothermal gradients observed in the case study reservoirs. Dashed lines are isotherms. Note that at gradients cooler than 40°C/km pass close to the vapour pressure curve, where rapid phase change leads to rapid density decrease. CO_2 at 2 km depth for these cool geothermal gradients will be in dense phase, whereas CO_2 density profiles for warmer geothermal gradients stay in the 'light' phase until greater than 3 km depths.

For cooler geothermal gradients CO_2 fluids remain dense until the phase transition depth, where rapid density decrease occurs over minimal change in depth. Seepage area for these fluids will therefore remain constant until the phase transition, whereafter greater permeability and area combinations are required for steady CO_2 flux. At the phase transition complex local effects from volume expansion will perturb flow.

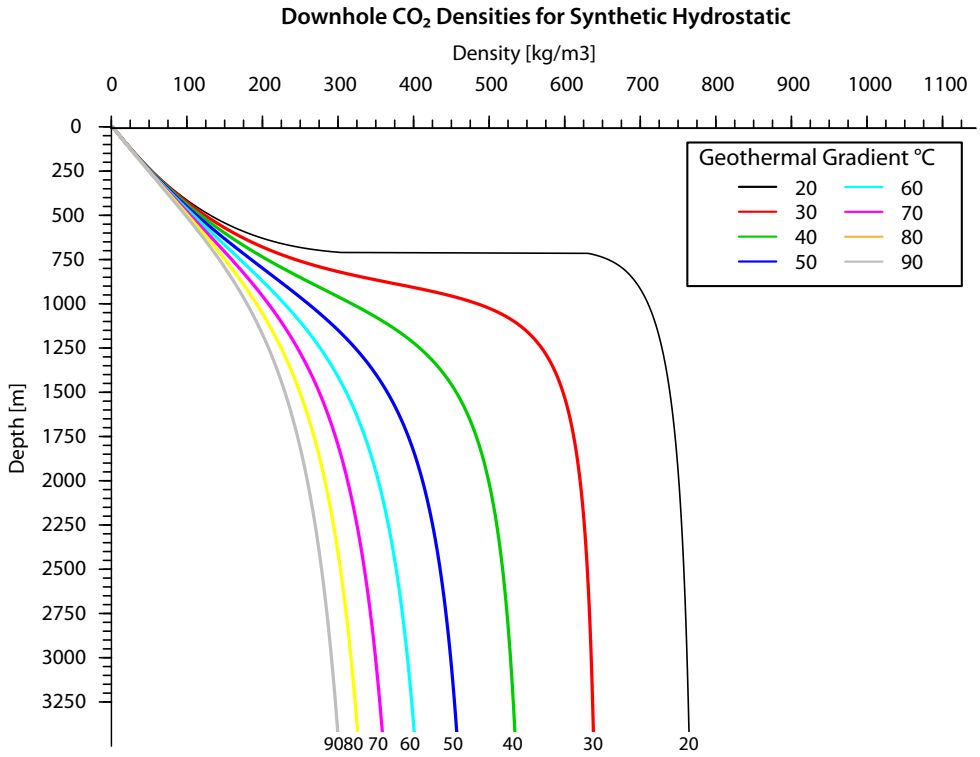

Figure 7.3: Downhole CO_2 density profiles at hydrostatic pressure conditions for the range of geothermal gradients observed in the case study reservoirs. Note that at gradients warmer than 40°C/km, the CO_2 incrementally decreases density as it ascends from depth, whereas CO_2 ascending in cooler environments will experience a rapid density decrease as fluids become shallower than 1000 m depth.

These considerations will affect CO_2 seep distribution at the surface. To enable rapid flux (100 t d^{-1}) of free phase CO_2 from a reservoir in gas phase (which here refers to 'light' phase CO_2, that is, CO_2 below the critical density, 464 kg/m^3), high permeability paths are necessary (section 5.1.5). These pathways are likely to be provided by fault damage zones. The density decrease from reservoir to surface is gradual, and the total decrease will be less than the critical density. For the same flux from a reservoir which contains dense phase CO_2, leaking fluids may not initially require high permeability pathways. However, fluid ascent to the surface is accompanied by a total density decrease of ~ 800 kg m^{-3}, therefore the area-permeability combinations required to conserve CO_2 flux will have to increase

significantly more than fluids initially leaking from the reservoir in gas phase. For dense CO_2 fluids, towards the phase transition high permeability pathway (faults) will become necessary to conserve CO_2 flux. Density decrease will cause CO_2 will spread until such pathway(s) are encountered and utilised. If no high permeability pathways are encountered, rapid CO_2 flux cannot occur. The area-permeability effects will be overestimated in these calculations since the pressure effect of CO_2 buoyancy is not considered here.Flow of free phase CO_2 fluids into the phreatic zone is therefore likely to be channelised via faults. In the vadose zone, the CO_2 may disperse laterally to form clusters and the location of the seep with respect to the CO_2-channeling fault is determined by local topography and outcropping rock characteristics (as shown in Chapters 3 - 4). It follows that dense phase CO_2 leaking from a reservoir may disperse more, and at greater depths, than if gas phase CO_2 fluids leak from the reservoir. It can therefore be hypothesised that reservoirs leaking dense phase CO_2 may develop seep clusters with a greater radius than reservoirs leaking free phase CO_2 (see figure 7.4).

This is a significant simplification of a complex process. Darcy flow is limited when considering the flow of buoyant fluids since buoyancy, frictional effects, and other complex fluid considerations are not accounted for. However, this is the best simple approximation to a complex problem for the scope of this research.

Figure 7.4: Schematic diagram representing CO_2 migration from reservoir to surface at the same rate for two similar geological settings which have different geothermal gradients. 'd' refers to CO_2 seeping in dense phase and 'g' refers to CO_2 seeping in 'light' or gas phase. **(A)** This scenario shows a CO_2 reservoir in a region with a cool geothermal gradient (28°C, like PSS1), and the depth-CO_2 density profile is shown to the right. Dense phase CO_2 leaks from the seal over a distributed area. As these fluids ascend, CO_2 density decreases and so, according to the Darcy flow equation, these fluids require greater seepage area or permeability combinations to sustain a steady CO_2 flux. CO_2 therefore disperses towards the phase transition, and flow becomes channelised along fractures and faults in the overburden. Later dispersion at depth leads to the development of a broad seep cluster at the surface [cntd overleaf].

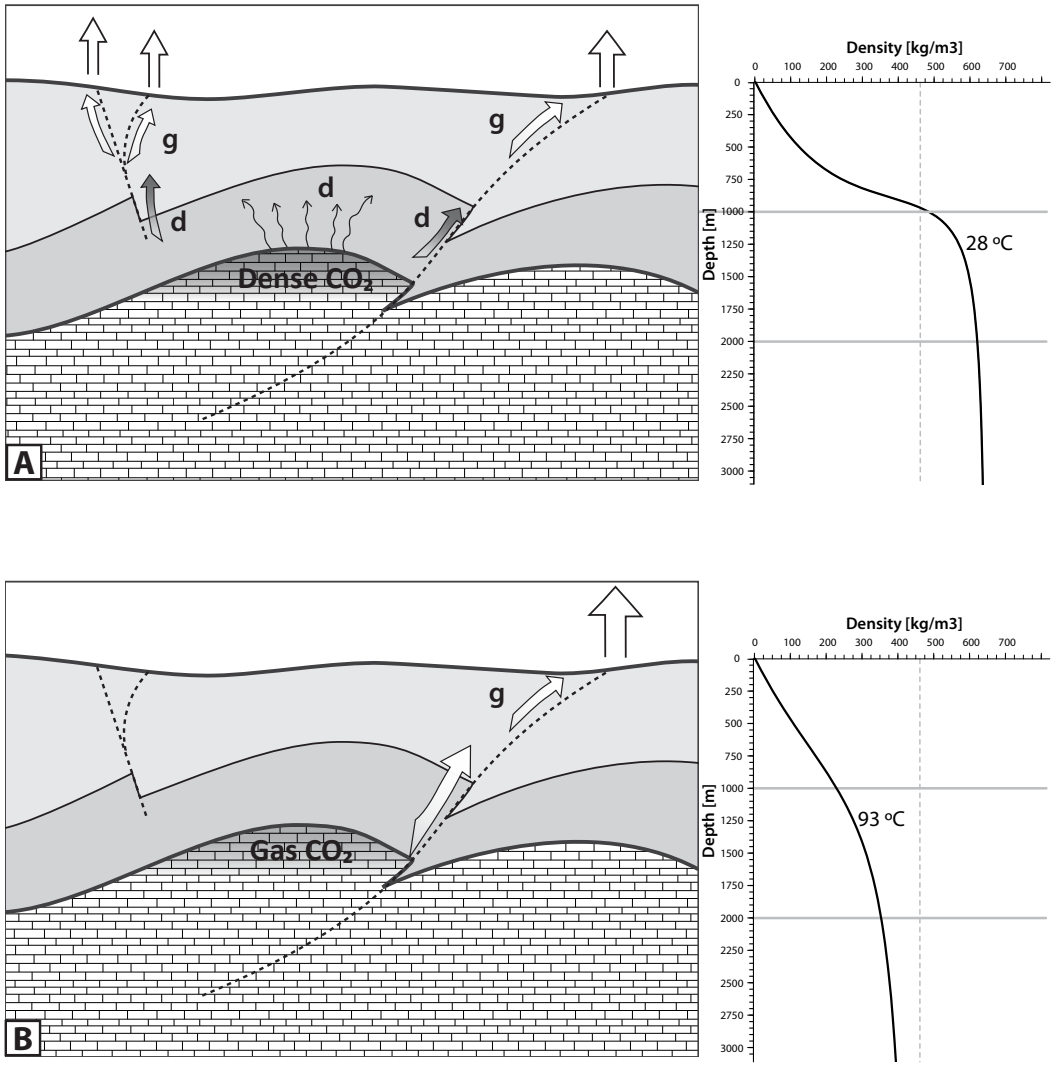

[cntd] **(B)** This scenario shows a CO_2 reservoir in a region with a warm geothermal gradient (93°C, like MF1),-CO_2 density decreases more gradually than scenarios (A), as can be seen from the depth density profile to the right. Gas ('light') phase CO_2 leaking from the reservoir requires a high permeability path for fluids to migrate at the same flux as fluids in (A). Fluids leak by the permeability provided by a non-sealing fault. A seep cluster of smaller radius than (A) might develop following CO_2 dispersion in the vadose zone.

7.2.2 Temperature and CO_2 Charge

We learn in Chapter 5 that formation waters can transport significant quantities of CO_2, but it is more likely that high flux venting clusters are fed by CO_2 seeping from the reservoir in free phase rather that dissolved phase. CO_2 saturated waters are, however, capable of charging CO_2 bearing structures by either pressure or temperature perturbation.

The hydraulic path of circulating CO_2 bearing waters will ascend and consequently experience a pressure reduction as they flow across an anticline structure. At depths greater than ~ 2 km, this will cause a decrease CO_2 solubility and CO_2 will be released from solution if these waters are saturated. Deep structures such as the Acerno or Pieve Santo Stefano reservoir could be charged by this mechanism. Let us consider the Pieve Santo Stefano reservoir as an example. Ignoring salinity effects, CO_2 saturated waters ascending from 5 km depth to 4 km depth would be associated with a solubility decrease of 0.5 molal. To supply 100 t d^{-1} to the reservoir requires 25 m^3 s^{-1} influx of ascending CO_2-saturated water to the reservoir.

For waters ascending in anticline structures shallower than ~ 2 km, the associated pressure decrease can be associated with an increase in CO_2 solubility as the CO_2 approaches the phase transition from dense to gas phase (as discussed in Chapter 5). To decrease the CO_2 carrying capacity of these waters, they must either be heated or mix with other waters of a different composition and temperature.

Figure 7.5 shows how waters circulating from the Apennines towards the Tyrrhenian in platform carbonate aquifers experience a decrease in CO_2 saturation potential as they are heated by the increasing geothermal conditions. For example, CO_2 saturated waters circulating at ~1000 m depth from a 40°C/km geothermal setting to 90°C/km geothermal setting will release half its dissolved CO_2. CO_2 could be delivered to CO_2 to reservoirs and seeps in the Tyrrhenian by this mechanism.

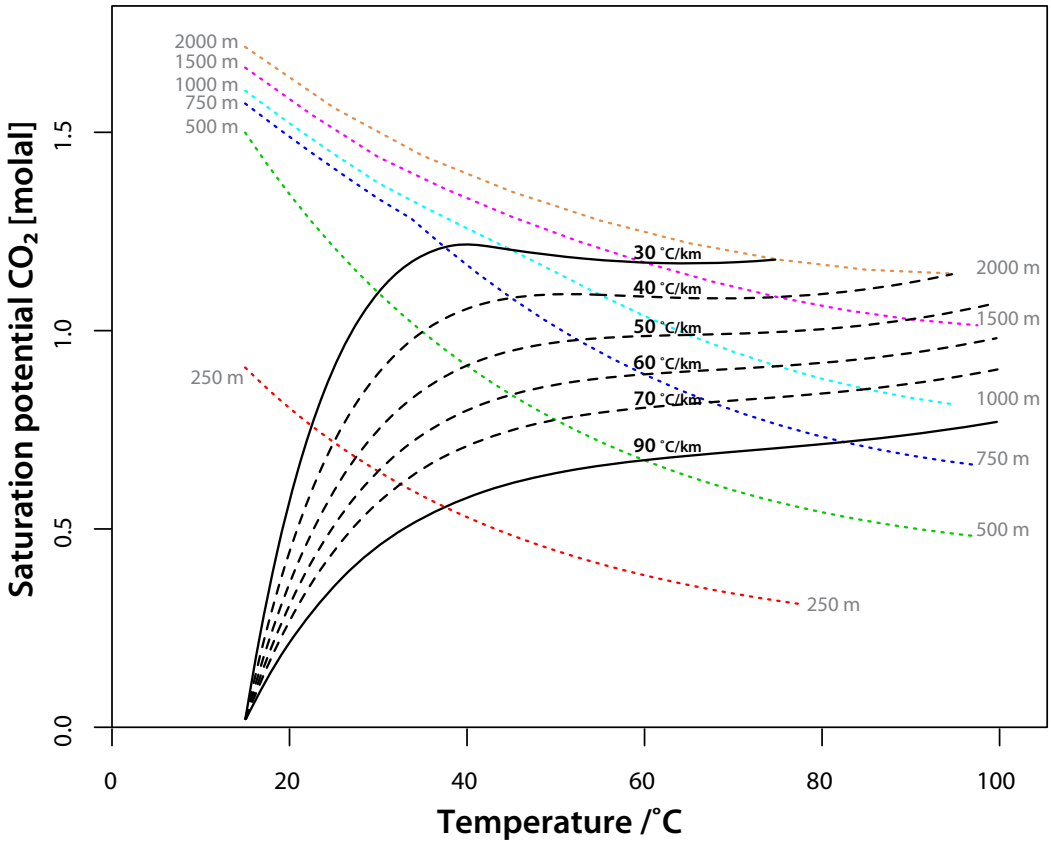

Figure 7.5: The effect of geothermal gradient on CO_2 carrying capacity of water. Black lines show change in CO_2 solubility and temperature for depth profiles for the range of geothermal gradients observed in case study wells (from 30-90°C/km). Depth contours labeled as dashed coloured lines. This plot shows how waters circulating from the Apennines towards the Tyrrhenian in platform carbonate aquifers can deliver CO_2 to reservoirs and seeps by simply being warmed as the geothermal gradient steepens. For example, CO_2 saturated waters circulating at ~1000 m depth from a 40°C/km geothermal setting to 90°C/km geothermal setting will release half its dissolved CO_2.

The Frigento reservoir structure has anomalous thermal conditions, and the reservoir crest is approximately 1000 m shallower than the surrounding carbonate platform units. If water is free to circulate in the water leg from outside of the structure, these waters would be ascending from 2000 m to 1000 m depth, and will be heated by at least 30 °C. The associated solubility drop will be ~0.4 molal and so to supply 100 t d^{-1} to the reservoir 20 m^3 s^{-1} of fresh water saturated with CO_2 must ascend and be heated.

The rate of CO_2 degassing at Mefite D'Ansanto, located above the Frigento reservoir, is extremely high (2000 t d^{-1} (Chiodini et al., 2010). To replenish the CO_2 reservoir at this rate, an influx of over 400 m^3 s^{-1} of fresh water saturated with CO_2 is necessary which would require extremely rapid hydraulic flow. Furthermore, CO_2 saturation of reservoir waters is unlikely since it required adequate CO_2 and water mixing. Importantly, reservoir pore waters are not CO_2 saturated. Well tests find fresh water in the reservoir, and the San Teodoro thermal spring, which has geochemical compositions that indicate rapid fluid ascent from a deep carbonate aquifer, does not degass CO_2 on emergence (see Chapter 5). CO_2 release by heating circulating CO_2 saturated groundwaters is therefore an unlikely mechanism for sustained CO_2 delivery to the Frigento reservoir.

It is perhaps more likely that CO_2 is delivered to the reservoir by faults. The R/Ra values of gasses at Mefite D'Ansanto indicate a strong mantle contribution to CO_2 degassing (Chiodini et al., 2010) and the seep is located very close to a décollement and terrain boundary (Ghisetti and Vezzani, 2002; Nicolai et al., 2007). It is reasonable to assume that the deformation associated with this deep décollement may encourage CO_2 delivery from deep sources and the thick sequence of thrust sheet top deposits which hide the décollement, as documented in the Trevico well (Improta et al., 2003; ViDEPI, 2009) guide buoyant CO_2 fluids into the carbonate anticline structure, where they accumulate. If there has been steady CO_2 flux since seepage first established over 2000 years ago (Chiodini et al., 2010), at least 1.46 Gt CO_2 has been released (see section 6.2).

It is difficult to consider which geological processes that can rapidly generate CO_2 at 2000 t d^{-1}, unless a local volcano-metamorphic source is present, as previous researchers have insinuated (Italiano et al., 2000). It may instead be that the reservoir is not being replenished at this rate (and therefore CO_2 is not being generated at this rate), in which case CO_2 accumulation occurred over a long time interval, and now the very large Frigento CO_2 reservoir is depleting.

7.2.3 Temperature and Seep Density

The effects of elevated geothermal gradient on CO_2 carrying capacity of formation waters can also account for the increase seep density in regions of high heat flow (see Chapter 4, (Collettini et al., 2008)). Warmed waters will not be able to dissolve large quantities of CO_2 and will therefore encourage dry gas seep development. Cooler circulating waters which are warmed as they flow into the region of elevated geothermal condition may release dissolved CO_2 as their CO_2 carrying capacity is decreased. This will be most pronounced for aquifers, since these have greater potential to dissolve large quantities of CO_2 in their formation waters than low permeability rock units.

7.3 Carbonate Dissolution and Precipitation

7.3.1 Dissolved Rock Volume

The geochemistry of some CO_2 springs in Italy show no mantle CO_2 enrichment and, overall, 33.2% of CO_2 in Apennine springs source from the dissolution of carbonate rocks (Chiodini et al., 2004). We calculate the mass of rock required to be dissolved to supply CO_2 at the observed rates assuming i) no external (mantle or biogenic) CO_2 contribution and ii) CO_2 dissolution contributes to 33.2% of the total dissolved CO_2.

Seepage at 10 $t_{(CO2)}d^{-1}$, sourcing only from the breakdown of $CaCO_3$, would result from 0.3 kg($CaCO_3$) s^{-1} or 23 t($CaCO_3$) d^{-1}. Given the density of these carbonate rocks (~2900 kg m^{-3}) this equates to ~ 7.8 m^3 of limestones either being heated or dissolving to release CO_2 each day. If CO_2 released by the dissolution of carbonates

contributes to 33.2% of the total CO_2 flux, 0.9 m^3 of limestones breakdown to release CO_2 each day. For the total CO_2 discharged from springs in central Italy (Chiodini et al., 2004), 33.2% from carbonate dissolution is equivalent to 0.002 km^3 rock volume per year.

If the area of degassing is simplified to a rectangle the extent of the Tyrrhenian sector (approximately 60 km x 600 km) and the platform carbonate units (APC and WCP) are considered to be minimum 5 km thick for this area (Ghisetti and Vezzani, 2002); the carbonate rock volume in the Tyrrhenian is 180,000 km^3.

Assuming annual carbonate dissolution and transport to the surface has been continuous at the same rate since travertine formation began (maximum dated travertine is 0.5 Ma (Minissale, 2004)) then ~1,200 km^3 total rock volume has been dissolved, which is 0.7% of the total carbonate rock volume in the Tyrrhenian. This is not a geologically unreasonable value. Porosity in APC units is usually fracture or vuggy porosity (Casabianca et al., 2002; Casero, 2004; Larsen et al.).

7.3.2 What keeps seep paths open?

CO_2 fluid flow along faults often cause mineral sealing of fractures by the precipitation of carbonate cements as CO_2 degasses from solution. Undersaturated CO_2 fluids will tend to dissolve rather than precipitate carbonate minerals. H_2S, present in most CO_2 seeps in Italy, will encourage this erosive process, since it readily dissolves water creating a strong acid. Strong CO_2 flux and associated high partial pressures may therefore conserve or enhance flow pathways. For fluid pathways at observed seep clusters to have been maintained for long time periods, they must not have been affected by cementation. In contrast, slow seepage or elevated CO_2 saturation will decrease CO_2 partial pressures, encouraging precipitation and eventual changes in fluid path.

Additionally, mixing water always leads to an aggressive water, oversaturated with CO_2. Therefore, where ascending CO_2 waters mix with cool meteoric waters, the resulting fluid is erosive and will dissolve the host carbonate units.

Chapter 8

Conclusions summary, and proposed future research

This research was motivated by the need to understand the controls on the location and consequences of different types of natural CO_2 seepage at the Earth surface. This has direct application to engineered CO_2 storage. It is important to ensure that geological stores are selected for characteristics that minimise the risk that injected CO_2 will migrate from the reservoir, and that seep pathways can be predicted in the unfortunate case that CO_2 does breach the store. Understanding the geological processes governing CO_2 migration and fate in the crust therefore informs site selection and characterisation procedure, seep risk assessment and targeted site monitoring strategy. Appreciating the risk of human death at CO_2 seep using real, historical data is significant for the public perception of onshore CO_2 storage operations, since public opposition can delay, suspend, or even terminate CCS developments.

This chapter closes the thesis by outlining the key conclusions of the research presented in Chapters 2 - 7, and the implications or recommendations to CCS

operations to ensure long term security of stored CO_2. Future research which could investigate the scientific questions arising from this research are proposed, to conclude.

8.1 Research Conclusions

The study of naturally occurring CO_2 seeps and reservoirs in Italy has provided insights into predicting natural seep paths of CO_2 fluids. This contributes to a body of knowledge which directly informs site selection procedure for carbon storage and maximise the long term storage potential for CCS. Thorough scientific understanding of the geological processes governing fluid escape is crucial to assure the scientific, political and public communities that safe, long-term carbon storage can be realised as an effective climate mitigation technology.

8.1.1 Health Risks of CO_2 Seeps

Studying risk from natural CO_2 seeps can guide assessment of potential health risks from leaking onshore CO_2 stores. Quantifying historical fatalities from CO_2 poisoning at CO_2 seeps in Italy find risk of accidental human death is 10^{-8} y^{-1} to the exposed population. This value is significantly lower than that of many socially accepted risks. Risk of human death is strongly influenced by seep surface expression, local conditions (e.g., topography and wind speed), CO_2 flux, and human behaviour leading to death. With appropriate hazard management, health risks from unplanned seepage at onshore storage sites can be adequately minimised. The current public concern regarding death by CO_2 leakage from onshore storage sites is therefore unfounded.

8.1.2 Seep Spatial Distributions and Characteristics

Natural analogues can provide insight into these geological controls on containment, migration and surface seepage of CO_2 fluids which is crucial for site selection for geological storage. Additionally, since risk of human death at CO_2 seeps is influenced by seep type, it is important to identifying the geological factors governing the expression of CO_2 fluids.

The relationship between seep spatial distribution, structural features, and CO_2 seep characteristics (type, flux, temperature) is statistically examined. Seeps distribute differently on two spatial scales corresponding to geological structure. On large scales (>5 km radius) seeps randomly distribute and align with regional structures. On local scales (<5 km radius) seeps are clustered and aligned with subsidiary geologic structures, and seep locations are influenced by fault maturity, the presence of lithological boundaries and seep type.

The nature of the CO_2 seeps and their distance from geologic structures are determined by the flow properties of outcropping lithology, together with local topography. Where low permeability rocks are outcropping there are numerous dry seeps exhibiting a range of fluxes. CO_2 'vents' occur along faults, and where CO_2 laterally supplied by these faults, emerges from the vadose zone, 'diffuse' dry seeps develop. Wet 'bubbling water' seeps arise where CO_2 supply enters the phreatic zone or an aquifer (e.g. fractured carbonates). 'Spring' seeps emerge where valleys erode into CO_2 aquifers and are wet, high flux seeps that are positioned close to lithological boundaries. These findings will assist seepage risk assessment and targeted surface monitoring strategy at engineered carbon stores.

8.1.4 Seeping and Sealing CO_2 reservoirs

The characteristics of sealing and seeping CO_2 rich reservoirs in Italy are investigated to elucidate the mechanisms enabling or preventing fluid escape.

These reservoirs retain CO_2 in gas or dense phase at various depths and pressure conditions. Sealing reservoirs show over pressured overburden, whereas seeping reservoirs are located close to modern extensional faulting and show overburden at hydrostatic conditions.

Fluid seep rates from top reservoir conditions are applied to investigate the geological conditions required for fluid escape. Rapid CO_2 flux will always be more achievable by seeping free phase CO_2. Significant (> 100 tonnes per day) leakage of dense phase CO_2 from the reservoir can be achieved by Darcy flow without the need for faults or enhanced permeability pathways. In contrast, to enable the same CO_2 flux for gas phase CO_2, fault permeabilities and areas are necessary since seepage through the overburden would require geometrically unlikely areal extent of seepage. Changes in CO_2 properties during ascent from the leaking reservoir therefore lead to fluid channeling along high permeability pathways such as faults.

Engineered carbon stores should therefore target stores away from modern extensional regional stresses and where overburden units exhibit reservoir pressures above hydrostatic. This ensures that the low permeability overburden units are not connected to the surface, increasing long duration security of performance of the store.

8.1.3 Total Flux from CO_2 Seeps

Total non volcanic sub areal CO_2 flux from dry gas seeps in the Italian sector are poorly constrained. To refine the annual budget of natural earth degassing, we estimate total flux from all types of natural non-volcanic CO_2 seeps in Italy. CO_2 release at discrete non-volcanic degassing sites is 3.5 ± 0.5 Mt y^{-1}. This is less than total estimates of CO_2 transport and release by Apennine spring waters in Central Italy.

Mean flux rates at these seeps are applied to commercial scale carbon storage scenarios to quantify the effect of these seep rates on long-term storage effectiveness. If a single seep established with the modelled mean seep flux rate for non-volcanic CO_2 seeps in Italy, such stores would remain 86-96% effective over 1,000 years. The store would be ineffective as a climate mitigation tool.

8.2 Suggested further research

The wealth of surface and subsurface information in Italy, together with the prevalence of CO_2 trapping and degassing phenomena, provide an excellent opportunity to develop scientific insight into the crustal plumbing of CO_2 fluids. The research presented in this thesis has addressed some of the overarching questions regarding geological controls on CO_2 seep locations, distributions and characteristics. However, there is considerable potential for further study of these analogues. The salient research questions that emerge from the research in this thesis are outlined below.

8.2.1 Future Study at CO_2 Seeps in Italy

Health effects

- *What temporal factors govern density pooling effects?*

  Monitoring at a CO_2 seep site could establish what wind speeds are required for CO_2 dispersal to non-fatal levels, and how this scales with flux, vegetation and season. This is important for understanding temporal factors that govern seep health risk, so hazardous weather conditions (those which encourage density pooling) can be identified.

- *Hazard perception at different seep types?*

  Seeps can be obvious manifestations, or they can be subtle surface features that are difficult to identify. Hazard perception can greatly reduce risk of CO_2 poisoning at CO_2 seeps. The conditions required to establish 'symptoms' of CO_2 degassing at the surface may be different according to seep type or local vegetation. The wealth of CO_2 seeps in Italy can be studied to identify thresholds that encourage seeps to manifest an apparent physical expression. This will develop current understanding of the risk to human health that different seeps and local characteristics present.

Seep Distributions

- *Do seep clusters represent CO_2 dispersion in the near surface and derive from a single 'parent' fluid path?*

  Noble gas geochemical investigation at seep clusters could identify whether wet and dry seeps in a cluster derive from the same 'parent' CO_2 fluid. The research in Chapter 3 and 4 concerns large scale geological features, and field research at seep clusters may identify the smaller scale geological structures (faults, lithological boundaries) that determine seep locations.

- *To what level have dry seeps interacted with groundwaters during ascent?*

  Detailed field study and noble gas geochemical investigation could assess where CO_2 seeps show little or no interaction with groundwater, and therefore are likely delivered to the surface by channelised flow. Perhaps CO_2 cannot seep to the surface without significant interaction with water during ascent, which is important since interaction with groundwater implies CO_2 attenuation. This may address the differences between bubbling water and diffuse seeps, and test the hypothesis for their formation presented in Sections 4.4 and 7.1.3.

- *How do CO_2 pathways vary through time?*

  On the short term, it is important to establish if CO_2 seeps will migrate, and if so, on what time scales and for what reasons. Long term studies at a variety of seep types would inform which seeps are sensitive to e.g. seasonal variation or e.g. seismic sequences. CO_2 vents have been observed to be affected by these factors, but it is unclear how other seep types respond.

  Travertine deposits are located near some CO_2 seeps (Section 4.4 and 5.1.4.3). It would be interested to geochemically study these travertines to establish if they represent paleo seep paths, and if so, what cause the seepage style to change. Climatic effects or tectonic effects, or even reservoir charge or reservoir depletion could change seepage style.

8.2.2 Future Research concerning CO_2 Reservoirs in Italy

There is large scope for more detailed investigation of the seeping and sealing case study reservoirs presented in Chapter 5. Reservoirs that directly leak CO_2 to the surface are rare, and so these provide unique opportunity for studying

the physical and chemical effects of CO_2 on reservoir fluids, and the site specific processes guiding fluid escape from the reservoir.

- *How does CO_2 effect reservoir rocks?*

  Core samples were collected during the hydrocarbon exploration drilling which discovered the CO_2 reservoirs studies in Chapter 5. Petrological and geochemical study of these reservoir rocks in the fertile CO_2 horizon, and the water leg (for CO_2 bearing waters and non-CO_2 bearing waters) could establish the effect of CO_2 on the reservoir rocks, and the proportion of chemical trapping that occurs in carbonate rocks.

- *Pressure diffusion in the overburden*

  Pressure diffusion modelling could calculate the timeframe necessary for pressure equilibration in flysch lithologies. This could inform whether the observed overburden overpressure is remnant from tectonic compression, or generated by other fluid processes.

- *Modelling of reservoir leakage*

  Geological models for these seeping and sealing reservoirs could be constructed for fluid flow simulation. These simulators may use more complex or more appropriate equations for buoyant fluid flow in rocks, taking buoyancy and friction effects into account. These models could assess in detail the geological requirements for the fluid seepage observed at the surface, and simulate potential mechanisms for fluid escape from the reservoir. Similar models of sealing CO_2 reservoirs may investigate in more detail wether the geological factors identified in Chapter 5 can account for the successful retention of CO_2.

- *Capacity estimates*

  Structural models of the sealing and seeping CO_2 reservoirs in Italy would allow more accurate CO_2 capacity estimates to be calculated for these reservoirs. These can be used to assess the percentage of CO_2 leaking from non-sealing stores, which would enable more precise deductions on the implications for storage security to be made than those in Section 3.4.

Appendix 1

Table A.1: Data table of all longitude (long) and latitude (lat) and characteristics of known Italian gas seeps from the Googas database (Chiodini and Valenzia, 2008). There are 6 different classifications of seep defined by their surface expression. Some locations exhibit two seep types. Flux is measured in tonnes per day (t d^{-1}) and class as 'low' (<1 t d^{-1}); 'medium' (1-10t/d); and 'very high' (>100 t d^{-1}). Safety is defined by the nature, if any, of historical incidences of CO_2 poisoning at the seep, involving animals ('animals'), humans ('humans') or both ('animals & humans'). No recorded incidents is denoted 'NRI'.

No.	Long	Lat	Label	Type	Flux	Temp/°C	Safety
1	12.6756	41.7547	Acqua Acetosa	Vent	Low	None	NRI
2	14.8930	37.5739	Acqua Grassa	Bubbling Water	High	18	Animals
3	15.2629	40.6113	Acqua Regina	Spring	High	None	NRI
4	11.8024	43.0820	Acquapuzzola Salcheto	Bubbling Water & Diffuse	High	6.5	Animals
5	15.0408	40.4574	Acque Salse	Spring	NQ	None	NRI
6	14.1703	40.8258	Agnano Fumarola	Fumarole	NQ	None	NRI
7	14.1730	40.8279	Agnano Pozzo	Spring	NQ	None	NRI
8	13.0315	41.9852	Agosta	Spring	High	None	NRI
9	15.4314	38.0095	Alec Terme Mare	Bubbling Water	NQ	None	NRI
10	15.4315	38.0103	Ali Terme Spiaggia	Diffuse	NQ	None	NRI
11	11.5391	43.3828	Ambra fiume	Bubbling Water	High	12	NRI
12	11.5389	43.3832	Ambra Pozzo 12	Well	High	41	NRI
13	11.5472	42.8231	Anteie 1	Vent	NQ	None	Animals
14	11.5454	42.8223	Anteie 2	Vent	NQ	None	Animals
15	14.9009	37.5571	Area degassante di Patern	Diffuse	Very High	18	Animals
16	15.1193	37.7016	Area degassante di Primoti-Dagala	Diffuse	High	18	NRI
17	11.6878	42.9226	Argillone 3	Bubbling Water & Diffuse	Medium	None	Animals
18	13.8450	42.5622	Astelina	Cold Vent	Low	None	NRI
19	15.6460	40.8689	Atella	Diffuse	NQ	None	NRI
20	11.0743	43.6637	Baccaiano	Bubbling Water & Diffuse	High	3	Animals
21	12.0711	42.4600	Bagnaccio	Bubbling Water	NQ	None	NRI
22	11.6033	43.2982	Bagni Freddi	Bubbling Water	Low	24.5	NRI
23	11.5350	42.8126	Banditella	Diffuse	Medium	12	NRI

No.	Long	Lat	Label	Type	Flux	Temp/°C	Safety
24	11.7372	44.3089	Bergullo	Cold Vent	Medium	None	NRI
25	15.4244	38.0051	Berlinghieri	Bubbling Water	NQ	22	NRI
26	15.1026	38.6381	Black Point	Bubbling Water	NQ	None	NRI
27	14.1421	40.8272	Bocca Grande-Solfatara of pozzuoli	Fumarole	Very High	163	NRI
28	11.6224	43.2164	Bogliole	Bubbling Water & Diffuse	Medium	21.5	Animals
29	11.6946	42.9271	Bollore	Spring and Diffuse	High	None	NRI
30	10.7156	43.4439	Borboi	Bubbling Water	Medium	17	NRI
31	11.7592	42.1444	Borgo Pantano	Bubbling Water	NQ	None	NRI
32	11.4263	43.3066	Borra ferruginosa	Bubbling Water	Low	28	NRI
33	11.5914	43.3012	Borro Temperone	Bubbling Water	Low	17.5	NRI
34	11.5925	43.2778	Bossoleto	Bubbling Water & Diffuse	High	22	Animals
35	15.1104	38.6387	Bottaro basso	Bubbling Water	NQ	None	NRI
36	15.1094	38.6372	Bottaro cratere	Bubbling Water	NQ	None	NRI
37	11.3248	43.1942	Buca Antarella	Diffuse & Vent	Medium	None	Animals
38	12.0713	42.4200	Bullicame	Spring	Low	40	NRI
39	14.9623	41.2242	Buonalbergo	Spring	NQ	None	NRI
40	12.1003	42.0900	Caldara di Manziana	Vent in Pool	Very High	None	Animals
41	12.1994	41.9686	Caldara di Palidoro	Bubbling Water & Diffuse	Very High	None	Animals
42	15.8023	40.4618	Calvello	Spring	NQ	None	NRI
43	15.1064	38.6384	Campo 7	Bubbling Water	NQ	None	NRI
44	10.8090	43.3912	Campo delle Monache	Bubbling Water	Low	22	NRI
45	11.6886	42.9325	Campo la Villa	Diffuse & Vent	Medium	None	Animals
46	11.8187	42.4658	Candia Pozzo 15	Well	High	17	NRI
47	13.0306	42.3946	Canetra	Spring	High	None	NRI
48	15.8467	40.9028	Cantarella	Diffuse	NQ	None	NRI
49	14.9325	38.1821	Capo Calave0	Bubbling Water	NQ	None	NRI
50	14.9334	38.1819	Capo Calave0	Diffuse	Low	25	NRI
51	15.0444	40.4485	Capo Fiume	Spring & Bubbling Water	NQ	None	NRI
52	14.0711	41.6374	Capo Volturno	Spring	High	None	NRI
53	12.8121	42.2332	Capore	Spring	High	None	NRI
54	12.0223	43.6331	Caprese Michelangelo 1	Vent in Pool	NQ	None	Animals
55	12.0226	43.6325	Caprese Michelangelo 2	Diffuse	NQ	10.8	NRI
56	12.0247	43.6320	Caprese Michelangelo 3	Bubbling Water	Medium	16	Animals

No.	Long	Lat	Label	Type	Flux	Temp/°C	Safety
57	12.0222	43.6319	Caprese Michelangelo 4	Vent	NQ	None	NRI
58	14.1972	40.9122	Casa	Well	NQ	None	Animals and Humans
59	13.8018	41.6817	Casa Ianni	Bubbling Water	Very High	None	Animals
60	10.8761	43.4890	Case Torricchi	Bubbling Water	Medium	24	NRI
61	14.2364	41.6261	Castel Romano Isernia	Bubbling Water	NQ	None	NRI
62	12.8648	37.9615	Castellammare del Golfo	Diffuse	Low	24	NRI
63	12.9829	41.5425	Catena	Spring	High	None	NRI
64	12.6139	41.7792	Cava dei Selci cava	Diffuse	High	None	Animals and Humans
65	12.6142	41.7819	Cava dei Selci vigneto	Diffuse	Medium	None	Animals and Humans
66	11.6176	43.2472	Cave Paradiso	Bubbling Water	Low	27	NRI
67	10.7871	43.6122	Chiecinella	Bubbling Water	Medium	None	NRI
68	14.1661	41.4339	Ciorlano Soffione	Vent in Pool	NQ	None	NRI
69	14.8836	37.5492	Contrada Pescheria	Diffuse	High	17	Animals and Humans
70	11.3025	44.7561	Corporeno	Cold Vent	High	None	NRI
71	16.8326	39.1825	Cotronei	Bubbling Water	NQ	34.1	NRI
72	12.1581	42.3028	Cretone	Well	NQ	None	NRI
73	15.2215	40.7135	Diamante	Vent in Pool	NQ	None	Animals
74	11.2846	43.1596	Doccio	Bubbling Water	Low	32	NRI
75	11.4550	44.3358	Dragone	Cold Vent	Low	None	NRI
76	13.8949	41.3146	Emissione grotta	Vent	NQ	None	NRI
77	14.7158	37.3375	Emissione Palagonia Ovest	Diffuse	High	18	NRI
78	15.5717	40.9452	Eudria	Vent in Pool	NQ	None	NRI
79	11.2913	43.0794	Farma Petriolo	Bubbling Water	Low	14	NRI
80	14.1231	41.2603	Ferrarelle-Riardo	Well	NQ	None	NRI
81	12.2303	42.9202	Fersinone	Vent	NQ	15.3	NRI
82	14.8005	38.5744	Filo di Branda	Bubbling Water	NQ	None	NRI
83	13.5546	41.6081	Fontana Liri	Spring	NQ	None	NRI
84	11.6809	42.9199	Fontanicchi Alto	Cold Vent	Medium	None	Animals
85	15.2358	40.6941	Fossa del Bue	Diffuse	NQ	None	Animals and Humans

No.	Long	Lat	Label	Type	Flux	Temp/°C	Safety
86	12.3593	42.8235	Fosso Biscina	Vent	High	13.4	Animals
87	11.6863	42.9214	Fosso Fontanicchi	Cold Vent	Medium	15	Animals
88	12.4844	42.1119	Fosso S.Antonino	Bubbling Water	NQ	None	NRI
89	14.0531	41.1900	Francolise (Calena Well)	Well	NQ	None	NRI
90	14.3675	42.2617	Frisa	Cold Vent	Low	None	NRI
91	15.0752	38.6454	Fumarola Calcara	Diffuse	NQ	None	NRI
92	14.9783	37.5856	Fumarola di Belpasso	Fumarole	Low	18.8	NRI
93	15.1231	37.6731	Fumarola di Passopomo	Fumarole	Low	62	NRI
94	15.1279	37.5798	Fumarola di Valverde	Fumarole	Low	30	NRI
95	12.0406	43.6288	Fungaia	Vent in Pool	High	16	NRI
96	13.3869	37.6253	Fuoco di Censo	Cold Vent	Low	None	NRI
97	15.0890	37.7000	Galleria drenante Acquasecca	Well	Medium	16	Animals and Humans
98	15.0844	37.7054	Galleria drenante di Vallone	Well	Medium	16	NRI
99	15.1535	37.6932	Galleria drenante Ponteferro	Well	High	16	Animals and Humans
100	15.1363	37.7990	Galleria drenante Rocca Campana	Well	High	16	NRI
101	10.9654	43.5251	Gambassi	Bubbling Water & Diffuse	Medium	12.7	NRI
102	15.4301	38.0097	Granata	Bubbling Water	NQ	28	NRI
103	15.4301	38.0097	Granata 2	Bubbling Water	NQ	31.9	NRI
104	15.4302	38.0096	Granata vasche di fango	Bubbling Water	NQ	None	NRI
105	15.2183	37.7679	Gurna di Fondachello	Bubbling Water	Low	15	NRI
106	11.6842	42.9215	Ingresso miniera	Cold Vent	Medium	None	NRI
107	13.8813	40.7196	Ischia-Donna Rachele	Fumarole	Medium	None	NA
108	12.4322	42.0086	Isola Farnese	Bubbling Water	NQ	None	NRI
109	14.8798	36.7716	Ispica	Diffuse	Low	21	NRI
110	11.6993	43.4824	Itac Pozzo 25	Well	High	17	NRI
111	11.8867	42.3644	La Rocca	Diffuse	NQ	27.5	NRI
112	13.1238	41.4554	Laghi del Vescovo	Spring & Diffuse	Low	None	NRI
113	12.6752	41.7430	Lago Albano	Bubbling Water	NQ	None	NRI
114	12.6843	41.7506	Lago Albano riva del	Diffuse	Low	None	NRI
115	10.8147	43.1541	Lago Boracifero	Bubbling Water	NQ	93	NRI
116	12.7212	41.9677	Lago della Regina-Acque Albule	Spring	Very High	None	Animals and Humans
117	12.7000	41.7236	Lago di Nemi	Diffuse	Low	None	NRI

No.	Long	Lat	Label	Type	Flux	Temp/°C	Safety
118	15.8467	40.9028	Lago Fetente	Cold Vent	Low	None	Animals
119	13.6938	41.6962	Lago Fibreno	Spring	Very High	None	NRI
120	14.6969	37.3256	Lago Nafteca	Cold Vent	Very High	18	Animals
121	12.5561	42.1561	Lago Puzzo (Capena)	Bubbling Water	NQ	None	NRI
122	10.8675	43.1662	Lagoncino gas1	Fumarole	NQ	96.7	NRI
123	10.8503	43.1757	Lagone	Bubbling Water	NQ	90	NRI
124	11.7903	42.5858	Latera Puzzolaie	Diffuse	Very High	22.6	Animals
125	11.8184	42.6178	Latera Silphur mine	Diffuse	Very High	None	Animals
126	16.1355	39.4604	Lattarico	Diffuse	Low	26	NRI
127	11.6860	42.9230	Lavinate	Diffuse & Vent in Pool	High	None	NRI
128	10.8537	43.1528	Le Biancane 1	Fumarole	NQ	90	NRI
129	10.8548	43.1542	Le Biancane 5	Fumarole	NQ	99.9	NRI
130	10.8539	43.1528	Le Biancane 8	Fumarole	NQ	129.4	NRI
131	11.6848	42.9348	Le colline	Diffuse & Vent	High	None	Animals and Humans
132	12.0597	42.4264	Le Zitelle-Viterbo	Bubbling Water	NQ	None	NRI
133	12.8811	35.8641	Linosa Island	Diffuse	Low	27	NRI
134	15.1100	38.6400	Lisca Bianca	Bubbling Water	NQ	None	NRI
135	11.6878	42.9319	Lo Spuntone 1	Diffuse & Vent	Medium	None	Animals
136	10.8393	43.1860	LP1	Fumarole	NQ	99.8	NRI
137	13.5995	37.3757	Maccalube di Aragona	Bubbling Water	Medium	11	NA
138	13.3791	37.4649	Maccalube di Bissana	Bubbling Water	Low	None	NRI
139	14.0906	37.4965	Maccalube di Terrapelata	Bubbling Water	Low	28.5	NRI
140	12.1143	42.1134	Macchia della manziana	Diffuse	NQ	None	NRI
141	15.4246	38.0048	Magnolia	Bubbling Water	NQ	31.9	NRI
142	15.0703	41.2585	Malvizza	Bubbling Water	NQ	None	NRI
143	11.6892	42.9226	Mammellone 1	Diffuse & Vent	Medium	15	Animals
144	12.3106	41.9628	Mazzano Romano (Acqua Salsa)	Bubbling Water	NQ	None	NRI
145	15.1463	40.9746	Mefite	Diffuse & Vent	Very High	30.2	Animals and Humans
146	15.1101	40.9902	Mefitiniella polla	Vent in Pool	NQ	None	Animals
147	14.6180	40.8151	Mercato Palazzo	Spring	High	None	NRI
148	10.7801	43.2774	Micciano	Vent	Medium	None	Animals

No.	Long	Lat	Label	Type	Flux	Temp/°C	Safety
149	12.3057	43.3083	Migianella	Vent in Pool	High	13.6	Animals
150	12.1008	42.1725	Mola D'Oriolo	Bubbling Water	NQ	None	Animals
151	11.8409	43.4530	Molinbianco	Well	Medium	14	NRI
152	13.8858	41.1260	Mondragone	Vent in Pool	NQ	None	NRI
153	13.8842	41.1294	Mondragone Padule	Bubbling Water	NQ	None	NRI
154	13.8858	41.1333	Mondragone S.Rocco 1(Concre. Well)	Bubbling Water	NQ	None	NRI
155	13.8903	41.1344	Mondragone S.Rocco 2 (Geoth.	Bubbling Water	NQ	None	NRI
156	13.8914	41.1328	Mondragone S.Rocco 3 (Iron	Bubbling Water	NQ	None	NRI
157	12.0187	42.0246	Monte Bischero	Bubbling Water	NQ	12	NRI
158	11.7736	44.0464	Monte Busca	Cold Vent	High	None	NRI
159	12.0396	42.0300	Monte Solferata	Diffuse & Vent in Pool	High	None	Animals
160	10.7767	43.8872	Montecatini Leopolpina	Well	Low	32	NRI
161	12.3773	42.4886	Montecchie	Diffuse	High	20	Animals
162	11.0005	43.3866	Montemiccioli	Bubbling Water & Diffuse	High	18	Animals
163	12.0790	42.1371	Monterano-Mignone 1	Diffuse	Medium	24.1	Animals
164	12.0781	42.1388	Monterano-Mignone 2	Diffuse	NQ	21.5	Animals
165	11.6687	42.4218	Monterozzi	Bubbling Water & Diffuse	NQ	20.3	NRI
166	11.2959	43.0972	Monti di Petriolo	Bubbling Water	Low	14	NRI
167	11.8492	43.4794	Montione	Bubbling Water	Low	15	NRI
168	14.6935	41.1215	Motta	Spring	NQ	None	NRI
169	10.8250	44.5147	Nirano	Cold Vent	High	None	NRI
170	10.6981	43.4360	Orciatico	Diffuse & Vent	High	None	Animals
171	11.6818	42.9242	Palazzo 2	Diffuse	High	None	NRI
172	11.1491	43.2691	Palazzo al Piano	Bubbling Water & Diffuse	Medium	None	NRI
173	12.0940	42.1702	Parco della Mola 1	Vent in Pool	Medium	22.5	NRI
174	12.0941	42.1699	Parco della Mola 2	Diffuse	High	None	NRI
175	11.6834	43.4765	Pergine	Bubbling Water	Low	8.5	NRI
176	11.6892	43.4796	Pergine Pozzo 14	Well	High	18.8	NRI
177	12.0327	42.5784	Piazzale Cava (i Morticini)	Diffuse	NQ	None	Animals and Humans
178	11.6741	43.0665	Pienza	Bubbling Water	High	28	NRI
179	10.4209	43.5687	Piersanti 2	Bubbling Water	Low	16	NRI

No.	Long	Lat	Label	Type	Flux	Temp/°C	Safety
180	12.0157	43.6554	Pieve S. Stefano Pozzo	Well	Very High	None	NRI
181	14.0483	42.6103	Pineto	Cold Vent	Low	None	NRI
182	11.3601	42.6525	Podere zolfiera	Diffuse & Vent	High	30	Animals
183	11.6823	42.9257	Poggio all'olivo	Bubbling Water	Low	14	Animals
184	12.0324	42.1380	Poggio Capecchio	Bubbling Water & Diffuse & Well	High	17.5	Animals
185	12.1367	42.5060	Poggio dell'Ulivo 1	Diffuse	Very High	27.5	NRI
186	12.1369	42.5031	Poggio dell'Ulivo 2	Diffuse & Vent in Pool	Very High	32.4	Animals
187	12.3846	42.4866	Poggio delle streghe	Diffuse	Medium	None	NRI
188	12.1288	42.5120	Poggio Foralupo	Bubbling Water & Diffuse	High	21.8	Animals
189	11.6443	43.2930	Poggio S Cecilia	Well	High	9	NRI
190	12.5578	41.5970	Polla FSGD Ardea	Bubbling Water	Medium	None	Animals
191	13.7892	41.6827	Polla Monticchio	Vent in Pool	Very High	None	Animals
192	14.1144	37.9650	Pollina	Diffuse	Low	None	NRI
193	12.5667	42.2500	Ponzano Romano	Bubbling Water	NQ	None	NRI
194	13.8634	41.2930	Pozzo 1	Well	NQ	None	Animals and Humans
195	10.8575	43.1719	Pozzo 2	Well	NQ	99.4	NRI
196	15.7592	40.3225	Pozzo Acqua Bianca	Bubbling Water	Low	29.7	Animals
197	11.9544	42.7382	Pozzo Alfina 13	Well	NQ	90	NRI
198	11.6032	43.2994	Pozzo Cimitero	Well	Medium	29	NRI
199	11.9928	42.6223	Pozzo Enel	Well	NQ	None	NRI
200	12.8729	41.4114	Pozzo Fogliano A	Well	NQ	21.4	Animals
201	12.8717	41.4109	Pozzo Fogliano B	Well	NQ	21.7	Animals
202	14.1836	41.4081	Pratella (Acqua Lete)	Bubbling Water	NQ	None	NRI
203	11.5977	43.2659	Puzzola di Rapolano	Bubbling Water	Medium	24.5	Animals
204	11.6065	43.2926	Querciolaia	Well	Low	37	NRI
205	12.2700	42.5606	Ramici Well	Well	NQ	15.5	NRI
206	10.5761	44.5578	Regnano	Cold Vent	High	None	NRI
207	11.2903	43.1415	Risaie Anas	Bubbling Water	Low	22	NRI
208	10.3269	44.6303	Rivalta	Cold Vent	Medium	None	NRI
209	12.0214	42.1479	Rota	Diffuse	NQ	None	NRI
210	12.0852	42.1330	Rovine di Monterano	Diffuse & Vent in Pool	NQ	21.7	Animals
211	10.6360	43.5146	S Leopoldo	Well	Medium	16	NRI
212	11.6125	42.6521	S Martino Fiora	Bubbling Water	Medium	22	NRI
213	11.8024	43.0717	S. Albino Pozzo 12	Well	High	None	NRI

No.	Long	Lat	Label	Type	Flux	Temp/°C	Safety
214	11.8020	43.0734	S. Albino vasca	Bubbling Water	High	26	NRI
215	14.9123	40.6738	S. Benedetto	Spring	High	None	NRI
216	11.8723	42.8710	S. Casciano Vasca	Bubbling Water	Low	41	NRI
217	14.6490	40.7906	S. M. Lavorate	Spring	High	None	NRI
218	11.4286	43.3080	S. Maria a Dofana	Bubbling Water	Medium	36	NRI
219	15.5725	40.9147	S. Maria De Luco	Bubbling Water	Low	None	Animals and Humans
220	14.5943	40.8327	S. Maria la Foce	Spring	High	None	NRI
221	14.8647	37.5681	Salinella del Fiume Simeto	Bubbling Water	Medium	18	NRI
222	14.8900	37.5725	Salinella Stadio di Patern	Bubbling Water	Medium	30	NA
223	14.9175	37.5447	Salinella Vallone Salato	Bubbling Water	High	20	NRI
224	12.0359	42.5689	Samac Pozzo A	Well	NQ	26	Animals
225	12.0368	42.5691	Samac Pozzo D	Well	NQ	None	Animals
226	12.5201	42.7232	San Faustino	Vent	Medium	16.8	NRI
227	14.1826	37.9221	San Mauro Castelverde	Diffuse	Low	25	NRI
228	12.6039	41.7783	Santa Maria delle Mole	Diffuse	High	None	NRI
229	12.8527	42.5022	Santa Susanna	Spring	High	None	NRI
230	11.2920	43.0799	Sasso Mortaione	Bubbling Water	Low	33	NRI
231	10.8667	43.1676	Sasso Pisano1	Fumarole	NQ	99.9	NRI
232	14.6953	36.7473	Scicli	Diffuse	Low	13	NRI
233	11.6276	42.7747	Selvena	Diffuse & Vent	High	18.9	Animals
234	13.8572	41.1408	Sinuessa	Vent in Pool	NQ	None	NRI
235	13.8572	41.1408	Sinuessa	Vent in Pool	NQ	None	NRI
236	12.1229	42.1168	Solfatara di Manziana	Diffuse	High	None	Animals
237	12.2961	42.2285	Solforata di Nepi	Bubbling Water	NQ	None	Animals
238	12.5333	41.7050	Solforata di Pomezia	Bubbling Water & Diffuse	Very High	None	Animals
239	13.0113	42.3688	Solregnti del Peschiera	Spring	Very High	None	NRI
240	15.5644	40.9094	Sorg Vellutina	Bubbling Water	NQ	None	NRI
241	10.8722	43.4985	Sorg. Palagio	Bubbling Water	Medium	22.5	NRI
242	10.8537	43.1528	Sorgente di Chiorba	Spring	NQ	57.8	NRI
243	14.5152	41.2251	Sorgente Grassano	Spring	Very High	None	NRI
244	14.1755	41.4000	Sorgente il Molinello	Spring	High	None	NRI
245	14.2536	41.1369	Sorgenti di Triflisco	Spring	Very High	None	NRI

No.	Long	Lat	Label	Type	Flux	Temp/°C	Safety
246	14.8300	38.5481	Spiaggia di Rinella	Diffuse	NQ	None	NRI
247	12.4932	42.4972	Stifone	Spring	Very High	None	NRI
248	12.0304	42.1223	Stigliano-Fosso Lenta	Spring	NQ	33	NRI
249	15.2454	40.6941	Strada	Diffuse	NQ	None	NRI
250	15.2462	40.6945	Strada polla	Bubbling Water	NQ	None	NRI
251	15.2456	40.6942	Strada polla2	Vent in Pool	NQ	None	NRI
252	13.8853	41.3097	Suio Lato Garigliano (polla)	Bubbling Water	NQ	None	NRI
253	13.8958	41.3133	Suio Piattaforma	Bubbling Water	NQ	None	NRI
254	13.8500	41.2942	Suio Piscina Naturalis	Bubbling Water	NQ	None	NRI
255	13.8964	41.3081	Suio Terme Tomassi	Bubbling Water	NQ	None	NRI
256	11.5563	42.4747	Tafone	Bubbling Water	NQ	None	NRI
257	14.0608	41.1886	Teano	Bubbling Water	NQ	None	NRI
258	14.5287	41.2223	Telese Terme	Bubbling Water	NQ	None	NRI
259	12.0589	42.3992	Terme de Papi	Bubbling Water	NQ	None	NRI
260	15.6570	40.7516	Terme di S. Cataldo	Bubbling Water & Diffuse	Low	None	Animals
261	14.1157	41.5015	Terme Pozzilli (Isernia)	Bubbling Water	NQ	None	NRI
262	15.2518	40.6829	Terme Rosa Pepe	Spring	NQ	None	NRI
263	11.5912	43.2797	Terme S. Giovanni	Well	Medium	38	NRI
264	11.6866	42.9227	The Hole	Diffuse & Vent	Medium	None	Animals
265	15.6842	40.5686	Tito	Spring	NQ	20.3	NRI
266	12.0302	42.1404	Tolfa 1	Bubbling Water & Diffuse	High	None	Animals
267	12.0299	42.1396	Tolfa 2	Bubbling Water	High	None	Animals
268	12.5945	41.4873	Tor Caldara (miniera grande)	Bubbling Water & Diffuse	Medium	25	Animals
269	12.5921	41.4897	Tor Caldara (miniera piccola)	Bubbling Water & Diffuse	High	None	NRI
270	12.5939	41.4884	Tor Caldara 3	Diffuse	NQ	None	NRI
271	11.9486	42.7456	Torre Alfina	Diffuse	NQ	10.5	NRI
272	11.7118	43.1815	Trequanda	Bubbling Water	Medium	14.5	NRI
273	15.2506	40.6738	Tufaro	Spring	NQ	22	NRI
274	12.2024	43.4522	Uppiano	Bubbling Water	NQ	22	Animals
275	10.8574	43.1606	V1_V2	Bubbling Water	NQ	97.3	NRI
276	11.3484	43.4359	Vagliagli	Diffuse & Vent	Medium	12	Animals
277	12.3706	42.1194	Valle del Baccano	Bubbling Water	NQ	None	NRI
278	15.2227	40.7058	Varchera	Vent in Pool	NQ	4.2	Animals
279	15.1103	38.6402	Vasca Bianca	Bubbling Water	NQ	None	NRI
280	13.8634	41.2930	Vasca inferno	Vent in Pool	NQ	None	NRI
281	15.2290	40.6949	Vecchio Mulino	Bubbling Water	NQ	None	NRI

No.	Long	Lat	Label	Type	Flux	Temp/°C	Safety
282	12.1133	42.2212	Veiano	Diffuse & Vent in Pool	Very High	17.9	Animals and Humans
283	12.1092	42.2194	Vejano Acquaforte	Bubbling Water	NQ	None	Animals
284	10.5985	43.0369	Venturina Calidario	Bubbling Water	Low	36	NRI
285	14.4256	40.8210	Vesuvio	Fumarole	Very High	95	NRI
286	11.5363	42.8532	Zancona	Bubbling Water	NQ	19.2	NRI

Appendix 2

Two-point correlation function script[16] (Python)

```
>> npoints  = len(data)
>>
>> # Generate bins for histograms
>> radii          = np.logspace(-2, 3, 50)
>> rinc           = np.diff(radii)
>> midradii       = radii[:-1] + rinc/2
>>
>> azbins         = np.linspace(0, 180, 19)
>> mid_azbins     = azbins[:-1] + np.diff(azbins)/2
>>
>> # Generate square matrices containing repeated lon, lat vectors
>> lon_1          = np.tile(data[:,0], [npoints,1])
>> lat_1          = np.tile(data[:,1], [npoints,1])
>>
>> lon_2          = np.transpose(lon_1)
>> lat_2          = np.transpose(lat_1)
>>
>> # Apply Geod inversion function to calculate distances, azimuths
>> #  g.inv(self, lons1, lats1, lons2, lats2, radians=False)
>> # Inverse Transformation: Returns forward and back azimuths, plus
>> distances between initial points (specified by lons1, lats) and
>> terminus points (specified by lons2, lats2).[17]
```

[16] Courtesy of Andrew F. Bell

[17] PSF, 2012, Pyproj class Geod, Python Software Foundation.

```
>>
>> # Specify WGS84 ellipsoid
>> g              = Geod(ellps='WGS84')
>>
>> az12, az21, rpairs = g.inv(lon_1[:-1,:-1], lat_1[:-1,:-1], lon_2
>>[:-1,:-1], lat_2[:-1,:-1])
>>
>> # Take upper triangle of square matrix and flatten
>> rpairs         = np.triu(rpairs, 1)/1000
>> azpairs        = np.triu(az12)
>>
>> rv             = rpairs.flatten()
>> azv            = azpairs.flatten()
>>
>> # Remove entries for "zero" distances
>> azv             = azv[rv>0]
>> rv             = rv[rv>0]
>>
>> # Re-scale azimuths -180-0 to 0-180
>> azv             = azv+180*(azv<0)
>>
>> # Find azimuths for r<10 and 10<=r<100 km
>> azv_10         = azv[rv<10]
>> azv_100        = azv[np.logical_and(10<=rv, 100>rv)]
```

Appendix 3

Table A.2: Geological units from the 1:500,000 ISPRA geological map which host CO_2 seeps. Rock descriptions were translated from Italian, simplified, and the rocks were then classified into specific rock types and grouped into rock category. Where two descriptions are similar, they represent different formation ages.

Category	Rock Type	Approximate Translation From Italian
Basin and Slope	Detrital Limestones	Marl sometimes with flint debris of slope facies
Basin and Slope	Detrital Limestones	Argillaceous micritic limestone and micro platform
Basin and Slope	Detrital Limestones	Detrital limestones and marly limestone of the escarpment

Category	Rock Type	Approximate Translation From Italian
Basin and Slope	Detrital Limestones	Detrital limestones and marly limestone of the escarpment
Basin and Slope	Detrital Limestones	Detrital limestones and marly limestone of the escarpment
Basin and Slope	Detrital Limestones	Detrital organogenic limestones and bench type
Basin and Slope	Detrital Limestones	Detrital organogenic limestones and bench type
Basin and Slope	Detrital Limestones	Detrital organogenic limestones and bench type
Basin and Slope	Muds and marls	Clayey and clayey-limestone
Basin and Slope	Muds and marls	Clays and marls sometimes olistostromes
Basin and Slope	Muds and marls	Clays and marls
Basin and Slope	Muds and Sands	Argillites with sandstones, pyroclastic rocks (average)
Basin and Slope	Pelagic Limestone	Marl sometimes with chert, pelagic facies
Basin and Slope	Pelagic Limestone	Marl and calcareous marl of pelagic facies
Basin and Slope	Pelagic Limestone	Limestone, marly limestone and marl, flint, pelagic
Basin and Slope	Pelagic Limestone	Limestone, marly limestone and marly pelagic clays
Basin and Slope	Pelagic Limestone	Micritic limestones and micro pelagic clay
Basin and Slope	Pelagic Limestone	Marly limestones and limestones with flint and a debris slope
Basin and Slope	Pelagic Limestone	Pelagic limestones and marly limestone
Basin and Slope	Pelagic Limestone	Marly limestones and limestones with chert, pelagic
Basin and Slope	Turbidite	Marly limestone (turbidite)
Basin and Slope	Turbidite	Marly limestone (turbidite)
Basin and Slope	Turbidite	Marly limestone (turbidite)
Basin and Slope	Turbidite	Marly limestone (turbidite)
Basin and Slope	Turbidite	Clay-limestone sometimes ophiolite-containing (turbidites)

Category	Rock Type	Approximate Translation From Italian
Basin and Slope	Turbidite	Clay-limestone (turbidites)
Basin and Slope	Turbidite	Clayey and clayey-calcareous (turbidite)
Basin and Slope	Turbidite	Clay (turbidite)
Basin and Slope	Turbidite	Arenaceous-marly (turbidites)
Basin and Slope	Turbidite	Arenaceous-marly (turbidites)
Basin and Slope	Turbidite	argillitic-turbidite sandstone
Basin and Slope	Turbidite	Arenaceous and arenaceous-marly (turbidite)
Basin and Slope	Turbidite	Arenaceous and arenaceous-marly
Basin and Slope	Turbidite	Marl limestone and marl facies of debris slope
Igneous	Andesites & Basalts	Trachytes and latiti (lavas, pyroclastics)
Igneous	Andesites & Basalts	Rhyo-dacite, rhyolites (lavas, ignimbrites)
Igneous	Andesites & Basalts	Latiandesiti and latibasalti (lavas, hyaloclastite, pyroclastic)
Igneous	Andesites & Basalts	Foiditi, tephrites (lavas, pyroclastics and ignimbrites)
Igneous	Andesites & Basalts	Dacite and latiandesiti (lavas and pyroclastics)
Igneous	Andesites & Basalts	Basalts, Spilia hyaloclastite (ophiolites and green stones)
Igneous	Andesites & Basalts	Basalts and tephrites sodium (hyaloclastite)
Igneous	Andesites & Basalts	Alkali basalts, trachy (lavas, pyroclastics)
Igneous	Andesites & Basalts	Alkali basalts (lava, hyaloclastite, pyroclastics)
Igneous	Andesites & Basalts	Andesite (lava and pyroclastic)
Igneous	Andesites & Basalts	Andesite (lava and pyroclastic)
Igneous	Dacites and Rhyolites	Rhyolites, Rhyo-dacite, latiti (lavas, ignimbrites and pyroclastic)
Igneous	Dacites and Rhyolites	Rhyo-dacite and rhyolites (ignimbrites and pyroclastic)

Category	Rock Type	Approximate Translation From Italian
Igneous	Dacites and Rhyolites	Rhyo-dacite and rhyolites (ignimbrites)
Igneous	Dacites and Rhyolites	Latiti, trachytes, phonolites (lavas, ignimbrites, pyroclastic)
Igneous	Dacites and Rhyolites	Phonolites and sodic trachyte (lava and ignimbrites)
Igneous	Diorites and Gabbro	Diorite and tonalite subject
Igneous	Diorites and Gabbro	Rare diorite and tonalite (cycles)
Igneous	Diorites and Gabbro	Quarzodioriti and diorites
Igneous	Diorites and Gabbro	Quarzodioriti and diorites (cycles)
Igneous	Diorites and Gabbro	Gabbro amphibolites
Igneous	Diorites and Gabbro	Gabbro
Igneous	Diorites and Gabbro	Diorite
Igneous	Granite and Granodiorite	Syenite
Igneous	Granite and Granodiorite	Syenite
Igneous	Granite and Granodiorite	Monzonite, monzodioriti, monzogabbri, rare granite cycle
Igneous	Granite and Granodiorite	Granite and granodiorite
Igneous	Granite and Granodiorite	Granite and granodiorite (cycles)
Igneous	Granite and Granodiorite	Granitoid gneiss (metamorphic foothills of varying degrees)
Igneous	Granite and Granodiorite	Gabbro and anorthosite (ophiolites and green stones)
Metamorphic	Metamorphics	Sepentinite and serpintineschist and chloroschist (ophiolites and green stones)
Metamorphic	Metamorphics	Quartz monzonite, and monzodioriti monzogabbri
Metamorphic	Metamorphics	Peridotites (ophiolites and green stones)
Metamorphic	Metamorphics	Migmatite (metamorphic foothills of varying degrees)
Metamorphic	Metamorphics	Mica schist (metamorphic foothills of medium grade)

Category	Rock Type	Approximate Translation From Italian
Metamorphic	Metamorphics	Metabasites, eclogites, amphibolites, green stones sl (ophiolites and green stones)
Metamorphic	Metamorphics	Granulites, amphibolites and gneiss with marble (metamorphic pre-Alpine high-grade)
Metamorphic	Metamorphics	Granulites with gabbro and diorite (high-grade metamorphic pre-Alpine)
Metamorphic	Metamorphics	Phyllites, porphyry, marble and slate green (low-grade metamorphic pre-Alpine)
Metamorphic	Metasediments	Areas with sedimentary successions broadly inclusive, tectonically complex
Metamorphic	Metasediments	Argilloscistose predominantly, sometimes carbonaceous
Metamorphic	Metasediments	Argilloscistose sometimes phyllitic
Metamorphic	Metasediments	Paragneiss and mica schist, phyllite, marble (metamorphic pre-Alpine medium-grade)
Metamorphic	Metasediments	Chaotic complexity of different ages'
Metamorphic	Metasediments	Clayey schists and limestone
Metamorphic	Metasediments	Limestone and marl in metamorphosed shales associated with radiolarites
Metamorphic	Metasediments	Clayey schists
Platform Interior	Evaporites	Chalky-sulphurous
Platform Interior	Evaporites	Evaporites often with marl
Platform Interior	Evaporites	Dolomite, limestone and sandstone, sometimes with evaporites
Platform Interior	Evaporites	Limestones and limestones with gypsum debris sometimes neritic and lagoonal
Platform Interior	Evaporites	Sandstones and clays (subordinate limestones and evaporites)
Platform Margin	Lmst and dolomite	Dolomite and neritic platform
Platform Margin	Lmst and dolomite	Dolomite and neritic platform
Platform Margin	Lmst and dolomite	Crystalline dolomite and neritic platform
Platform Margin	Lmst and dolomite	Neritic limestones and dolomites and crimson platform

Category	Rock Type	Approximate Translation From Italian
Platform Margin	Lmst and dolomite	Limestone and dolomite
Platform Margin	Lmst and dolomite	Neritic limestones and dolomitic limestones and platform
Platform Margin	Lmst and sst	Organogenic limestones, calcarenites
Platform Margin	Lmst and sst	Sandstones, shales with carbonate lenses
Platform Margin	Lmst and sst	Sandstone and limestone
Platform Margin	Platform Carbonate	Organogenic neritic limestones and platform
Platform Margin	Platform Carbonate	Organogenic neritic limestones and Biodetrital and platform
Platform Margin	Platform Carbonate	Organogenic neritic limestones and Biodetrital and platform
Platform Margin	Platform Carbonate	Neritic limestones and platform
Platform Margin	Platform Carbonate	Neritic limestones and platform
Platform Margin	Platform Carbonate	Biodetrital neritic limestones and limestones and platform
Platform Margin	Platform Carbonate	Neritic limestones and calcarenites and platform
Platform Margin	Platform Carbonate	Limestone
Platform Margin	Platform Carbonate	Limestone
Terrestrial	Conglomeritic Sands	Predominantly sandstone
Terrestrial	Conglomeritic Sands	Sands and conglomerates
Terrestrial	Conglomeritic Sands	Sands and conglomerates
Terrestrial	Conglomeritic Sands	Sands and conglomerates
Terrestrial	Conglomeritic Sands	Clastic deposits sometimes with marl
Terrestrial	Conglomeritic Sands	Arenaceous-conglomeratic clastic deposits
Terrestrial	Conglomeritic Sands	Conglomerates, sandstones and clays mainly lake
Terrestrial	Conglomeritic Sands	Conglomerates and sandstones

Category	Rock Type	Approximate Translation From Italian
Terrestrial	Conglomeritic Sands	Breccias and conglomerates
Terrestrial	Conglomeritic Sands	Conglomerates and sandstones, including coastal, lagoon limestones
Terrestrial	Conglomeritic Sands	Sandstones and conglomerates, sometimes turbidite
Terrestrial	Conglomeritic Sands	Lacustrine sandstones and conglomerates
Terrestrial	Conglomeritic Sands	Sandstones and conglomerates with lenses of anthracite (coal)
Terrestrial	Conglomeritic Sands	Sandstones and conglomerates
Terrestrial	Glacial Cover	Lakes and Glaciers
Terrestrial	Glacial Cover	Debris, floods, terraced and fluviolacustri fluvioglacial
Terrestrial	Glacial Cover	Glacial deposits
Terrestrial	Glacial Cover	Clay
Terrestrial	Glacial Cover	Clays
Terrestrial	Quaternary Cover	Debris, alluvial deposits and fluviolacustri, beaches present
Terrestrial	Quaternary Cover	Fluviolacustri and lake deposits
Terrestrial	Quaternary Cover	Eolian deposits
Terrestrial	Quaternary Cover	Flood terraces
Terrestrial	Travertine	Travertine

Appendix 4

A.4.1 Depth to TVD

In the following, Depthmin/Depthmax are the upper/lower bounds of depth data, such as formations, deviation, mud weights etc. Depdev records the depths where deviation information exists.

```
>> ## Loop to fit depth-dev information at 1m intervals
>> i = 0    ;     depth_curr = 0    ;     angle_curr = 0
>> depth_next = depdev_top[i+1]    ;     angle_next = dev_rad[i+1]

>> inc      = 1              # Increments of 1 m
>> i        = i + 1
>>
>> ## loop over downhole depths
>> for (j in 1: max(Depthmin)){
+     if  ( (i<length(dev_rad)-1 ) && (j > depth_next) ){
+           # move to next depth-dev pair if depth j is great enough
+           theta = dev_rad[i]
+           inc = cos(theta)        ## 1 m intervals
+           i = i+1
+           depth_curr = depdev_top[i] ;  depth_next = depdev_top[i
+1]
+           angle_curr = dev_rad[i]    ;  angle_next = dev_rad[i+1]
+     }
+
+     if(j==1){ TVD[j]  = inc ; theta = 0 }
+     else { TVD[j]     = TVD[j-1] + inc }
+
+     TVD_angles [j]    = theta
+ }
>>
>> Depthmin = TVD[Depthmin] # Convert all Depthmin/max to TVD
>> Depthmax = TVD[Depthmax]
>> depth = TVD
```

A 4.2 Calculating pressure from mudweights

```
>> # Identify depths where mudweight data exist
>> minDepthMuds   = Depthmin[which(mudWeight>0)]
>>
>> # Depths with mud weight information
>> maxDepthMuds   = Depthmax[which(mudWeight>0)]
>> mudWeights     = mudWeight[which(mudWeight>0)]
>>
>> # Mud weight in g/L to ppg
>> mudPppg        = mudWeights*0.0083454
>> mudP_grad      = mudPppg*0.052*0.0068948*(3.281)
>> # Mud P grad (MPa/km) where 0.0068948 is conversion from psi to
>> # MPa, 0.052 is conversion from ppg to psi
>>
>> # Make continuous P-Z data
>> mudP = c()
>> depth = seq(1, max(TVD))
>>
>> mudP[1:minDepthMuds[1]] = depth[1:minDepthMuds[1]]*mudP_grad[1]
>>
>> for (i in 1:(length(minDepthMuds)-1)){
+     mudP[minDepthMuds[i]:minDepthMuds[i+1]] = depth[minDepthMuds
  [i]
+ :minDepthMuds[i+1]]*mudP_grad[i]
+     }
>>
>> mudP[minDepthMuds[i+1]:maxDepth] = depth[minDepthMuds[i+1]:
maxDepth] * mudP_grad[i]
>>
>> # Correction for overestimating pressure from muds
>> mudP = mudP*0.9
```

A 4.3 CO_2 Properties and P-T Uncertainty

This function calculates the effects of depth/pressure and temperature uncertainty on CO_2 properties, as outlined in the supplementary methods of Chapter 6. These uncertainties are applied at 10 m intervals beyond 250 m TVD. To calculate the upper and lower standard deviations, the results of the 1000 computations

(randomly distributed around the measured T and P according to the standard deviation assigned) are sorted into a list, and the 25th and 975th value saved.

```
>> sample = 1000
>> for (i in 1:length(depth)){
+   if (depth[i]>=250){
+       print(paste("**  Processing UC in Stepped Mud Pressures", i))
+       steppedMudPressure   = rnorm(sample, pressures[i], 0.1)
+       steppedMudTemps      = rnorm(sample, temps[i], (5/3))
+
+       sortTemps     = sort(steppedMudTemps)
+       upperT[i]     = sortTemps[P.975]
+       lowerT[i]     = sortTemps[P.025]
+       sortPressures = sort(steppedMudPressure)
+       upperP[i]     = sortPressures[P.975]
+       lowerP[i]     = sortPressures[P.025]
+
+       CO2.Densities.SteppedMudUC=c()
+       CO2.Viscosity.SteppedMudUC=c()
+
+       phaseChangeOccurs_mud = FALSE
+
+       if(length(steppedMudPressure)>0){
+          for(l in 1:length(steppedMudPressure)){
+          P = steppedMudPressure[l]; T = steppedMudTemps[l]
+
+              phaseChangePressure=CO2.getPhaseChangePressure(T, P)
+
+              satTempAtThisP    = CO2.getTempFromVapPressure( P )
+              satVapourDensity  = CO2.getSatVapDensity
( satTempAtThisP )
+              dewPointDensity  = CO2.getDewPointDensity
( satTempAtThisP )
+
+           ## Set density range to ensure correct solution is found
+                     if  (  P  <  phaseChangePressure)  {  +
       densityRange = c(0.01, satVapourDensity[1]) }
+              if ( P >= phaseChangePressure) {
+                 densityRange = c(dewPointDensity[1],22)
+                 phaseChangeOccurs_mud = TRUE}
+              if ( P > P_c2 ){
+                 densityRange = c(0.01,22) }
+
+              temp = CO2.getDewPointDensity(T)
```

```
+
+             if ( (P > P_c2) && (T < T_c) ) {
+                 densityRange = c(temp[1],22) }
+
+             answer<-optimise
(CO2.getHuangDensityDifference,densityRange,P=P,T=T, tol=0.000001)
+             CO2.Densities.SteppedMudUC[l] = answer[[1]] * 44.010
+             CO2.Viscosity.SteppedMudUC[l] =
CO2.getViscosityFromDensity (CO2.Densities.SteppedMudUC[l], T)}
+
+      sortDensity   = sort(CO2.Densities.SteppedMudUC)
+      upperD[i]     = sortDensity[P.975]
+      lowerD[i]     = sortDensity[P.025]
+      sortViscosity = sort(CO2.Viscosity.SteppedMudUC)
+      upperV[i]      = sortViscosity[P.975]
+      lowerV[i]      = sortViscosity[P.025]
+
+          }}}
```

Appendix 5

A.5 Supplementary Figures for Down well Conditions

In the following figures, four plots for each well are shown. Clockwise from left (see schematic), these are:

- **A:** Depth - temperature plots, showing the interpolated 1 km(blue, dotted) and 2 km (black, dotted) gradients, and formation temperatures where available (red triangles). The temperature gradient used in CO_2 property calculations is coloured red, and the asterix marks the top of the reservoir unit (often the APC). Where no, or poor, temperature data exists, the 1 km geotherm is preferentially used.

- **B:** Vapour pressure curve, plots down well temperature and pressure environment (dark blue) and the upper and lower error bounds (grey). Coloured dashed lines are lines of vapour pressure, which are labelled. Red asterix marks the conditions at the top of the reservoir unit.
- **C**: Pressure density curve, showing the down well profile in red, and error upper and lower bounds in grey. Coloured lines of equal density, in increments of 100 kg/m^3. Reservoir top shown by brown line and labeled.
- **D:** Down well density difference between CO_2 saturated water and CO_2. Reservoir top shown by labeled brown line.

A	**B**
C	**D**

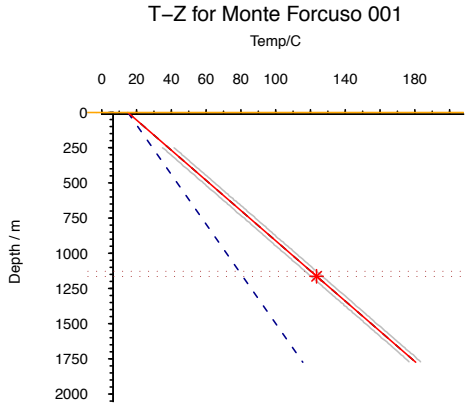
T–Z for Monte Forcuso 001
Temp/C
0 20 40 60 80 100 140 180
Depth / m
0 250 500 750 1000 1250 1500 1750 2000

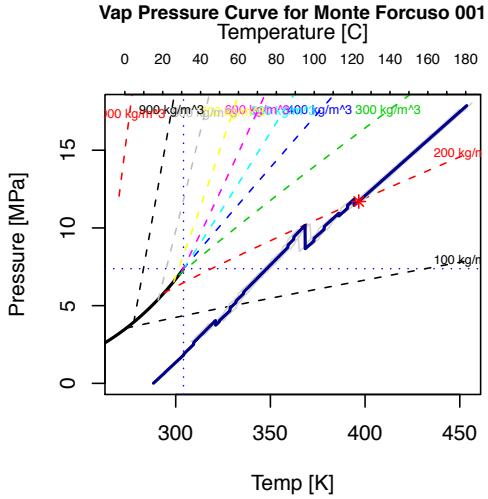
Vap Pressure Curve for Monte Forcuso 001
Temperature [C]
0 20 40 60 80 100 120 140 160 180
Pressure [MPa]
0 5 10 15
300 350 400 450
Temp [K]

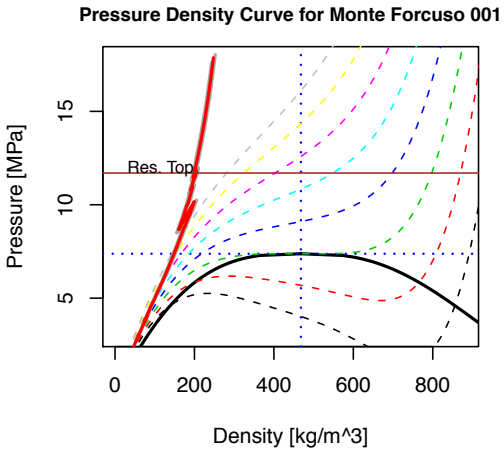
Pressure Density Curve for Monte Forcuso 001
Pressure [MPa]
5 10 15
Res. Top
0 200 400 600 800
Density [kg/m^3]

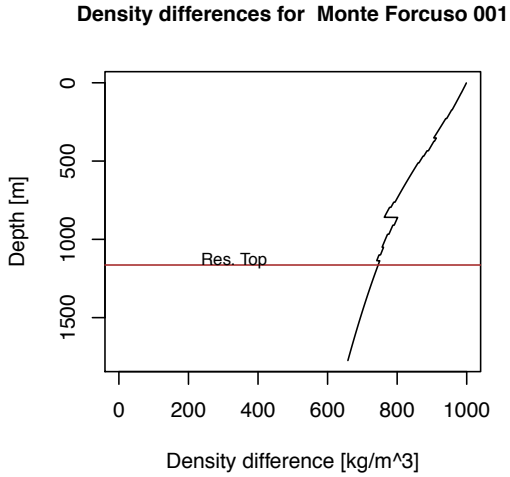
Density differences for Monte Forcuso 001
Depth [m]
0 500 1000 1500
Res. Top
0 200 400 600 800 1000
Density difference [kg/m^3]

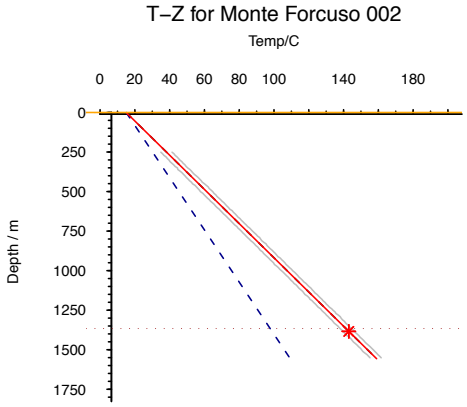
T–Z for Monte Forcuso 002
Temp/C
0 20 40 60 80 100 140 180
0 250 500 750 1000 1250 1500 1750
Depth / m

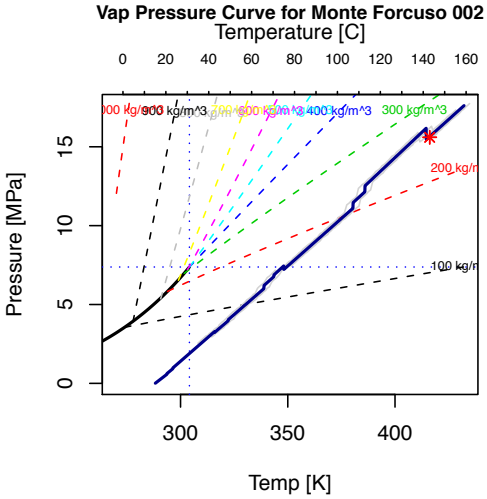
Vap Pressure Curve for Monte Forcuso 002
Temperature [C]
0 20 40 60 80 100 120 140 160
900 kg/m^3
400 kg/m^3
300 kg/m^3
200 kg/m
100 kg/m
Pressure [MPa]
0 5 10 15
300 350 400
Temp [K]

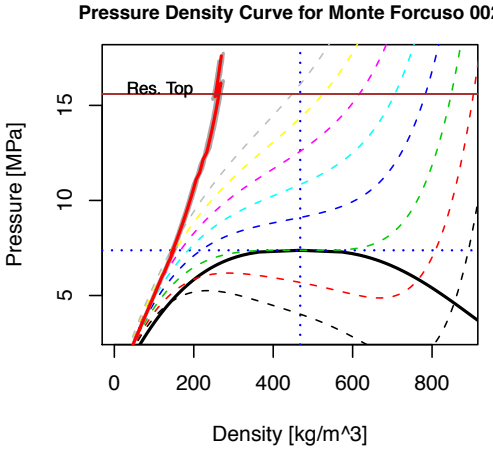
Pressure Density Curve for Monte Forcuso 002
Res. Top
Pressure [MPa]
5 10 15
0 200 400 600 800
Density [kg/m^3]

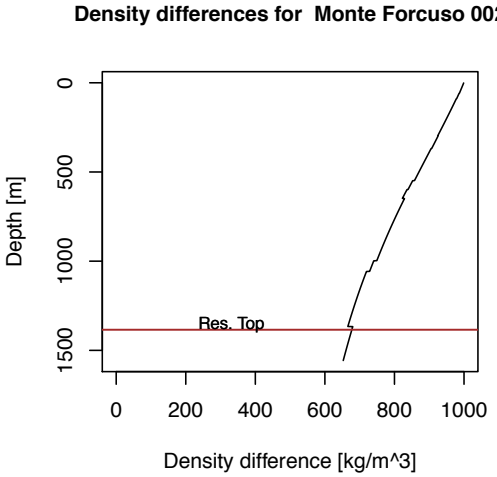
Density differences for Monte Forcuso 002
Res. Top
Depth [m]
0 500 1000 1500
0 200 400 600 800 1000
Density difference [kg/m^3]

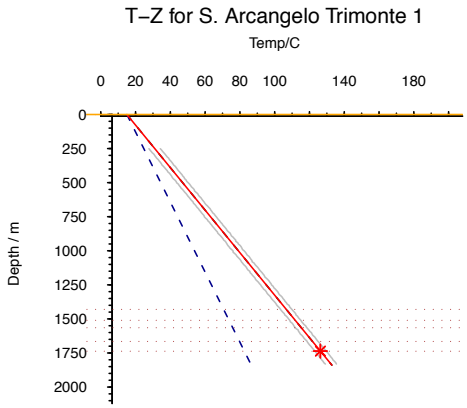
T–Z for S. Arcangelo Trimonte 1
Temp/C
0 20 40 60 80 100 140 180
Depth / m
0 250 500 750 1000 1250 1500 1750 2000

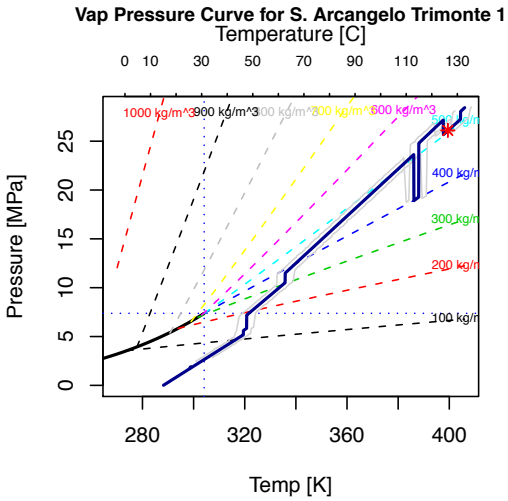
Vap Pressure Curve for S. Arcangelo Trimonte 1
Temperature [C]
0 10 30 50 70 90 110 130
1000 kg/m^3
900 kg/m^3
600 kg/m^3
400 kg/m
300 kg/m
200 kg/m
100 kg/m
Pressure [MPa]
0 5 10 15 20 25
280 320 360 400
Temp [K]

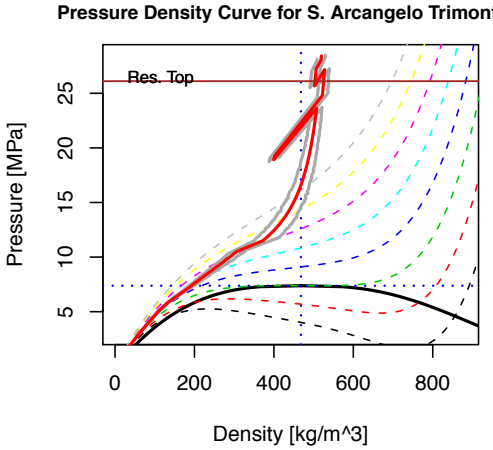
Pressure Density Curve for S. Arcangelo Trimonte 1
Res. Top
Pressure [MPa]
5 10 15 20 25
0 200 400 600 800
Density [kg/m^3]

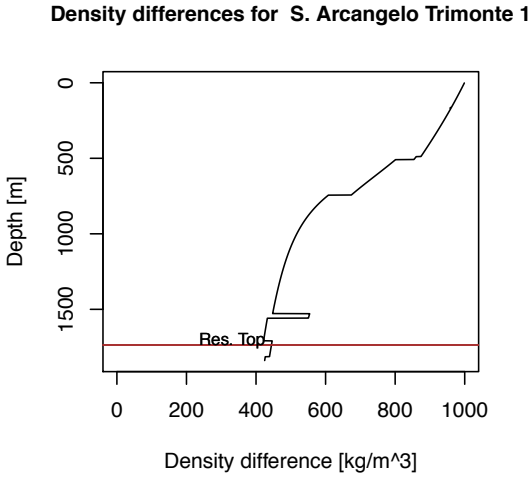
Density differences for S. Arcangelo Trimonte 1
Depth [m]
0 500 1000 1500
Res. Top
0 200 400 600 800 1000
Density difference [kg/m^3]

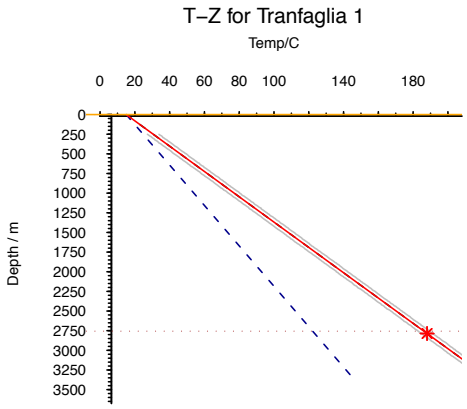
T–Z for Tranfaglia 1
Temp/C
0 20 40 60 80 100 140 180
Depth / m
0 250 500 750 1000 1250 1500 1750 2000 2250 2500 2750 3000 3250 3500

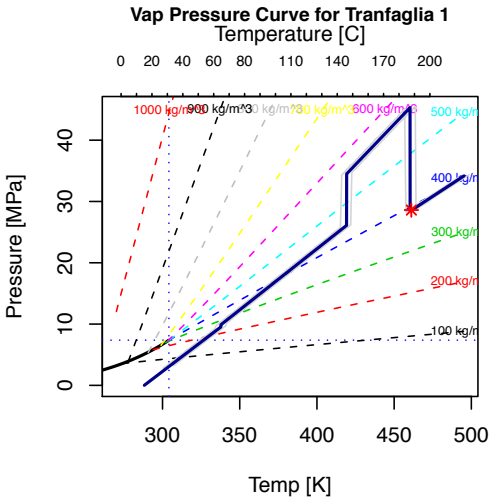
Vap Pressure Curve for Tranfaglia 1
Temperature [C]
0 20 40 60 80 110 140 170 200
1000 kg/m^3
900 kg/m^3
500 kg/m^3
400 kg/m^3
300 kg/m^3
200 kg/m^3
100 kg/m^3
Pressure [MPa]
0 10 20 30 40
300 350 400 450 500
Temp [K]

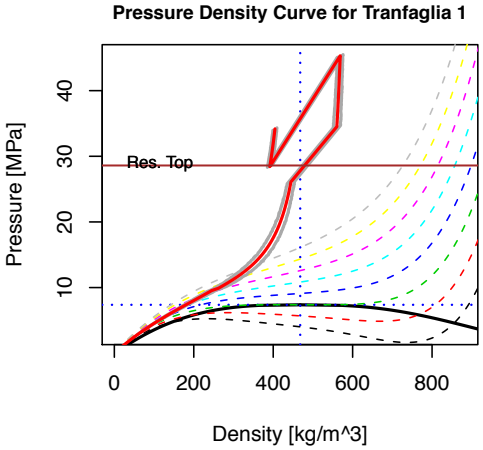
Pressure Density Curve for Tranfaglia 1
Res. Top
Pressure [MPa]
10 20 30 40
0 200 400 600 800
Density [kg/m^3]

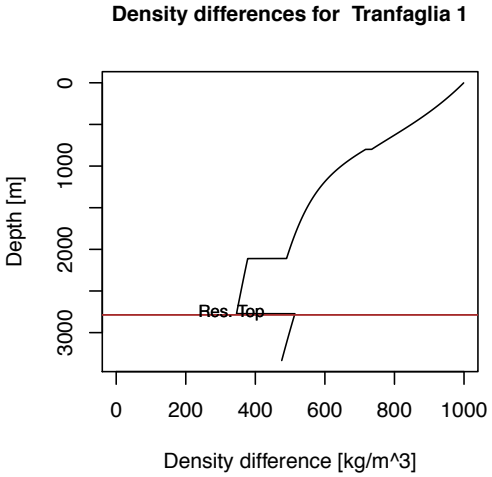
Density differences for Tranfaglia 1
Res. Top
Depth [m]
0 1000 2000 3000
0 200 400 600 800 1000
Density difference [kg/m^3]

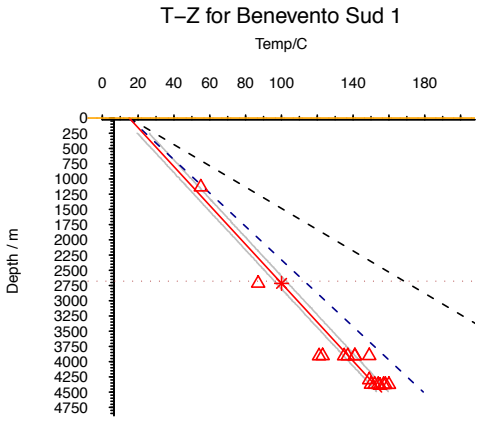
T–Z for Benevento Sud 1
Temp/C
0 20 40 60 80 100 140 180
Depth / m
0 250 500 750 1000 1250 1500 1750 2000 2250 2500 2750 3000 3250 3500 3750 4000 4250 4500 4750

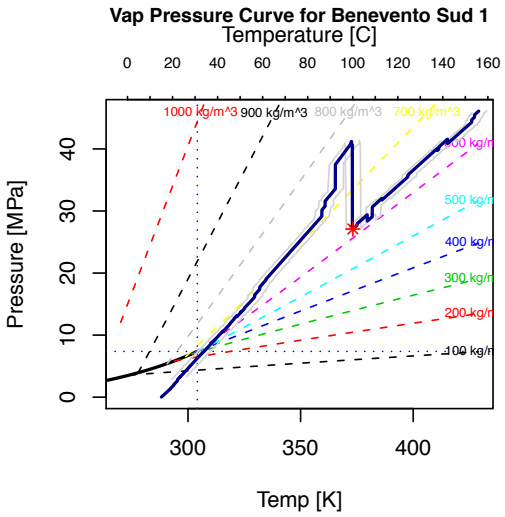
Vap Pressure Curve for Benevento Sud 1
Temperature [C]
0 20 40 60 80 100 120 140 160
1000 kg/m^3 900 kg/m^3 800 kg/m^3 700 kg/m^3
600 kg/m
500 kg/m
400 kg/m
300 kg/m
200 kg/m
100 kg/m
Pressure [MPa]
0 10 20 30 40
300 350 400
Temp [K]

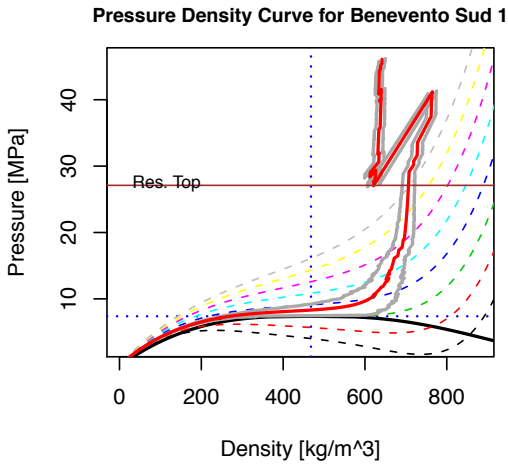
Pressure Density Curve for Benevento Sud 1
Res. Top
Pressure [MPa]
10 20 30 40
0 200 400 600 800
Density [kg/m^3]

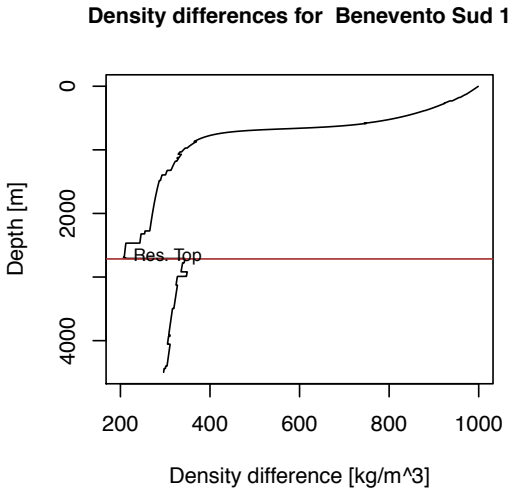
Density differences for Benevento Sud 1
Res. Top
Depth [m]
0 2000 4000
200 400 600 800 1000
Density difference [kg/m^3]

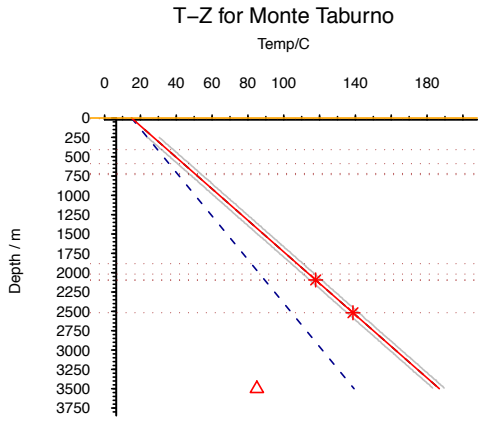
T–Z for Monte Taburno
Temp/C
0 20 40 60 80 100 140 180
Depth / m
0 250 500 750 1000 1250 1500 1750 2000 2250 2500 2750 3000 3250 3500 3750

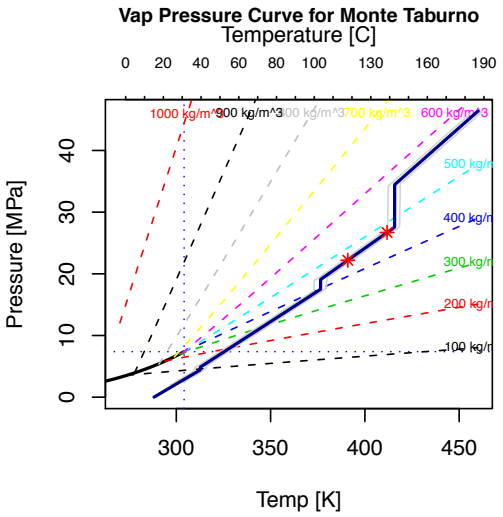
Vap Pressure Curve for Monte Taburno
Temperature [C]
0 20 40 60 80 100 130 160 190
1000 kg/m^3 900 kg/m^3 800 kg/m^3 700 kg/m^3 600 kg/m^3
500 kg/m
400 kg/m
300 kg/m
200 kg/m
100 kg/m
Pressure [MPa]
0 10 20 30 40
300 350 400 450
Temp [K]

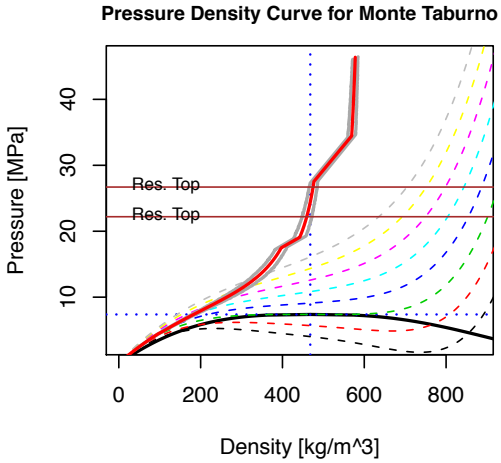
Pressure Density Curve for Monte Taburno
Res. Top
Res. Top
Pressure [MPa]
10 20 30 40
0 200 400 600 800
Density [kg/m^3]

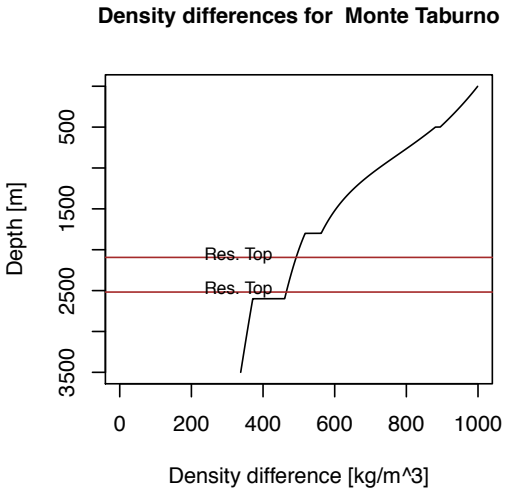
Density differences for Monte Taburno
Res. Top
Res. Top
Depth [m]
3500 2500 1500 500
0 200 400 600 800 1000
Density difference [kg/m^3]

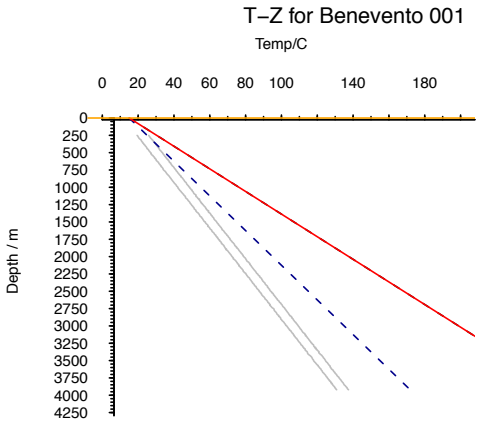
T–Z for Benevento 001
Temp/C
0 20 40 60 80 100 140 180
Depth / m
0 250 500 750 1000 1250 1500 1750 2000 2250 2500 2750 3000 3250 3500 3750 4000 4250

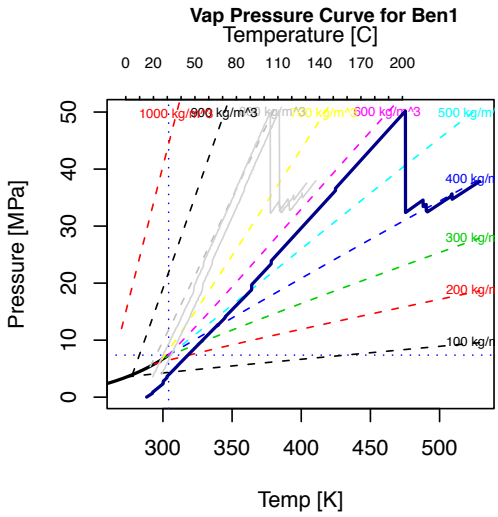
Vap Pressure Curve for Ben1
Temperature [C]
0 20 50 80 110 140 170 200
1000 kg/m^3
900 kg/m^3
600 kg/m^3
500 kg/m^3
400 kg/m^3
300 kg/m^3
200 kg/m^3
100 kg/m^3
Pressure [MPa]
0 10 20 30 40 50
300 350 400 450 500
Temp [K]

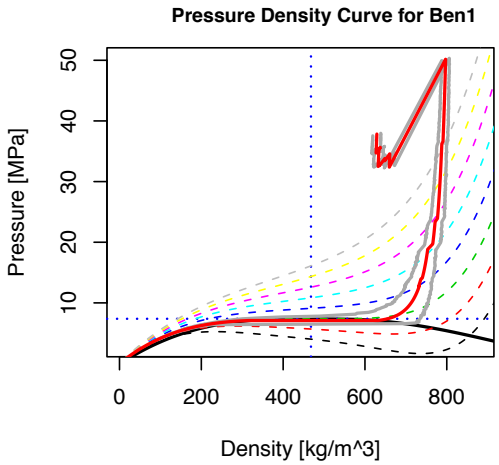
Pressure Density Curve for Ben1
Pressure [MPa]
10 20 30 40 50
0 200 400 600 800
Density [kg/m^3]

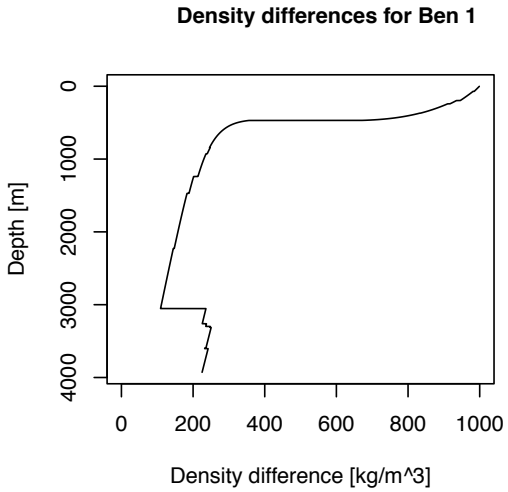
Density differences for Ben 1
Depth [m]
0 1000 2000 3000 4000
0 200 400 600 800 1000
Density difference [kg/m^3]

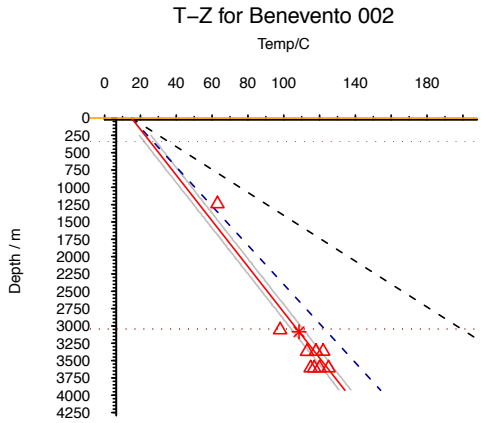
T–Z for Benevento 002
Temp/C
0 20 40 60 80 100 140 180
Depth / m
0 250 500 750 1000 1250 1500 1750 2000 2250 2500 2750 3000 3250 3500 3750 4000 4250

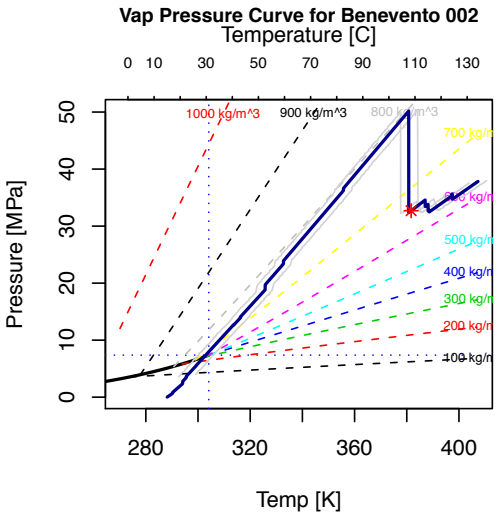
Vap Pressure Curve for Benevento 002
Temperature [C]
0 10 30 50 70 90 110 130
1000 kg/m^3
900 kg/m^3
800 kg/m^3
700 kg/m^3
600 kg/m^3
500 kg/m^3
400 kg/m^3
300 kg/m^3
200 kg/m^3
100 kg/m^3
Pressure [MPa]
0 10 20 30 40 50
280 320 360 400
Temp [K]

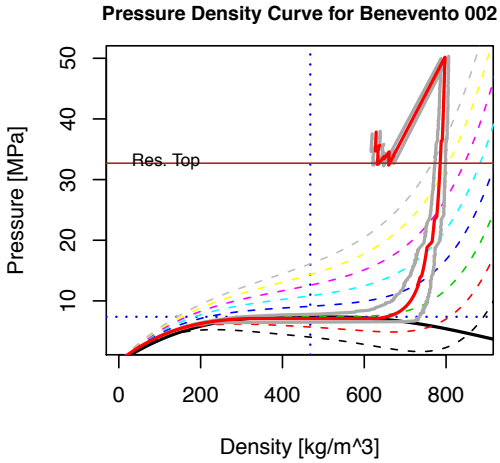
Pressure Density Curve for Benevento 002
Res. Top
Pressure [MPa]
10 20 30 40 50
0 200 400 600 800
Density [kg/m^3]

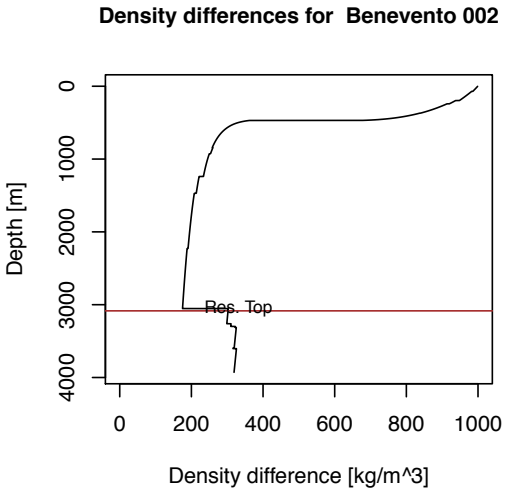
Density differences for Benevento 002
Res. Top
Depth [m]
0 1000 2000 3000 4000
0 200 400 600 800 1000
Density difference [kg/m^3]

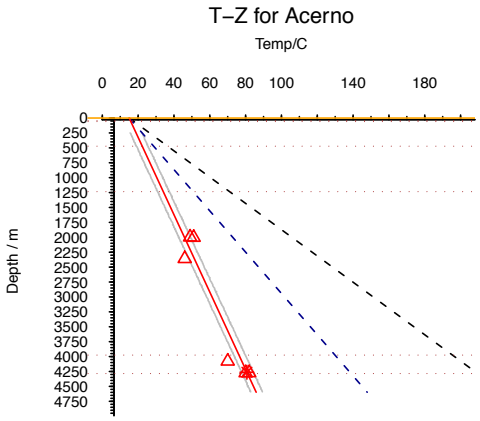
T–Z for Acerno
Temp/C
0 20 40 60 80 100 140 180
Depth / m
0 250 500 750 1000 1250 1500 1750 2000 2250 2500 2750 3000 3250 3500 3750 4000 4250 4500 4750

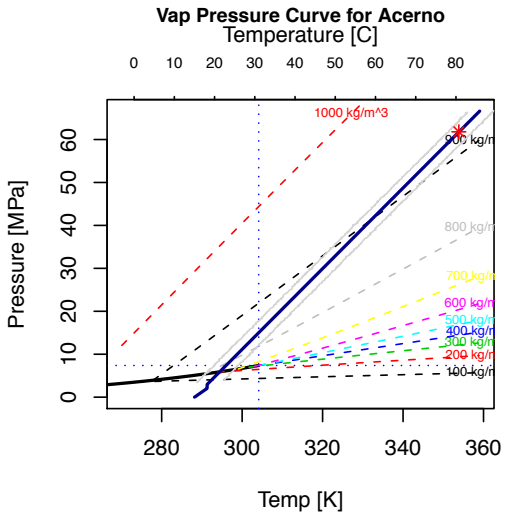
Vap Pressure Curve for Acerno
Temperature [C]
0 10 20 30 40 50 60 70 80
1000 kg/m^3
900 kg/m
800 kg/m
700 kg/m
600 kg/m
500 kg/m
400 kg/m
300 kg/m
200 kg/m
100 kg/m
Pressure [MPa]
0 10 20 30 40 50 60
280 300 320 340 360
Temp [K]

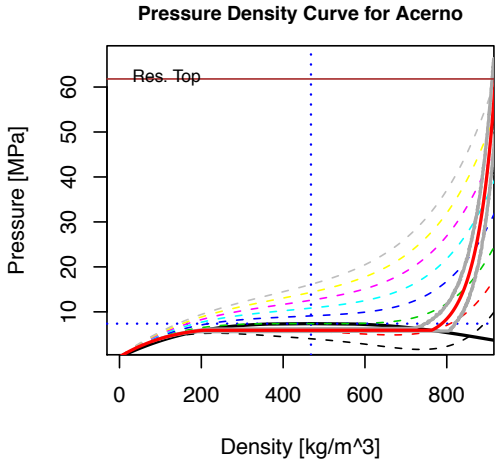
Pressure Density Curve for Acerno
Res. Top
Pressure [MPa]
10 20 30 40 50 60
0 200 400 600 800
Density [kg/m^3]

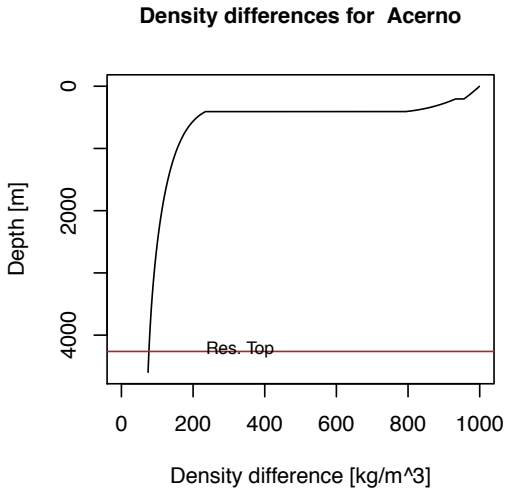
Density differences for Acerno
Depth [m]
0 2000 4000
Res. Top
0 200 400 600 800 1000
Density difference [kg/m^3]

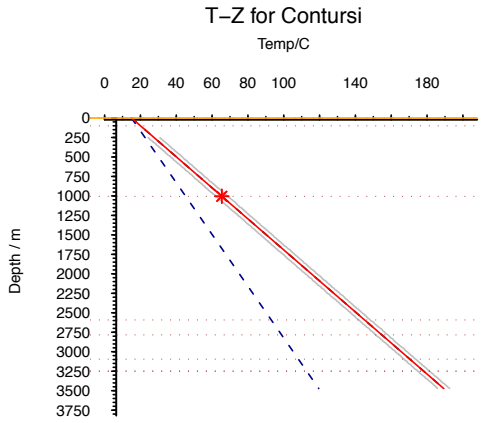
T–Z for Contursi
Temp/C
0 20 40 60 80 100 140 180
Depth / m
0 250 500 750 1000 1250 1500 1750 2000 2250 2500 2750 3000 3250 3500 3750

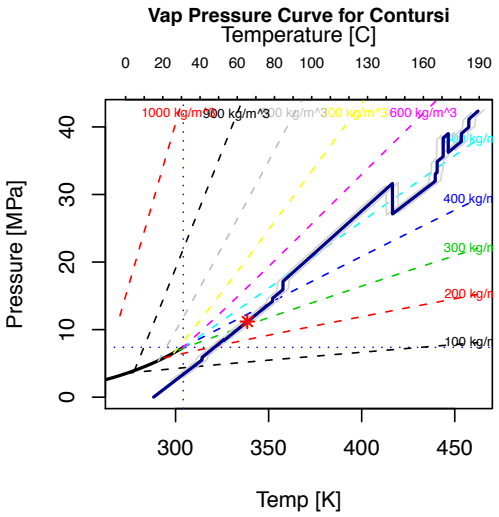
Vap Pressure Curve for Contursi
Temperature [C]
0 20 40 60 80 100 130 160 190
1000 kg/m^3
900 kg/m^3
600 kg/m^3
400 kg/m
300 kg/m
200 kg/m
100 kg/m
Pressure [MPa]
0 10 20 30 40
300 350 400 450
Temp [K]

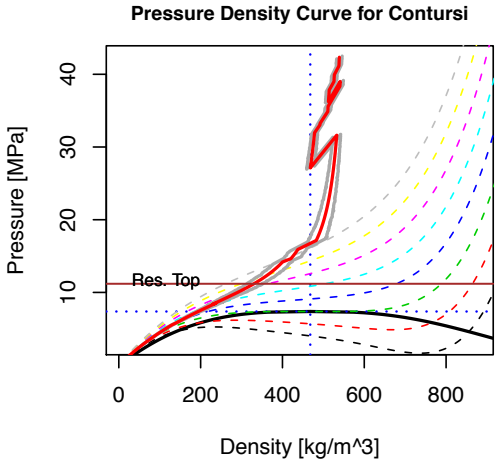
Pressure Density Curve for Contursi
Res. Top
Pressure [MPa]
10 20 30 40
0 200 400 600 800
Density [kg/m^3]

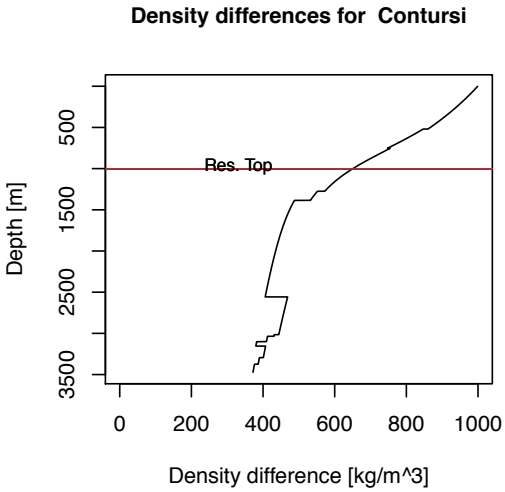
Density differences for Contursi
Res. Top
Depth [m]
3500 2500 1500 500
0 200 400 600 800 1000
Density difference [kg/m^3]

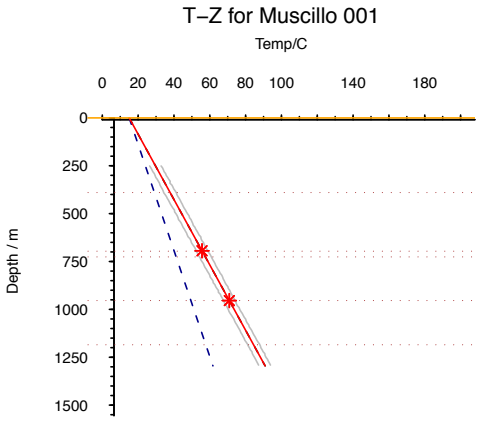
T–Z for Muscillo 001
Temp/C
0 20 40 60 80 100 140 180
0 250 500 750 1000 1250 1500
Depth / m

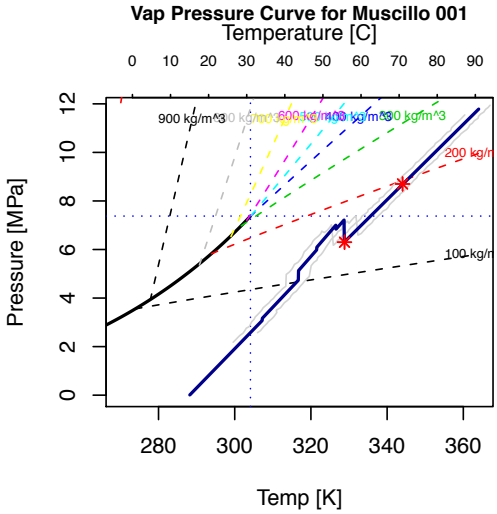
Vap Pressure Curve for Muscillo 001
Temperature [C]
0 10 20 30 40 50 60 70 80 90
900 kg/m^3
200 kg/m
100 kg/m
0 2 4 6 8 10 12
Pressure [MPa]
280 300 320 340 360
Temp [K]

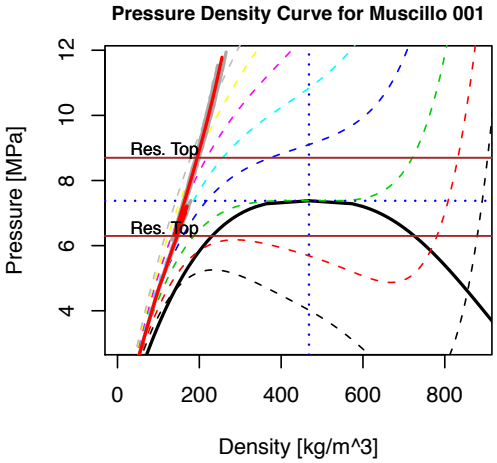
Pressure Density Curve for Muscillo 001
Res. Top
Res. Top
4 6 8 10 12
Pressure [MPa]
0 200 400 600 800
Density [kg/m^3]

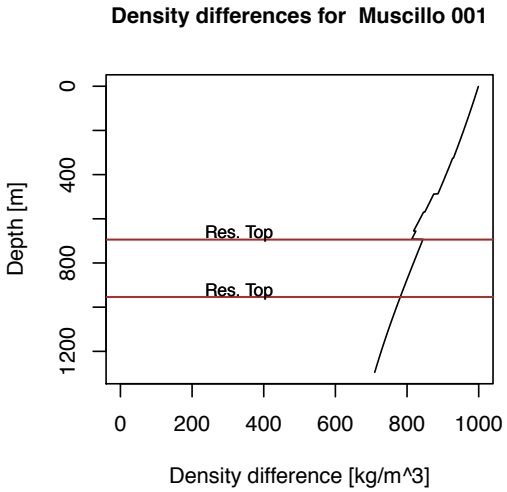
Density differences for Muscillo 001
Res. Top
Res. Top
0 400 800 1200
Depth [m]
0 200 400 600 800 1000
Density difference [kg/m^3]

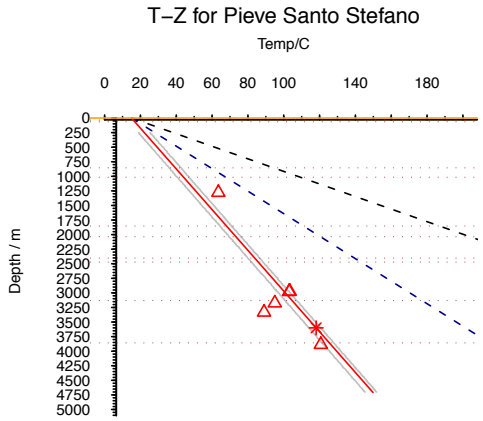
T–Z for Pieve Santo Stefano
Temp/C
0 20 40 60 80 100 140 180
Depth / m
0 250 500 750 1000 1250 1500 1750 2000 2250 2500 2750 3000 3250 3500 3750 4000 4250 4500 4750 5000

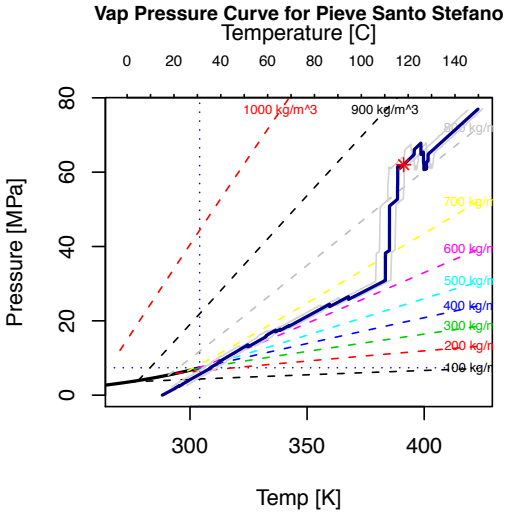
Vap Pressure Curve for Pieve Santo Stefano
Temperature [C]
0 20 40 60 80 100 120 140
1000 kg/m^3
900 kg/m^3
700 kg/m
600 kg/m
500 kg/m
400 kg/m
300 kg/m
200 kg/m
100 kg/m
Pressure [MPa]
0 20 40 60 80
300 350 400
Temp [K]

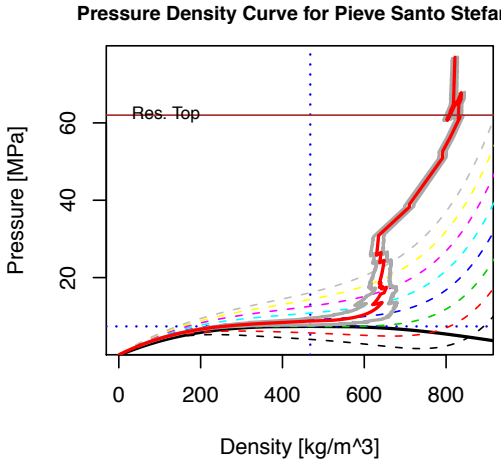
Pressure Density Curve for Pieve Santo Stefano
Res. Top
Pressure [MPa]
20 40 60
0 200 400 600 800
Density [kg/m^3]

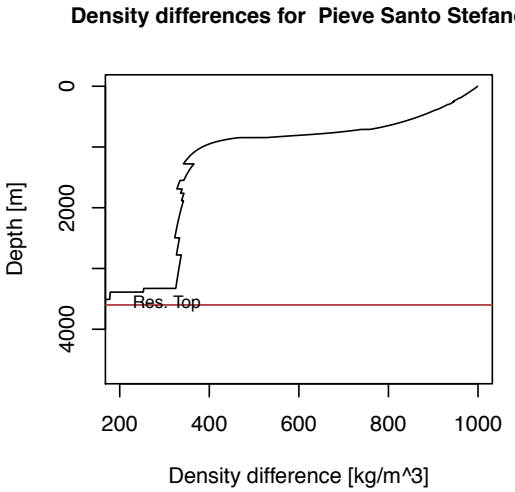
Density differences for Pieve Santo Stefano
Depth [m]
0 2000 4000
Res. Top
200 400 600 800 1000
Density difference [kg/m^3]

References

The Natural Analogues for the Storage of CO_2 in the Geological Environment (NASCENT) project focussed on evaluating European natural CO_2 deposits.

2008, Climate Change Act c.27.

Adekoya, N., and Nolte, K.B., 2005, Struck-by-lightning deaths in the United States: Journal of Environmental Health, v. 67, p. 45-50.

Agosta, F., Alessandroni, M., Antonellini, M., Tondi, E., and Giorgioni, M., 2010, From fractures to flow: A field-based quantitative analysis of an outcropping carbonate reservoir: Tectonophysics, v. 490, p. 197-213.

Agosta, F., Alessandroni, M., Tondi, E., and Aydin, A., 2009, Oblique normal faulting along the northern edge of the Majella Anticline, central Italy: Inferences on hydrocarbon migration and accumulation: Journal of Structural Geology, v. 31, p. 674-690.

Agosta, F., and Kirschner, D.L., 2003, Fluid conduits in carbonate-hosted seismogenic normal faults of central Italy: Journal of Geophysical Research-Solid Earth, v. 108.

Agosta, F., Mulch, A., Chamberlain, P., and Aydin, A., 2008, Geochemical traces of CO_2-rich fluid flow along normal faults in central Italy: Geophysical Journal International, v. 174, p. 758-770.

Agosta, F., Prasad, M., and Aydin, A., 2007, Physical properties of carbonate fault rocks, fucino basin (Central Italy): implications for fault seal in platform carbonates: Geofluids, v. 7, p. 19-32.

Allis, R., Chidsey, T., Gwynn, W., Morgan, C., White, S., Adams, M., and Moore, J., 2001, Natural CO_2 Reservoirs on the Colorado Plateau and Southern Rocky Mountains: Candidates for CO_2 sequestration, DOE/NETL 1st National Conference of Carbon Sequestration Washington D.C, p. 19.

Anderson, T.R., and Fairley, J.P., 2008, Relating permeability to the structural setting of a fault-controlled hydrothermal system in southeast Oregon, USA: Journal of Geophysical Research-Solid Earth, v. 113.

Annunziatellis, A., Beaubien, S.E., Bigi, S., Ciotoli, G., Coltella, M., and Lombardi, S., 2008, Gas migration along fault systems and through the vadose zone in the Latera

caldera (central Italy): Implications for CO_2 geological storage: International Journal of Greenhouse Gas Control, v. 2, p. 353-372.

Bachu, S., and Bennion, B., 2008a, Effects of in-situ conditions on relative permeability characteristics of CO(2)-brine systems: Environmental Geology, v. 54, p. 1707-1722.

Bachu, S., and Bennion, D.B., 2008b, Interfacial Tension between CO_2, Freshwater, and Brine in the Range of Pressure from (2 to 27) MPa, Temperature from (20 to 125) ¬∞C, and Water Salinity from (0 to 334,Äâ000) mg¬∑L,àí1: Journal of Chemical & Engineering Data, v. 54, p. 765-775.

Baines, S.J., and Worden, R.H., 2001, Geological CO_2 disposal: Understanding the long term fate of CO_2 in naturally occurring accumulations, *in* Williams, D.J., Durie, B., McMullan, P., Paulson, C., and Smith, A., eds., 5th International Conference on Greenshouse Gas Control Technologies: Cairns, Australia, p. 311-316.

—, 2004, The long-term fate of CO_2 in the subsurface: natural analogues for CO_2 storage. In: Baines, S. J. & Worden, R. H. (eds) 2004. Geological Storage of Carbon Dioxide. : Geological Society, London, Special Publications, v. 233, p. 59 – 86. .

Ballentine, C., Burgess, R., and Marty, B., 2002, Tracing Fluid Transport and Interaction in the Crust, *in* Porcelli, D., Ballentine, C., and Wieler, R., eds., Noble Gases in Geochemistry and Cosmochemistry, Volume 47: Reviews in Mineralogy and Geochemistry, Mineralogical Society of America.

Barba, S., Carafa, M.M.C., Mariucci, M.T., Montone, P., and Pierdominici, S., 2009, Present-day stress-field modelling of southern Italy constrained by stress and GPS data: Tectonophysics.

Barberi, F., Carapezza, M.L., Ranaldi, M., and Tarchini, L., 2007, Gas blowout from shallow boreholes at Fiumicino (Rome): Induced hazard and evidence of deep CO_2 degassing on the Tyrrhenian margin of Central Italy: Journal of Volcanology and Geothermal Research, v. 165, p. 17-31.

Bateson, L., Vellico, M., Beaubien, S.E., Pearce, J.M., Annunziatellis, A., Ciotoli, G., Coren, F., Lombardi, S., and Marsh, S., 2008, The application of remote-sensing techniques to monitor CO_2-storage sites for surface leakage: Method development and testing at Latera (Italy) where naturally produced CO_2 is leaking to the atmosphere: International Journal of Greenhouse Gas Control, v. 2, p. 388-400.

Beaubien, S.E., Ciotoli, G., Coombs, P., Dictor, M.C., Kruger, M., Lombardi, S., Pearce, J.M., and West, J.M., 2008, The impact of a naturally occurring CO_2 gas vent

on the shallow ecosystem and soil chemistry of a Mediterranean pasture (Latera, Italy): International Journal of Greenhouse Gas Control, v. 2, p. 373-387.

Beaubien, S.E., Ciotoli, G., and Lombardi, S., 2003, Carbon dioxide and radon gas hazard in the Alban Hills area (central Italy): Journal of Volcanology and Geothermal Research, v. 123, p. 63-80.

Becker, T.P., and Lynds, R., 2012, A geologic deconstruction of one of the world's largest natural accumulations of CO_2, Moxa arch, southwestern Wyoming: Aapg Bulletin, v. 96, p. 1643-1664.

Bennion, D., and Bachu, S., 2008, Drainage and Imbibition Relative Permeability Relationships for Supercritical CO_2/Brine and H2S/Brine Systems in Intergranular Sandstone, Carbonate, Shale, and Anhydrite Rocks: SPE Reservoir Evaluation & Engineering, v. 11, p. 487-496.

Bertello, F., Fantoni, R., Franciosi, R., Gatti, V., Ghielmi, M., and Pugliese, A., 2010, From thrust-and-fold belt to foreland: hydrocarbon occurrences in Italy: Geological Society, London, Petroleum Geology Conference series, v. 7, p. 113-126.

Bickle, M.J., 2009, Geological carbon storage: Nature Geoscience, v. 2, p. 815-818.

Billi, A., 2005, Attributes and influence on fluid flow of fractures in foreland carbonates of southern Italy: Journal of Structural Geology, v. 27, p. 1630-1643.

Bleacher, J.E., Glaze, L.S., Greeley, R., Hauber, E., Baloga, S.M., Sakimoto, S.E.H., Williams, D.A., and Glotch, T.D., 2009, Spatial and alignment analyses for a field of small volcanic vents south of Pavonis Mons and implications for the Tharsis province, Mars: Journal of Volcanology and Geothermal Research, v. 185, p. 96-102.

Bogdanov, I.I., Mourzenko, V.V., Thovert, J.F., and Adler, P.M., 2007, Effective permeability of fractured porous media with power-law distribution of fracture sizes: Physical Review E, v. 76, p. 036309.

Bonini, M., 2008, Elliptical mud volcano caldera as stress indicator in an active compressional setting (Nirano, Pede-Apennine margin, northern Italy): Geology, v. 36, p. 131-134.

—, 2009a, Mud volcano eruptions and earthquakes in the Northern Apennines and Sicily, Italy: Tectonophysics, v. 474, p. 723-735.

—, 2009b, Structural controls on a carbon dioxide-driven mud volcano field in the Northern Apennines (Pieve Santo Stefano, Italy): Relations with pre-existing steep discontinuities and seismicity: Journal of Structural Geology, v. 31, p. 44-54.

Bradbury, J., Ray, I., Peterson, T., Wade, S., Wong-Parodi, G., and Feldpausch, A., 2009, The Role of Social Factors in Shaping Public Perceptions of CCS: Results of Multi-State Focus Group Interviews in the US, *in* Gale, J., Herzog, H., and Braitsch, J., eds., Greenhouse Gas Control Technologies 9, Volume 1: Energy Procedia, p. 4665-4672.

Brozzetti, F., 2011, The Campania-Lucania Extensional Fault System, southern Italy: A suggestion for a uniform model of active extension in the Italian Apennines: Tectonics, v. 30.

Calabro, R.A., Corrado, S., Di Bucci, D., Robustini, P., and Tornaghi, M., 2003, Thin-skinned vs. thick-skinned tectonics in the Matese Massif, Central-Southern Apennines (Italy): Tectonophysics, v. 377, p. 269-297.

Carapezza, M.L., Badalamenti, B., Cavarra, L., and Scalzo, A., 2003, Gas hazard assessment in a densely inhabited area of Colli Albani Volcano (Cava dei Selci, Roma): Journal of Volcanology and Geothermal Research, v. 123, p. 81-94.

Carapezza, M.L., and Tarchini, L., 2007, Accidental gas emission from shallow pressurized aquifers at Alban Hills volcano (Rome, Italy): Geochemical evidence of magmatic degassing?: Journal of Volcanology and Geothermal Research, v. 165, p. 5-16.

Cardellini, C., 2010: Dipartimento di Scienze della Terra, Università di Perugia.

Carminati , E., Lustrino, M., Cuffaro, M., and Doglioni, C., 2010, Tectonics, magmatism and geodynamics of Italy: What we know and what we imagine, *in* M. Beltrando, A.P., M. Mattei, S. Conticelli, C. Doglion, ed., The Geology of Italy: tectonics and life along plate margins, Journal of the Virtual Explorer, Volume 36.

Casabianca, D., Bosence, D., and Beckett, D., 2002, Reservoir potential of Cretaceous platform-margin Breccias, Central Italian Apennines: Journal of Petroleum Geology, v. 25, p. 179-202.

Casero, P., 2004, Structural setting of petroleum exploration plays in Italy, *in* Crescenti, U., ed., Geology of Italy: Special Volume of the Italian Geologic Society for the IGC 32 Florence-2004, Società Geologica Italiana.

—, 2005, Southern Apennines geologic framework and related petroleum systems, Atti Ticinensi di Scienze della Terra, Volume 10: Serie Speciale:The record of thermal history in sedimentary successions: Rome.

Cello, G., Gambini, R., Mazzoli, S., Read, A., Tondi, E., and Zucconi, V., 2000, Fault zone characteristics and scaling properties of the Val d'Agri Fault System (Southern Apennines, Italy): Journal of Geodynamics, v. 29, p. 293-307.

Chalbaud, C., Robin, M., Lombard, J.M., Martin, F., Egermann, P., and Bertin, H., 2009, Interfacial tension measurements and wettability evaluation for geological CO_2 storage: Advances in Water Resources, v. 32, p. 98-109.

Chiodini, G., 2010: INGV, Naples.

Chiodini, G., Baldini, A., Barberi, F., Carapezza, M.L., Cardellini, C., Frondini, F., Granieri, D., and Ranaldi, M., 2007, Carbon dioxide degassing at Latera caldera (Italy): Evidence of geothermal reservoir and evaluation of its potential energy: J. Geophys. Res., v. 112, p. B12204.

Chiodini, G., Caliro, A., Cardellini, C., Frondini, F., Inguaggiato, S., and Matteucci, F., 2011, Geochemical evidence for and characterization of CO_2 rich gas sources in the epicentral area of the Abruzzo 2009 earthquakes: Earth and Planetary Science Letters, v. 304, p. 389-398.

Chiodini, G., Cardellini, C., Amato, A., Boschi, E., Caliro, S., Frondini, F., and Ventura, G., 2004, Carbon dioxide Earth degassing and seismogenesis in central and southern Italy: Geophysical Research Letters, v. 31.

Chiodini, G., and Frondini, F., 2001, Carbon dioxide degassing from the Albani Hills volcanic region, Central Italy: Chemical Geology, v. 177, p. 67-83.

Chiodini, G., Frondini, F., Cardellini, C., Parello, F., and Peruzzi, L., 2000, Rate of diffuse carbon dioxide Earth degassing estimated from carbon balance of regional aquifers: The case of central Apennine, Italy: Journal of Geophysical Research-Solid Earth, v. 105, p. 8423-8434.

Chiodini, G., Frondini, F., and Ponziani, F., 1995, Deep Structures and Carbon-Dioxide Degassing in Central Italy: Geothermics, v. 24, p. 81-94.

Chiodini, G., Granieri, D., Avino, R., Caliro, S., Costa, A., Minopoli, C., and Vilardo, G., 2010, Non-volcanic CO_2 Earth degassing: Case of Mefite d'Ansanto (southern Apennines), Italy: Geophysical Research Letters, v. 37, p. 11303.

Chiodini, G., and Valenza, M., 2008, Googas - the catalogue of Italian gas emissions, Volume 2009.

—, 2009, Googas - the catalogue of Italian gas emissions, Volume 2009.

Chiodini, G., Valenza, M., Cardellini, C., and Frigeri, A., 2008, A New Web-Based Catalog of Earth Degassing Sites in Italy: EOS, v. 37, p. 341–342.

Chiodini, G., Valenza, M., Cardellini, C., Frigeri, A.,, 2008, A New Web-Based Catalog of Earth Degassing Sites in Italy: EOS, v. 37, p. 341–342.

Cinti, D., Procesi, M., Tassi, F., Montegrossi, G., Sciarra, A., Vaselli, O., and Quattrocchi, F., 2011, Fluid geochemistry and geothermometry in the western sector of the Sabatini Volcanic District and the Tolfa Mountains (Central Italy): Chemical Geology, v. 284, p. 160-181.

Ciotoli, G., Etiope, G., Guerra, M., Lombardi, S., Duddridge, G.A., and Grainger, P., 2005, Migration of gas injected into a fault in low-permeability ground: Quarterly Journal of Engineering Geology and Hydrogeology, v. 38, p. 305-320.

Clark, P.J.E., F.C., 1954, Distance to nearest neighbor as a measure of spatial relationships in populations. : Ecology, v. 35, p. 445-453.

COGS, The Carbon Monoxide Gas Safety Society, CO-Gas Safety's Statistics of Deaths and Injuries.

Collettini, C., and Barchi, M.R., 2002, A low-angle normal fault in the Umbria region (Central Italy): a mechanical model for the related microseismicity: Tectonophysics, v. 359, p. 97-115.

Collettini, C., Cardellini, C., Chiodini, G., De Paola, N., Holdsworth, R.E., and Smith, S.A.F., 2008, Fault weakening due to CO_2 degassing in the Northern Apennines: short- and long-term processes, *in* WIBBERLEY, C.A.J., KURZ, W., IMBER, J., HOLDSWORTH, R. E. & COLLETTINI, C. , ed., The Internal Structure of Fault Zones: Implications for Mechanical and Fluid-Flow Properties, Volume 299, The Geological Society of London, p. 175-194.

Collettini, C., and Holdsworth, R.E., 2004, Fault zone weakening and character of slip along low-angle normal faults: insights from the Zuccale fault, Elba, Italy: Journal of the Geological Society, v. 161, p. 1039-1051.

Costa, A., Chiodini, G., Granieri, D., Folch, A., Hankin, R.K.S., Caliro, S., Avino, R., and Cardellini, C., 2008, A shallow-layer model for heavy gas dispersion from natural sources: Application and hazard assessment at Caldara di Manziana, Italy: Geochemistry Geophysics Geosystems, v. 9.

Council, E.P.a.o.t., 2009, Directive 2009/31/EC on the geological storage of carbon dioxide. Official Journal of the European Union, , L 140/114 to L 140/135.

Curewitz, D., and Karson, J.A., 1997, Structural settings of hydrothermal outflow: Fracture permeability maintained by fault propagation and interaction: Journal of Volcanology and Geothermal Research, v. 79, p. 149-168.

D'Alessandro, W., 2006, Gas hazard: an often neglected natural risk in volcanic areas, *in* Martin-Duque, J.F., Brebbia, C.A., Emmanouloudis, D.E., and Mander, U., eds., Geo-Environment and Landscape Evolution II - Evolution, Monitoring, Simulation, Management and Remediation of the Geological Envirnoment and Landscape, Volume 89: Wit Transactions on Ecology and the Environment, WIT Press, p. 369-378.

DCLG, 2009, Department for Communities and Local Government: Housing and Planning Statistics 2009.

De Paola, N., Collettini, C., Trippetta, F., Barchi, M.R., and Minelli, G., 2007, A mechanical model for complex fault patterns induced by evaporite dehydration and cyclic changes in fluid pressure: Journal of Structural Geology, v. 29, p. 1573-1584.

Desbarats, J., Upham, P., Riesch, H., Reiner, D., Brunsting, S., Best-Waldhober, M.d., Duetschke, E., Sala, C.O.a.R., and McLachlan, C., 2010, Near-CO_2 (FP7) Review of the public participation practices for CCS and non-CCs projects in Europe., Insititue for European Environmental Policy.

Di Bucci, D., Massa, B., Tornaghi, M., and Zuppetta, A., 2006, Structural setting of the Southern Apennine fold-and-thrust belt (Italy) at hypocentral depth: The Calore Valley case history: Journal of Geodynamics, v. 42, p. 175-193.

Di Luccio, F., Ventura, G., Di Giovambattista, R., Piscini, A., and Cinti, F.R., Normal faults and thrusts reactivated by deep fluids: The 6 April 2009 M-w 6.3 L'Aquila earthquake, central Italy: Journal of Geophysical Research-Solid Earth, v. 115, p. 15.

Di Stefano, R., I. Bianchi, M. G. Ciaccio, G. Carrara, E. Kissling, 2011, Three-dimensional Moho topography in Italy: New constraints from receiver functions and controlled source seismology: Geochemistry, Geophysics, Geosystems, v. 12.

Dockrill, B., and Shipton, Z.K., 2010, Structural controls on leakage from a natural CO_2 geologic storage site: Central Utah, U.S.A: Journal of Structural Geology, v. 32, p. 1768-1782.

DoH, 2008, Carbon monoxide: Are you at risk?: Carbon monoxide: Are you at risk?, Department of Health, p. 14.

Duchi, V., Minissale, A., Vaselli, O., and Ancillotti, M., 1995, Hydrogeochemistry of the Campania region in southern Italy: Journal of Volcanology and Geothermal Research, v. 67, p. 313-328.

EEA, 2012, Annual European Union greenhouse gas inventory 1990–2010 and inventory report 2012, *in* Agency, E.E., ed.

Esposito, A., Giordano, G., and Anzidei, M., 2006a, The 2002 - 2003 submarine gas eruption at Panarea volcano (Aeolian Islands, Italy): Volcanology of the seafloor and implications for the hazard scenario: Marine Geology, v. 227, p. 119-134.

—, 2006b, The 2002,Äì2003 submarine gas eruption at Panarea volcano (Aeolian Islands, Italy): Volcanology of the seafloor and implications for the hazard scenario: Marine Geology, v. 227, p. 119-134.

Etiope, G., Fridriksson, T., Italiano, F., Winiwarter, W., and Theloke, J., 2007a, Natural emissions of methane from geothermal and volcanic sources in Europe

: Journal of Volcanology and Geothermal Research, v. 165, p. 76 - 86.

Etiope, G., Guerra, M., and Raschi, A., 2005, Carbon dioxide and radon geohazards over a gas-bearing fault in the Siena Graben (Central Italy): Terrestrial Atmospheric and Oceanic Sciences, v. 16, p. 885-896.

Etiope, G., and Martinelli, G., 2009, "Pieve Santo Stefano" is not a mud volcano: Comment on Structural controls on a carbon dioxide-driven mud volcano field in the Northern Apennines (by Bonini, 2009): Journal of Structural Geology, v. 31, p. 1270-1271.

Etiope, G., Martinelli, G., Caracausi, A., and Italiano, F., 2007b, Methane seeps and mud volcanoes in Italy: Gas origin, fractionation and emission to the atmosphere: Geophysical Research Letters, v. 34.

Faccenna, C., Soligo, M., Billi, A., De Filippis, L., Funiciello, R., Rossetti, C., and Tuccimei, P., 2008, Late Pleistocene depositional cycles of the Lapis Tiburtinus travertine (Tivoli, Central Italy): Possible influence of climate and fault activity: Global and Planetary Change, v. 63, p. 299-308.

Faulkner, D.R., Jackson, C.A.L., Lunn, R.J., Schlische, R.W., Shipton, Z.K., Wibberley, C.A.J., and Withjack, M.O., 2010, A review of recent developments concerning the structure, mechanics and fluid flow properties of fault zones: Journal of Structural Geology, v. 32, p. 1557-1575.

Faulkner, D.R., Lewis, A.C., and Rutter, E.H., 2003, On the internal structure and mechanics of large strike-slip fault zones: field observations of the Carboneras fault in southeastern Spain: Tectonophysics, v. 367, p. 235- 251.

Fleet, A., Wycherley, H., and Shaw, H., 1998, Large volumes of carbon dioxide in sedimentary basins: Mineralogical Magazine, v. 62(A), p. 460-462.

Ford, T.D., and Pedley, H.M., 1996, A review of tufa and travertine deposits of the world: Earth-Science Reviews, v. 41, p. 117-175.

Frezzotti, M., L. Peccerillo, A. Panza, G. May, 2009, Carbonate metasomatism and CO_2 lithosphere-asthenosphere degassing beneath the western mediterranean: An integrated model arising from petrological and geophysical data. : Chemical Geology v. 262, p. 108-120.

Frondini, F., Caliro, S., Cardellini, C., Chiodini, G., and Morgantini, N., 2009, Carbon dioxide degassing and thermal energy release in the Monte Amiata volcanic-geothermal area (Italy): Applied Geochemistry, v. 24, p. 860- 875.

Frondini, F., Chiodini, G., Caliro, S., Cardellini, C., Granieri, D., and Ventura, G., 2004, Diffuse CO_2 degassing at Vesuvio, Italy: Bulletin of Volcanology, v. 66, p. 642-651.

Gambardella, B., Cardellini, C., Chiodini, G., Frondini, F., Marini, L., Ottonello, G., and Zuccolini, M.V., 2004, Fluxes of deep CO_2 in the volcanic areas of central-southern Italy: Journal of Volcanology and Geothermal Research, v. 136, p. 31-52.

Geothopica, 2010, Geothermal resources national inventory, Volume 2010, CNR Geosciences and Earth Resources Institute.

Ghisetti, F., and Vezzani, L., 2002, Normal faulting, transcrustal permeability and seismogenesis in the Apennines (Italy): Tectonophysics, v. 348, p. 155-168.

Gilfillan, S., Ballentine, C., Lollar, B.S., Stevens, S., Schoell, M., and Cassidy, M., 2008, Quantifying the precipitation and dissolution of CO_2 within geological carbon storage analogues: Geochimica Et Cosmochimica Acta, v. 72, p. A309-A309.

Gilfillan, S.M.V., 2006, Deep Magmatic Degassing and the Colorado Plateau Uplift: Manchester, University of Manchester.

Gilfillan, S.M.V., Lollar, B.S., Holland, G., Blagburn, D., Stevens, S., Schoell, M., Cassidy, M., Ding, Z.J., Zhou, Z., Lacrampe-Couloume, G., and Ballentine, C.J., 2009, Solubility trapping in formation water as dominant CO_2 sink in natural gas fields: Nature, v. 458, p. 614-618.

Goldscheider, N., Madl-Szonyi, J., Eross, A., and Schill, E., Review: Thermal water resources in carbonate rock aquifers: Hydrogeology Journal, v. 18, p. 1303-1318.

Gudmundsson, A., Berg, S.S., Lyslo, K.B., and Skurtveit, E., 2001, Fracture networks and fluid transport in active fault zones: Journal of Structural Geology, v. 23, p. 343-353.

Haszeldine, R.S., 2009, Carbon Capture and Storage: How Green Can Black Be?: Science, v. 325, p. 1647-1652.

Haugan, P.M., and Joos, F., 2004, Metrics to assess the mitigation of global warming by carbon capture and storage in the ocean and in geological reservoirs: Geophysical Research Letters, v. 31, p. L18202.

Hebach, A., Oberhof, A., Dahmen, N., Kv∂gel, A., Ederer, H., and Dinjus, E., 2002, Interfacial Tension at Elevated PressuresMeasurements and Correlations in the Water + Carbon Dioxide System: Journal of Chemical & Engineering Data, v. 47, p. 1540-1546.

Heinicke, J., Braun, T., Burgassi, P., Italiano, F., and Martinelli, G., 2006, Gas flow anomalies in seismogenic zones in the Upper Tiber Valley, Central Italy: Geophysical Journal International, v. 167, p. 794-806.

Heinicke, J., Italiano, F., Koch, U., Martinelli, G., and Telesca, L., 2010, Anomalous fluid emission of a deep borehole in a seismically active area of Northern Apennines (Italy): Applied Geochemistry, v. 25, p. 555-571.

Heinicke, J., Italiano, F., Lapenna, V., Martinelli, G., and Nuccio, P.M., 2000, Coseismic geochemical variations in some gas emissions of Umbria region (Central Italy): Physics and Chemistry of the Earth Part a-Solid Earth and Geodesy, v. 25, p. 289-293.

Hepple, R.P., 2005, Chapter 26 - Human Health and Ecological Effects of Carbon Dioxide Exposure, Carbon Dioxide Capture for Storage in Deep Geologic Formations: Amsterdam, Elsevier Science, p. 1143-1172.

Hepple, R.P., and Benson, S.M., 2003, Implications of surface seepage on the effectiveness of geologic storage of carbon dioxide as a climate change mitigation strategy, 261-266 p.

—, 2005, Geologic storage of carbon dioxide as a climate change mitigation strategy: performance requirements and the implications of surface seepage: Environmental Geology, v. 47, p. 576-585.

Holloway, S., Pearce, J.M., Hards, V.L., Ohsumi, T., and Gale, J., 2007, Natural emissions of CO_2 from the geosphere and their bearing on the geological storage of carbon dioxide: Energy, v. 32, p. 1194-1201.

Huang, F., Li, M., Le, L., and Starling, K., 1985, An accurate equation of state for carbon dioxide: Journal of Chemical Engineering of Japan, v. 18, p. 490–496.

Huc, M., and Main, I.G., 2003, Anomalous stress diffusion in earthquake triggering: Correlation length, time dependence, and directionality: J. Geophys. Res., v. 108, p. 2324.

IEA, 2009, Technology Roadmap: Carbon capture and storage.: Paris.

Improta, L., Bonagura, M., Capuano, P., and Iannaccone, G., 2003a, An integrated geophysical investigation of the upper crust in the epicentral area of the 1980, Ms=6.9, Irpinia earthquake (Southern Italy): Tectonophysics, v. 361, p. 139-169.

Improta, L., Iannaccone, G., Capuano, P., Zollo, A., and Scandone, P., 2000, Inferences on the upper crustal structure of Southern Apennines (Italy) from seismic refraction investigations and subsurface data: Tectonophysics, v. 317, p. 273-297.

Improta, L., Zollo, A., Bruno, P.P., Herrero, A., and Villani, F., 2003b, High-resolution seismic tomography across the 1980 (Ms 6.9) Southern Italy earthquake fault scarp: Geophysical Research Letters, v. 30.

IPCC, 2005, IPCC Special Report on Carbon Dioxide Capture and Storage. Prepared by Working Group III of the Intergovernmental Panel on Climate Change, *in* Metz, B., O. Davidson, H. C. de Coninck, M. Loos, and L. A. Meyer, ed., p. 442 pp.

—, 2007a, Climate Change 2007: Synthesis Report. , *in* Team), C.W., Pachauri, R.K., and Reisinger, A., eds., Contribution of Working Groups I, II and III to the Fourth Assessment Report of the Intergovernmental Panel on Climate Change: Geneva, Switzerland, IPCC, p. 104.

—, 2007b, Climate Change 2007: Synthesis Report, Summary for Policy Makers, *in* Pachauri, R.K., and Reisinger, A., eds., Contribution of Working Groups I, II and III to the Fourth Assessment Report of the Intergovernmental Panel on Climate Change: IPCC, Geneva, Switzerland. pp 10, Core Writing Team.

—, 2007c, Technical Summary. Climate Change 2007: Impacts, Adaptation and Vulnerability. , *in* M.L. Parry, O.F.C., J.P. Palutikof, P.J. van der Linden and C.E. Hanson, ed., Contribution of Working Group II to the Fourth Assessment Report of the Intergovernmental Panel on Climate Change, p. 23-78.

Irwin, W.P., and Barnes, I., 1980, Tectonic Relations of Carbon Dioxide Discharges and Earthquakes: Journal of Geophysical Research, v. 85, p. 3115-3121.

ISPRA, 2007, ITaly HAzard from CApable faults (ITHACA), Volume 2011.

—, 2010, ISPRA GeoMapViewer Volume 2010, ISPRA.

ISTAT, 2001, 14th General Population and Housing Census: Legal Population Italian National Institute of Statistics.

—, 2006a, Italian National Institute of Statistics, Demography in Figures, Total Population in Italy.

—, 2006b, Italian National Institute of Statistics, Health Statistics, Road Accidents, Killed and Injured.

—, 2009, Italian National Institute of Statistics, Demography in Figures, Total Population in Italy.

Italiano, F., Bonfanti, P., Pizzino, L., and Quattrocchi, F., 2010, Geochemistry of fluids discharged over the seismic area of the Southern Apennines (Calabria region, Southern Italy): Implications for Fluid-Fault relationships: Applied Geochemistry, v. 25, p. 540-554.

Italiano, F., Martelli, M., Martinelli, G., and Nuccio, M., 2000, Geochemical evidence of melt intrusions along lithospheric faults of the Southern Apennines, Italy: Geodynamic and seismogenic implications: Journal of Geophysical Research, v. 105, p. 13569 - 13578.

Italiano, F., Martinelli, G., and Plescia, P., 2008, CO_2 degassing over seismic areas: The role of mechanochemical production at the study case of Central Apennines: Pure and Applied Geophysics, v. 165, p. 75-94.

Jarvis, A., H.I. Reuter, A. Nelson, E. Guevara, 2008, Hole-filled SRTM for the globe Version 4, available from the CGIAR-CSI SRTM 90m Database (http://srtm.csi.cgiar.org).

Jenden, P.D., Hilton, D.R., Kaplan, I.R., and Craig, H., 1993, Abiogenic hydrocarbons in and mantle helium in oil and gas fields, *in* Howell, D.G., ed., The future of energy gases (U.S. Geological Survey Professional Paper), Volume 1570, U.S. Geological Survey, p. 31-56.

Jenness, J., 2005, Distance/Azimuth Tools (dist_az_tools.avx) extension for ArcView 3.x, v. 1.6. , *in* Enterprises, J., ed.

Johnsson, F., Reiner, D., Itaoka, K., and Herzog, H., 2009, Stakeholder attitudes on Carbon Capture and Storage-An international comparison: International Journal of Greenhouse Gas Control, v. 4, p. 410-418.

Kampman, N., Burnside, N.M., Bickle, M., Shipton, Z.K., Ellam, R.M., and Chapman, H., 2010, Coupled CO_2-leakage and in situ fluid-mineral reactions in a natural CO_2 reservoir, Green River, Utah: Geochimica Et Cosmochimica Acta, v. 74, p. A492-A492.

Katz, B.J., Dittmar, E.I., and Ehret, G.E., 2000, A geochemical review of carbonate source rocks in Italy: Journal of Petroleum Geology, v. 23, p. 399-424.

Kerrick, D.M., 2001, Present and past nonanthropogenic CO(2) degassing from the solid Earth: Reviews of Geophysics, v. 39, p. 565-585.

Kirk, K., 2011, Natural CO_2 flux literature review for the QICS project, Energy Programme, British Geological Survey Comissioned Report, p. 38.

Kurz, W., Imber, J., Wibberley, C.A., Holdsworth, R.E., and Collettini, C., 2008, The internal structure of fault zones: fluid flow and mechanical properties, *in* Kurz, W., Imber, J., Wibberley, C.A., Holdsworth, R.E., and Collettini, C., eds., The Internal Structure of Fault Zones: Implications for Mechanical and Fluid-Flow Properties: Geolological Society of London Special Publications, Geological Society of London, p. 376.

Larsen, B., Grunnaleite, I., and Gudmundsson, A., How fracture systems affect permeability development in shallow-water carbonate rocks: An example from the Gargano Peninsula, Italy: Journal of Structural Geology, v. 32, p. 1212-1230.

Lewicki, J.L., Birkholzer, J., and Tsang, C.F., 2007, Natural and industrial analogues for leakage of CO_2 from storage reservoirs: identification of features, events, and processes and lessons learned: Environmental Geology, v. 52, p. 457-467.

Likhachev, E., 2003, Dependence of water viscosity on temperature and pressure: Technical Physics, v. 48, p. 514-515.

Lindeberg, E., 2002, The quality of a CO_2 repository: what is the sufficient retention time of CO_2 stored underground. , *in* Gale, J., and Kaya, Y., eds., Proceedings of 6th greenhouse gas control technologies conference: Kyoto, Elsevier, p. 255-260.

Lu, J.M., Wilkinson, M., Haszeldine, R.S., and Fallick, A.E., 2009, Long-term performance of a mudrock seal in natural CO_2 storage: Geology, v. 37, p. 35-38.

Mariucci, M.T., Pierdominici, S., Pizzino, L., Marra, F., and Montone, P., 2008, Looking into a volcanic area: An overview on the 350 m scientific drilling at Colli Albani (Rome, Italy): Journal of Volcanology and Geothermal Research, v. 176, p. 225-240.

Martinelli, G., and Judd, A., 2004, Mud volcanoes of Italy: Geological Journal, v. 39, p. 49-61.

Marziano, G.I., Gaillard, F., and Pichavant, M., 2007, Limestone assimilation and the origin of CO_2 emissions at the Alban Hills (Central Italy): Constraints from experimental petrology: Journal of Volcanology and Geothermal Research, v. 166, p. 91-105.

Masini, M., Bigi, S., Poblet, J., Bulnes, M., Di Cuia, R., and Casabianca, D., 2011, Kinematic evolution and strain simulation, based on cross-section restoration, of the Maiella Mountain: an analogue for oil fields in the Apennines (Italy), *in* Poblet, J., and Lisle, R.J., eds., Kinematic Evolution and Structural Styles of Fold-and-Thrust Belts, Volume 349: Geological Society Special Publication, p. 25-44.

McDermott, C.I., Randriamanjatosoa, A.L., Tenzer, H., and Kolditz, O., 2006, Simulation of Heat Extraction from Crystalline Rocks: The Influence of Coupled Processes on Differential Reservoir Cooling.: Geothermics, v. 35, p. 321-344.

McGee, K.A., and Gerlach, T.M., 1998, Annual cycle of magmatic CO_2 in a tree-kill soil at Mammoth Mountain, California: Implications for soil acidification: Geology, v. 26, p. 463 - 466.

Miller, S.A., Collettini, C., Chiaraluce, L., Cocco, M., Barchi, M., and Kaus, B.J.P., 2004, Aftershocks driven by a high-pressure CO_2 source at depth: Nature, v. 427, p. 724-727.

Minissale, A., 2004, Origin, transport and discharge of CO_2 in central Italy: Earth-Science Reviews, v. 66, p. 89-141.

Minissale, A., Evans, W.C., Magro, G., and Vaselli, O., 1997a, Multiple source components in gas manifestations from north-central Italy: Chemical Geology, v. 142, p. 175-192.

Minissale, A., Kerrick, D.M., Magro, G., Murrell, M.T., Paladini, M., Rihs, S., Sturchio, N.C., Tassi, F., and Vaselli, O., 2002, Geochemistry of Quaternary travertines in the region north of Rome (Italy): structural, hydrologic and paleoclimatic implications: Earth and Planetary Science Letters, v. 203, p. 709-728.

Minissale, A., Magro, G., Martinelli, G., Vaselli, O., and Tassi, G.F., 2000, Fluid geochemical transect in the Northern Apennines (central-northern Italy): fluid genesis and migration and tectonic implications: Tectonophysics, v. 319, p. 199-222.

Minissale, A., Magro, G., Vaselli, O., Verrucchi, C., and Perticone, I., 1997b, Geochemistry of water and gas discharges from the Mt. Amiata silicic complex and surrounding areas (central Italy): Journal of Volcanology and Geothermal Research, v. 79, p. 223-251.

Mitchell, T.M., and Faulkner, D.R., 2012, Towards quantifying the matrix permeability of fault damage zones in low porosity rocks: Earth and Planetary Science Letters, v. 339, p. 24-31.

Morellato, C., Redini, F., and Doglioni, C., 2003, On the number and spacing of faults: Terra Nova, v. 15, p. 315-321.

Morner, N.A., and Etiope, G., 2002, Carbon degassing from the lithosphere: Global and Planetary Change, v. 33, p. 185-203.

Nara, Y., Meredith, P.G., Yoneda, T., and Kaneko, K., 2011, Influence of macro-fractures and micro-fractures on permeability and elastic wave velocities in basalt at elevated pressure: Tectonophysics, v. 503, p. 52-59.

Naylor, M., Wilkinson, M., and Haszeldine, R.S., 2011, Calculation of CO_2 column heights in depleted gas fields from known pre-production gas column heights: Marine and Petroleum Geology, v. 28, p. 1083-1093.

Nelson, S.T., Mayo, A.L., Gilfillan, S., Dutson, S.J., Harris, R.A., Shipton, Z.K., and Tingey, D.G., 2009, Enhanced fracture permeability and accompanying fluid flow in the footwall of a normal fault: The Hurricane fault at Pah Tempe hot springs, Washington County, Utah: Geological Society of America Bulletin, v. 121, p. 236-246.

Nicolai, C., Gambini, R., and Ed. by A. Mazzotti, E.P.P.S., 2007, Structural architecture of the Adria-platform-and-basin system.: Bolletino della Società Geologica Italiana, p. 21–37.

O'Nions, R.K., and Oxburgh, E.R., 1988, Helium, Volatile Fluxes and the Development of Continental-Crust: Earth and Planetary Science Letters, v. 90, p. 331-347.

Oldenburg, C.M., and Lewicki, J.L., 2006, On leakage and seepage of CO_2 from geologic storage sites into surface water: Environmental Geology, v. 50, p. 691-705.

Osborne, M.J., and Swarbrick, R.E., 1997, Mechanisms for generating overpressure in sedimentary basins; a reevaluation: Aapg Bulletin, v. 81, p. 1023-1041.

Paluszny, A., and Matthai, S.K., 2010, Impact of fracture development on the effective permeability of porous rocks as determined by 2-D discrete fracture growth modeling: J. Geophys. Res., v. 115, p. B02203.

Patacca, E., and Scandone, P., 2007, Geology of the Southern Apennines: Bolletino della Società Geologica Italiana, v. Special Issue no. 7 ed. by A. Mazzotti, E. Patacca and P. Scandone, p. 75 - 119.

Patacca, E., Scandone, P., Di Luzio, E., Cavinato, G.P., and Parotto, M., 2008, Structural architecture of the central Apennines: Interpretation of the CROP 11 seismic profile from the Adriatic coast to the orographic divide: Tectonics, v. 27.

Pearce, J., 2005/6, Natural analogues for the geological storage of CO_2. Final report of the Nascent project (IEAGHG Report).

Peebles, P.J.E., 1980, The Large-Scale Structure of the Universe: Princeton, Princeton University Press.

Peng, R.D., Bobb, J.F., Tebaldi, C., McDaniel, L., Bell, M.L., and Dominici, F., 2010, Towards a Quantitative Estimate of Future Heat Wave Mortality under Global Climate Change: Environ Health Perspect.

Pentecost, A., 1995, Geochemistry of Carbon-Dioxide in 6 Travertine-Depositing Waters of Italy: Journal of Hydrology, v. 167, p. 263-278.

Pruess, K., 2004, Numerical simulation of CO_2 leakage from a geologic disposal reservoir, including transitions from super- to subcritical conditions, and boiling of liquid CO_2: SPE Journal, v. 9, p. 237-248.

—, 2008, Leakage of CO_2 from geologic storage: Role of secondary accumulation at shallow depth: International Journal of Greenhouse Gas Control, v. 2, p. 37-46.

Quattrocchi, F., and Calcara, M., 1998, Test-sites for earthquake prediction experiments within the Colli Albani region: Physics and Chemistry of The Earth, v. 23, p. 915-920.

Raschi, A., Miglietta, F., Tognetti, R., and van Gardingen, P.R., 1997, Plant Responses to Elevated CO_2: Evidence from Natural Springs. : Cambridge, United Kingdom., Cambridge University Press, 272 p.

Reveillere, A., and Rohmer, J., 2011, Managing the risk of CO_2 leakage from deep saline aquifer reservoirs through the creation of a hydraulic barrier: Energy Procedia, v. 4, p. 3187-3194.

Richards-Dinger, K., Stein, R.S., and Toda, S., 2010, Decay of aftershock density with distance does not indicate triggering by dynamic stress: Nature, v. 467, p. 583-U105.

Roberts, G.P., 2008, Visualisation of active normal fault scarps in the Apennines, Italy: a key to assessment of tectonic strain release and earthquake rupture., *in* De Paor, D., ed., Google Earth Science, Journal of the Virtual Explorer, Volume 30.

Roberts, J.J., Wood, R.A., and Haszeldine, R.S., 2011, Assessing the health risks of natural CO_2 seeps in Italy: Proceedings of the National Academy of Sciences of the United States of America, v. 108, p. 16545-16548.

Roberts, J.J., Wood, R.A., Haszeldine, R.S., and Bell, A., 2012, Structural Controls on Natural CO_2 Seeps in Italy as Analogs for Long Duration CO_2 Storage.

Sani, F., Del Ventisette, C., Montanari, D., Coli, M., Nafissi, P., and Piazzini, A., 2004, Tectonic evolution of the internal sector of the Central Apennines, Italy: Marine and Petroleum Geology, v. 21, p. 1235-1254.

Santo, A., Ascione, A., Prete, S.D., Crescenzo, G.D., and Santangelo, N., 2011, Collapse sinkholes distribution in the carbonate massifs of central and southern Apennines: Acta Carsologica, v. 40, p. 95-112.

Savary, V., Berger, F., Dubois, M., Lacharpagne, J.-C., Pages, A., Thibeau, S., and Lescanne, M., 2012, The solubility of CO_2 + H2S mixtures in water and 2M NaCl at 120 deg C and pressures up to 35MPa: International Journal of Greenhouse Gas Control, v. 10, p. 123-133.

Scott, V., Gilfillan, S., Markusson, S., Chalmers, H., and Haszeldine, R.S., 2012, Last Chance for CCS.: Nature Climate Change.

Scrocca, D., 2005, Deep structure of the southern Apennines, Italy: Thin-skinned or thick-skinned?: Tectonics, v. 24.

Serpelloni, E., Anzidei, M., Baldi, P., Casula, G., and Galvani, A., 2005, Crustal velocity and strain-rate fields in Italy and surrounding regions: new results from the analysis of permanent and non-permanent GPS networks: Geophysical Journal International, v. 161, p. 861-880.

—, 2006, GPS measurement of active strains across the Apennines: Annals of Geophysics, v. 49, p. 319-329.

Shackley, S., Reiner, D., Upham, P., de Coninck, H., Sigurthorsson, G., and Anderson, J., 2009, The acceptability of CO_2 capture and storage (CCS) in Europe: An assessment of the key determining factors Part 2. The social acceptability of CCS and the wider impacts and repercussions of its implementation: International Journal of Greenhouse Gas Control, v. 3, p. 344-356.

Shaffer, G., 2010, Long-term effectiveness and consequences of carbon dioxide sequestration: Nature Geoscience, v. 3, p. 464-467.

Shiner, P., Beccacini, A., and Mazzoli, S., 2004, Thin-skinned versus thick-skinned structural models for Apulian carbonate reservoirs: constraints from the Val d'Agri Fields, S Apennines, Italy: Marine and Petroleum Geology, v. 21, p. 805-827.

Smets, B., Tedesco, D., Kervyn, F.o., Kies, A., Vaselli, O., and Yalire, M.M., 2010, Dry gas vents ("mazuku") in Goma region (North-Kivu, Democratic Republic of Congo): Formation and risk assessment: Journal of African Earth Sciences, v. 58, p. 787-798.

Smith, S.A.F., Collettini, C., and Holdsworth, R.E., 2008, Recognizing the seismic cycle along ancient faults: CO_2-induced fluidization of breccias in the footwall of a sealing low-angle normal fault: Journal of Structural Geology, v. 30, p. 1034-1046.

Solomon, S., D. Qin, M. Manning, R.B. Alley, T. Berntsen, N.L. Bindoff, Z. Chen, A. Chidthaisong, J.M. Gregory, G.C. Hegerl, M. Heimann, B. Hewitson, B.J. Hoskins, F. Joos, J. Jouzel, V. Kattsov, U. Lohmann, T. Matsuno, M. Molina, N. Nicholls, J. Overpeck, G. Raga, V. Ramaswamy, J. Ren, M. Rusticucci, R. Somerville, T.F. Stocker, P. Whetton, R.A. Wood and D. Wratt, 2007, Technical Summary, *in* Solomon, S., D. Qin, M. Manning, Z. Chen, M. Marquis, K.B. Averyt, M. Tignor and H.L. Miller, ed., Climate Change 2007: The Physical Science Basis. Contribution of Working Group I to the Fourth Assessment Report of the Intergovernmental Panel on Climate Change: Cambridge, United Kingdom and New York, NY, USA, Cambridge University Pres.

Sorey, M.L., Evans, W.C., Kennedy, B.M., Farrar, C.D., Hainsworth, L.J., and Hausback, B., 1998, Carbon dioxide and helium emissions from a reservoir of magmatic gas beneath Mammoth Mountain, California: Journal of Geophysical Research-Solid Earth, v. 103, p. 15303-15323.

Span, R., and Wagner, W., 1996, A new equation of state fo carbon dioxide covering the fluid region from the triple point temperature to 1100 K at pressures up to 800 MPa: J Phys Chem Ref Data, v. 25, p. 1509 - 1596.

Spycher, N., and Pruess, K., 2005, CO_2-H2O mixtures in the geological sequestration of CO_2 center dot. II. Partitioning in chloride brines at 12-100 degrees C and up to 600 bar: Geochimica Et Cosmochimica Acta, v. 69, p. 3309-3320.

Spycher, N., Pruess, K., and Ennis-King, J., 2003, CO_2-H2O mixtures in the geological sequestration of CO_2. I. Assessment and calculation of mutual solubilities from 12 to 100 degrees C and up to 600 bar: Geochimica Et Cosmochimica Acta, v. 67, p. 3015-3031.

Stevens, S.H., Pearce, J.M., and Rigg, A.A.J., 2001, Natural Analogs for Geologic Storage of CO_2: An Integrated Global Research Program, First National Conference on Carbon Sequestration

U.S. Department of Energy: National Energy Technology Laboratory

Washington, D.C., p. 12.

Strahler, A.N., 1952, Dynamic Basis of Geomorphology: Geological Society of America Bulletin, v. 63, p. 923-&.

Streit, J.E., and Cox, S.F., 2001, Fluid pressures at hypocenters of moderate to large earthquakes: J. Geophys. Res., v. 106, p. 2235-2243.

Tarboton, D.G., Bras, R.L., and Rodrigueziturbe, I., 1991, On the Extraction of Channel Networks from Digital Elevation Data: Hydrological Processes, v. 5, p. 81-100.

Tassi, F., Fiebig, J., Vaselli, O., and Nocentini, M., 2012, Origins of methane discharging from volcanic-hydrothermal, geothermal and cold emissions in Italy: Chemical Geology, v. 310-311, p. 36-48.

Tyrrell, T., Shepherd, J.G., and Castle, S., 2007, The long-term legacy of fossil fuels: Tellus B, v. 59, p. 664-672.

Vaselli, O., 2012, Dr: Università degli Studi di Firenze.

Vaselli, O.T., F.; Minissale, A.; Capaccioni, B.; Macro, G.; Evans, W. C., 1997, Geochemistry of natural gas manifestions from the Upper Tiber Valley (central Italy): Mineralogica et Petrographica Acta, v. 40, p. 201-212.

ViDEPI, 2009, Visibility of petroleum exploration data in Italy (ViDEPI) project, *in* Casero, P., Bruni, A., Epifan, L., Giorgio Luigini, G., Alessandra Pensa, A., Simoncini, D., and Santocchi, N., eds., Volume 2009, Ministero dello sviluppo economico - UNMIG, Società Geologica Italiana, Assomineraria.

Voltattorni, N., Caramanna, G., Cinti, D., Galli, G., Pizzino, L., and Quattrocchi, F., 2006, Study of Natural CO_2 Emissions in Different Italian Geological Scenarios, *in* Lombardi, S., Altunina, L.K., and Beaubien, S.E., eds., Advances in the Geological Storage of Carbon Dioxide, Volume 65: NATO Science Series, Springer Netherlands, p. 175-190.

Voltattorni, N., Sciarra, A., Caramanna, G., Cinti, D., Pizzino, L., and Quattrocchi, F., 2009, Gas geochemistry of natural analogues for the studies of geological CO_2 sequestration: Applied Geochemistry, v. 24, p. 1339-1346.

WHO, 2009, Protecting health from climate change: Connecting science, policy and people, World Health Organization, p. 36.

Wibberley, C.A.J., and Shipton, Z.K., 2010, Fault zones: A complex issue: Journal of Structural Geology, v. 32, p. 1554-1556.

Wilkinson, M., Gilfillan, S.M.V., Haszeldine, R.S., and Ballentine, C.J., 2009, Plumbing the depths – testing natural tracers of subsurface CO_2 origin and migration, Utah, USA.: American Association of Petroleum Geologists Studies in Geology, v. 59.

Yang, C.-Y., and Manga, M., 2009, Earthquakes and Water: Berlin / Heidelberg, Springer.

Yielding, G., Freeman, B., and Needham, D.T., 1997, Quantitative fault seal prediction: Aapg Bulletin-American Association of Petroleum Geologists, v. 81, p. 897-917.

Zweigel, P., Lindeberg, E., Moen, A., and Wessel-Berg, D., 2004, Towards a methodology for top seal efficacy assessment for underground CO_2 storage.